AN EXPERIMENTAL INVESTIGATION OF THE USE OF AIR JET VORTEX GENERATORS TO CONTROL SHOCK INDUCED BOUNDARY LAYER SEPARATION.

By Martin Kiran Rao.

Thesis Submitted for the Degree of Doctor of Philosophy.

City University

Department of Aeronautics

September 1988.

CONTENTS

LIST OF FIGURES

6.2 Comparison of shock locii for the 8%, 10% and 14% bumps with no vortex generators.

6.3 Comparison of P_2 loci on the 8% bump (No vg and vanes)

6.4 Comparison of P_2 loci on the 10% bump (No vg and vanes)

6.5 Comparison of P_2 loci on the 14% bump (No vg and vanes)

6.6 Comparison of shock loci on the 8% bump (No vgs and vanes).

6.7 Comparison of shock loci on the 10% bump (No vgs and vanes).

6.8 Comparison of shock loci on the 14% bump (No vgs and vanes).

6.9 Experimental Pressure Distributions with Corresponding Schlieren Image for the 10% Bump with no vortex generators.

6.10 Experimental Pressure Distributions with Corresponding Schlieren Image for the 10% Bump with vane generators.

6.11 Boundary Layer Profiles With no vortex generators.

6.12 Boundary Layer Profiles With Vane Generators.

6.13 Experimental Pressure Distributions with Corresponding Schlieren Image for the 10% Bump with Small Air Jets (P_b/P_o=1.2)

6.14 Experimental Pressure Distributions with Corresponding Schlieren Image for the 10% Bump with Large Air Jets (θ=60°,P_b/P_o=1.2).

6.15 Boundary Layer Profiles With Small Air Jet Vortex Generators (P_b/P_o=1.6, ϕ=30°).

6.16 Boundary Layer Profiles With Large Air Jet Vortex Generators (P_b/P_o=1.5, θ=60°).

6.17 Influence of Jet Direction on Cross Flow Component.

6.18 Boundary Layer Profiles With Small Air Jet Vortex Generators (P_b/P_o=1.6, ϕ=45°).

6.19 Experimental Pressure Distributions with Corresponding Schlieren Image for the 14% Bump with Small Air Jets (ϕ=30°, P_b/P_o=1.6).

6.20 Experimental Pressure Distributions with Corresponding Schlieren Image for the 14% Bump with Small Air Jets (ϕ=45°, P_b/P_o=1.6).

6.21 Boundary Layer Profiles With Large Air Jet Vortex Generators (P_b/P_o=1.2, θ=60°).

6.22 Boundary Layer Profiles With Large Air Jet Vortex Generators (P_b/P_o=1.5, θ=60°).

6.23 Comparison of shock loci on the 8% bump (No vgs and Round jets θ=90° P_b/P_o=1.0)

6.24 Comparison of shock loci on the 8% bump (No vgs and Round jets θ=60° and θ=90° P_b/P_o=1.0)

6.25 Comparison of shock loci on the 8% bump (No vgs and Round and Rectangular jets θ=60° P_b/P_o=1.0)

6.26 Comparison of shock loci on the 8% bump (vanes and Small rectangular jets P_b/P_o=1.0 and 1.2)

6.27 Comparison of shock loci on the 10% bump (vanes and Small rectangular jets P_b/P_o=1.2 and 1.6)

6.28 Comparison of shock loci on the 14% bump (vanes and Small rectangular jets P_b/P_o=1.2 and 1.6)

6.29 Experimental Pressure Distributions for the 10% Bump with small Air Jet Vortex Generators (ϕ=30°, P_b/P_o=1.6).

6.30 Experimental Pressure Distributions for the 14% Bump with small Air Jet Vortex Generators (ϕ=30°, P_b/P_o=1.6).

6.31 Experimental Pressure Distributions for the 14% Bump with small Air Jet Vortex Generators (ϕ=45°, P_b/P_o=1.2).

6.32 Experimental Pressure Distributions for the 14% Bump with small Air Jet Vortex Generators (ϕ=45°, P_b/P_o=1.6).

6.33 Comparison of shock loci on the 14% bump (Small rectangular jets ϕ=30° and 45° at P_b/P_o=1.6)

6.34 Comparison of Pressure Distributions for the 14% Bump small Air Jet Vortex Generators (ϕ=30°and 45°, P_b/P_o=1.6).

6.35 Comparison of shock loci on the 10% bump (Large air jets P_b/P_o=1.8 and vanes)

6.36 Comparison of shock loci on the 10% bump (Large air jets P_b/P_o=1.8, 1.2 and 1.0)

ACKNOWLEDGEMENTS

I would like to thank the Department of Aeronautics at City University and British Aerospace P.L.C. for giving me the opportunity to carry out the research which is reported in this thesis.

I would especially like to thank my supervisors, Dr. M. M. Freestone and Prof. H.H. Pearcey, for their help during the course of this project.

I would also like to thank the technical staff in the Department for their time and effort in preparing the wind tunnel models, especially Mr. R. Lomas for helping me with the operation of the tunnel.

Finally, I would like to thank my wife Alison for her support and help in writing this thesis.

ABSTRACT

Air jet vortex generators were originally investigated by R.A. Wallis. Results showed that their effectiveness in delaying shock induced boundary layer separation was not as good as conventional vane type generators. Recent low speed wind tunnel tests carried out at City University indicated that the strength of the vortex could be increased considerably by using rectangular jet exits rather than round ones as used by Wallis. On this basis an investigation into air jet vortex generators was undertaken to find out whether similar improvements in vortex strength may be gained at transonic speeds and hence achieve a more effective method of controlling shock induced boundary layer separation.

It was felt that in order to design air jet vortex generators it would be necessary to understand the mechanism by which an air jet forms a vortex, and to evaluate the effects of various jet parameters on vortex size, strength and position. The parameters investigated in this thesis were: (i) exit shape (ii) exit size (iii) jet direction (iv) jet inclination and (v) blowing pressure. The tests were conducted using a combination of high speed wind tunnel tests and flow visualisation in a water tunnel.

The wind tunnel tests used the half aerofoil or 'bump technique' as used by Wallis. Bumps with thickness to chord ratios of 8%, 10% and 14% were tested. Increasing the thickness of the bumps resulted in higher local Mach numbers ahead of the shock and hence an increase in the severity of the shock induced separation. Vane vortex generators designed using the criteria laid down by H.H. Pearcey were used to establish a datum of control effectiveness.

As a result of this investigation a method by which an air jet forms a vortex has been proposed together with a hypothesis on the influence of the various jet parameters. The results have shown that air jet vortex generators can be designed to be more effective than conventional vane type generators.

Based on the work reported in this thesis a set of design guidelines has been proposed together with suggestions for further work.

STATEMENT OF CONFIDENTIALITY

On request of the sponsors, British Aerospace Plc., access to this thesis is restricted and it may not be copied in part or in whole until October 1995.

NOTATION

c	Chord of half aerofoil
$C_{L\ max}$	Maximum lift coefficient
C_{pb}	Boundary Layer Pressure Coefficient $(P_{ob}-P)/(P_{oe}-P)$
d	Diameter of round jet exit
D	Pitch of vortex generators
h	Height of vane vortex generators
l	Jet exit length
L	Length of vane vortex generator
M	Mach number
P	Local static pressure
P (TE)	Static pressure at the trailing edge
P_b	Blowing pressure
P_o	Freestream Stagnation pressure
P_{ob}	Stagnation Pressure in Boundary Layer
P_{oe}	External Flow Stagnation Pressure
P_p	Preston tube pressure
P_1	Static pressure just ahead of the shock
P_2	Static pressure just downstream of the shock or, alternatively, just downstream of the rapid rise through the region of shock/ boundary layer interaction (which includes the re-attachment if the separation bubble is of limited length).
t_v	Thickness of vane vortex generator
t/c	Thickness/chord ratio of the bump
U	Local velocity in the boundary layer
U_e	Freestream velocity

V	Mean Jet Velocity
V_y	Induced Lateral Velocity
w	Width of rectangular air jet
x/c	Chordwise position on the bump
x/c_{shock}	Chordwise position of the shock wave
Y	Height normal to the surface of the bump
α	Incidence of the vanes to the freestream
Γ	Circulation of the vortex
θ	Boundary layer momentum thickness
θ	Direction of jet exits
ϕ	Inclination of jet exits

Abbreviations

Lg	Large air jet vortex generator
Sm	Small air jet vortex generator
Vg	Vortex generator

1.0 INTRODUCTION

1.1 Historical Background

As the speed of an aircraft increases into the high subsonic range, a region of supersonic flow can develop over the wings. When both subsonic and supersonic regions co-exist the aircraft is said to be flying in the transonic regime. The region of supersonic flow is usually terminated by a shock wave and the effect of this shock wave is to impose an adverse pressure gradient on the flow. Depending on the flow conditions, this can result in a region of boundary layer separation occurring downstream of the shock. This type of separation is called shock induced boundary layer separation.

This separation can lead to drastic changes in the flow over the wings of an aircraft, which in turn can lead to a degradation in its performance. This can manifest itself as a reduction in lift, an increase in drag, and large changes in the pitching moment. Flow separation can also give rise to increased vibration and noise and associated increases in structural loads, fatigue damage and crew and passenger discomfort.

In order to avoid the problems associated with shock induced separation, the flight envelope of the aircraft can be restricted so that it will be unlikely to encounter the problems associated with shock induced boundary layer separation. This could however render the aircraft uncompetitive in today's aggressive markets. For this reason the most common solution to the problem has been to

design the wing so that only weak shocks are encountered at the design cruise conditions. For the off-design conditions (i.e. at increased lift coefficient or increased Mach number) devices are used to influence the boundary layer so that the adverse effects of shock induced separation are delayed. An example of such devices are vane vortex generators and figure 1.1 shows how they may be incorporated on an aircraft's wing.

The development of vane vortex generators was carried out by Pearcey (1) and his co-workers in the early 1950's. Since then, vane vortex generators have been used successfully to delay the onset of the problems associated with shock induced separation. The disadvantage of vane vortex generators however is that there is a small but significant drag penalty associated with their use. Several attempts have been made to reduce the drag penalty associated with vane vortex generators including optimisation of the vane planform, size and distribution and the use of retractable vanes. The scope for improvement is however limited since the vane vortex generators have to be of a certain size to work effectively and retractable vanes are mechanically too complex.

An alternative method to delay shock induced separation was investigated by Wallis (2) in 1958. Wallis proposed that discrete jets of air, blown across the span of the wing could interact with the local flow to produce vortices similar to those produced by the vane vortex generators. It was proposed that the advantages of using air jet vortex generators would be to reduce the drag penalty compared with the conventional vane vortex generators. In addition several rows of air jet vortex

generators could be incorporated on a wing and individual rows could be selected to give the optimum boundary layer control depending on the position of the shock. Also, the air jet vortex generators would still operate in a region of separated flow unlike the vane vortex generators. Figure 1.2 illustrates the round air jet exits used by Wallis. His research showed that these round air jet vortex generators were able to delay the onset of shock induced separation, but they were less effective than the vane vortex generators.

Although the work carried out by Wallis looked promising no additional research into optimising or developing an understanding of the air jet parameters appears to have been published until 1985 when Freestone (3) showed that significant improvements could be achieved by making the jet exits rectangular rather than round. Further improvements could also be gained by angling the jets slightly downstream, giving the jets a downstream component as seen in figure 1.3. Although Freestone's tests were carried out with low speed flows he proposed that similar improvements could be achieved for jets issuing into high subsonic or supersonic flows. This was the basis of the investigation discussed in this thesis.

1.2 Research Objectives

The objectives of the research discussed in this thesis are as follows,

- To develop an understanding of the method by which an air jet forms a vortex.

- To investigate the influence of the shape, size, direction and air jet blowing pressure on the characteristics of the resulting vortex.

- To test the ability of a row of air jet vortex generators to delay the onset of shock induced boundary layer separation and to compare their effectiveness against conventional vane vortex generators.

- To formulate a set of guidelines which may be used in the design process for practical applications of air jet vortex generators.

1.3 Research Programme

Flow visualization was considered to be the most effective way to investigate the method by which an individual air jet, issuing from the surface of a wing into the local stream, interacts to form a vortex. Of the various techniques available at City University a simulation by water channel testing was considered to be the most suitable. Although water channel tests may not duplicate the exact conditions experienced in air, it was felt that the results would give an indication of the interaction process.

Extensive transonic wind tunnel tests were also carried out. Tests were carried out on half aerofoil models with no vortex generators in order to establish the extent of shock induced boundary layer separation present. Vane vortex generators were then added to provide a datum against which the various air jet vortex generator

configurations could be compared. Three bumps of different thickness to chord ratios were used to investigate the effect of increasing local Mach numbers ahead of the shock waves. Static pressure measurements, together with schlieren photography and boundary layer rake investigations were used to evaluate the flow conditions.

The results were analysed to identify the effect of the various air jet design parameters on the vortex formation and to hypothesise on the development of the vortices as the travelled downstream and interacted with the shock wave and the boundary layer in order to explain their effect in delaying the onset of separation. Comparisons between the various vortex generator configurations were made and a set of design guidelines proposed.

Vane Vortex Generators

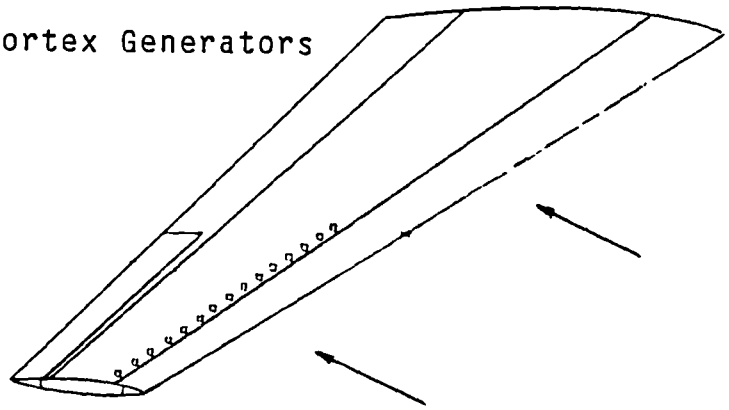

Counter-rotating Generators

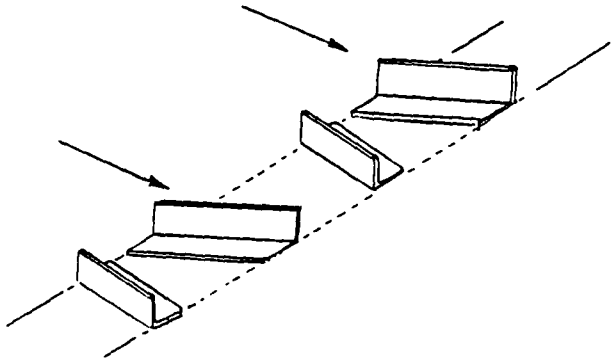

Co-rotating Generators

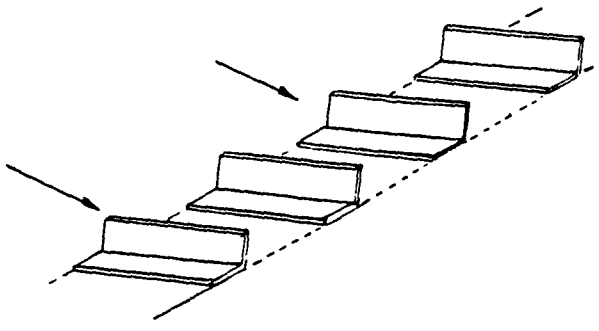

Figure 1.1 Vane Vortex Generators

Figure 1.2 Round Jet Exits

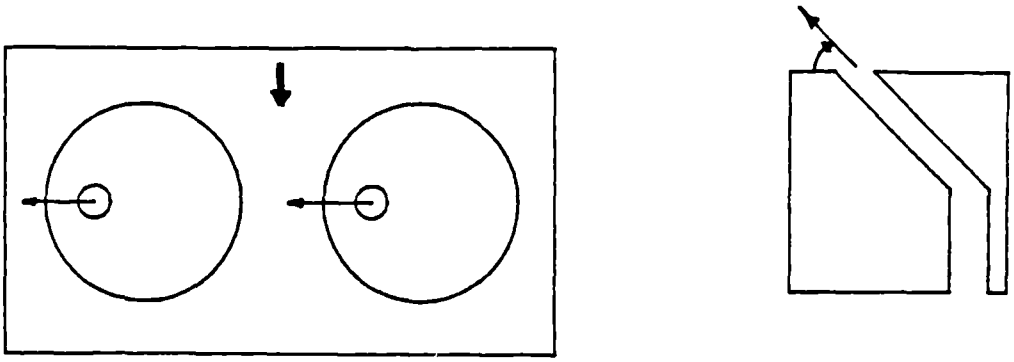

Figure 1.3 Rectangular Jet Exits

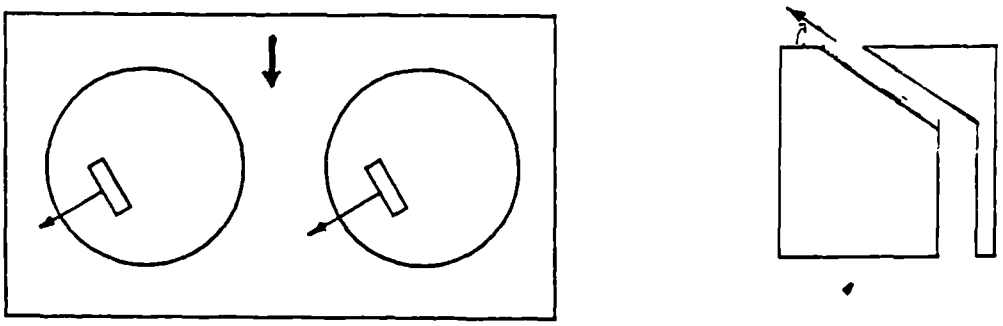

2.0 SHOCK INDUCED BOUNDARY LAYER SEPARATION AND ITS' CONTROL.

This chapter describes the development of transonic flow over a two-dimensional aerofoil. Particular attention is paid to the development of shock induced boundary layer separation and the relationships between the flow parameters used to identify it. The adverse effects of shock induced boundary layer separation on the performance characteristics of an aerofoil are mentioned and several methods currently used to delay the onset of this type of separation are discussed.

2.1 Development of Transonic Flow over an Aerofoil.

Transonic flow is said to exist when regions of subsonic and supersonic flow exist simultaneously on the surface of a body. The development of transonic flow over an aerofoil can be achieved by either increasing the freestream Mach number or increasing the aerofoil incidence. To assist in the description of this flow the effect of increasing Mach number and incidence are treated separately.

Consider a two-dimensional lifting aerofoil with a turbulent boundary layer. Initially an aerofoil at fixed incidence is considered over a range of freestream Mach numbers. The development of the flow over this aerofoil is illustrated in Figures 2.1a-d together with their associated pressure distributions. The flow characteristics, with Mach number as the variable, are presented in Figure 2.3. The parameters presented are trailing edge pressure (P_{TE}), the pressure immediately downstream of the shock wave (P_2), the position of the shock wave (x/c_{shock}), and the lift coefficient (C_L). Definitions of these parameters are given in Appendix E.

The conditions illustrated in Figures 2.1 are indicated in Figures 2.3 to assist in the description of the flow development.

The development of the flow over the aerofoil is represented schematically in Figures 2.1. With increasing freestream Mach number a region of supersonic flow forms first on the upper surface of the aerofoil. This supersonic region is terminated by a weak shock wave (see figure 2.1a). The corresponding pressure distribution shows this shock wave as a steep pressure rise, and this pressure rise results in a thickening of the boundary layer at the foot of the shock. If the flow were inviscid, the shock wave would be normal to the surface and the associated pressure rise would be that predicted by the Rankine-Hugoniot equations. In practice the presence of the boundary layer means that the pressure rise achieved through the shock is reduced. There is no separation downstream of the shock, and as shown by the pressure distribution, there is a good pressure recovery to the trailing edge.

As the freestream Mach number is increased, the shock wave moves progressively downstream and increases in strength (see figure 2.1b). The resulting pressure rise causes the boundary layer to separate at the foot of the shock and in this case it re-attaches a short distance downstream enclosing a region of separation known as a 'bubble'. At this stage the presence of the bubble has little effect on the pressure recovery from the foot of the shock to the trailing edge. Figures 2.3 shows the aerofoil characteristics for increasing Mach number. Between the conditions shown in figures 2.1a and 2.1b the increase in Mach number has resulted in a downstream movement of the shock, an decrease in the pressure at the foot of the shock, a reduction in the trailing edge pressure, and an increase in the lift coefficient.

As the Mach number is increased further, the shock wave has increased in strength and the resulting separation bubble has increased significantly in length (see figure 2.1c). The associated pressure distribution shows that this separation has a significant effect on the overall pressure recovery both through the shock and downstream to the trailing edge. Clearly this separation will have a significant effect on the flow at the trailing edge and also therefore on the flow on the lower surface. The interrelationship between the flow over the upper and lower surface is governed by the fact that the wake cannot support any appreciable pressure difference between its two edges and hence the pressure of the upper and lower surfaces must be nearly equal at the trailing edge.

For the case shown in Figure 2.1c the separation on the upper surface greatly reduces the trailing edge pressure. Assuming the flow remains attached on the lower surface, the reduction in trailing edge pressure can only be achieved by an acceleration of the flow and hence a rearward movement of the lower surface shock. The changes on the lower surface will in turn affect the upper surface and this interaction will continue until some equilibrium is established in the development of the flow on the two surfaces relative to each other. This condition is usually associated with unsteady phenomena known as buffeting where there are fluctuations in the loading of the aerofoil.

Figures 2.3 detailing the characteristics of the aerofoil shows that the rate at which the shock progresses downstream, over the upper surface, with increasing Mach number is reduced. The trailing edge pressure and the pressure at the foot of the shock have both diverged significantly and the lift coefficient has decreased. These features are clear indicators of significant shock induced boundary layer separation. Other

effects of shock induced boundary layer separation include changes in pitching moment which, when applied to a real aircraft, can result in control problems.

A further increase in Mach number (see figure 2.1d) results in both shocks moving downstream to the trailing edge and the aerofoil is said to be in the supersonic range.

Considering now the situation where the Mach number is kept constant and the aerofoil incidence is increased. The flow conditions are illustrated in Figures 2.2a-d together with their associated pressure distributions. The flow characteristics, with aerofoil incidence now as the variable, are presented in figures 2.3. Notice that the general flow development with increasing incidence follows similar trends to those outlined for the previous constant Mach number example.

As the incidence is increased the shock wave forms on the upper surface of the aerofoil and it moves progressively downstream and increases in strength as incidence is increased further. As with the previous example, a separation bubble forms at the foot of the shock and increases in length until a point is reached where the bubble extends beyond the trailing edge of the aerofoil. The severe effects of shock induced boundary layer separation, as described in the previous example, are indicated by the trailing edge pressure diverging. Also the shock position moves forward and the lift curve slope reduces.

In both cases described above the effect of increasing Mach number or incidence resulted in increasing shock strength which in turn led to significant shock induced boundary layer separation.

For most wings of low or moderate sweepback the locus drawn through the values of incidence or lift coefficient at which trailing edge pressure diverges as Mach number is increased, or the values of Mach number for which trailing edge pressure diverges as incidence or lift coefficient is increased is a good guide to the onset of significant effects of separation, which often includes buffeting. This will be referred to as the "separation onset boundary" throughout this thesis.

A typical boundary is shown in Figure 2.4. For safety, an adequate margin must be maintained between the boundary and the locus drawn through the cruise operating conditions (see dotted line in Figure 2.4). In practice, for many wing designs, the cruise operating conditions can be determined by the separation onset boundary (or buffet boundary) and the need to ensure adequate margins. In such cases, the separation onset boundary has to be improved, i.e. displaced to the right and upwards in Figure 2.4, in order to achieve a better cruise performance. One method of effecting this is to use vortex generators.

2.2 Types of Shock Induced Boundary Layer Separation.

In the previous section the development of shock induced boundary layer separation over an aerofoil was discussed. This discussed a specific type of separation and there are in fact other types. Reference (4) and more recently in reference (5) categorises the way in which shock induced boundary layer separation develops over an aerofoil into two main classifications, referred to as Type A and Type B.

The development of shock induced boundary layer separation described earlier in Section 2.1 is of Type A. This is where the separation occurs at the foot of the shock enclosing a

separation bubble. Then with increasing Mach number or incidence the separation bubble increases in length until it extends beyond the trailing edge.

In Type B flows more severe adverse pressure gradients over the rear of the aerofoil results in a separation region spreading forward from the trailing edge. The Type B classification is sub divided into three categories depending on the way in which this rear separation interacts with the shock. The various sub classes of Type B are illustrated in Figure 2.5. When the rear separation occurs only after the formation of the bubble at the foot of the shock the flow is classified as Type B1. Type B2 is where the rear separation occurs soon after the occurrence of the shock wave but before the shock is strong enough to promote a separation bubble. Type B3 occurs when the rear separation is present before the shock wave has developed.

Type A separations are most common over aerofoils where the adverse pressure gradients encountered near the trailing edge are not particularly severe. For aerofoils with a high degree of rear camber the adverse pressure gradients near the trailing edge are more severe and this typically results in Type B separation.

Although aerofoils with significant rear camber are more common nowadays this thesis deals only with Type A flows. The reasons for this are that it is only the initial development of air jet vortex generators which is being considered at present and the rear separation that occurs in Type B flows would present an additional complication. Besides which, it is reasonable to assume that if vortex generators are able to influence the boundary layer such that shock induced boundary layer separation of Type A is delayed then the same vortex generators will have a beneficial effect in delaying Type B separations.

These assumptions can be justified by remembering that the development of vane vortex generators was carried out by investigating their effectiveness on Type A separations (reference 1) and yet they are being successfully applied to modern aerofoils experiencing Type B separations.

2.3 Methods of Boundary Layer Control.

In section 2.1 the development of shock induced boundary layer separation was described and the adverse effects of this separation on an aerofoil were mentioned. In order to delay these adverse effects it is possible to employ a method of boundary layer control and in this section some methods are described. As this thesis is concerned with the development of air jet vortex generators particular attention is paid to the effect a row of vortices has in delaying shock induced boundary layer separation.

Before describing the various methods of boundary layer control a summary of the interaction between a shock wave and a turbulent boundary layer is presented. A more detailed description can be found in references 1 and 5.

The cause of shock induced separation is the inability of a boundary layer to withstand the adverse pressure gradient imposed by a shock wave. In the external flow these pressure gradients are extremely large but at the surface they are softened by the interaction with the boundary layer. The softening process acts by thickening the subsonic part of the layer which in turn deflects the supersonic part and the external flow away from the surface. This generates a band of compression waves in the supersonic part of the layer which propagate into the external flow. The boundary layer thus

converts a sharp pressure rise into a more gradual one. As the shock strength increases (by increasing Mach number or incidence) the adverse pressure gradients associated with the compression waves increases until a point is reached where the flow in the inner part of the layer separates.

As mentioned earlier the shock induced separation can be delayed by influencing the boundary layer and various methods currently being used are described.

The concept of the vane vortex generator was introduced by Bruynes and Taylor and was developed by Pearcey (1) into one of the most common and successful methods of controlling shock induced boundary layer separation. The generators consist of a row of small plates or aerofoils that project normal from the surface with each one set at an angle of incidence to the local flow to produce a single trailing vortex (see Figure 2.6). The row of vanes can all be set at the same angle to produce a row of co-rotating vortices (Figure 2.6) or can be set in pairs of positive and negative angles to produce pairs of counter rotating vortices. Other less common types of vane vortex generators exits including biplane and wing type generators and further details can be found in reference 1.

The vortices produced by the vane vortex generators are partially submerged in the boundary layer. The dominant factor in delaying the onset of shock induced separation is the re-energisation of the inner part of the boundary layer. This process is a result of the downward velocities induced by the vortices which sweep high momentum fluid into the inner layers and at the same time the upward induced velocities sweep away the low momentum air from the boundary layer into the

freestream. Since the vortices are travelling in a streamwise direction they provide a continuous source of forced mixing.

Figure 2.7a (1) illustrates the interaction of a pair of co-rotating vortices in terms of contours of total head loss. Where the flow is being transferred towards the surface the boundary layer will tend to be thinned and its velocity profile will become fuller and, where the fluid is being transferred away from the surface the opposite will occur.

The interaction of a pair of co-rotating vortices on a boundary layer is illustrated in Figure 2.8, again as contours of total head loss. For an effective array of co-rotating vortices, D/h=6 (vane spacing to height ratio), the vortex cores are clearly shown. Also, the thinned part of the boundary layer on the downward side of the vortices is clearly illustrated as well as the thickened boundary layer on the upward side of the vortex. This pattern is clearer for D/h=6 than it is for D/h=4 where it can be seen that the thinned parts of the boundary layer getting less thin and the vortex cores becoming less intense. For D/h=2, the pattern is not at all established since the vortices are too close and interfere with each other.

From these observations Pearcey (1) deduced that there is a minimum value of D/h (around 4) below which the momentum transfer mentioned above is not present due to adjacent vortices interfering with each other. For values of D/h greater than four there was little variation in the ability of these vortices to delay the onset of shock induced separation. A maximum value obviously exits and Pearcey recommended that D/h should not exceed ten.

Recent work by Freestone (10) proposed a theoretical model demonstrating the influence of spacing on the effectiveness of a row of co-rotating vortices. This theory was based on a potential flow analysis of the maximum spanwise variation in the lateral velocity induced by a row of co-rotating vortices and their images. The results of Freestones (10) theoretical investigation are presented in Figure 2.7b in terms of maximum variation of induced lateral velocity per unit span versus vortex generator spacing to height ratio (D/h). Superimposing Pearcey's (1) vane vortex generator design guidelines it can be seen that there is a reasonable correlation.

Pairs of counter rotating vortices also influence the boundary layer by momentum transfer and introduce regions of thinned and thickened boundary layers. Figure 2.9 shows the interaction of two pairs of counter rotating vortices in terms of contours of total head loss. It can be seen that between the two pairs of vortices the boundary layer is thinned and thickened between the individual vortices making up the pair. Although counter rotating vortices are not as sensitive to spacing as co-rotating vortices they do have a tendency to lift of the surface as they progress downstream. This is illustrated in Figure 2.9 and this limits their effectiveness when used to delay shock induced boundary layer separation.

A variation on the vane vortex generator is the air jet vortex generator, which is under investigation in this thesis. The vortices are formed by the interaction between jets of air issuing from the surface and the mainstream flow. The resulting vortices then have a similar effect as the vortices produced by the vanes which may result in a delay in the onset of shock induced boundary layer separation. The advantages of air jets is that they need only be engaged when required and hence there will be a reduced drag penalty. Also, air jets will be able to

work in separated flows as the jets can penetrate a separated region and interact with the freestream to produce a vortex to help reattach the flow and delay the adverse effects of shock induced boundary layer separation. In addition multiple row of air jets can be built into a wing and the most appropriate row can automatically be selected to give the best control of separation.

As mentioned earlier other methods of delaying shock induced boundary layer separation are available. These include spanwise blowing and a passive method using a porous surface.

Spanwise blowing works by introducing high momentum air upstream of the shock which helps delay the onset of shock induced boundary layer separation. The disadvantage of this technique is that high quantities of air are required if the system is to be effective for a wide range of shock positions.

The concept of a passive system of controlling shock induced boundary layer separation is described in in Reference 8. Part of the upper surface of an aerofoil is replaced with a porous surface which covers a plenum chamber (see Figure 2.10). When a shock wave is located over the porous surface the pressure gradient associated with the shock introduces a flow through the plenum chamber from downstream of the shock to just upstream of it. The blowing ahead of the shock has the effect of softening the shock and thus reducing its strength and the adverse pressure gradient imposed by it on the boundary layer. The suction aft of the shock reduces the boundary layer thickness which helps to delay the onset of separation. A disadvantage of this technique is that it is only effective when the shock is located on the porous surface.

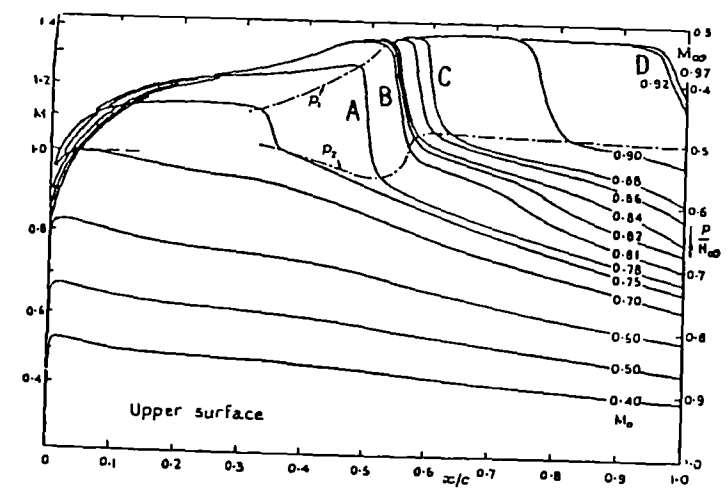

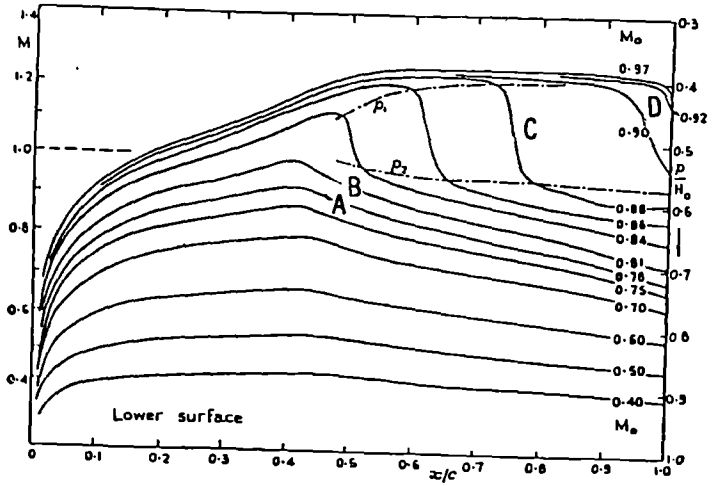

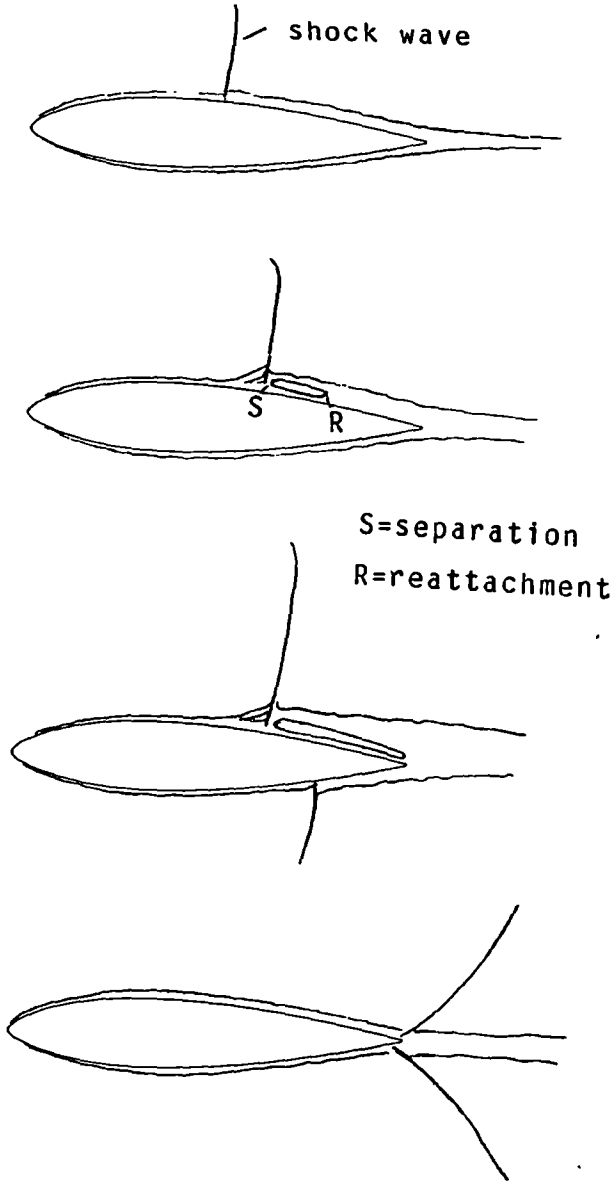

Figure 2.1 Sketches of the Flow Over an Aerofoil and the Associated Pressure Distributions (Fixed Incidence)

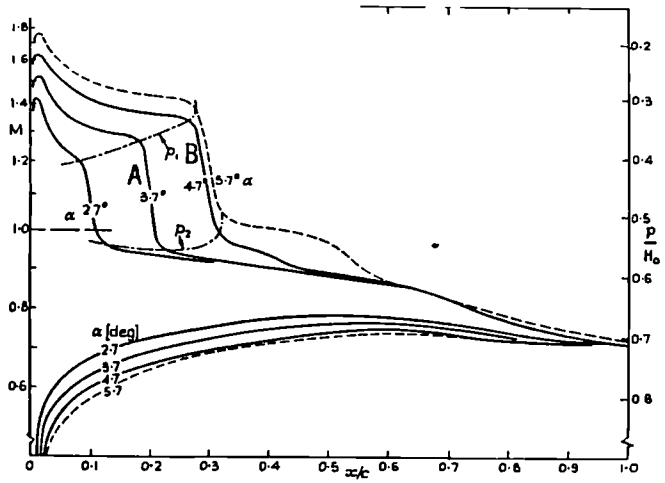

A: $\alpha = 3.7°$

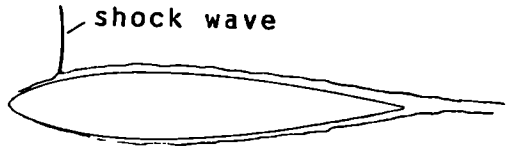

B: $\alpha = 4.7°$

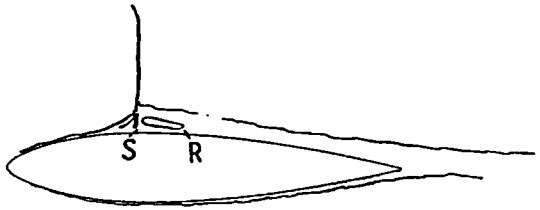

S=separation
R=reattachment

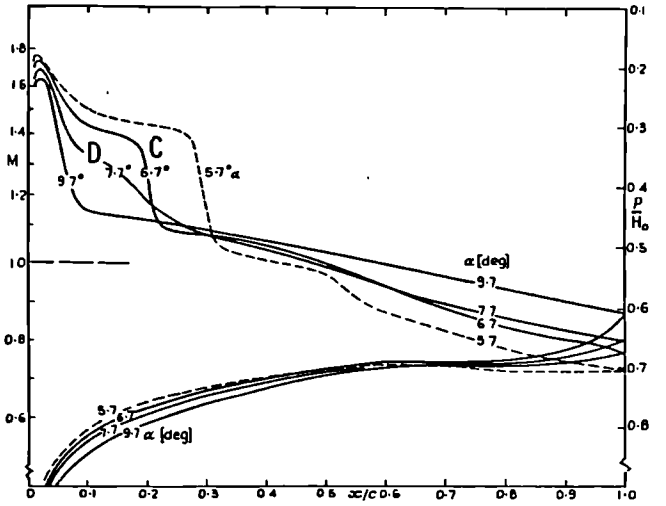

C: $\alpha = 6.7°$

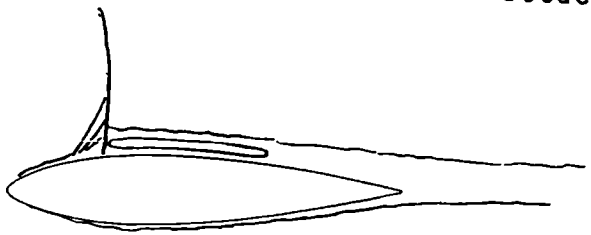

D: $\alpha = 7.7°$

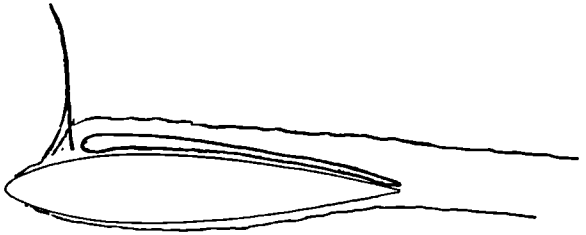

Figure 2.2 Sketches of the Flow Over an Aerofoil and the Associated Pressure Distributions (Fixed Mach Number)

Fixed Mach Number

Fixed Incidence

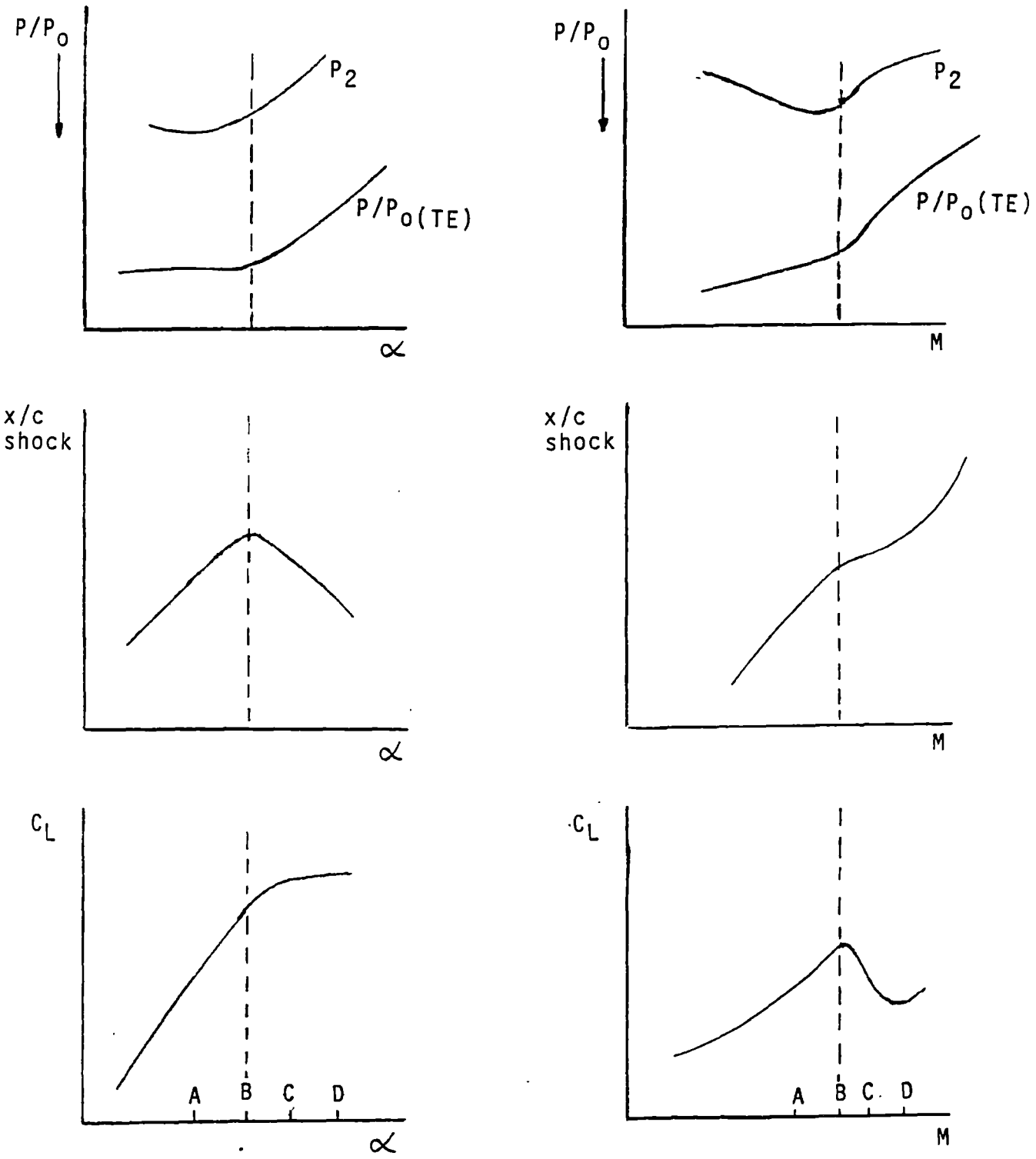

Figure 2.3 Comparison of Aerofoil Characteristics

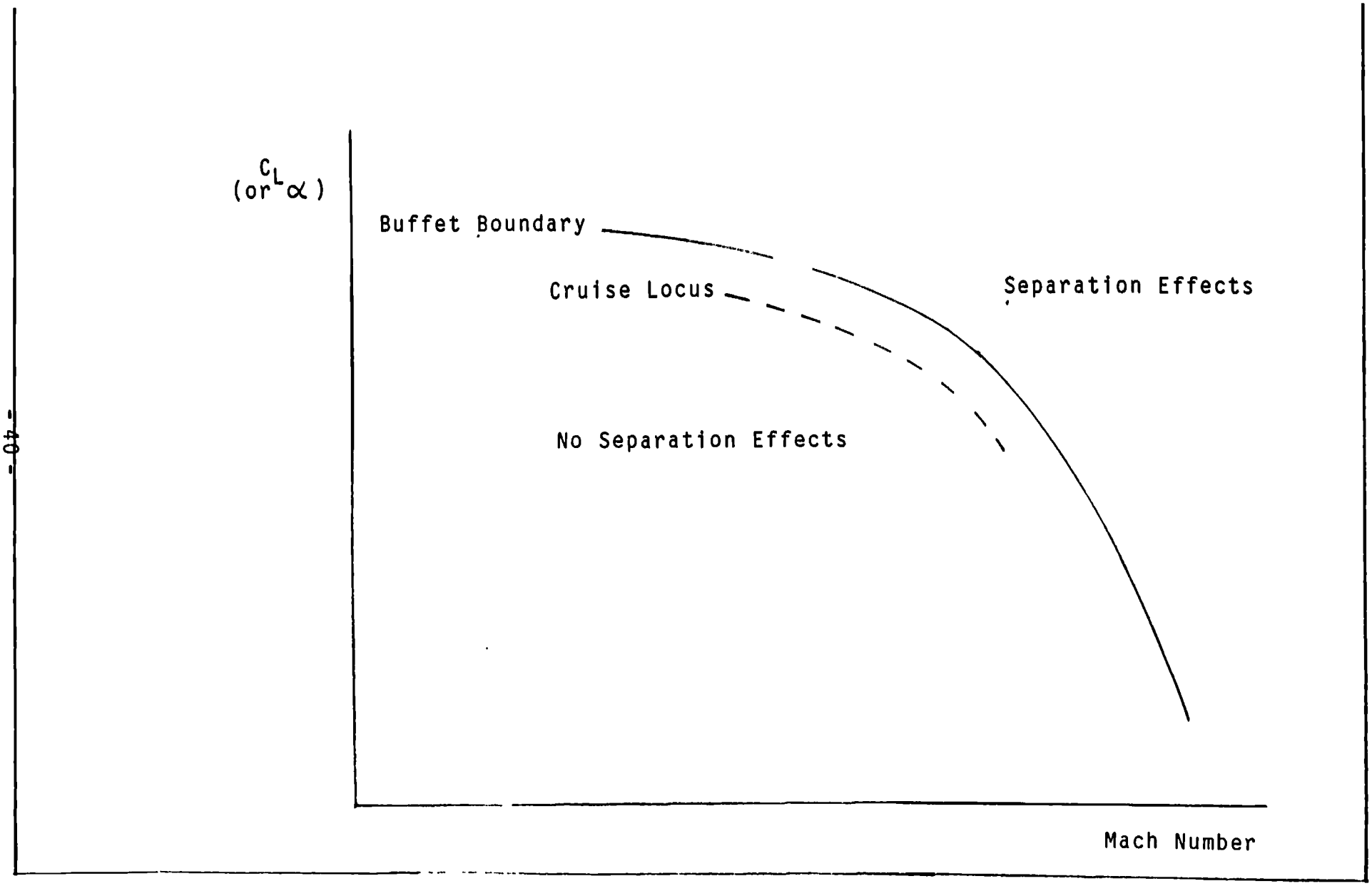

Figure 2.4 Typical Buffet Boundary

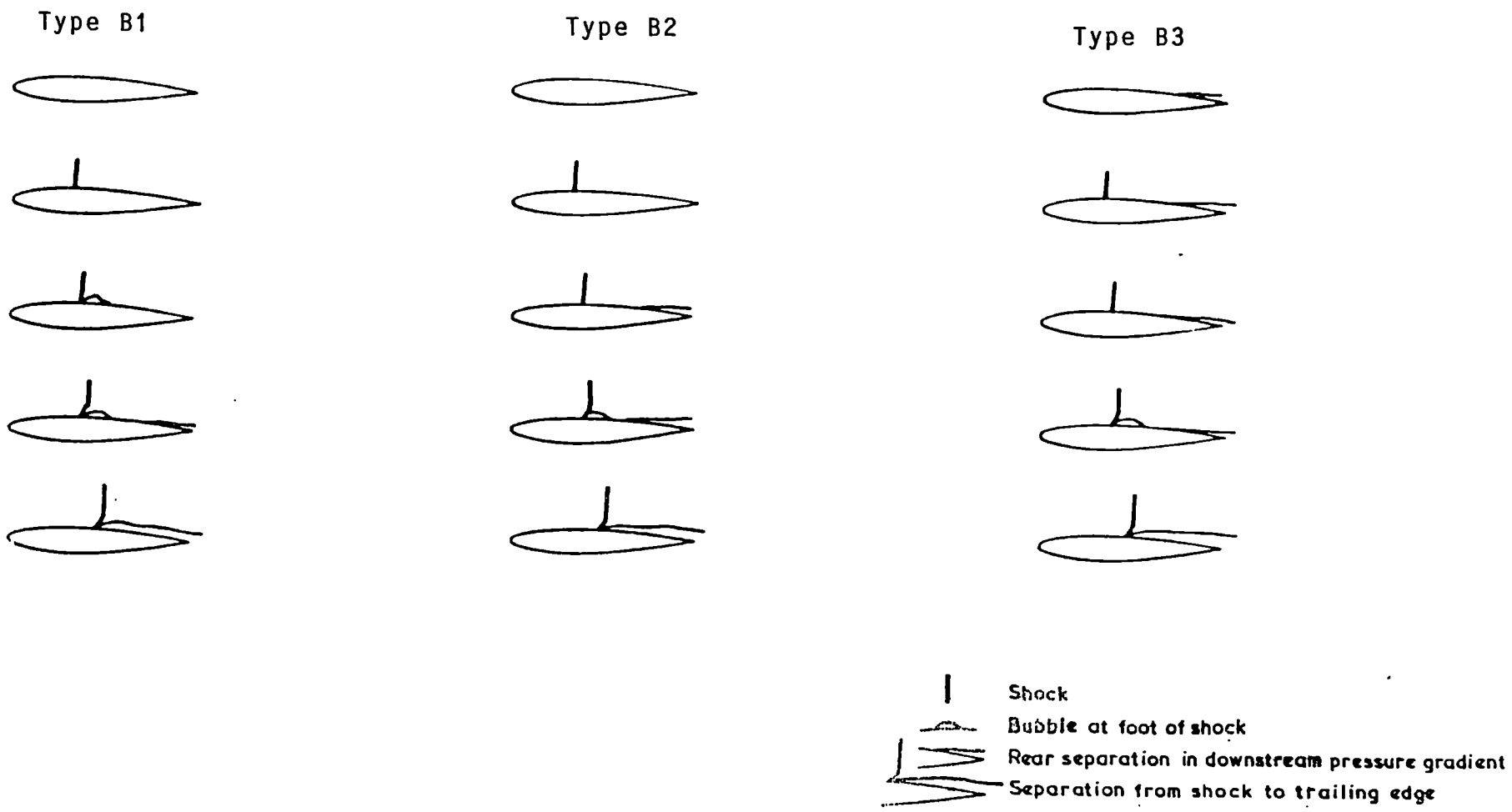

Figure 2.5 Type B Shock Induced Boundary Layer Separation

Vane Vortex Generators

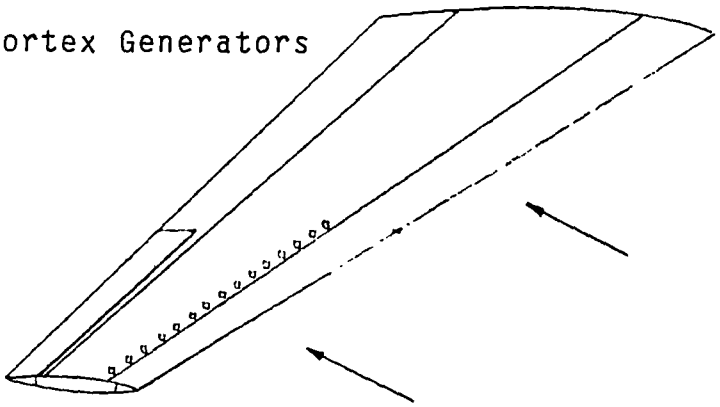

Counter-rotating Generators

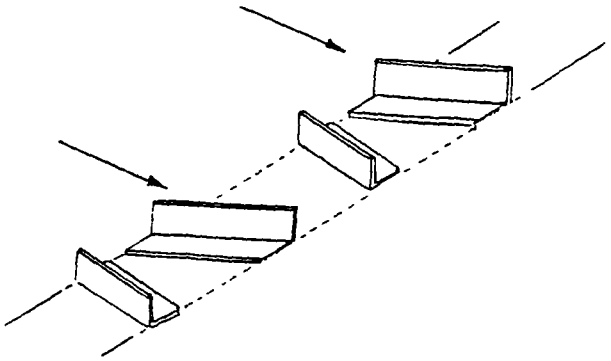

Co-rotating Generators

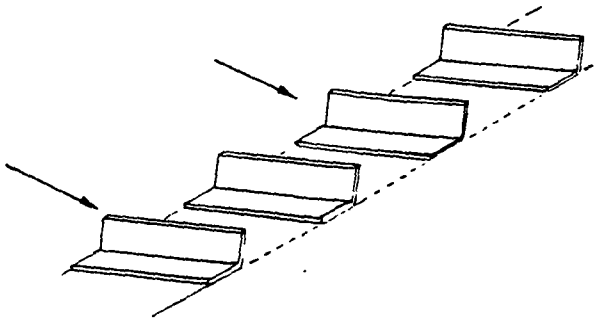

Figure 2.6 Vane Vortex Generators

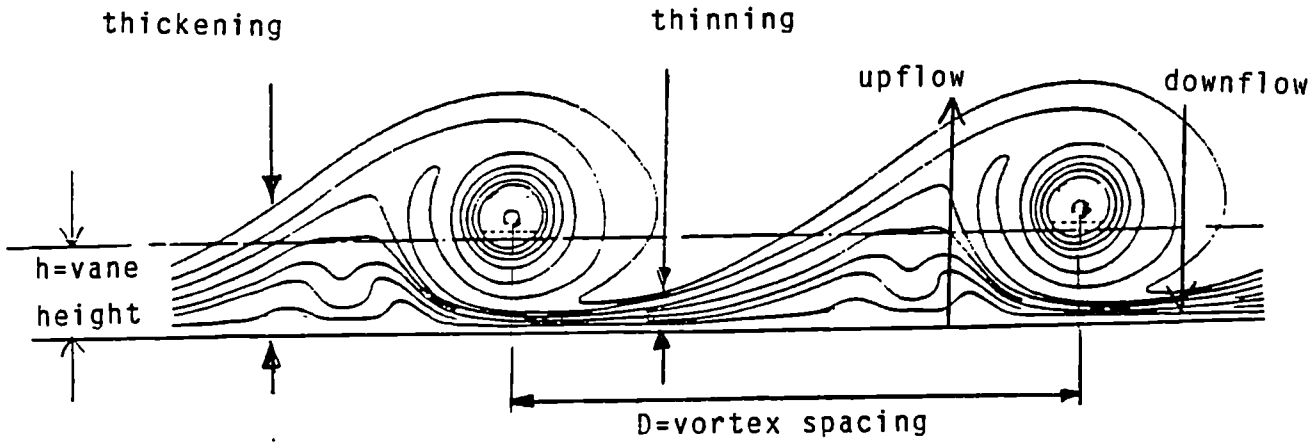

Figure 2.7a Vortex Boundary Layer Interaction

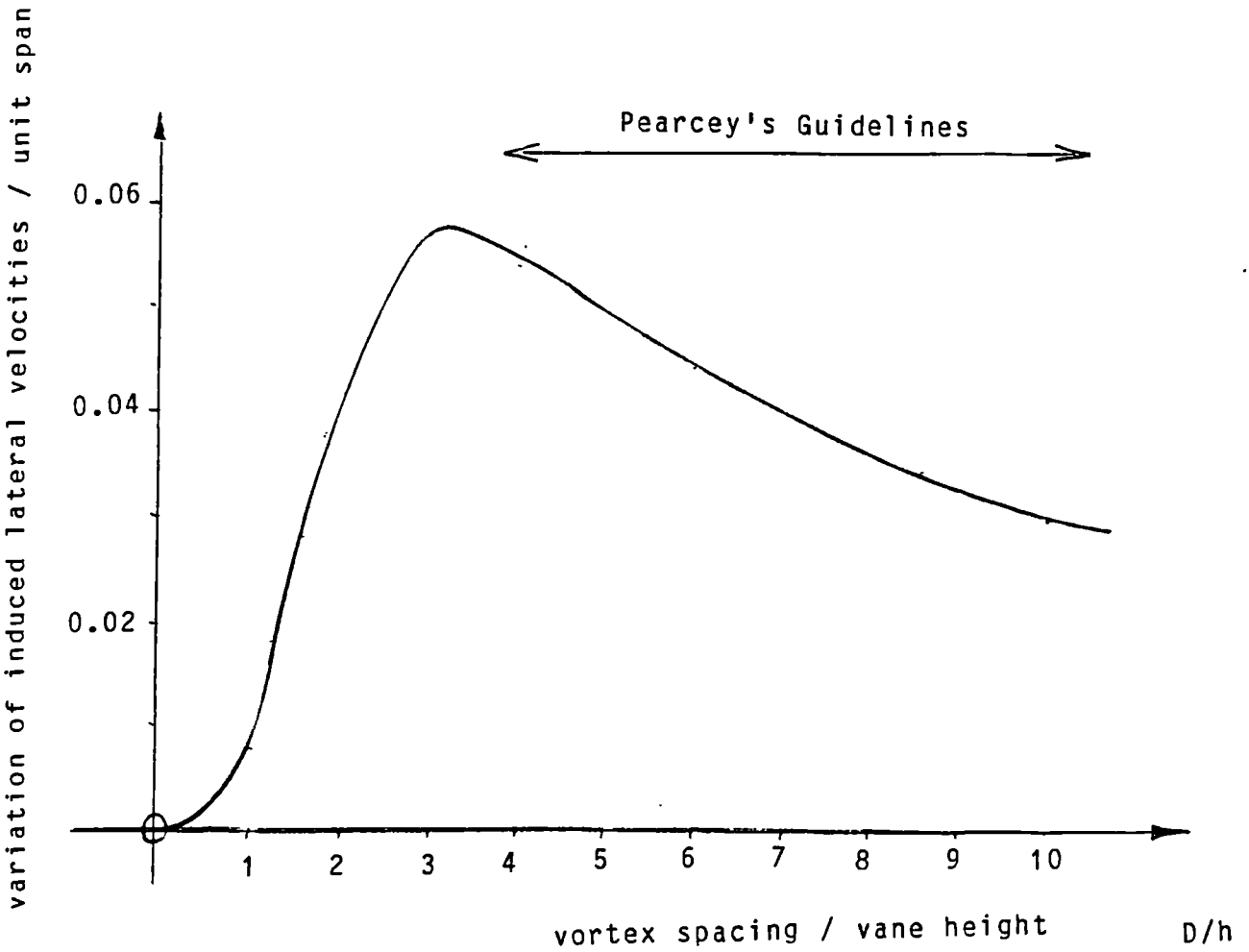

Figure 2.7b Theoretical Influence of Vortex Spacing

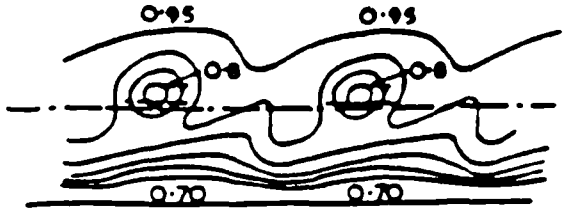

D/h=generator spacing/generator height

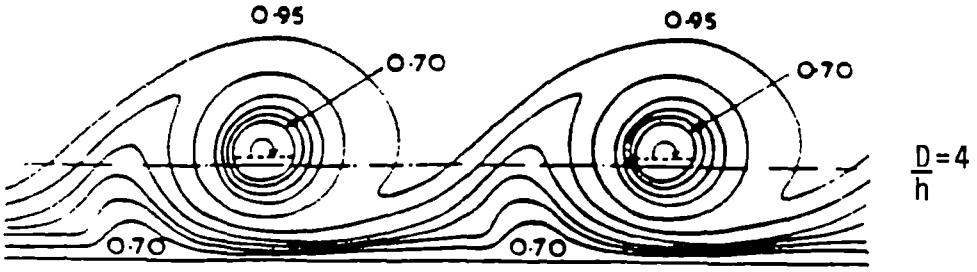

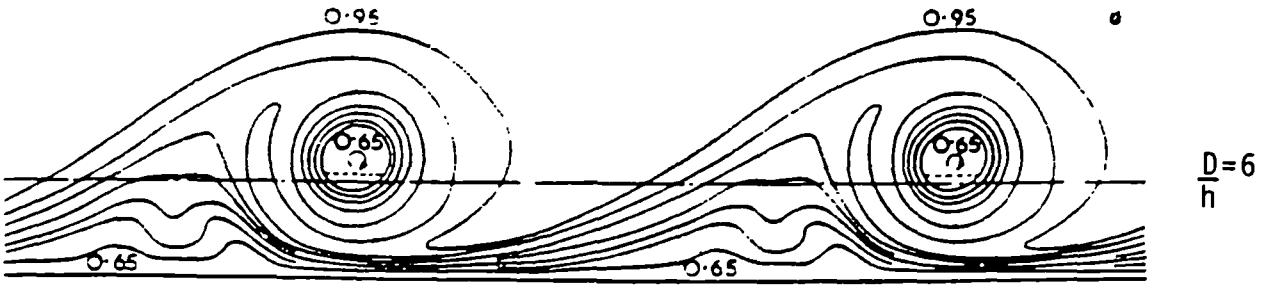

Figure 2.8 Contours of Total Head Loss for Co-Rotating Vortices at a Fixed Distance Downstream of the Generators

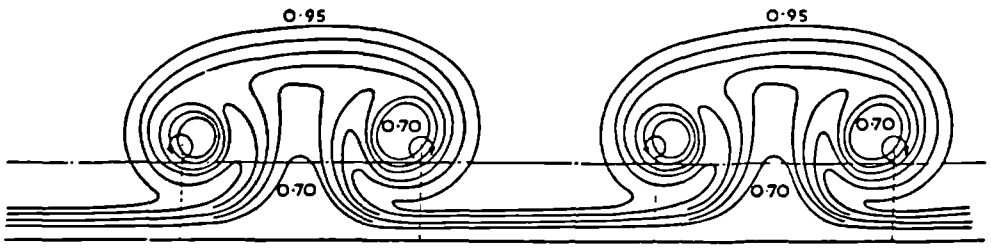

x/D=distance downstream/generator spacing

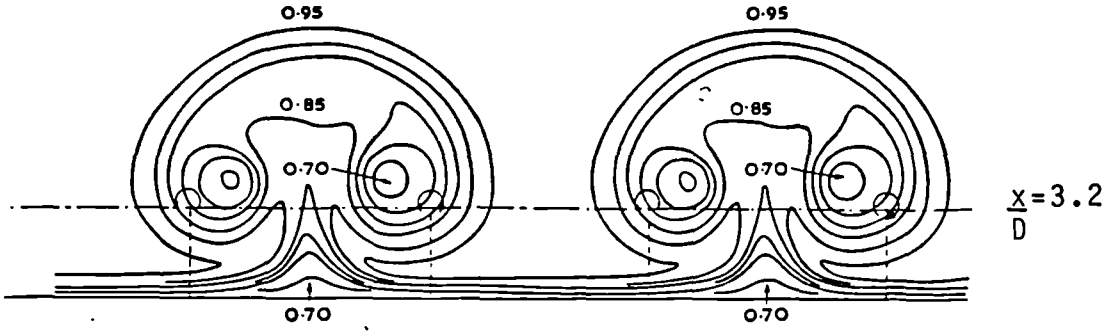

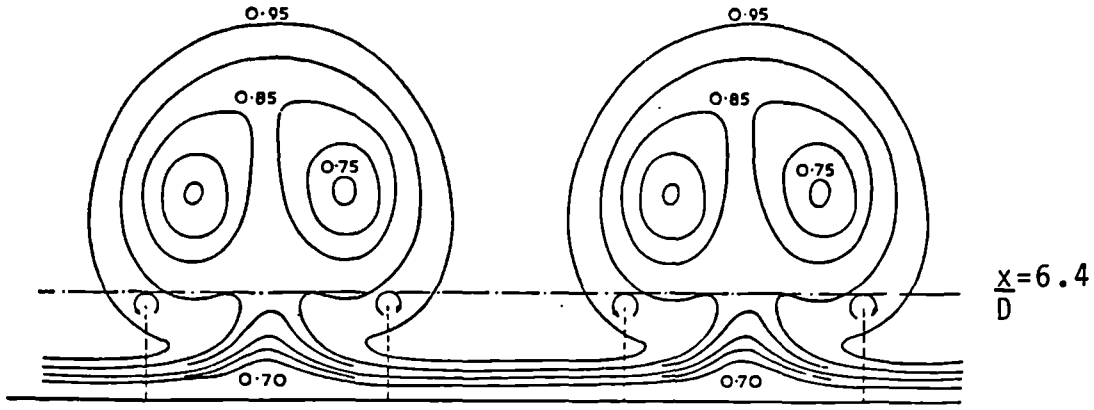

Figure 2.9 Contours of Total Head Loss for Counter- Rotating Vortices that are Initially Equally Spaced.

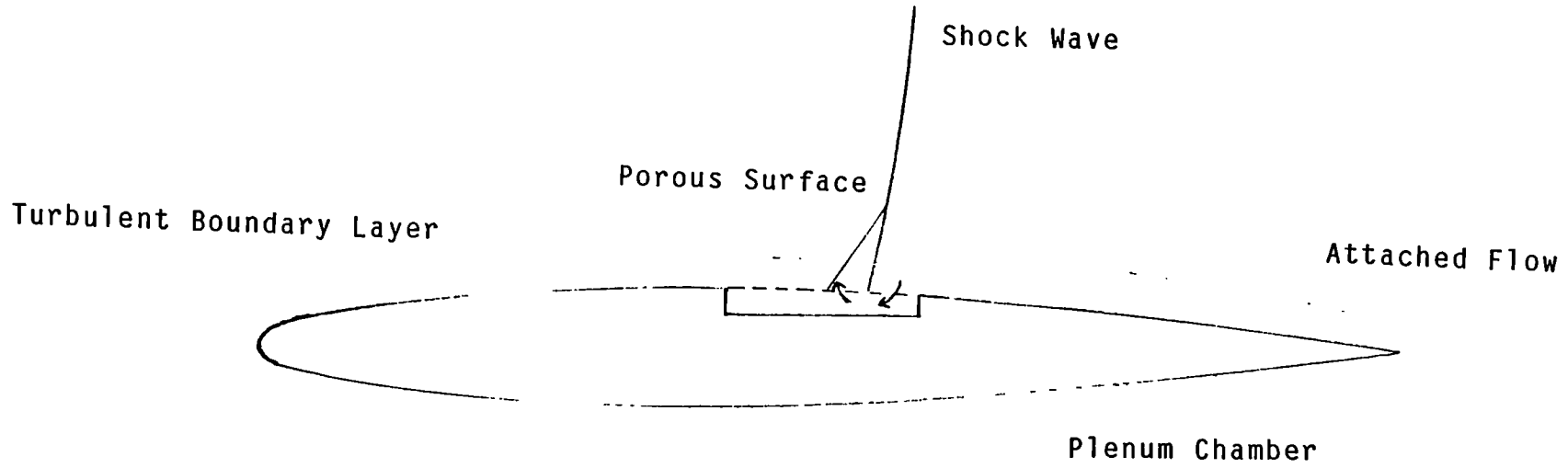

Porous surface creates recirculating airflow and increased communication across the shock wave

Figure 2.10 The Concept of a Porous Surface to Control Shock Induced Boundary Layer Separation

3.0 MODEL DESIGN AND EXPERIMENTAL SET UP.

In this chapter the criteria used for the design of the models is described. This includes the reasoning behind the choice of a half aerofoil and the design of the vane and air jet vortex generators. This is followed by a description of the experimental test facilities used in this work, including the water channel and the transonic wind tunnel. Finally the data acquisition methods are outlined.

3.1 Model Design Criteria

Previous work carried out on air jet vortex generators, by Wallis (2), and vane vortex generators, by Pearcey (1), made use of the half aerofoil or 'bump' technique. The main advantage of this technique is that for a given working section height, the test Reynolds number can be increased since a model with a larger chord can be used without significantly increasing the interference in the working section.

In chapter 2 the development of shock induced boundary layer separation over an aerofoil was described. The adverse effects of this separation on an aerofoil's performance were mentioned. The divergence of the trailing edge pressure and the pressure downstream of the shock, in addition to the pausing of the shock position, for increasing freestream Mach number (or incidence) were identified as indicators of the significant shock induced boundary layer separation. These features were also identified when significant shock induced boundary layer

separation was present on a bump (references 1 and 2). Also, some of the development work on vane vortex generators was carried using the bump technique. Since vane vortex generators are now successfully being used in practice on complete aerofoils it is reasonable to assume that the development work of air jet vortex generators on a bump model will also transfer successfully onto a complete aerofoil. For the reasons mentioned above, a bump model was used in this series of tests. A further advantage of the bump model in this series of tests is that the installation of the air supply for the air jets would be simplified.

Mounting the bump in the floor of the tunnel, however, meant that the boundary layer that develops ahead of the model must be removed so that the investigation can be carried out with a turbulent boundary layer of more realistic thickness. Details of the method used for sucking away the boundary layer ahead of the bump can be found in Appendix A. Another disadvantage of the bump technique is that the effect of increasing incidence cannot easily be investigated. This was overcome by using bumps with various thickness to chord ratios. Increasing the thickness to chord ratio of the bump has the effect of increasing the local Mach numbers and hence simulates an increase in incidence.

3.1.1 Design of the Half Aerofoil (Bump)

The shape of the bump was the same as that used by both Wallis (2) and Pearcey (1). This shape was obtained from a family of analytic aerofoil geometries developed by Tanner (12).

For this investigation three bumps of 8%, 10% and 14% thickness to chord ratio were used. The 8% bump was selected in order to repeat some of the work carried out by Wallis (2). The 10% and 14% bumps were designed to investigate the effect of increasing the local Mach number ahead of the shock. The extrapolation method used to predict the thickness to chord ratio required for a given maximum Mach number is detailed in Appendix F.

The floor of the wind tunnel was removed and replaced with the test rig which incorporated the bump (see Figure 3.1). Ahead of the bump a perforated liner was fitted above a plenum chamber, which in turn was connected to a low pressure source. This enabled the tunnel wall boundary layer to be partially removed so as to leave a thin turbulent layer, of more realistic thickness, near the leading edge of the bump (see Appendix A).

The bump had a chord of 304.8mm and spanned the working section of the wind tunnel (254mm). Test Reynolds numbers based on chord length were typically 5×10^6. Theoretical calculation carried out using VGK20 (18), assuming a complete aerofoil in free air with a Reynolds number based on chord of 5×10^6, gave a θ/C at 60% chord of 0.0016. A typical momentum thickness of the boundary layer ahead of the shock was measured on the bump at 60% chord and was found to give $\theta/C=0.0020$ (this gave a Reynolds number based on θ of $0.9X10^4$). Since the theoretical value of the momentum thickness is lower than the experimental value, it suggests that the suction ahead of the bump may not have been totally effective in removing the boundary layer. Based on simple turbulent boundary layer calculations (i.e.

$\theta/C \propto 1/R^{0.2}$) it is reasonable to assume that the effective Reynolds number based on chord was around 3×10^6.

3.1.2 Vane Vortex Generator Design.

To establish a datum against which to measure the effectiveness of air jet vortex generators, a set of co-rotating vane vortex generators was designed. The size and position of these vanes was found using the guidelines laid down by Pearcey (1). In his report Pearcey showed that the spacing (D) of co-rotating vortex generators is the single most important parameter and suggested that for optimum design the ratio of spacing to the height (h) of the vane must be greater than four and less than ten. The guidelines also recommend that the height of the vanes should be approximately 1% of the chord of the aerofoil and the vane length (l) should be four time the height. The criteria for selecting the chordwise position of the vane vortex generators was that the generators should always be in a region of attached flow and should be just upstream of the point where separation would occur without the boundary layer control.

Figure 3.2 shows the arrangement of the vane vortex generators used in this investigation. Using Pearcey's guidelines, the height (h) of the vanes was 3.05mm which resulted in a required length (l) of 12.2mm. The spacing of the vanes was 25.4mm giving a D/h ratio of 8.3. All vanes were set at an incidence of 20 degrees.

In order to establish the chordwise position of the vanes, preliminary tests on the bump were carried out with no

vortex generators. This showed that shock induced separation was only evident for shock positions downstream of 45% chord. Thus a chordwise position of 35% was selected for the vortex generators.

To incorporate the vane vortex generators into the existing bump a section was removed and replaced by a perspex insert, as shown in Figure 3.3. The insert contained nine cylindrical plugs of 20mm diameter and 25.4mm apart. The plugs were interchangeable, either containing vane vortex generators, smooth surfaces or as will be explained later, air jets. Once fitted into the perspex insert, the plugs could be rotated and locked at any angle, setting the vanes at the required incidence to the freestream.

3.1.3 Air Jet Vortex Generator Design

In order to repeat some of Wallis' (2) work a set of air jet vortex generators with round exits was designed. The criteria used to determine the diameter (d) and the inclination (Ø) of the jet exits were scaled from Wallis' (2) preliminary studies. A diameter of 3.81mm and an inclination of 45 degrees was used for this set of generators (see Figure 3.4). Cylindrical plugs, similar to those used for the vane vortex generators, were used to house a set of air jet vortex generators with round jet exits.

The work carried out by Freestone (3), on air jet vortex generators, showed that a significant increase in vortex strength and persistency could be achieved by using a rectangular rather than round jet exits.

In order to investigate the effect of exit shape, size and inclination, three sets of air jet vortex generators with rectangular exits were designed and constructed.

(i) A set of 'small' air jet vortex generators with a length (l) of 7.62mm and a width (w) of 1.59mm were selected as these gave approximately the same cross sectional area of jet as the round jet exits mentioned above (see Figure 3.5). Hence for similar blowing pressures, comparisons could be made for roughly equal mass flow rates. The jet inclination (Ø) was 30 degrees.

(ii) To investigate the effect of jet inclination a second set of 'small' air jets was constructed with the inclination increased from 30 degrees to 45 degrees (see Figure 3.5).

(iii) To investigate the effect of increasing jet aspect ratio, a set of 'large' rectangular air jet vortex generators were manufactured, see Figure 3.6. These were of the same width as the 'small' jets, and the length was increased to 12.7mm. The jet inclination was again 30 degrees.

3.2 Experimental Facilities

This section describes the experimental test facilities that were used in this investigation. This includes a description of the water channel and the transonic wind tunnel facility.

3.2.1 Water Channel

In order to investigate the way the freestream and the jet flows interact to form a vortex, a flow visualisation in the water channel at City University was carried out. A single jet was mounted in a test rig which was attached to the sidewall of the channel (as shown in Figure 3.7).The model was manufactured from perspex and was designed to enable the various jet exit shapes and direction to be tested. A plenum chamber, used to supply the jet exits, was fed by an external water supply. The 'blowing' pressure of the jet was adjusted by varying the head of water. To observe the interaction between the mainstream and the jet, a coloured dye (Potassium Permanganate) was used. The dye could either be introduced via the jet or through a series of small holes upstream of the jet exit.

The water channel in which the flow visualisation model was immersed was 15m long 0.5m deep and 0.3m wide and was configured to give a flow speed of 1m/s. Jet exit lengths between 0.05m and 0.1m were investigated.

3.2.2 Transonic Wind Tunnel

The wind tunnel used for the investigation discussed in this thesis was the T5 transonic facility at City University. This is an intermittent wind tunnel with run time of approximately ten seconds. It has a closed return circuit, and is driven by four wall jets located downstream of the working section. These wall jets are fed from a controlled compressed air system. The excess air in the circuit is vented into the laboratory and the working

section stagnation pressure and temperature remain almost constant and are approximately equal to those of the ambient atmosphere.

The working section is 760mm long and 254mm wide and the working section height increases linearly from 190mm to 206mm over its useful length of 610mm. Figure 3.8 shows a diagrammatic representation of the T5 wind tunnel.

The roof and floor of the wind tunnel may either be fitted with slotted walls with an open area ratio of 12% for transonic flow (M=0.6 to 1.1), or with solid contoured walls for supersonic flow (M=1.5). The side walls are fitted with circular windows of 228mm diameter and they may be positioned to enable observation of either the fore or aft area of the working section. Further details of the wind tunnel can be found in reference 11.

3.2.3 Choice of Wind Tunnel Liner

For this series of tests the model incorporating the bump was mounted in the floor of the tunnel. The roof of the tunnel was fitted with one of the slotted liners normally used for transonic testing (see Figure 3.9) and tests were carried out with no vortex generators fitted to the bump. Early results showed that the extent of the shock induced boundary layer separation was not as severe as that observed on the tests carried out by Wallis (2). The main reason for the difference in the results was attributed to the fact that Wallis had used a solid liner above the half aerofoil model. Appendix C discusses these differences and shows that more comparable results were achieved when the

slots were sealed and the tests carried out with a solid liner.

The investigation into the extent of the shock induced boundary layer separation was continued with the sealed liner. The results showed that sealing the liner led to a significant increase in the severity of the shock induced separation. Although the results were still not identical to those of Wallis, they were judged to be an adequate test for the air jet vortex generators.

3.2.4 Air Supply for Air Jet Vortex Generators

An objective of this research project was to investigate the effect of blowing pressure and to do this an external high pressure air supply was required. A high pressure supply which had a maximum controlled delivery pressure of 550KPa (gauge) was used.

The flexible hose from the high pressure supply was connected to an access port of 12.5mm diameter on the T5 facility. This was in turn connected to a plenum chamber which supplied the individual air jets via nine flexible hoses of 12.5mm diameter. Figure 3.10 shows a sketch of this set up.

This system was used to supply the air for the tests carried out on the 8% thick bump. During the investigation several inadequacies were found in the design of the blowing system, most important of which was that the blowing pressure was not the same at each exit. This variation in blowing pressure was probably associated with

the fact that the lengths of the individual feed pipes from the plenum chamber to the jet exits were not all the same. Also some of the feed tubes tended to kink and become partially blocked. To overcome this problem a new plenum chamber was designed which would give a more even pressure distribution for the jet exits. Figure 3.11 shows a sketch of the new plenum chamber. Tests on the 8% bump were repeated and the system was also used successfully in the tests carried out on the 10% and 14% thick 'bumps'.

In order to measure the blowing pressure of the air jet vortex generators a differential pressure transducer, with a range of 172KPa, was connected via a pressure tapping to the plenum box.

3.3 Wind Tunnel Data Acquisition.

The various data acquisition methods used in this investigation are described in this section. Also, the computerised pressure recording system developed for this investigation is described.

3.3.1 Chordwise Pressure Tappings

Approximately 36 brass pressure tappings of 1.0mm internal diameter were fitted along the centre line of each bump. Appendices B.1, B.2 and B.3 show the chordwise positions for the tappings on the 8%, 10% and 14% bumps respectively.

3.3.2 Boundary Layer Rake

The boundary layer investigation was carried out on the 14% bump. A boundary layer rake (see figure 3.12) was used to measure the local velocity profile close to the bump surface, and this was positioned at 60% chord. The rake was designed to minimise its effect on the flow over the model. The bump was manufactured with a flush fitting metal insert which held the rake. The rake could be securely fixed into one of four spanwise locations enabling boundary layer profiles to be measured from the centre line of one vortex generator towards the adjacent generator in 6.35mm intervals. Figure 3.13 shows a diagrammatic representation of the apparatus.

3.3.3 Schlieren Photography

Schlieren photography was used to observe the shock boundary layer interaction as well as the vortices produced by the various generators.

The sidewalls of the T5 wind tunnel were fitted with circular windows of 228mm diameter. The windows could be positioned to observe either the forward or rear section of the bump. The schlieren investigation was carried out with a continuous light source, and the knife edge was set parallel to the floor. The image was focused onto a Polaroid camera using 400ASA film. Details of the interpretation of the schlieren photographs can be found in Appendix D.

3.3.4 Computerised Pressure Recording System.

The pressure recording device available on the T5 wind tunnel at the start of this experimental investigation was a bank of mercury manometers which were clamped once the desired steady state conditions were reached. The individual pressures were then recorded by hand and analysed later.

It was decided at an early stage in this project to remove the bank of mercury manometers and replace it with a computerised system employing an electrical pressure transducer linked to a 48 port pressure scanning switch (Scanivalve model D, hereafter called scanivalve). A schematic diagram of the system is shown in Figure 3.14. It is described in a logical order, beginning at the model end of the system.

From each pressure tapping on the model a continuous plastic tube leads to a clamping mechanism which is used to seal off all tubes simultaneously. The distance between the pressure tapping and the clamping mechanism is minimised to reduce the response time of the system.

Beyond the clamp each tube is connected to a small reservoir. The reservoir is intended to alleviate the effects of clamping the tube, which would otherwise increase the pressure in the sealed part of the duct. Similarly the scanivalve connects a small volume of air (at arbitrary pressure) to each reservoir in turn. If this small volume is tiny by comparison with the reservoir volume then the pressure after connection is negligibly

different from the unconnected reservoir pressure. Each reservoir is in turn connected to a port on a scanivalve multiport connector. The scanivalve incorporates a Druck PDCR 22/35L pressure transducer which has a differential range of 104kPa (15psi). On command from the micro computer a voltage is recorded. The scanivalve is then stepped to connect the next port and the next value is recorded. All the pressure readings are taken as difference from atmosphere since one end of the transducer is left open to the atmosphere.

The pressure transducer is powered by a 5v bridge supply. The output of the transducer is then amplified by a Fylde FE254 GA amplifier adjusted so as to give an output range of 0 to 1.0 volts corresponding to a pressure range of approximately 0 to 100kPa below atmosphere. Calibration of the transducer was carried out using a mercury manometer and the results showed a linear variation to within $\pm$0.25% over the required range of pressures. The mercury manometer used for the calibration could be read to within $\pm$0.01inHg.

The amplified output is input to a 12 bit analog to digital converter (OASIS MADC 12, see reference 14), which can yield an accuracy of 0.3mV. In terms of pressure this is an error of $\pm$ 28 Pa or $\pm$ 0.004inHg which compares with an accuracy of about $\pm$ 0.1 inHg achieved with the mercury manometer bank. The data acquisition system showed excellent repeatability throughout the investigation.

When all forty eight ports connected to the scanivalve are scanned the voltages are recorded on floppy disk. The calibration factor together with the ambient pressure and temperature are also saved.

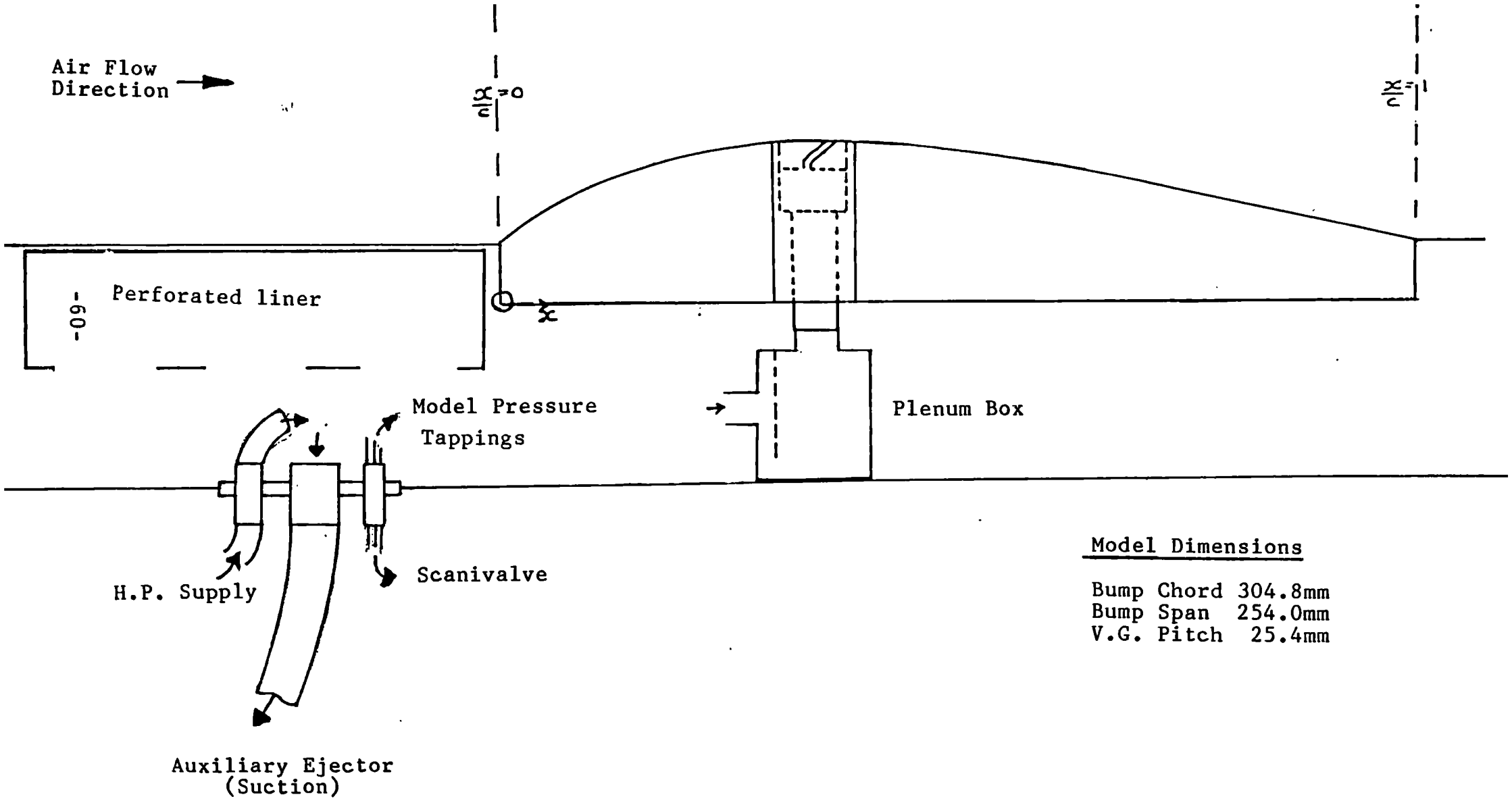

Figure 3.1 General Layout of Wind Tunnel Model

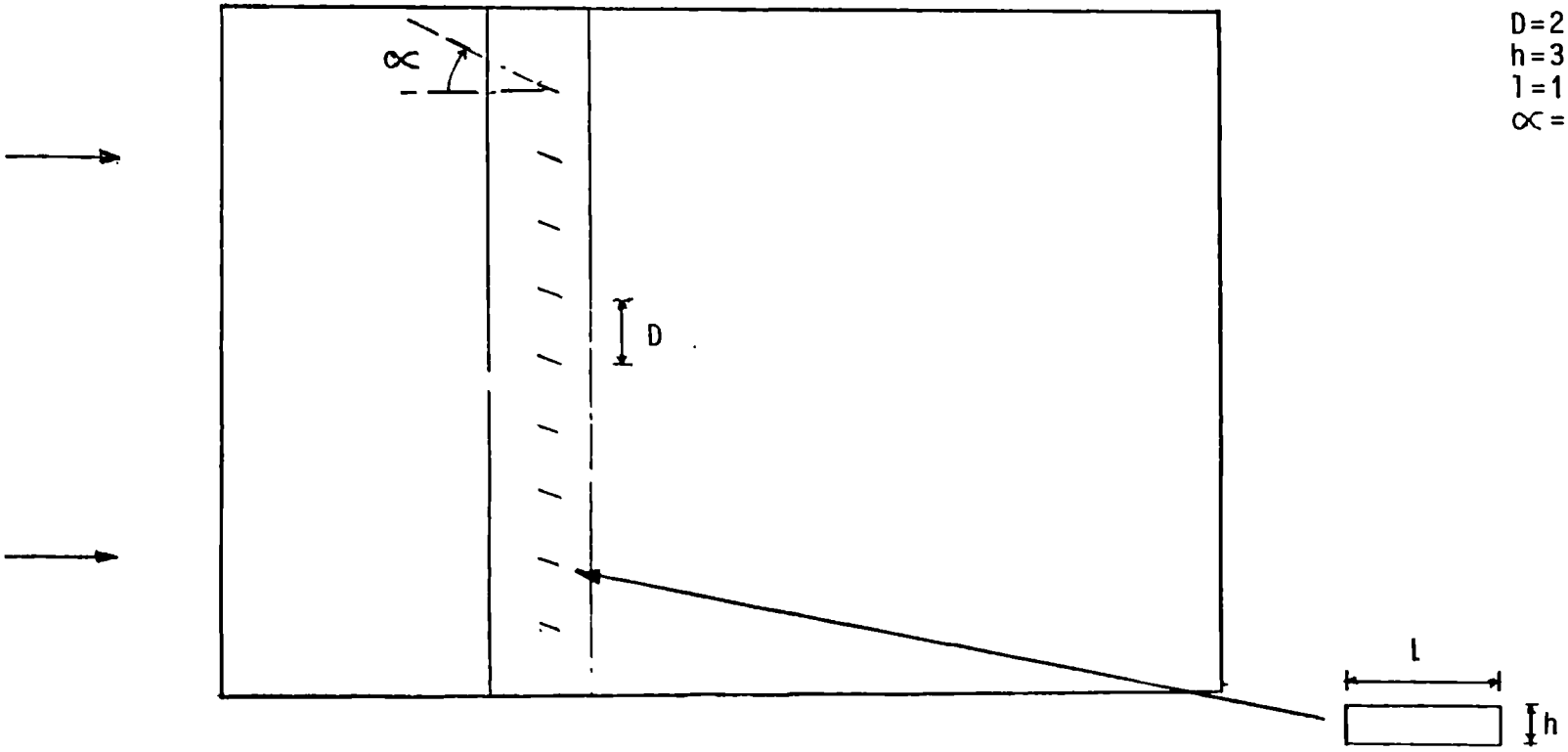

Figure 3.2 Vane Vortex Generator Layout

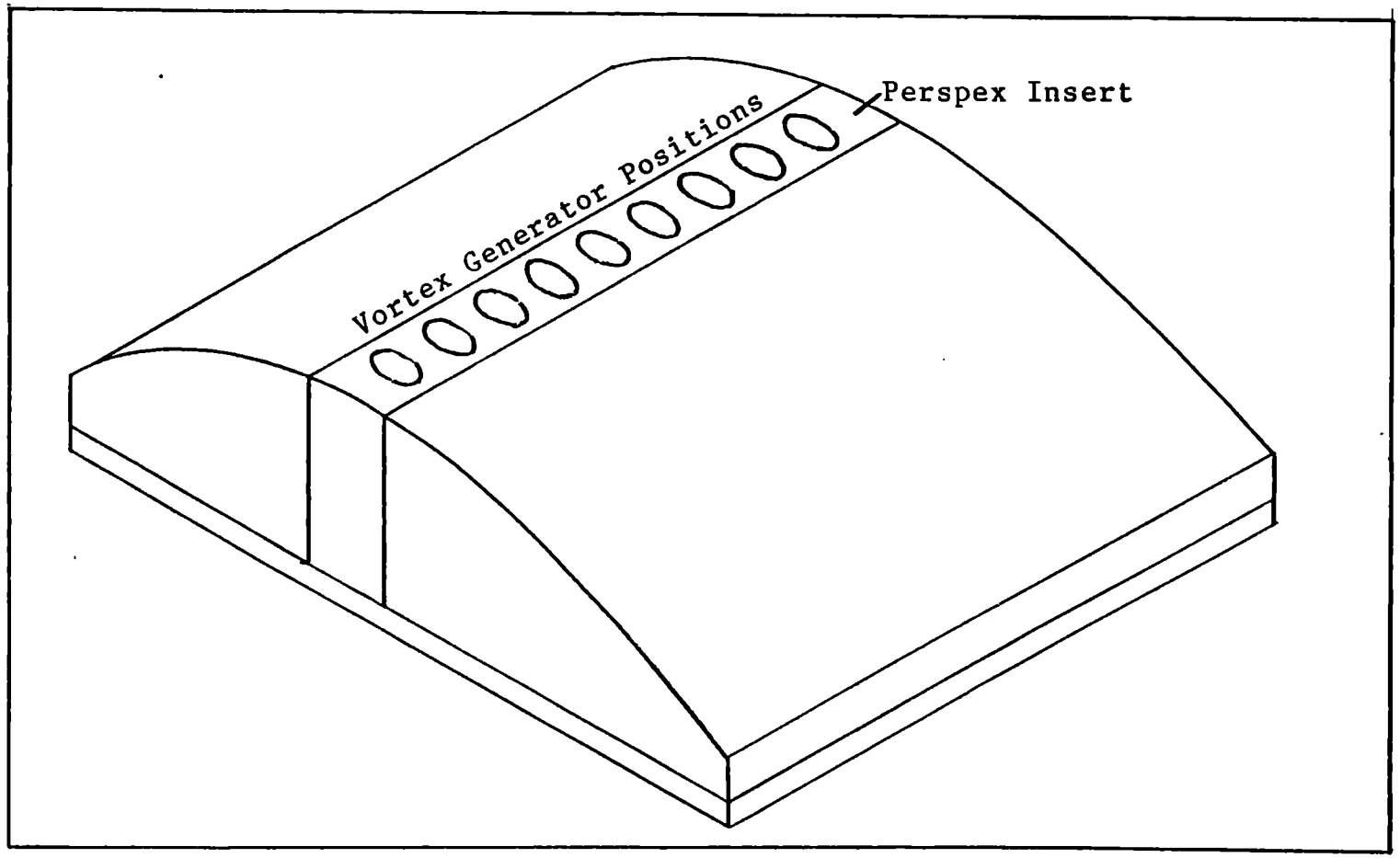

Figure 3.3 Diagrammatic Representation of a Half Aerofoil Model

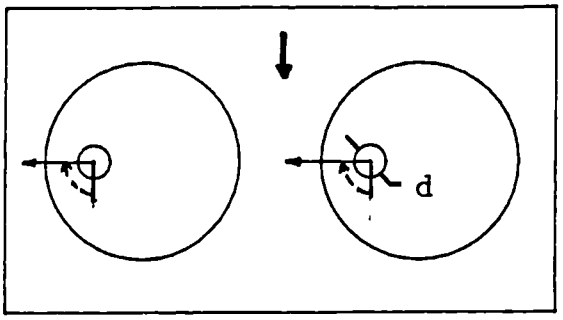

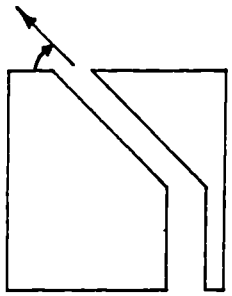

(a) Jet Direction: θ=90° Jet Inclination: ϕ=45°

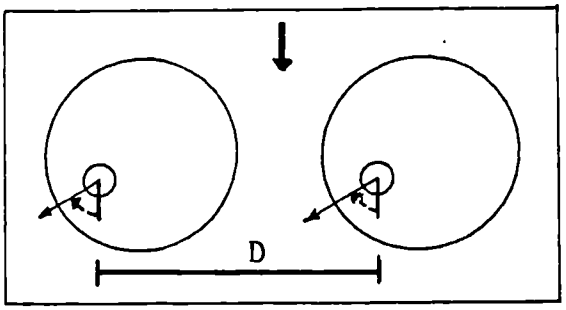

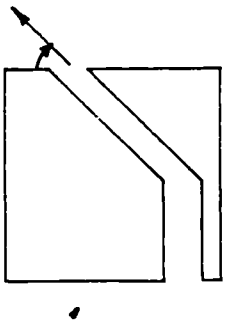

(b) Jet Direction: θ=60° Jet Inclination: ϕ=45°

Figure 3.4 Air Jet Vortex Generators with Round Exits

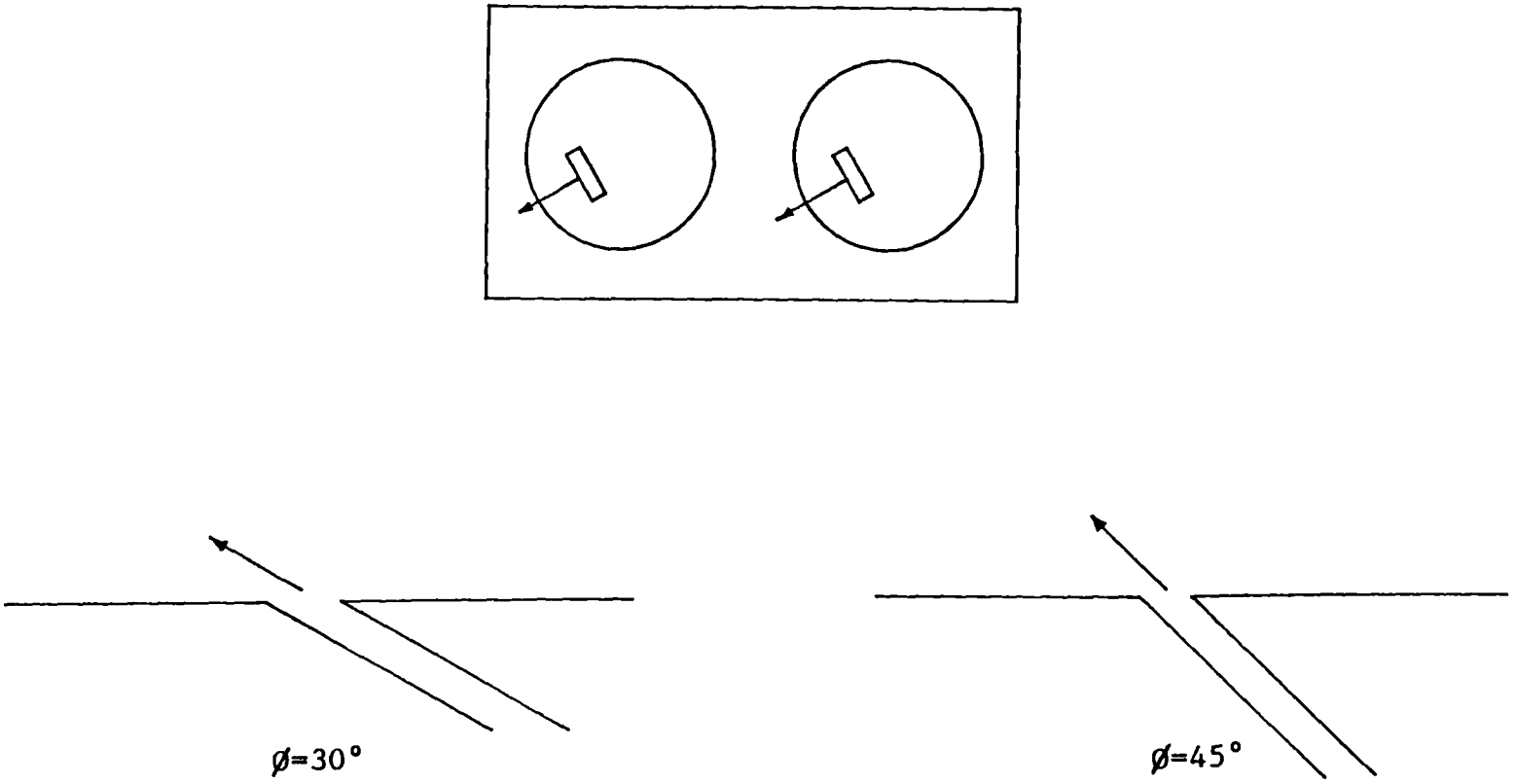

Figure 3.5 Comparison Between Small Jet Exits (0=30° and 0=45°)

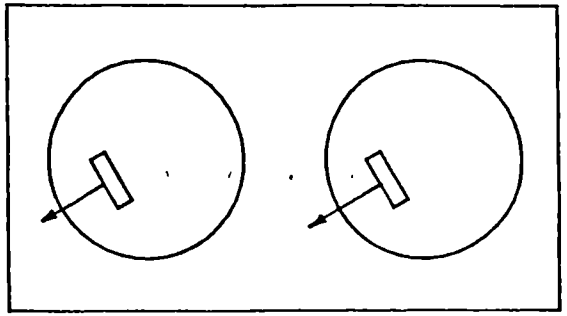

Small Exits

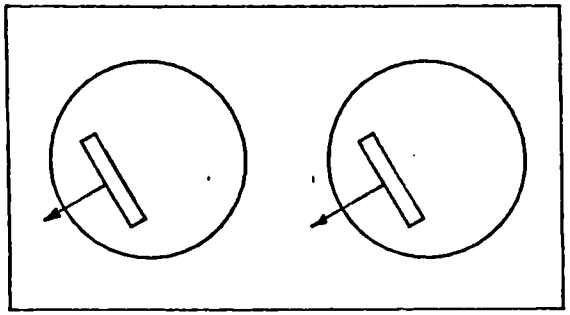

Large Exits

Figure 3.6 Comparison Between Large and Small Jet Exits

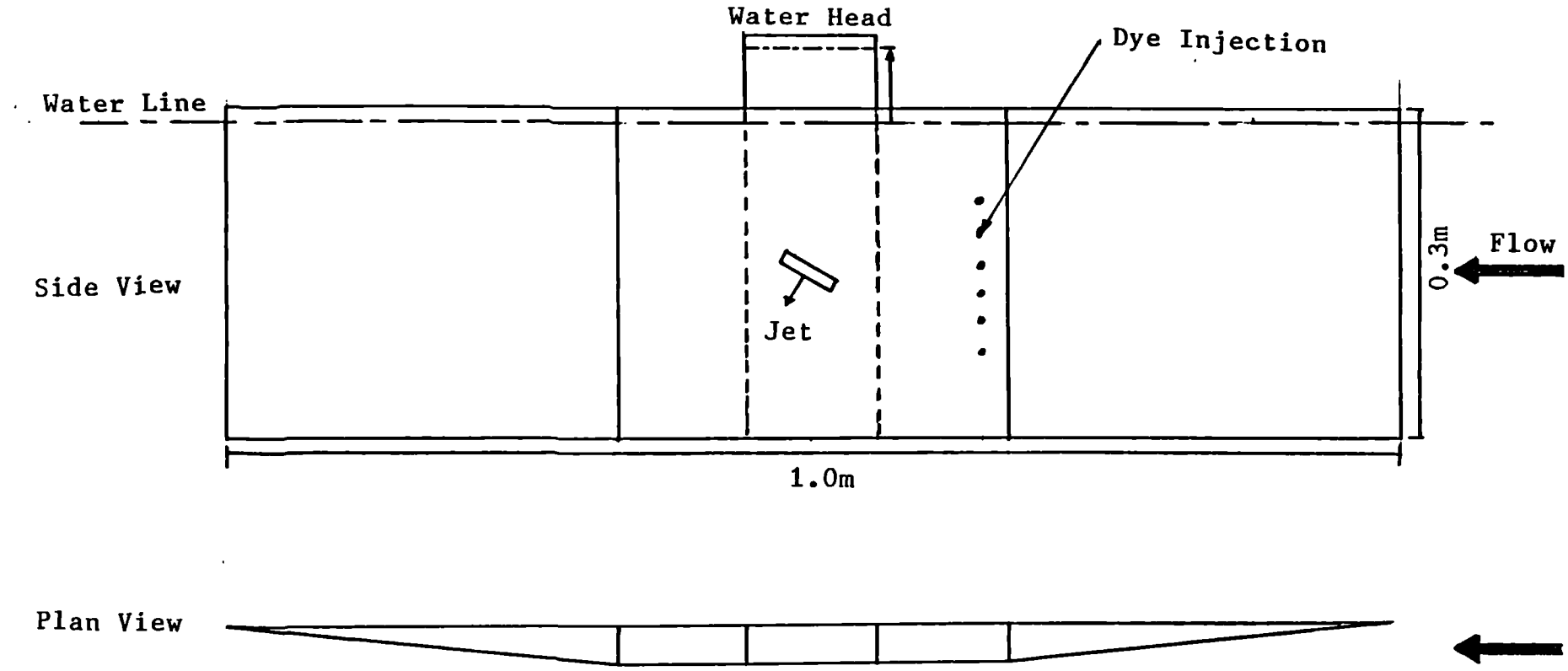

Figure 3.7 Schematic Diagram of Water Tunnel Model

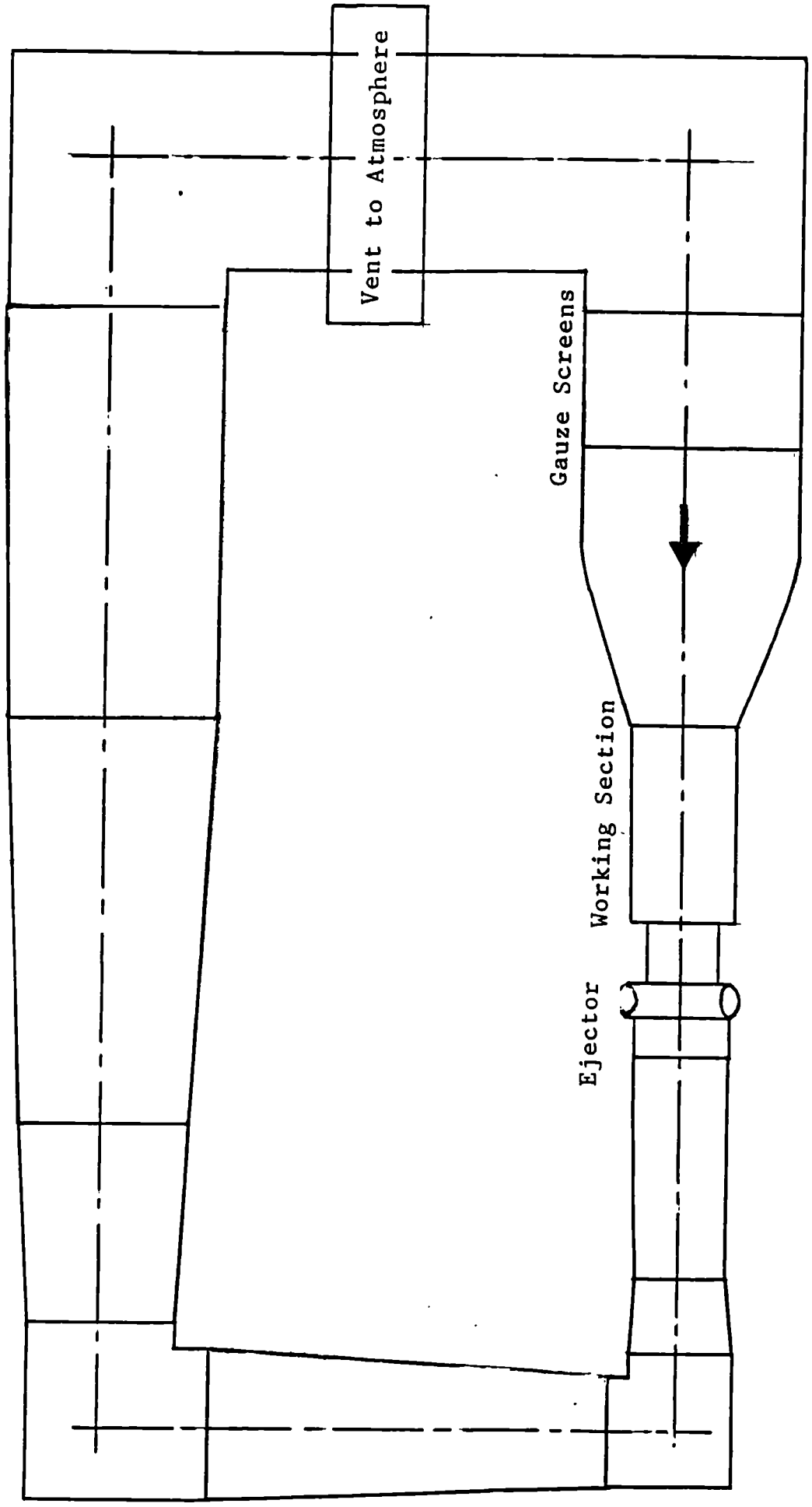

Figure 3.8 T5 Wind Tunnel Layout

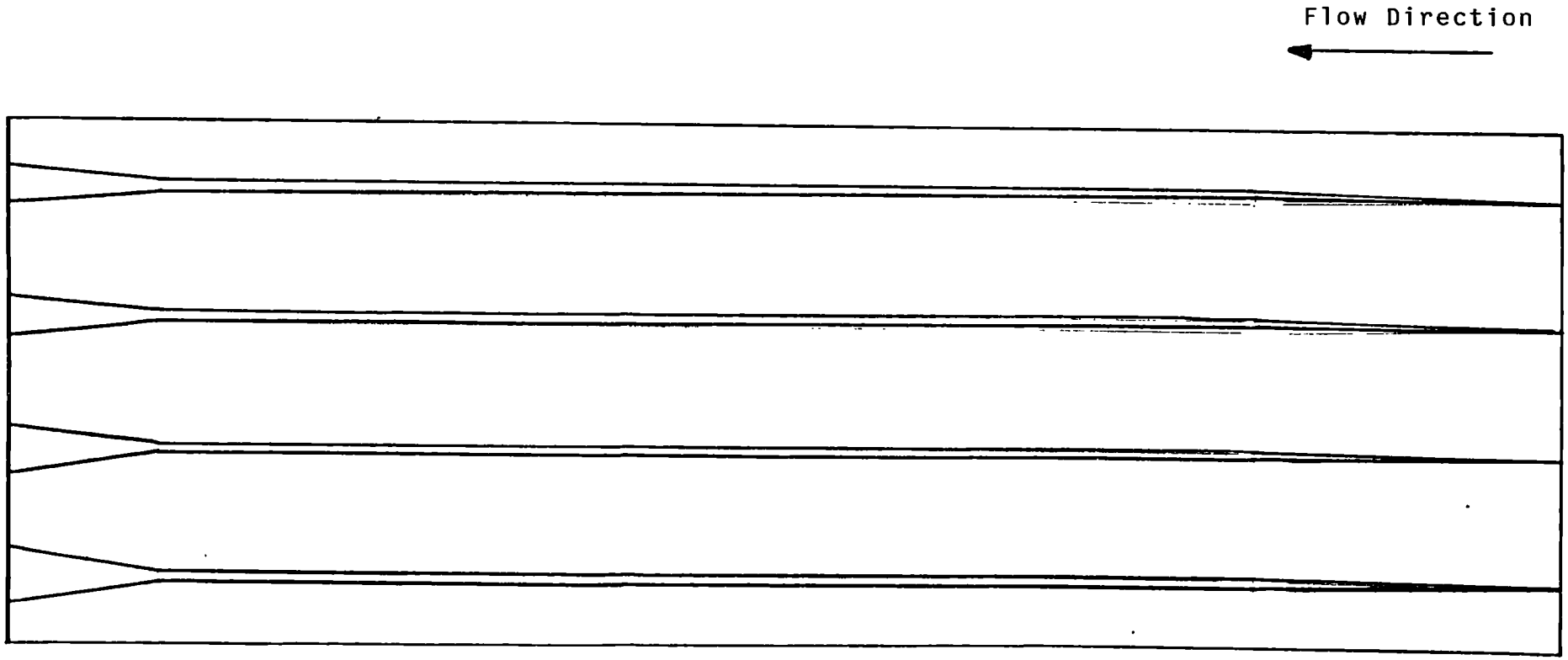

Figure 3.9 Diagrammatic Representation of the Slotted Liner

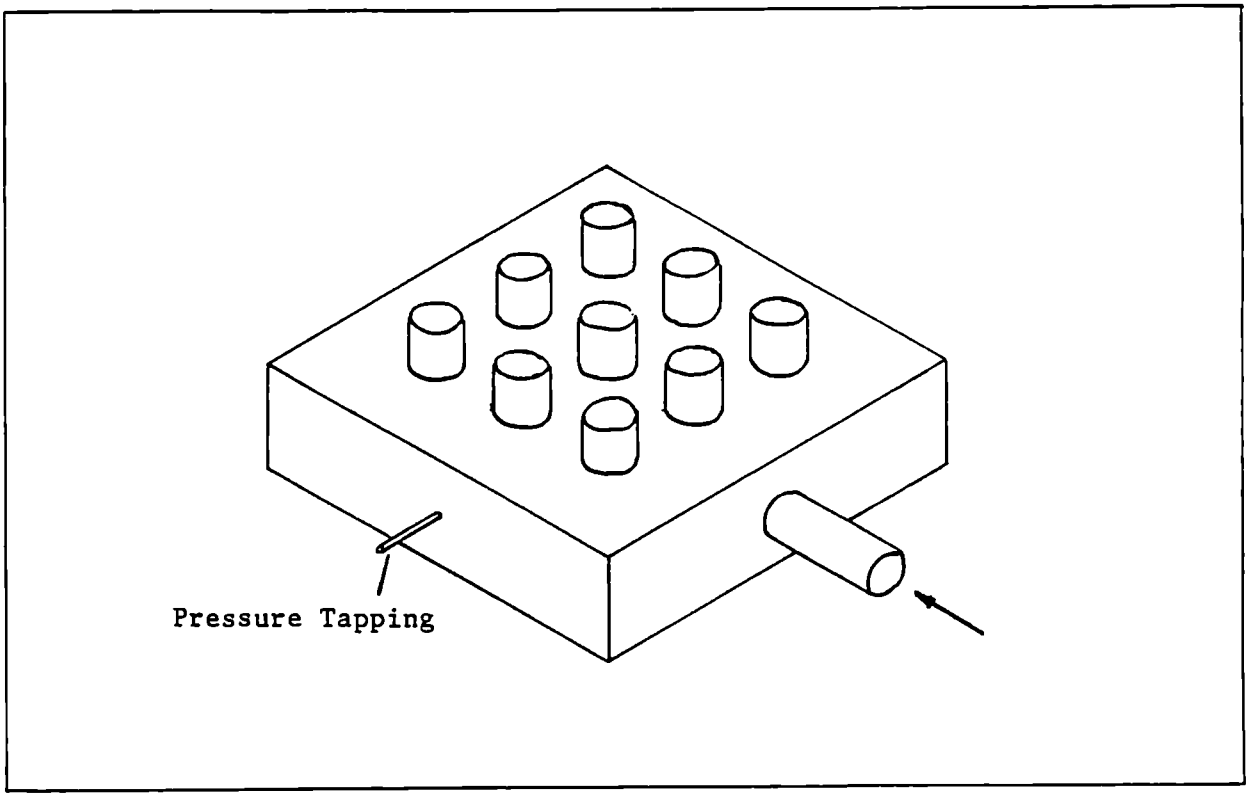

Figure 3.10 Sketch of First Plenum Chamber

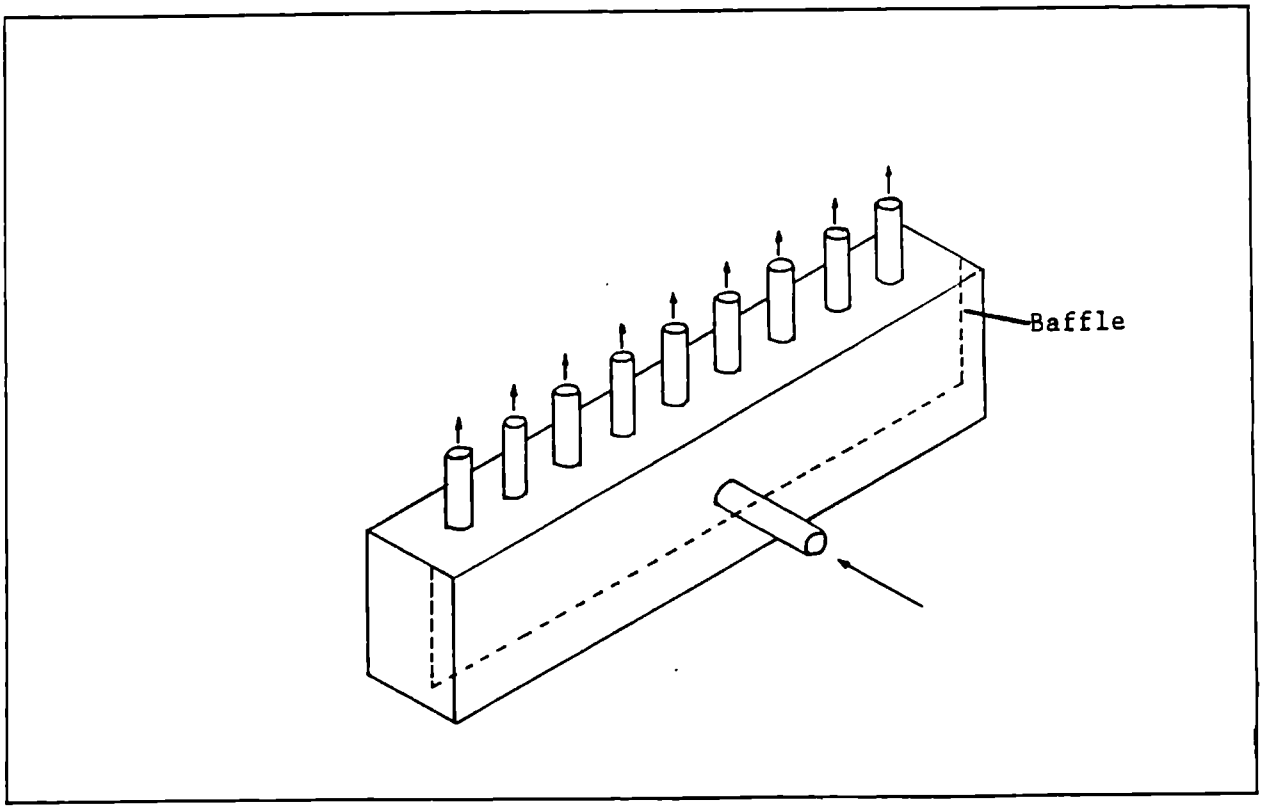

Figure 3.11 Sketch of Modified Plenum Chamber

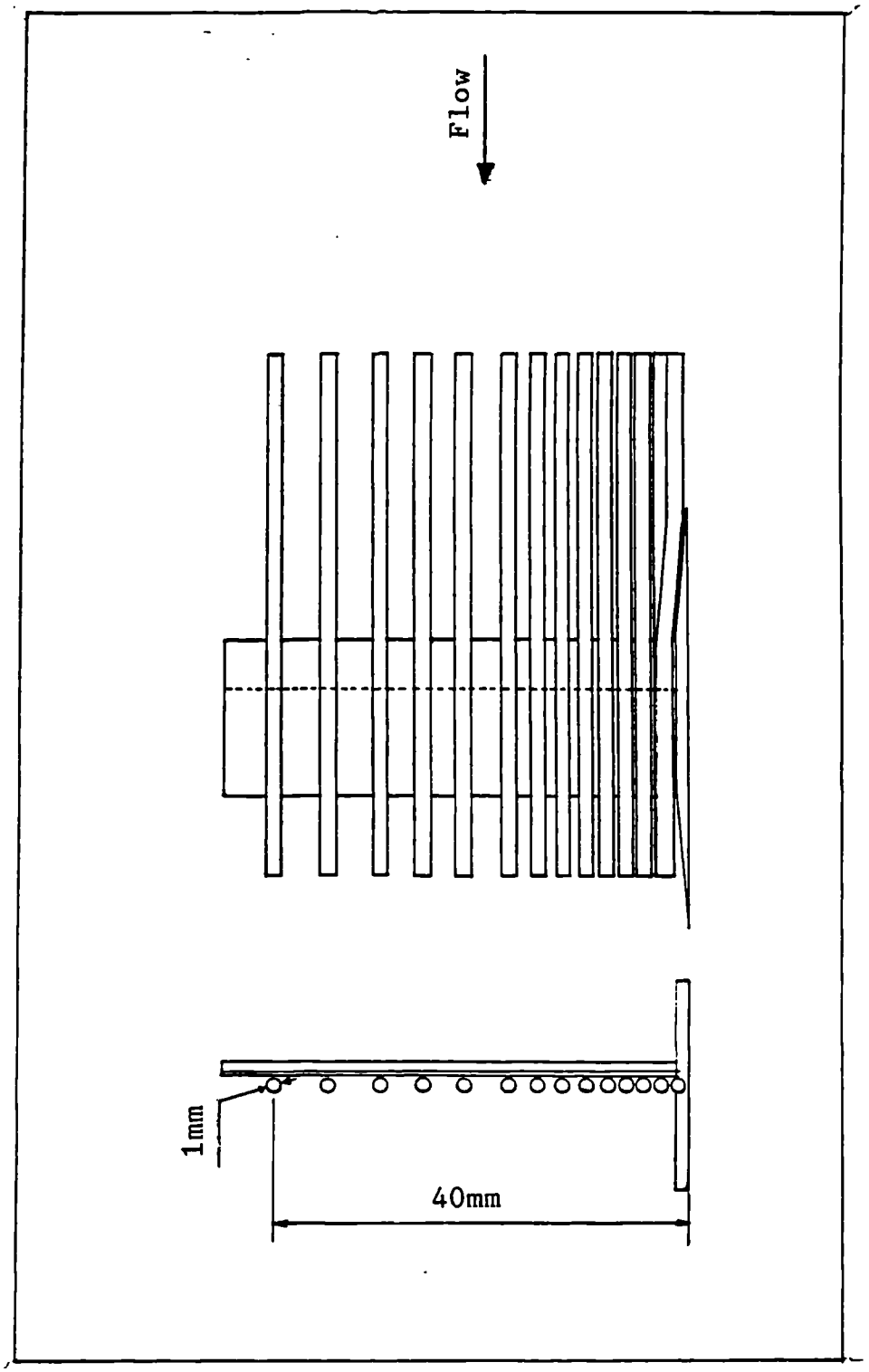

Figure 3.12 Diagrammatic Representation of the Boundary Layer Rake

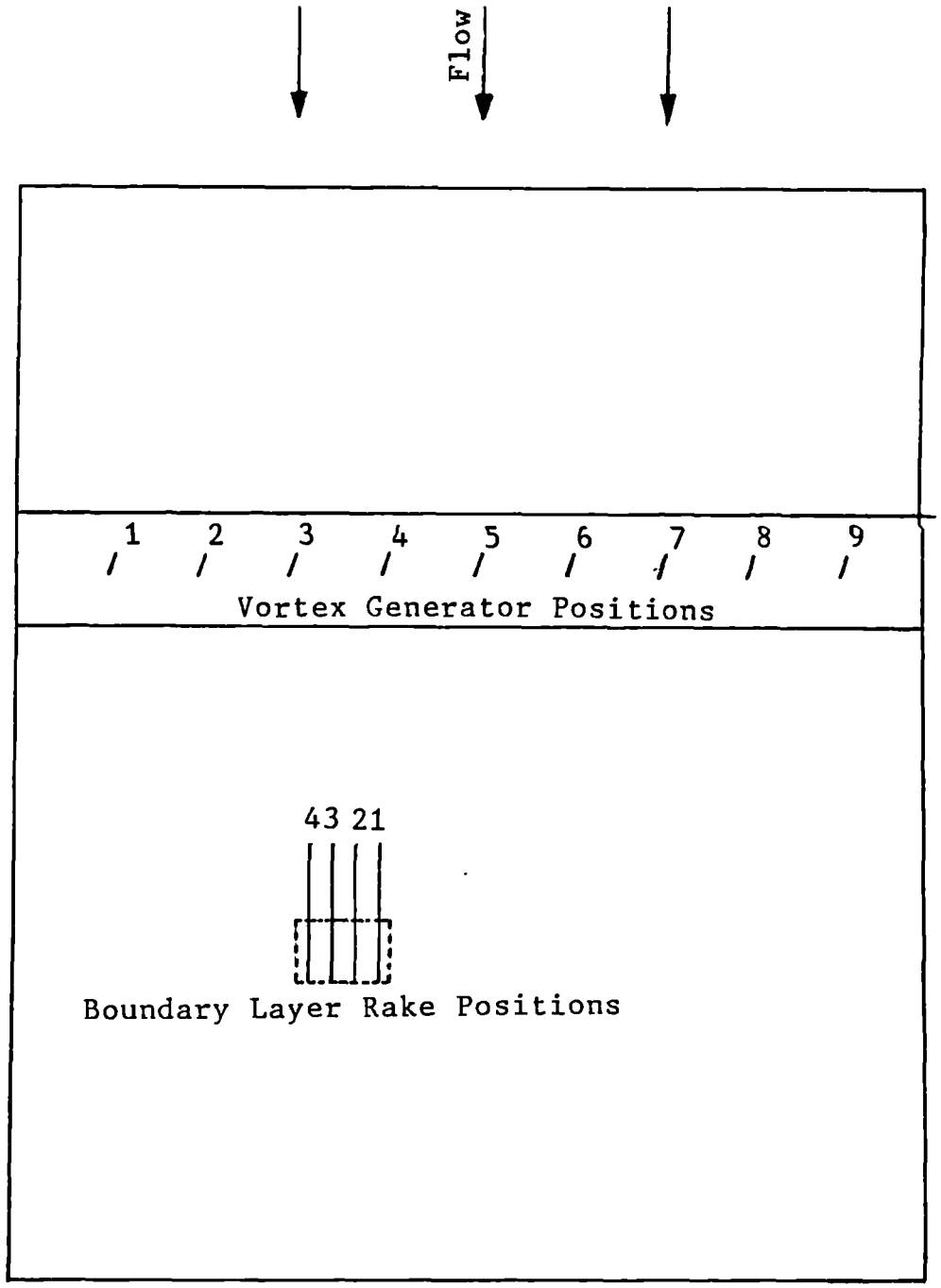

Figure 3.13 Model Arrangement for Boundary Layer Rake Investigation

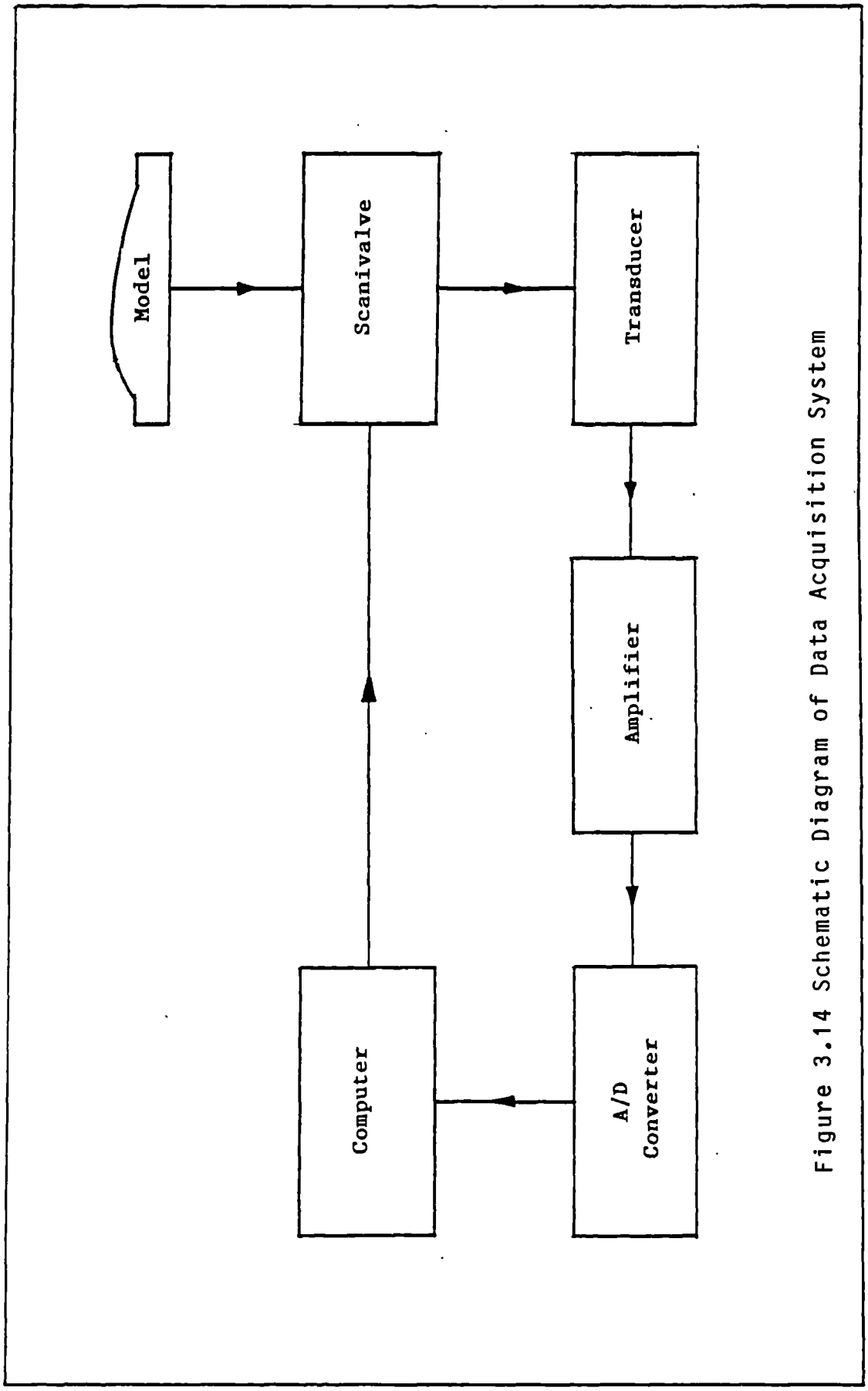

Figure 3.14 Schematic Diagram of Data Acquisition System

4.0 EXPERIMENTAL PROCEDURES

In this section the experimental procedure for the water channel and wind tunnel tests are described.

4.1 Water Channel Test

The water channel test rig was set up for the desired jet configuration and then immersed into the channel and secured to one of the sidewalls. The water channel was set to give a flow speed of 1m/s. The desired jet blowing pressure was achieved by adjusting the mass flow rate of the pipe feeding the plenum chamber.

Once steady conditions had been achieved the dye was introduced via the jet or through small holes just upstream of the jet. The resulting flow was observed from various angles.

4.2 Wind Tunnel Tests

The required set of cylinderical plugs, incorporating either a smooth surface or a vortex generator configuration, was installed in the perspex insert. The insert was then fitted into the bump. The sidewalls of the wind tunnel were secured with the windows in the aft position in order to use the schlieren to observe the flow over the rear half of the bump.

When air jet vortex generators were being investigated the desired blowing pressure was set using the pressure gauge on the high pressure control valve. The tests for all configurations were then carried out using the following procedure. The pressure at the downstream end of the model was varied to simulate increasing freestream Mach number to take the shock from its initial point of formation to the trailing edge. When steady conditions were achieved (typically after 8 seconds), the pressure tubing was clamped and the pressures were logged and analysed using the micro computer. At the time of clamping a schlieren photograph was generally taken.

During the boundary layer investigation the rake was securely fitted into one of the four positions between generator position 3 and 4. With the required vortex generator installed, the wind tunnel was operated as described above. The data was recorded using the micro computer and processed on-line to give the results in terms of the pressure coefficient C_{pb} (see Appendix G). Schlieren photographs were taken to ensure that the shock location was within acceptable limits when tests were repeated with the rake in another spanwise position. Accuracy to within 2% chord was achieved using this technique.

5.0 EXPERIMENTAL RESULTS

The experimental results obtained for this investigation are presented in this chapter. The results cover the observations from the water channel investigation and the data obtained from the three half aerofoil sections tested in the high speed wind tunnel. Also included are the results from the boundary layer investigation on the 14% thick bump. The presentation and method of analysis of the wind tunnel results is described in detail.

5.1 Observations from the Water Channel Investigation

In this section the observations from the water channel tests are described. This includes a hypothesis on the method of vortex formation and a description of the influence of the jet parameters on the characteristics of the resulting vortex.

Observations of the interaction between the mainstream and the jet flow are illustrated in Figure 5.1. It can be seen that the mainstream is diverted either side of the jet. Just downstream of the jet exit the mainstream flow which was initially diverted away from the direction of the jet flow is entrained towards it and passes beneath it, wrapping itself around the jet to form a vortex.

During the course of this flow visualization investigation the influence of the jet direction, blowing pressure and exit length were investigated and the following observations were made.

(i) It was found that for a given jet configuration, a critical blowing pressure existed below which a vortex was not formed. The critical blowing pressure was found to decrease as

the jet direction was given a downstream component. Figure 5.2 shows qualitatively how the critical blowing pressure was found to vary with jet direction. Notice that as the direction of the jet is given a particular downstream component a minimum critical pressure is reached. Any further increase in the downstream component results in a rise in the critical blowing pressure. With the jet blown in the same direction as the mainstream ($\theta=0°$), a pair of counter-rotating vortices was formed.

(ii) For a given jet configuration any increase in blowing pressure, above the critical value, resulted in an increase in the helical flow speed near the vortex. This was interpreted as an increase in vortex strength.

(iii) The effect of increasing the jet length was investigated and it was observed that a vortex with a larger diameter was formed as a result of increasing the length of the jet exit. The diameter of the vortex is defined as the width of the observed helical flow.

5.2 Presentation and Method of Analysis of the Chordwise Pressure Distributions

The basic results for each configuration are a family of pressure distributions (P/Po vs x/c). Figures 5.3a and 5.3b show typical sets of pressure distributions both with and without vortex generators. For both cases the pressure upstream of the shock falls smoothly (local Mach number increases) until a plateau is reached where the pressure remains constant for any further decrease in trailing edge pressure. These upstream pressure distributions provided the locus of the shock upstream pressure P_1 (see Reference 15). The locus of the shock downstream pressure P_2 (see broken

lines) indicates one characteristic feature of shock induced boundary layer separation. This feature is the failure of P_2 to rise with the falling P_1 (see Figure 5.3b) but rather to fall instead in line with a near constant value of the ratio P_2/P_1 (see Figure 5.3a). This type of separation is defined as Type A shock induced separation (see Reference 4) with a separation bubble developing at the foot of the shock and extending rearwards to the trailing edge without causing or agrevating a second separation moving forward from the trailing edge (Type B). The growth of the bubble is indicated by the progressive flattening of the downstream pressure recovery from the shock rearwards, while the shock is held in a fixed position. This feature is referred to as "shock pause".

The addition of vortex generators has a significant effect on the pressure distributions. Comparing Figure 5.3a with 5.3b it can be seen that pressure rises through the shock and downstream to the trailing edge are much greater when vortex generators are used. As will be seen from the pressure distributions, there is some ambiguity in the position of the P_2 locus. This reflects the alternative definitions given in the Notations.

The difference between these can be illustrated by reference to Figures 5.7 and 5.11 respectively. In the first, for a plane bump, the P_2 locus drawn represents the pressure immediately downstream of the shock itself, at first in the absence of separation and later, from the third curve onwards, in the presence of separation. For these later curves, the shock in question is the forward oblique leg with separation occurring at its foot. P_2 then corresponds approximately to the pressure at separation.

In Figure 5.11, for the bump with vane vortex generators, the P_2 locus is drawn according to the second definition because the rapid pressure rise continues through the localised re-attachment. For this example, the re-attachment remains confined within the chord of the model allowing this definition of P_2 to be used throughout.

Returning to Figure 5.3, we see that for 5.3a the first definition seems appropriate for the whole range of shock positions, whereas the second seems more appropriate in 5.3b, but for the earlier shock positions only.

Again in Figure 5.15, the second definition can be used for the first two curves, but it is then necessary to switch to the first definition because re-attachment is no longer localised. This discontinuity between the two branches gives us an idea of the pressure rise achieved through the re-attachment region itself. It is clear that a less ambiguous method is required for assessing the effectiveness of vortex generators and the method used is described below.

The effects of separation and the effectiveness of vortex generators is obtained from the second type of graph presented here in Figure 5.5. These are plots of shock position against trailing edge pressure and the advantage of assessing the results in this way is that a knowledge of the freestream Mach number is not required. This is of particular importance in this series of tests because the flow through the working section was choked and hence the freestream Mach number could not be determined.

This assessment results from the following considerations. For a given bump consider the flow with and without shock induced boundary layer separation. The pressure distributions over the

bump are presented for attached and separated flows in Figures 5.4 A to C. For constant shock position the pressure distributions show that the effect of separation is to given a reduced pressure recovery to the trailing edge. For constant trailing edge pressure the shock position of the attached flow is further downstream. Finally for constant Mach number, separation effects both shock position and trailing edge pressure. The fourth graph presented in Figure 5.4 shows the loci of the shock position versus the trailing edge pressure. In the absence of separation the shock would move progressively downstream as indicated by curve 1. Separation greatly reduces the pressure recovery through the shock and leads to curve 2. When comparing curves 1 and 2 the comparison for fixed shock position is between A1 and A2 and B1 and B2 compares fixed trailing edge pressure. When comparing fixed Mach number the comparison is between the points C1 and C2. More importantly, points A1, B1 and C1 lie on curve 1 and points A2, B2 and C2 lie on curve 2. Hence, even when the freestream Mach number is not known the effects of separation can still be determined since the comparison is between curves 1 and 2 rather than points C1 and C2.

In this way Figure 5.5 summarises the comparison between the results with vane type generators and those without generators. It the absence of generators there was a shock pause from $P/Po_{(TE)}$ of 0.75 to 0.6, not present when generators were used. A slight decrease in the rate of shock movement occurs in the latter case for $P/Po_{(TE)}$ less than 0.6 and probably corresponds to the situation where the shock has moved out of the most effective range of the influence of the generators. The most effective range would therefore be for $P/Po_{(TE)}$ from about 0.75 to 0.6. It should be emphasised that, even beyond this range, the extent of the separation that does develop is very much less than in the absence of generators.

The effects of shock induced separation can also be seen in the schlieren photographs. Figure 5.6a and 5.6b show examples of schlieren photographs with and without shock induced separation. In Figure 5.6a the boundary layer (dark band above the surface) has separated just aft of the shock and has remained separated right down to the trailing edge. Figure 5.6b shows that the effect of the vortex generators is to reduce separation and the small bifurcated foot of the shock indicates that the separation is now very localised. The schlieren image of a vortex appears as a pale and dark band above the boundary layer and the diameter of the vortex is defined as the width of these bands. More detailed information on the schlieren set up and interpretation of the photographs can be found in Appendix D.

Table 5.1 shows the various configurations investigated in this thesis. Figure numbers for the pressure distributions and the shock loci for the individual cases are shown. Table 5.2 shows the configurations for which schlieren pictures were taken and the figure numbers where they can be found.

5.3 Presentation and Method of Analysis of the Boundary Layer Results

The boundary layer investigation was carried out on the 14% bump. Details of the experiment can be found in section 3.5.

Boundary layer profiles for each shock position and vortex generator configuration are presented as a set of four profiles. Position (a) refers to the location behind the centre line of generator 4 and positions (b), (c) and (d) are spaced at 6.35mm ($\frac{1}{4}$ inch) intervals towards generator 3 (see

Figure 3.13). A schlieren photograph is included to help illustrate the flow conditions.

The profiles are presented as a non-dimensional pressure coefficient (C_{pb}) versus height (Y) normal to the surface. The derivation of C_{pb} can be found in Appendix G and the height Y is plotted in millimetres. The shape of the profile indicates the condition of the boundary layer, with a fuller profile indicating attached flow, see Figure 5.67a. If there is separated flow in the boundary layer or the boundary layer is close to separation this means that the pitot rake method of measurement can no longer be interpreted reliably and correctly in terms of C_{pb}. However where the pitot pressure becomes close to static pressure (as C_{pb} tends to 0) at a significant distance from the surface it is safe to deduce the presence of separation, as in Figure 5.67b.

The presence of streamwise vortices embedded or partially embedded in the boundary has an influence on the pitot pressures measured. It is apparent from the vortices observed that there is large reduction in static pressure within the core and a significant drop in pitot pressure. The location of the greatest drop in pitot pressure gives an indication of the centre of the vortex core. (see Figure 5.67c). In principle the magnitude of the pitot pressure reduction and its vertical extent could be used to give an indication of maximum rotational speed and strength of the vortex, but a more thorough set of tests would be required than was carried out for this thesis. It is suffice to say that a more pronounced pressure drop can be associated with a vortex of increased strength. Another method of assessing the strength of the individual vortices would be to monitor the lateral displacement of the vortices as they translated downstream. This method of assessing vortex strength is based on the fact that a row of co-rotating vortices near a solid surface will

translate laterally across the flow under the influence of the reflections. Again, however, insufficient data is available from this series of tests to give any worthwhile comparisons of vortex strength.

The diameter of the vortex is defined as the width of the region of reduced pressure. This is consistent with the definition of vortex diameter put forward for the schlieren photographs and observed flows in the water channel tests.

The configurations for which boundary layer profiles were measured are shown in Table 5.3.

					Figure Numbers	
Configuration	Bump t/c	θ deg	Ø deg	Pb/Po	Press Dist	Shock loci
No V.G.'s	8%	-	-	-	5.7	5.10
No V.G.'s	10%	-	-	-	5.8	5.10
No V.G.'s	14%	-	-	-	5.9	5.10
Vanes	8%	-	-	-	5.11	5.14
Vanes	10%	-	-	-	5.12	5.14
Vanes	14%	-	-	-	5.13	5.14
Round Air Jet	8%	90	45	1.0	5.15	5.17
Round Air Jet	8%	60	45	1.0	5.16	5.17
Small Rec Jet	8%	60	30	1.0	5.18	5.19
Small Rec Jet	8%	60	30	1.2	-	5.19
Small Rec Jet	10%	60	30	1.2	5.20	5.22
Small Rec Jet	10%	60	30	1.6	5.21	5.22
Small Rec Jet	14%	60	30	1.2	5.23	5.25
Small Rec Jet	14%	60	30	1.6	5.24	5.25
Small Rec Jet	14%	60	45	1.2	5.26	5.28
Small Rec Jet	14%	60	45	1.6	5.27	5.28
Large Rec Jet	10%	60	30	1.0	5.29	5.32
Large Rec Jet	10%	60	30	1.2	5.30	5.32
Large Rec Jet	10%	60	30	1.8	5.31	5.32
Large Rec Jet	10%	75	30	1.8	5.33	5.35
Large Rec Jet	10%	45	30	1.2	5.34	5.35
Large Rec Jet	14%	60	30	1.2	5.36	5.38
Large Rec Jet	14%	60	30	1.5	5.37	5.38

Table 5.1 Index of Pressure Distributions and Shock Loci

Configuration	Bump t/c	θ deg	ϕ deg	Pb/Po	Figure Numbers	
No V.G.'s	10%	-	-	-	5.39	5.40
No V.G.'s	14%	-	-	-	5.41	5.42
Vanes	10%	-	-	-	5.43	5.44
Vanes	14%	-	-	-	5.45	5.46
Small Rec Jet	10%	60	30	1.2	5.47	5.48
Small Rec Jet	10%	60	30	1.6	5.49	5.50
Small Rec Jet	14%	60	30	1.2	5.51	5.52
Small Rec Jet	14%	60	30	1.6	5.53	5.54
Small Rec Jet	14%	60	45	1.2	5.55	5.56
Small Rec Jet	14%	60	45	1.6	5.57	5.58
Large Rec Jet	10%	60	30	1.2	5.59	5.60
Large Rec Jet	10%	60	30	1.8	5.61	5.62
Large Rec Jet	14%	60	30	1.2	5.63	5.64
Large Rec Jet	14%	60	30	1.5	5.65	5.66

Table 5.2 Index of Schlieren Photographs

Configuration	Bump t/c	θ deg	ϕ deg	Pb/Po	Boundary Layer Profile
No V.G.'s	14%	-	-	-	5.68 to 5.71
Vanes	14%	-	-	-	5.72 to 5.75
Small Rec Jet	14%	60	30	1.2	5.76 to 5.79
Small Rec Jet	14%	60	30	1.6	5.80 to 5.82
Small Rec Jet	14%	60	45	1.6	5.83 to 5.86
Large Rec Jet	14%	60	30	1.2	5.87 to 5.89
Large Rec Jet	14%	60	30	1.5	5.90 to 5.93

Table 5.3 Index of Boundary Layer Profiles

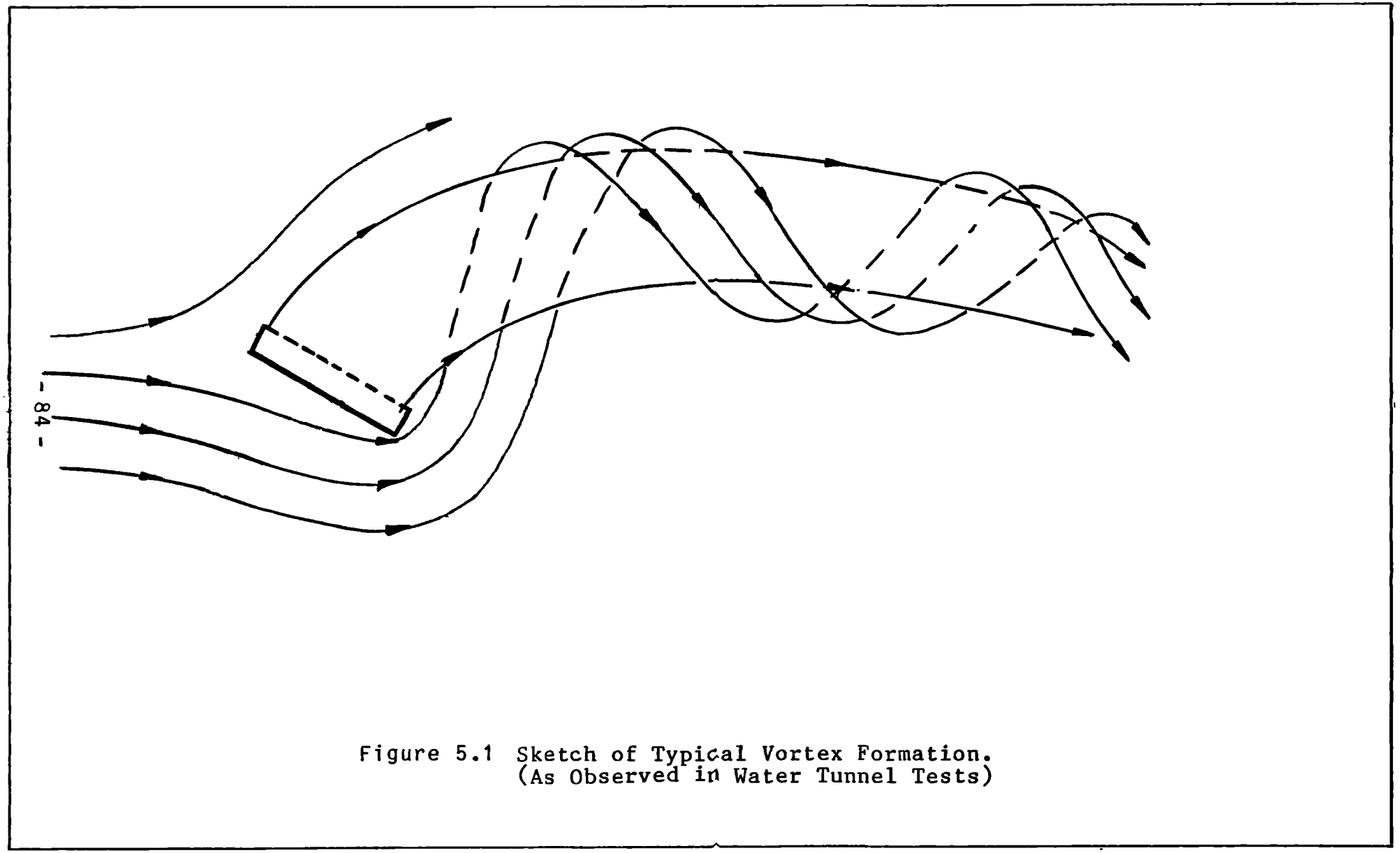

Figure 5.1 Sketch of Typical Vortex Formation.
(As Observed in Water Tunnel Tests)

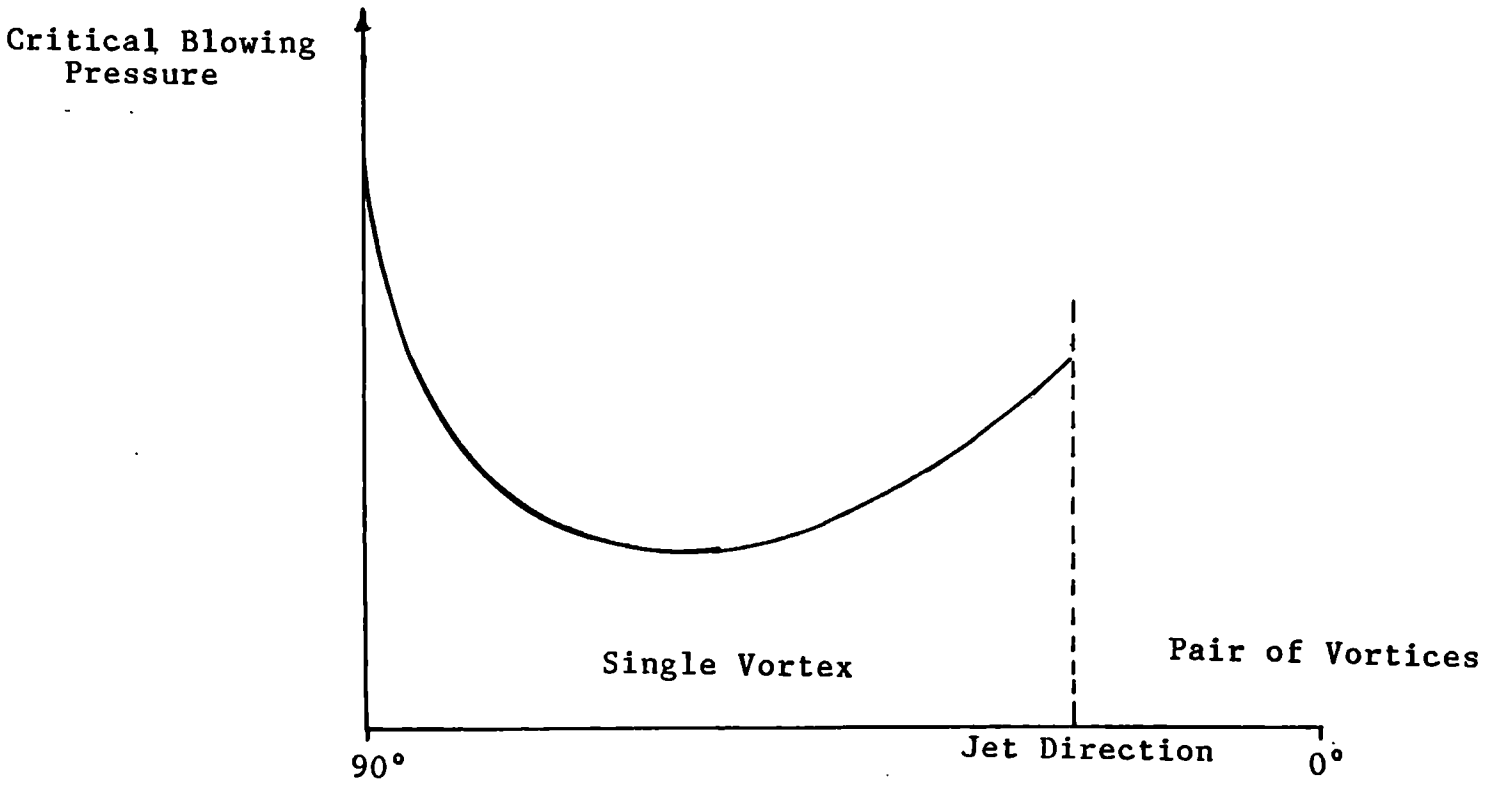

Figure 5.2 Qualitative Graph Showing the Variation in Critical Blowing Pressure with Jet Direction.

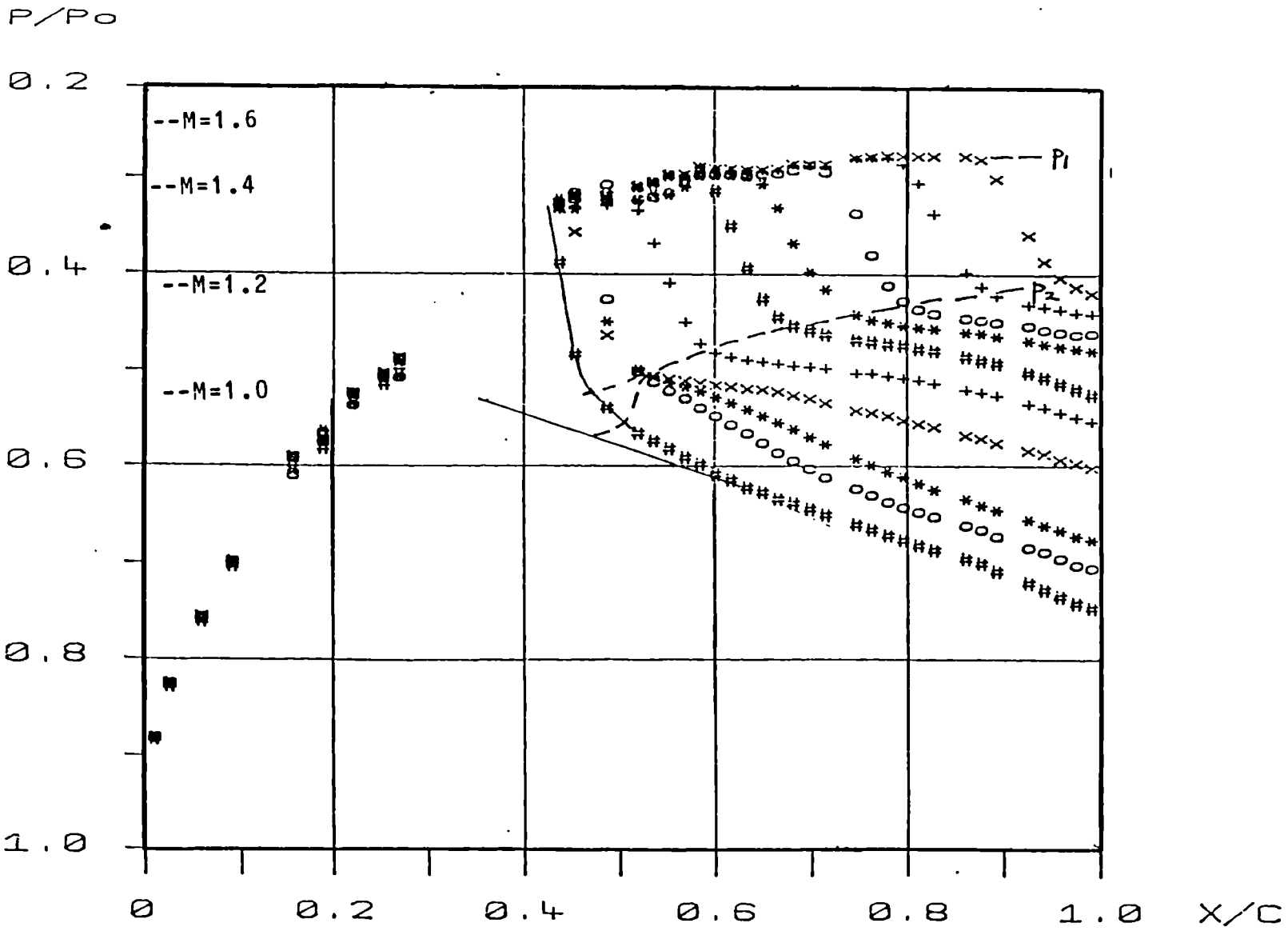

Figure 5.3a Experimental Pressure Distributions for the 10% Bump with No Vortex Generators.

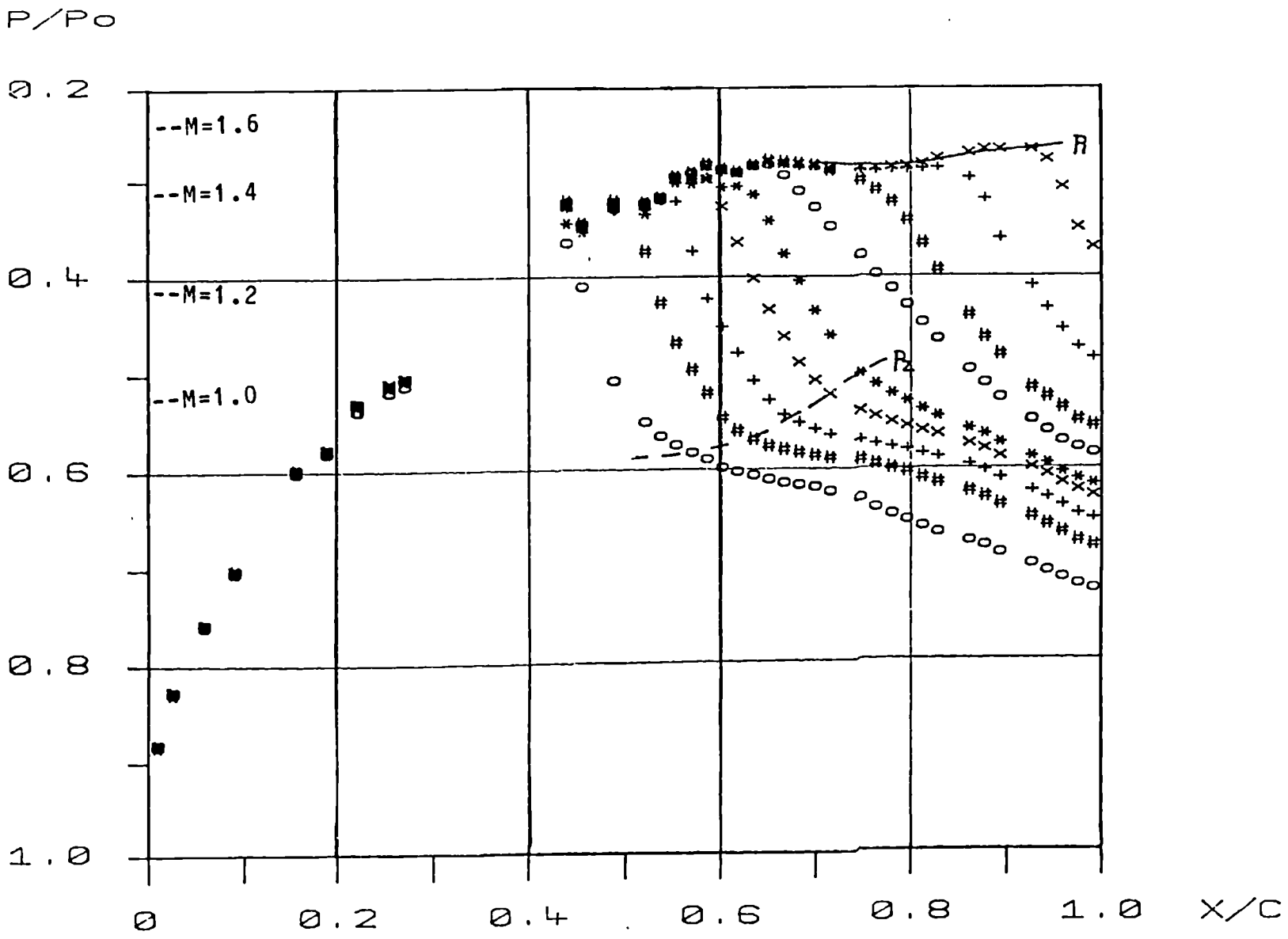

Figure 5.3b Experimental Pressure Distributions for the 10% Bump with Vane Vortex Generators (α =20°).

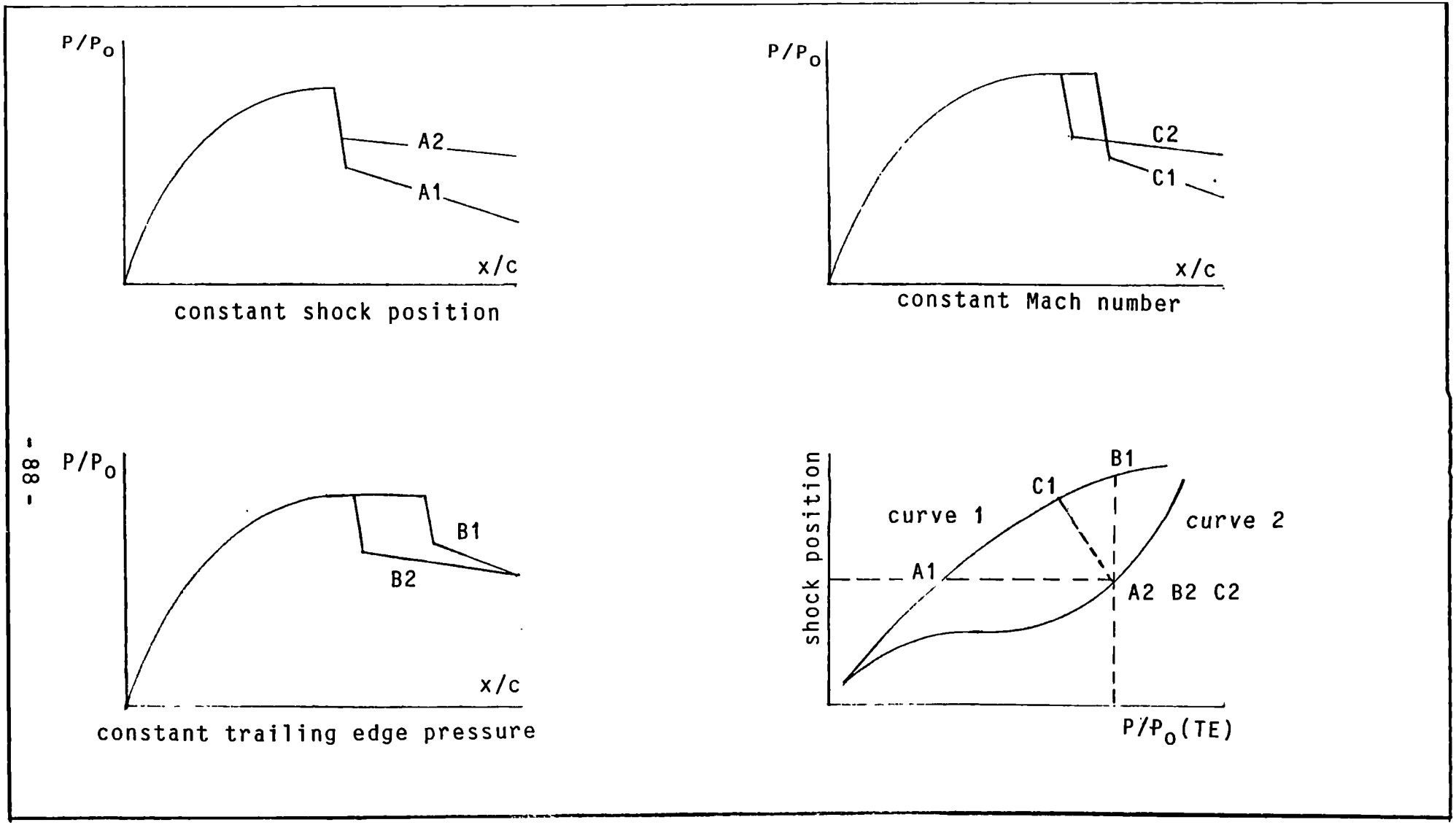

Figure 5.4 Justification for Using the Loci of Shock Position against Trailing Edge Pressure

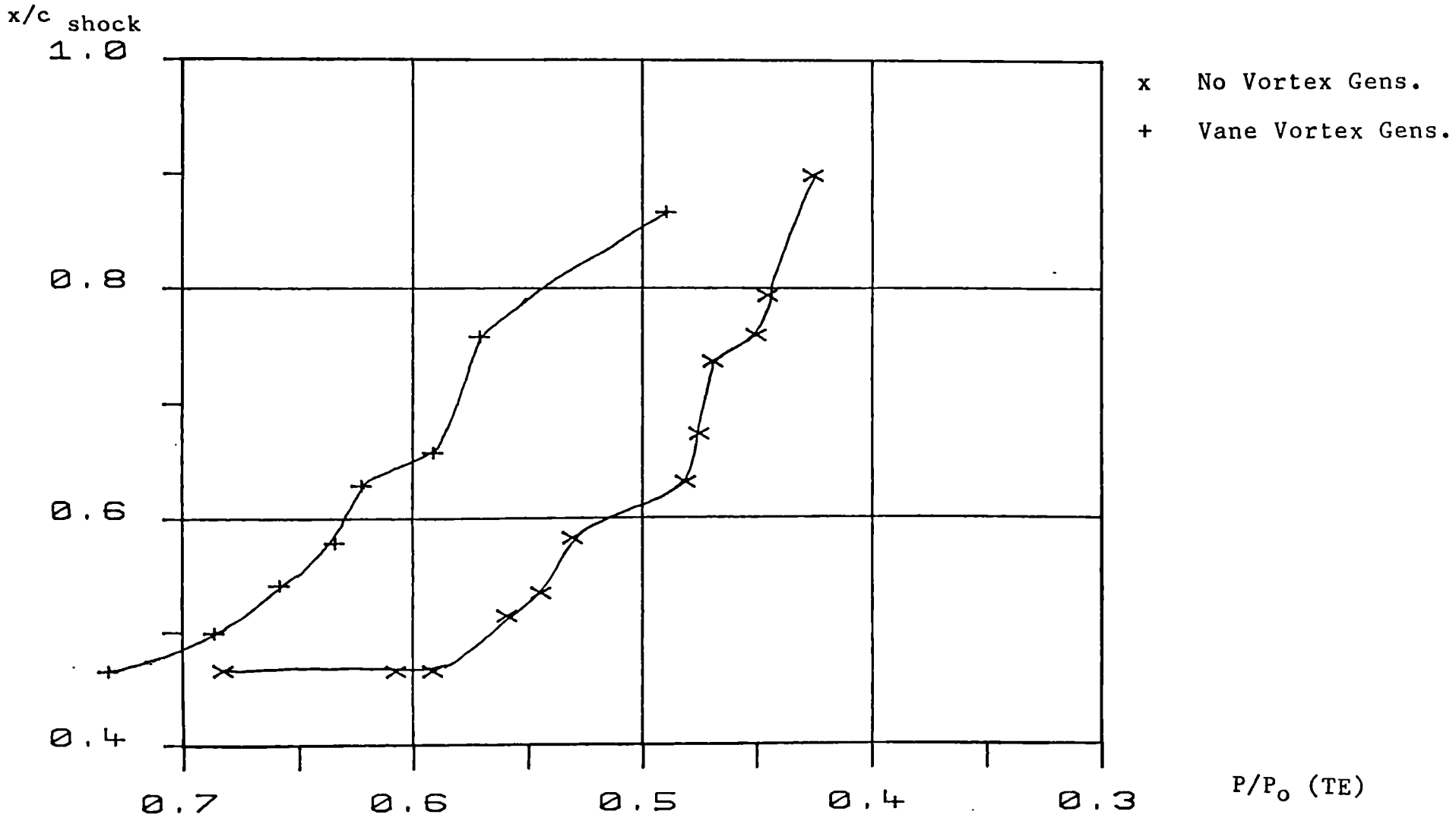

Figure 5.5 Loci of Shock Position Against Trailing Edge Pressure for the 10% Bump with No Vortex Generators and Vane Vortex Generators.

No Vortex Generators (Separated Flow)

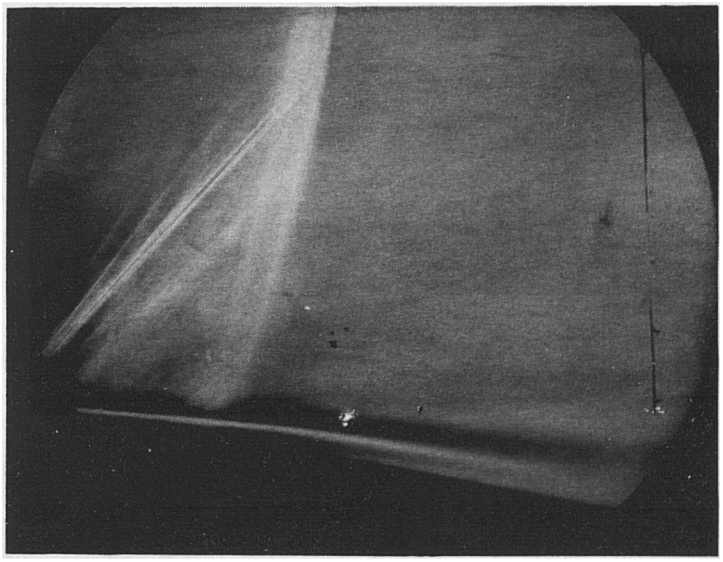

Vane Vortex Generators (Attached Flow)

Figure 5.6 Comparison of Schlieren Photographs

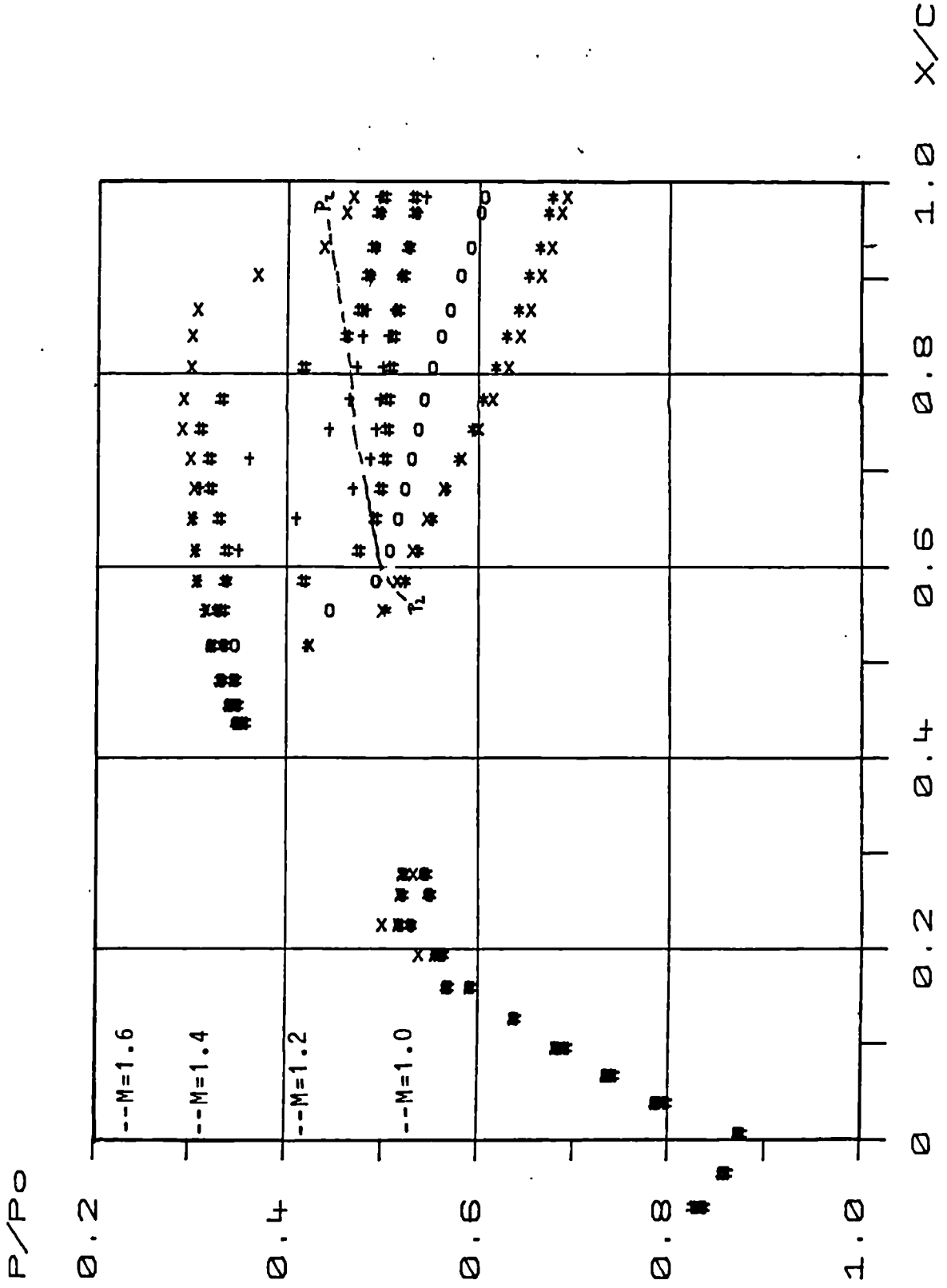

Figure 5.7 Experimental Pressure Distributions for the 8% Bump with No Vortex Generators.

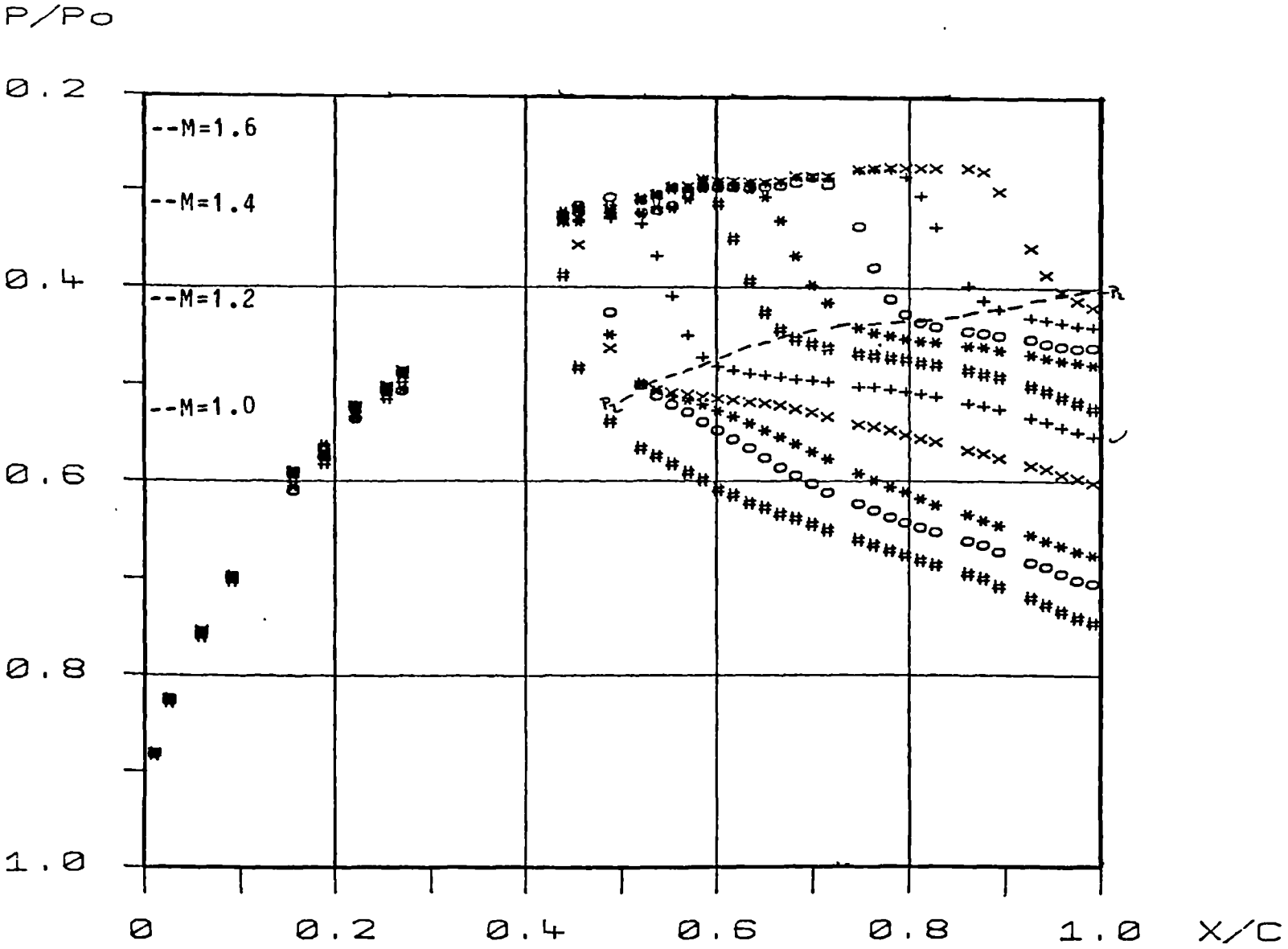

Figure 5.8 Experimental Pressure Distributions for the 10% Bump with No Vortex Generators.

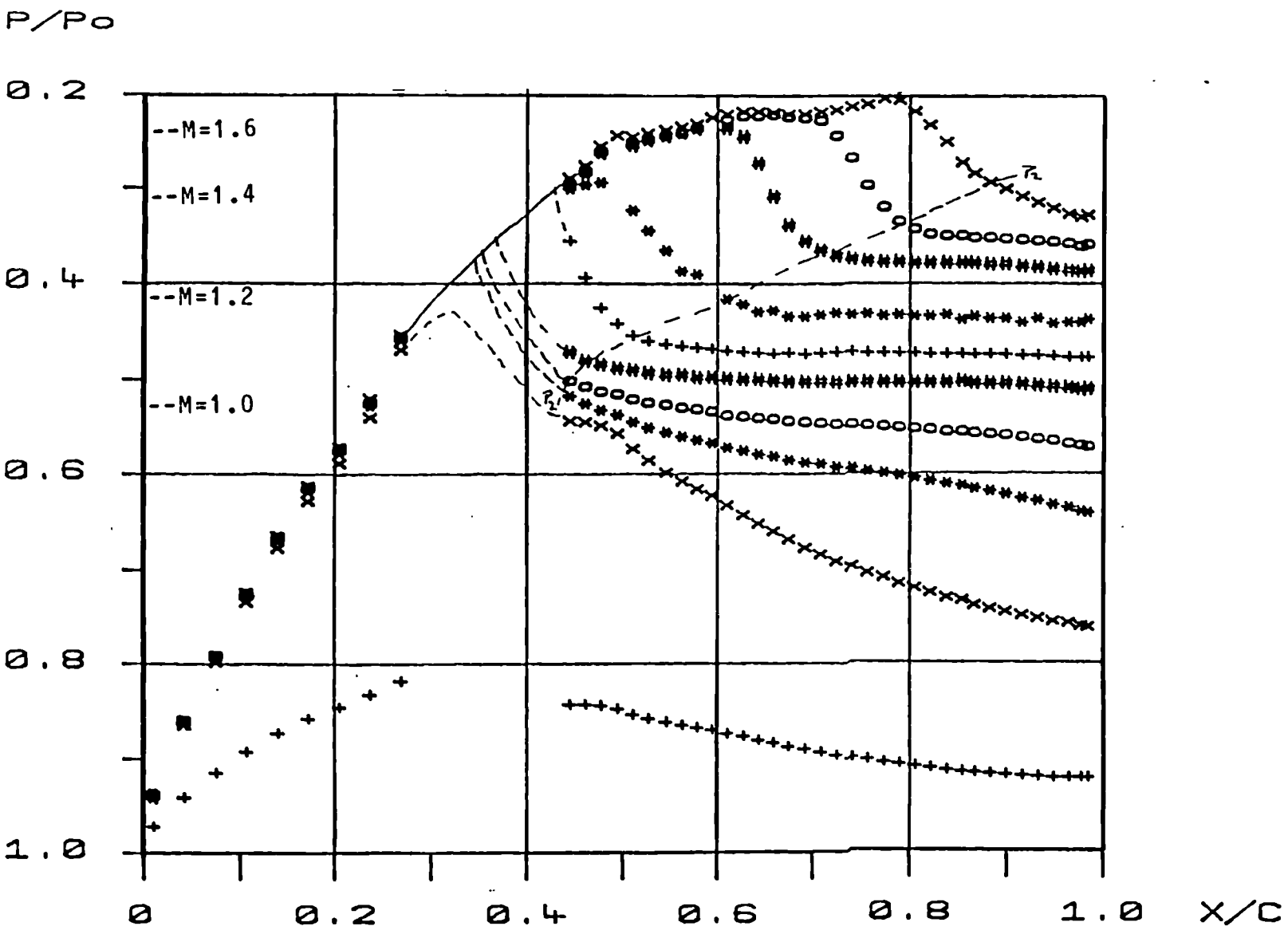

Figure 5.9 Experimental Pressure Distribution for the 14% Bump with No Vortex generators.

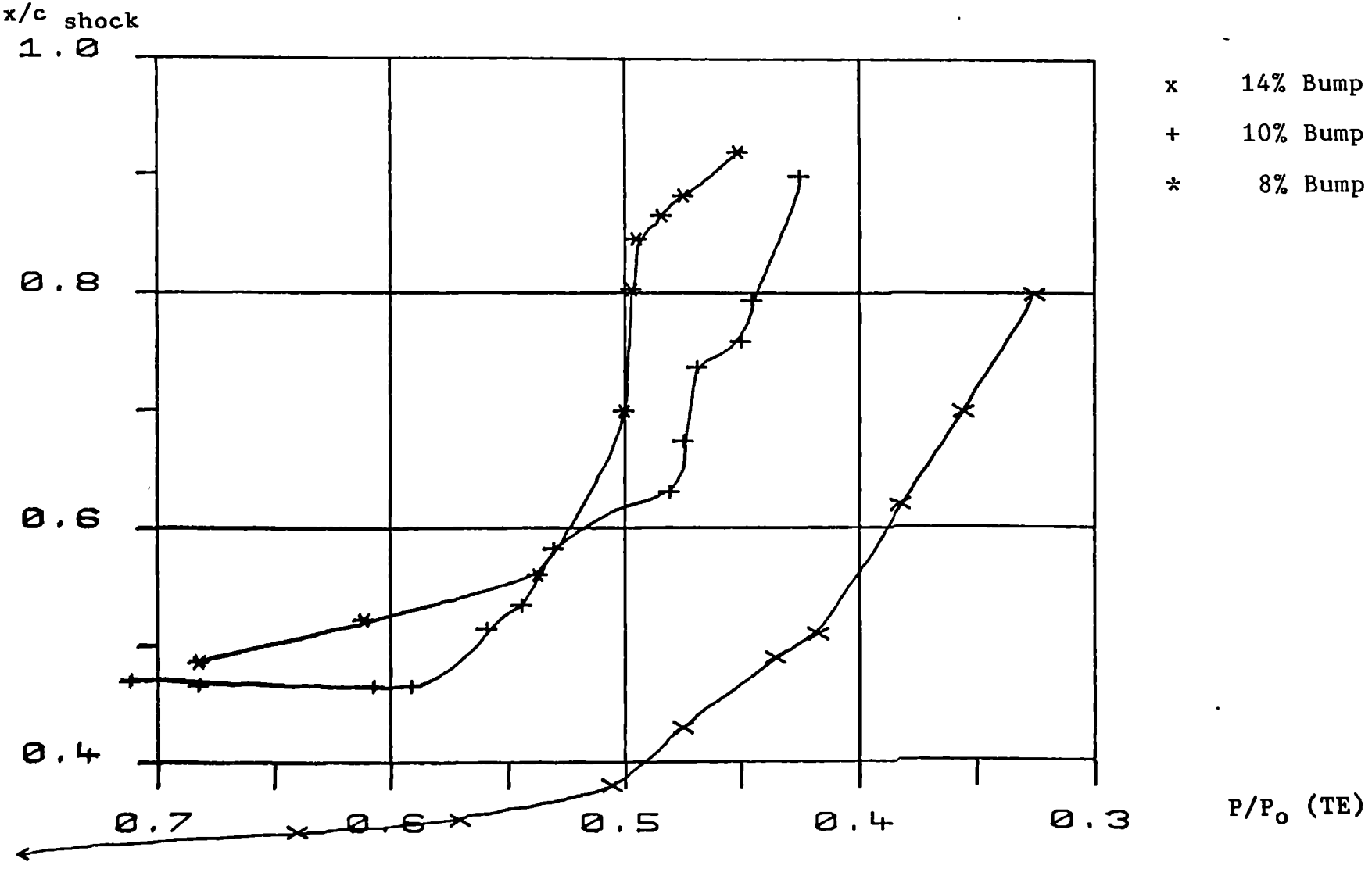

Figure 5.10 Comparison of the Loci of Shock Position Against Trailing Edge Pressure for the Three Bumps with No Vortex Generators.

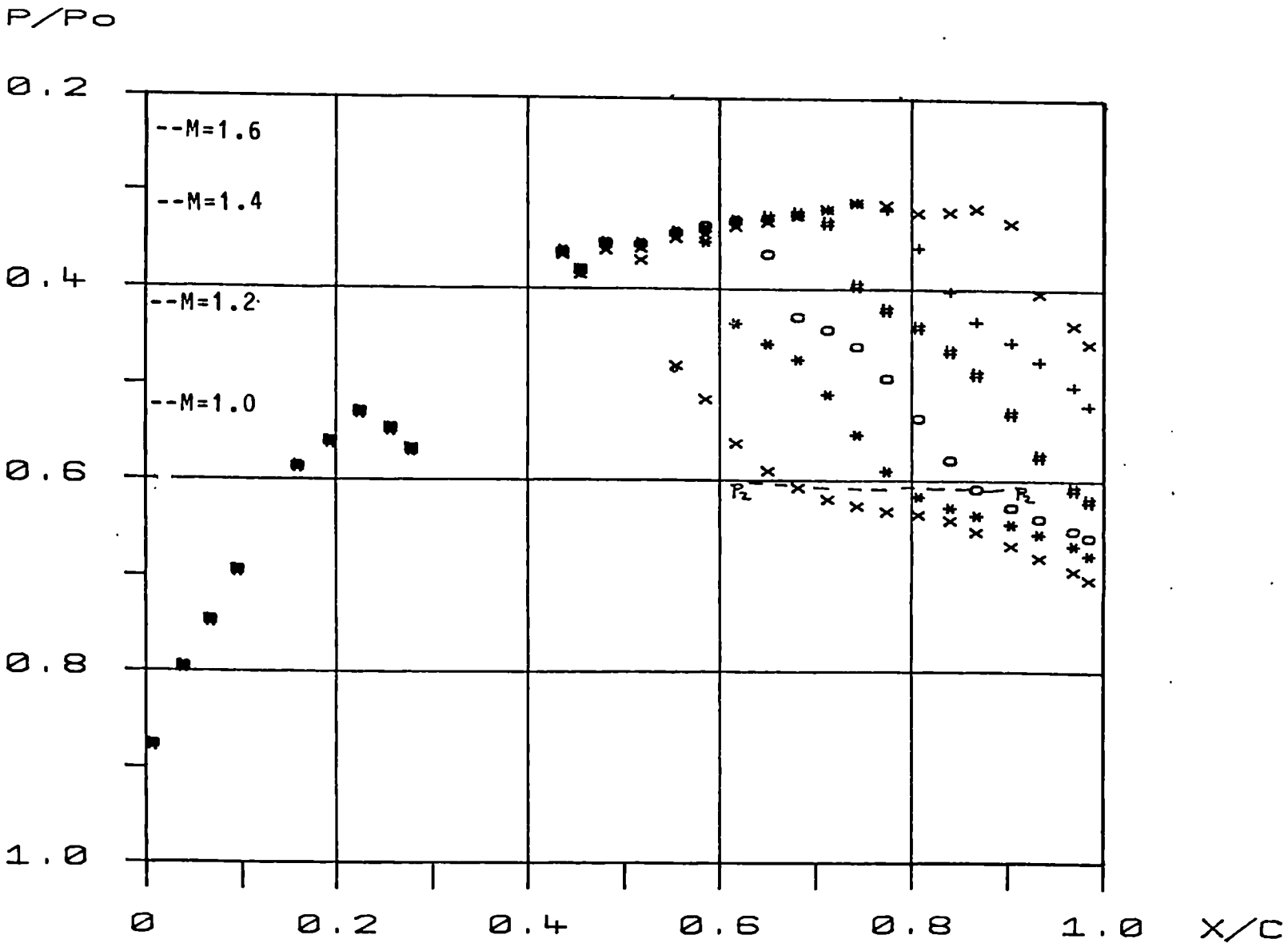

Figure 5.11 Experimental Pressure Distributions for the 8% Bump with Vane Vortex Generators.

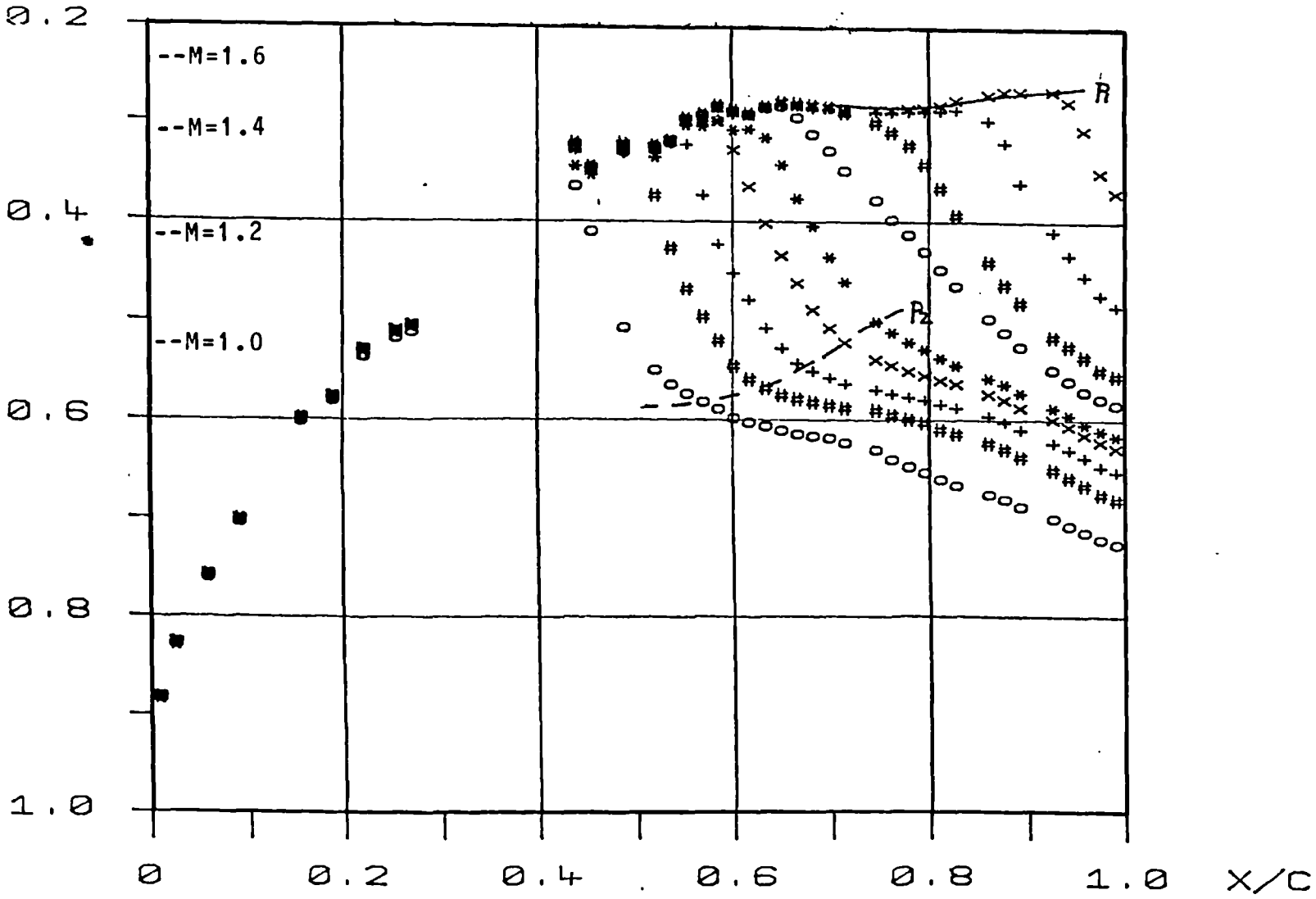

Figure 5.12 Experimental Pressure Distributions for the 10% Bump with Vane Vortex Generators.

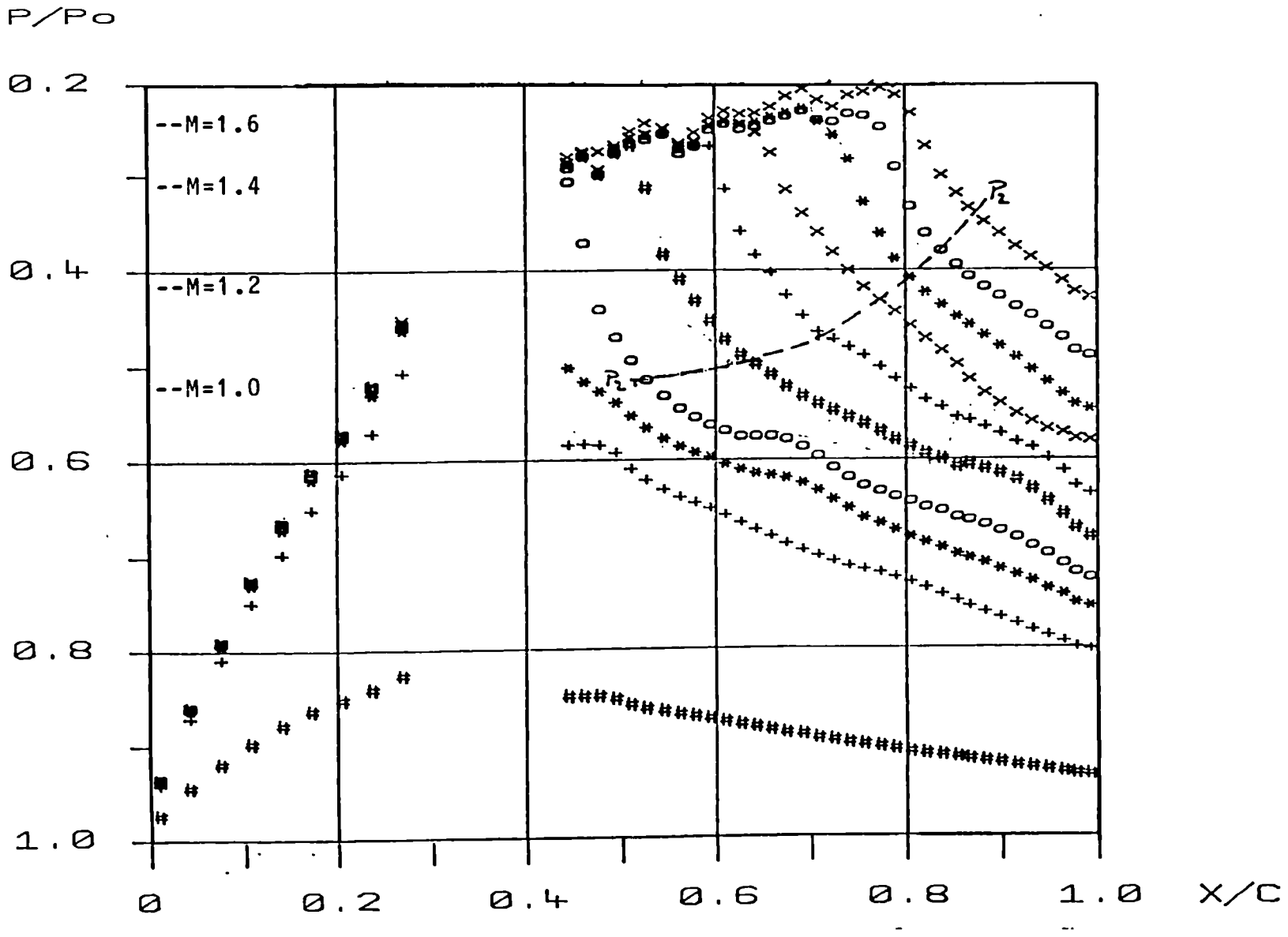

Figure 5.13 Experimental Pressure Distributions for the 14% Bump with Vane Vortex Generators.

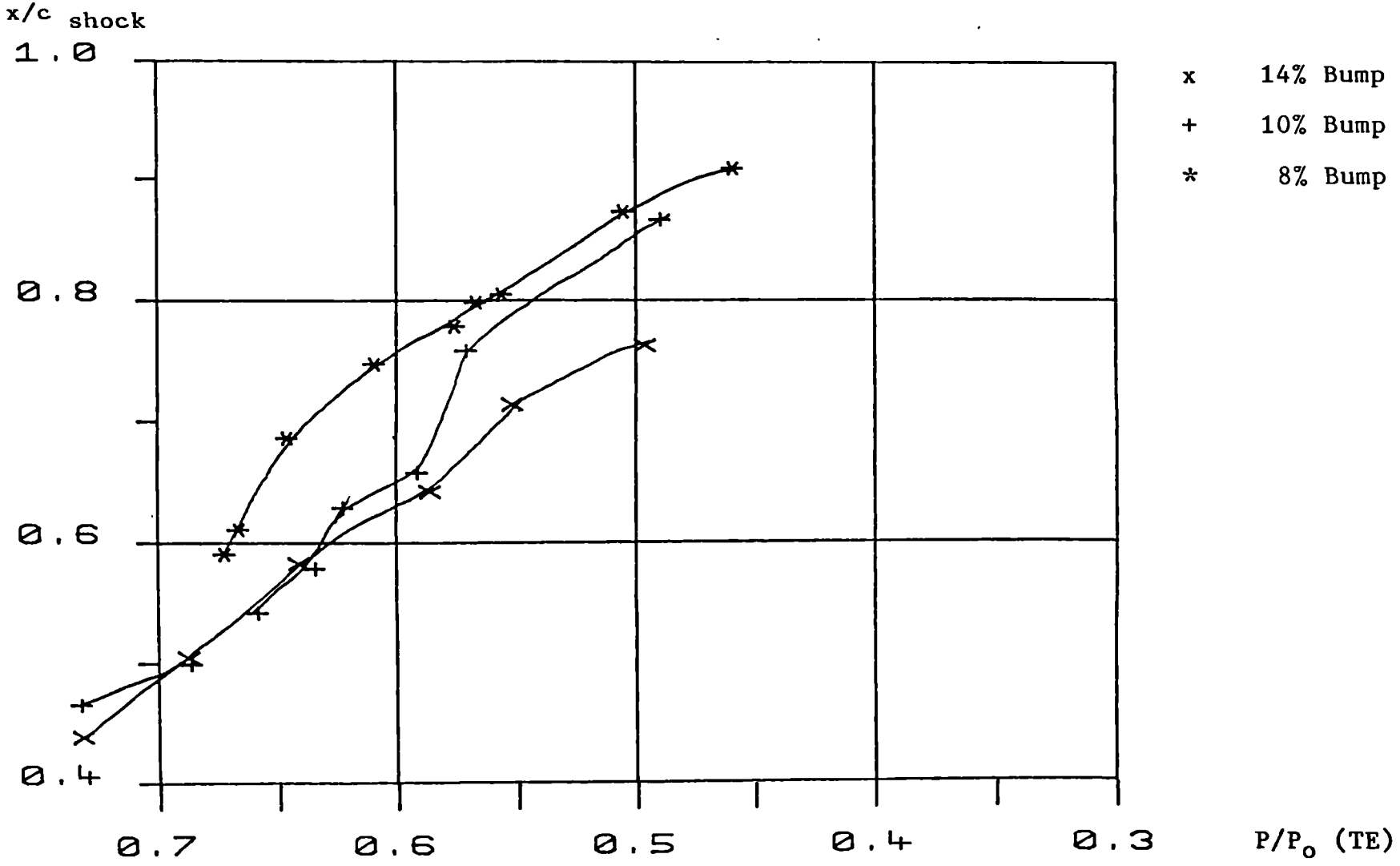

Figure 5.14 Comparison of the Loci of Shock Position Against Trailing Edge Pressure for the Three Bumps with Vane Vortex Generators.

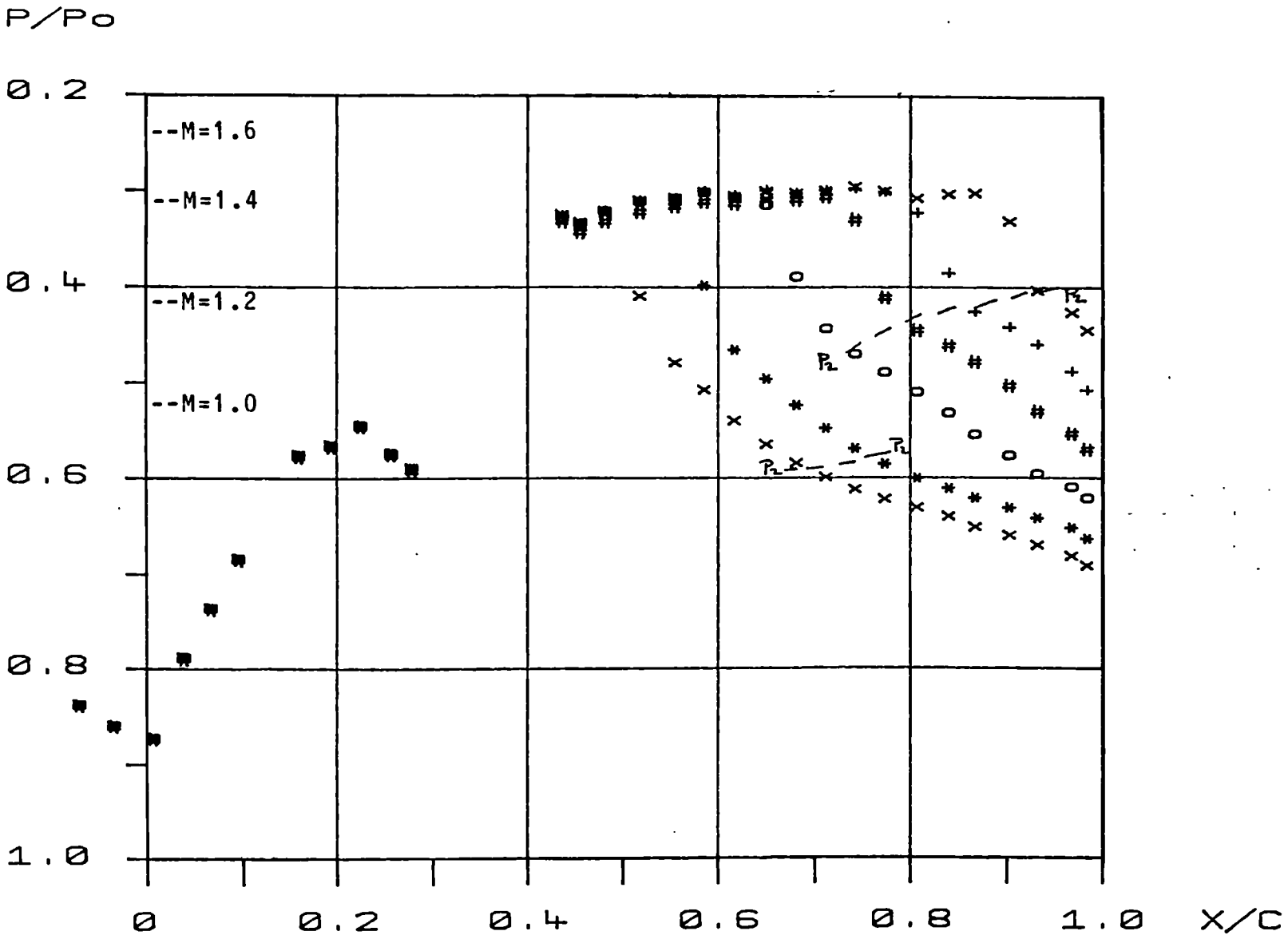

Figure 5.15 Experimental Pressure Distributions for the 8% Bump with Round Air Jet Vortex Generators (θ=90° P_b/P_o=1.0).

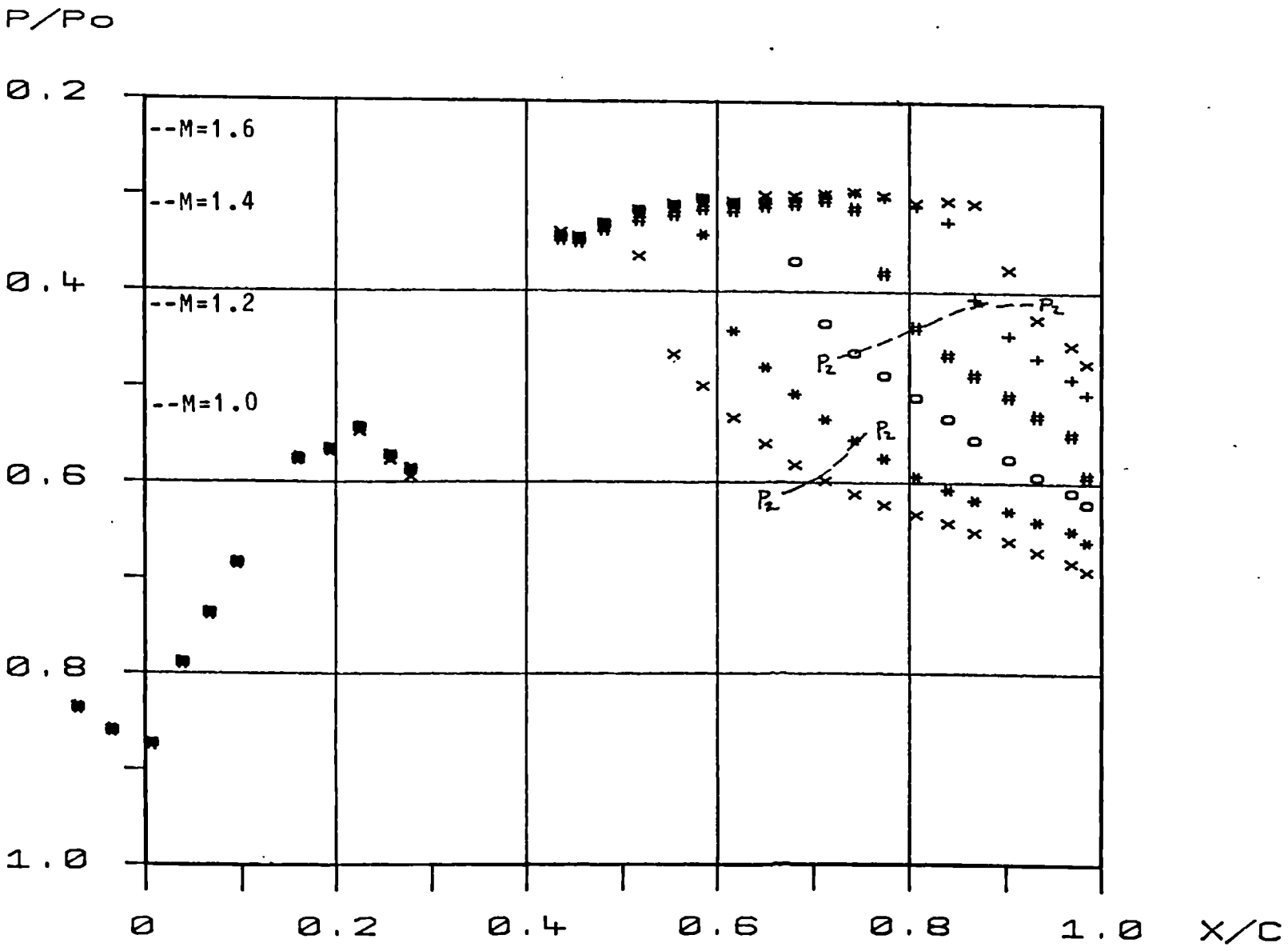

Figure 5.16 Experimental Pressure Distributions for the 8% Bump with Round Air Jet Vortex Generators (θ=60° P_b/P_o=1.0).

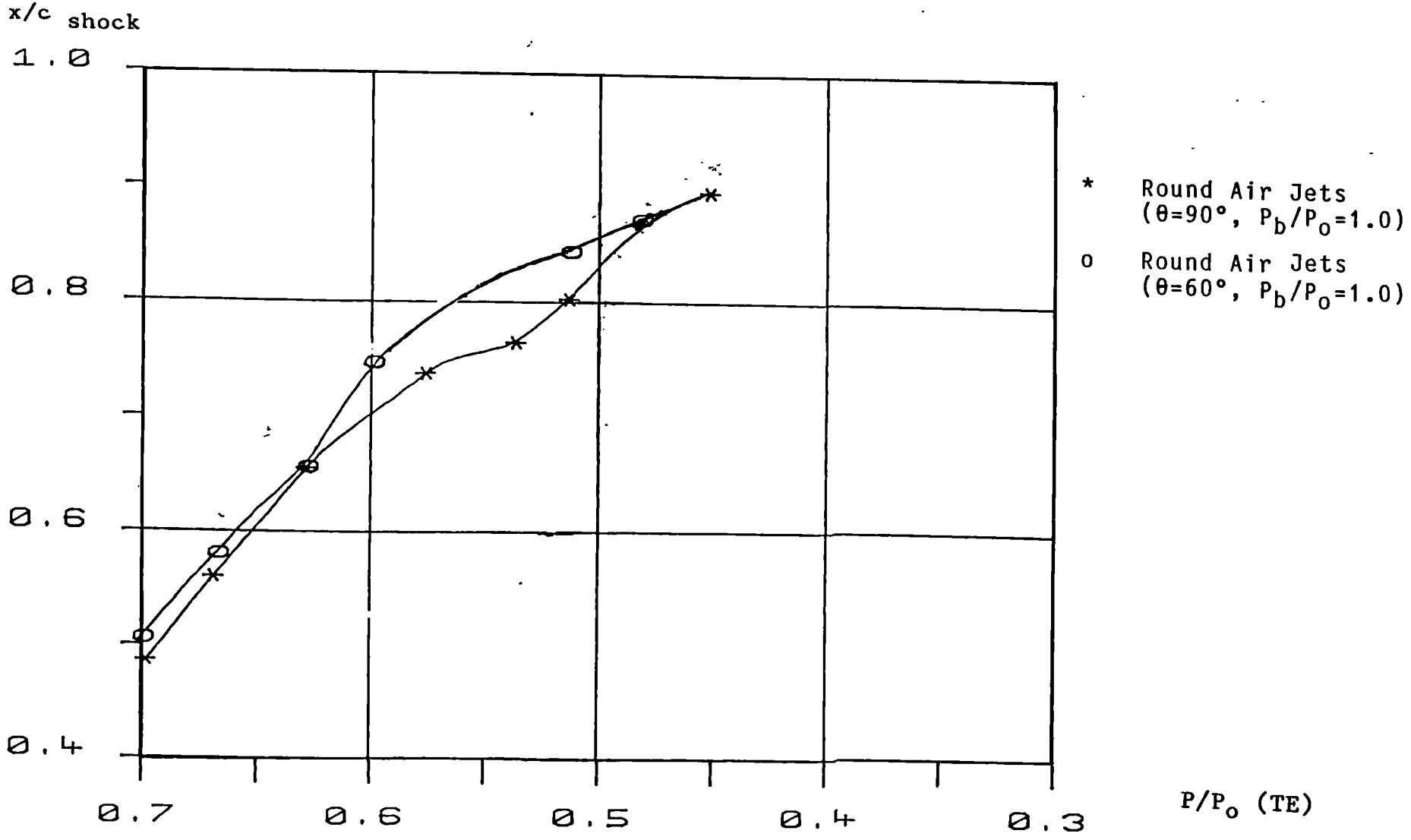

Figure 5.17 Comparison of the loci of Shock Position Against Trailing Edge Pressure for the 8% Bump.

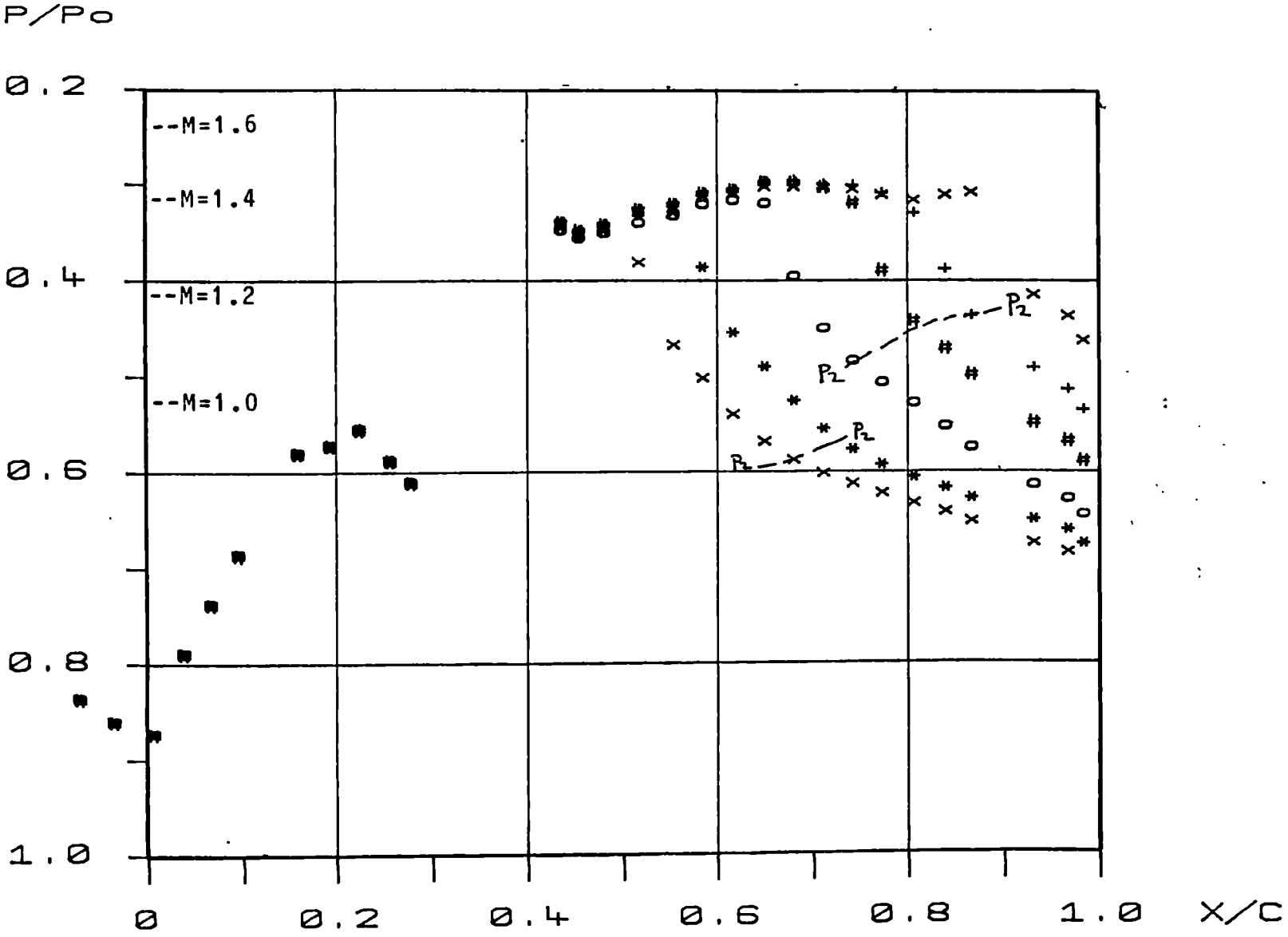

Figure 5.18 Experimental Pressure Distributions for the 8% Bump with Rectangular Air Jet Vortex Generators ($\theta=60°$ $P_b/P_o=1.0$).

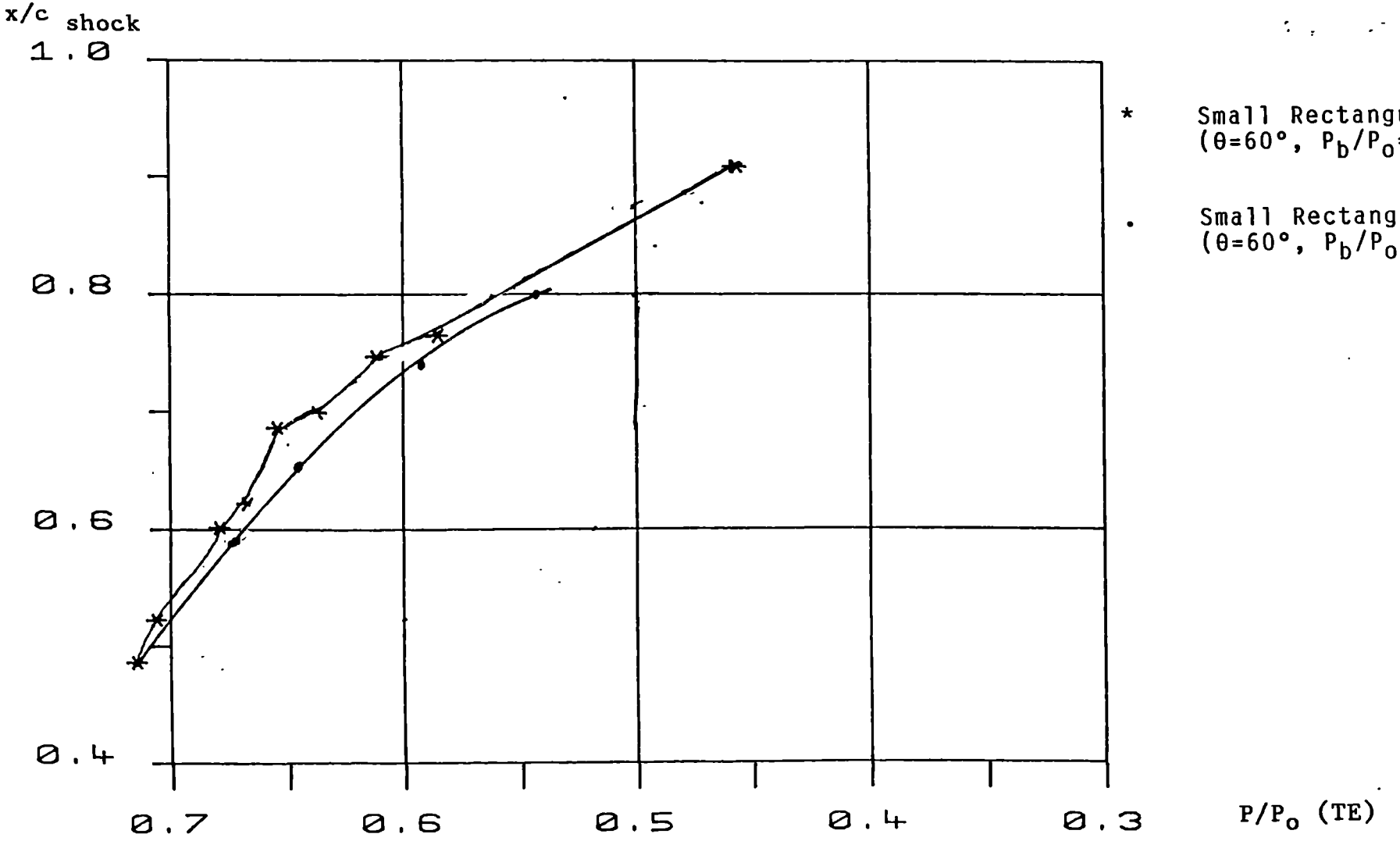

Figure 5.19 Comparison of the loci of Shock Position Against Trailing Edge Pressure for the 8% Bump.

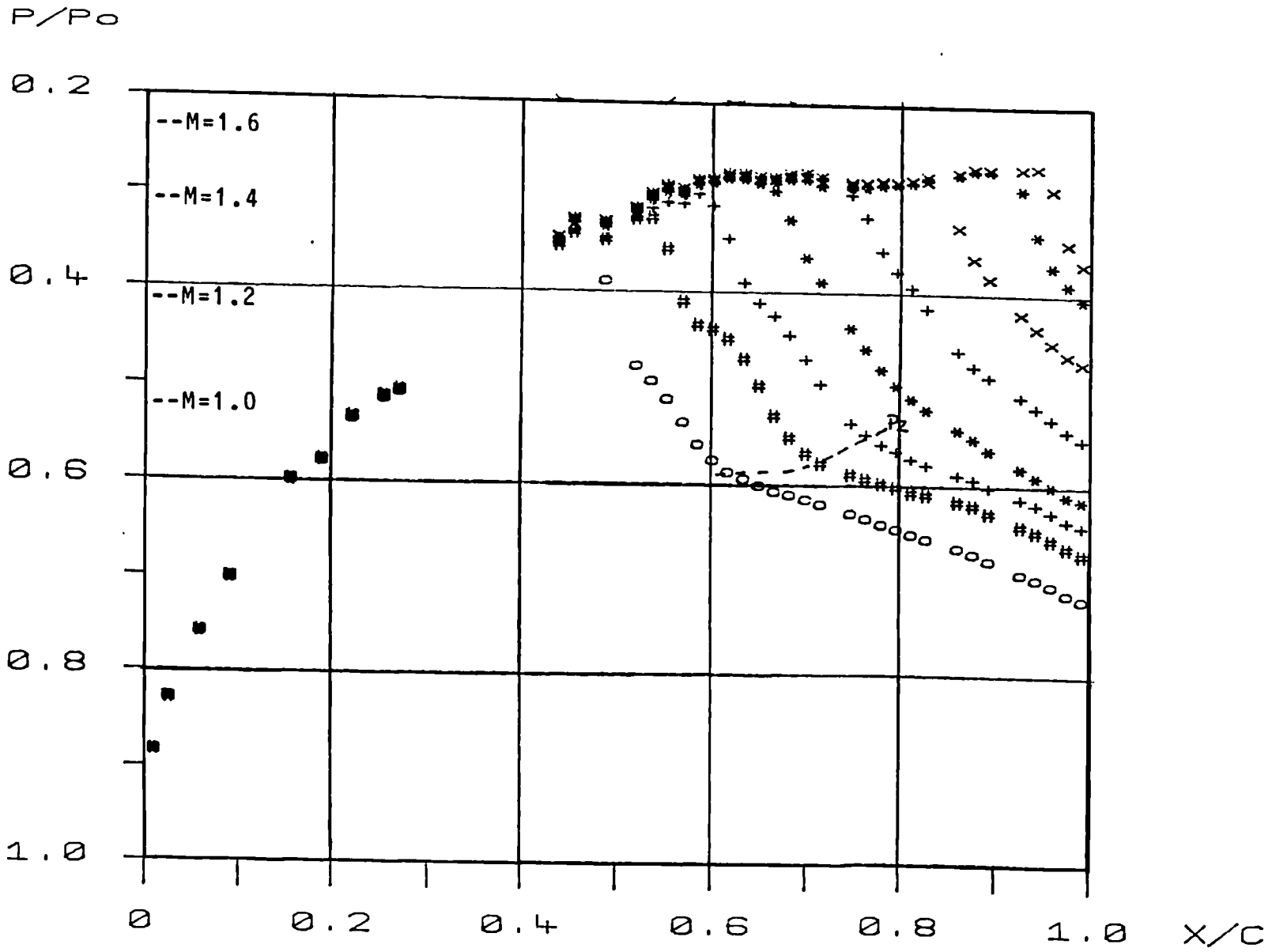

Figure 5.20 Experimental Pressure Distributions for the 10% Bump with Small Air Jet Vortex Generators (P_b/P_o=1.2

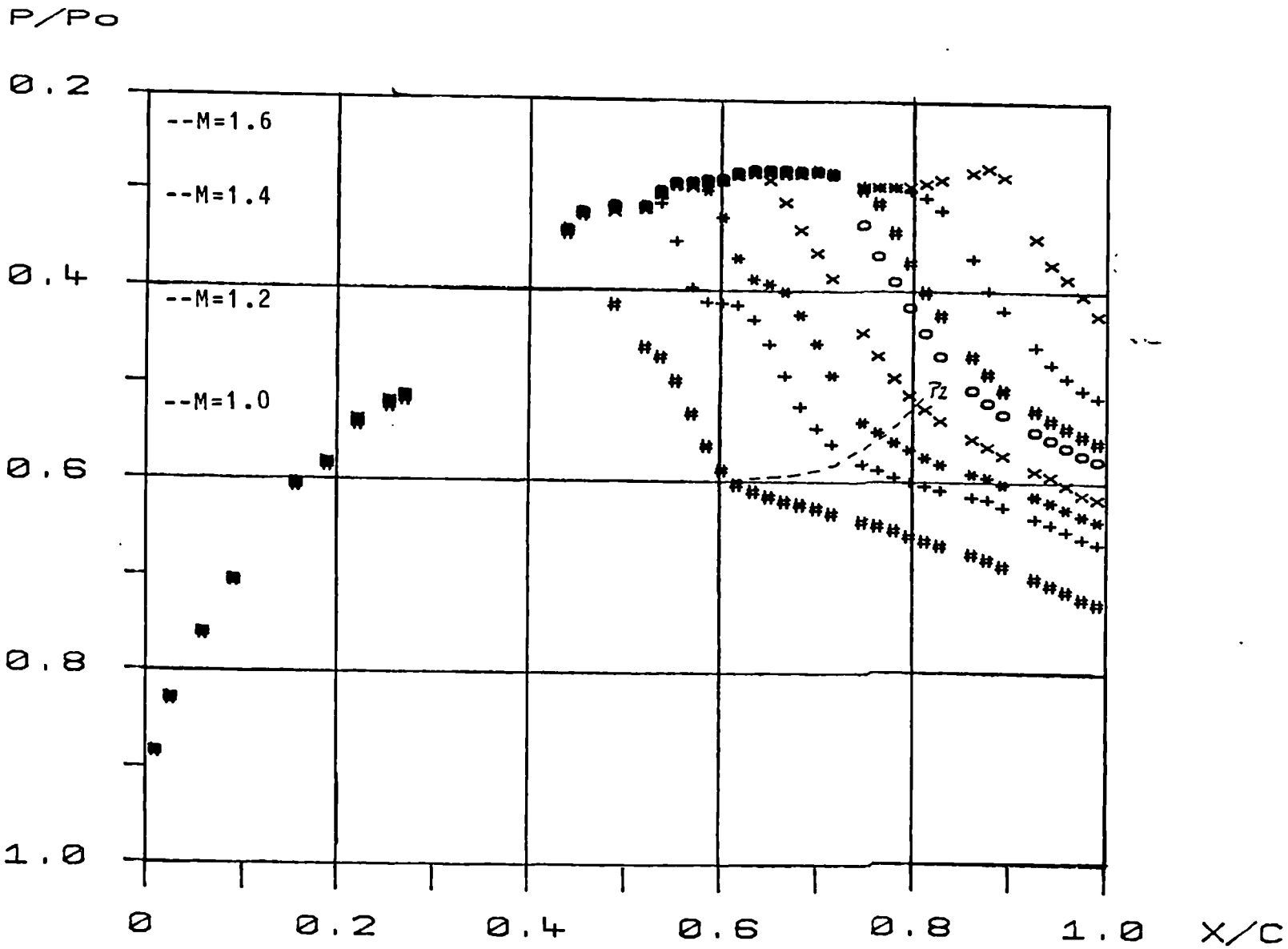

Figure 5.21 Experimental Pressure Distributions for the 10% Bump with Small Air Jet Vortex Generators (P_b/P_o=1.6)

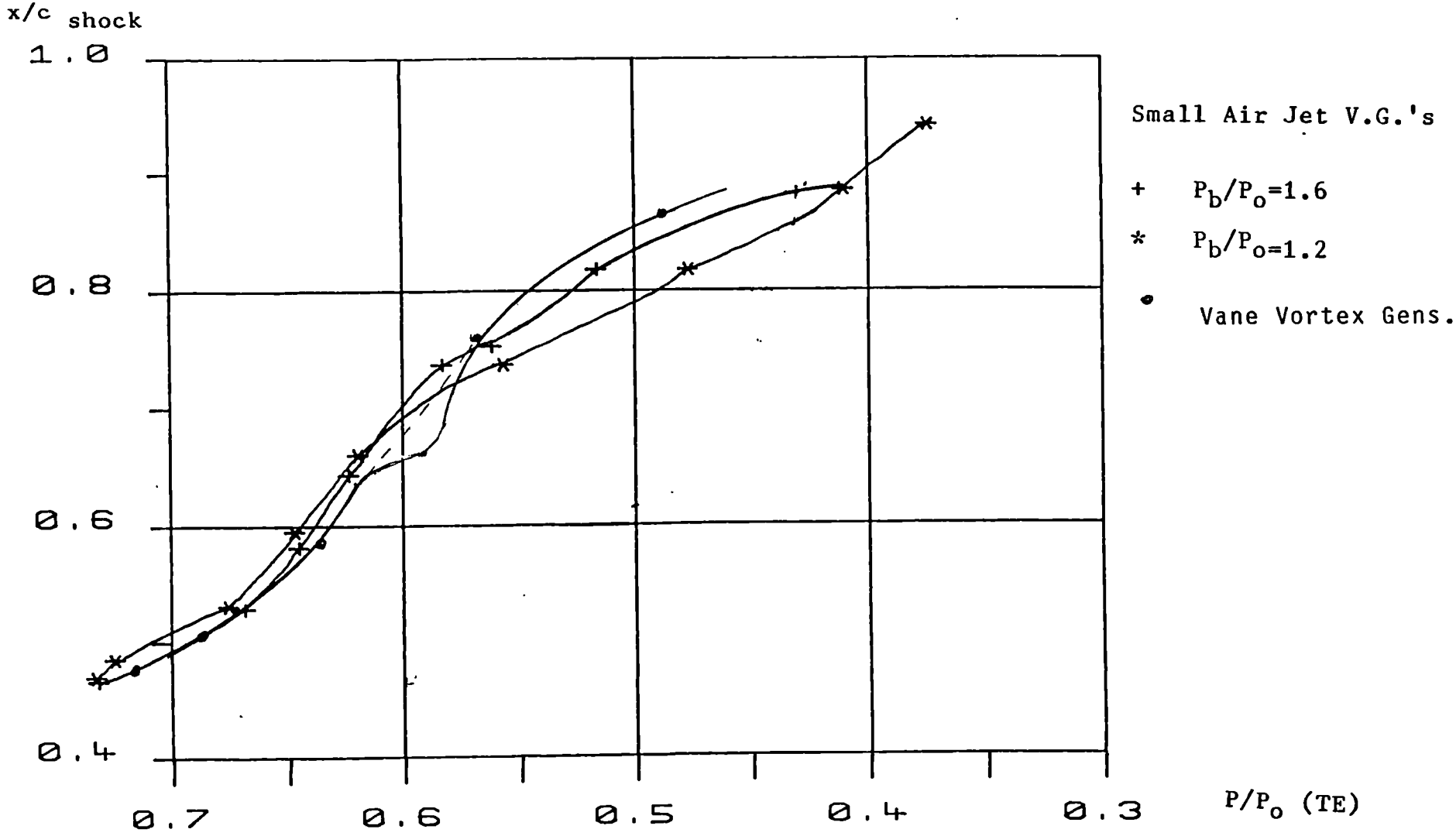

Figure 5.22 Comparison of the Loci of Shock Position Against Trailing Edge Pressure for the 10% Bump.

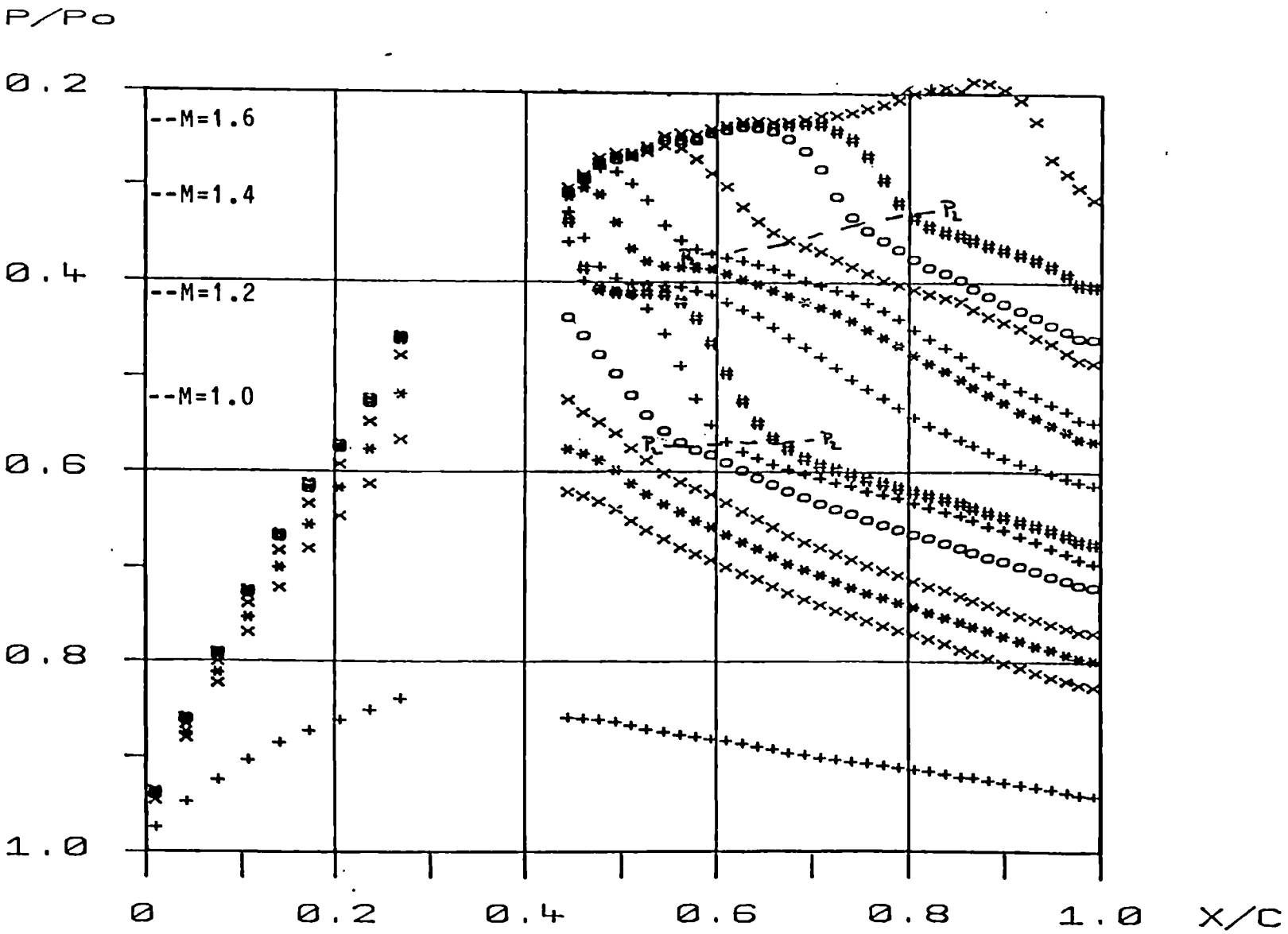

Figure 5.23 Experimental Pressure Distributions for the 14% Bump with Small Air Jet Vortex Generators ($\emptyset$=30°, P_b/P_o=1.2).

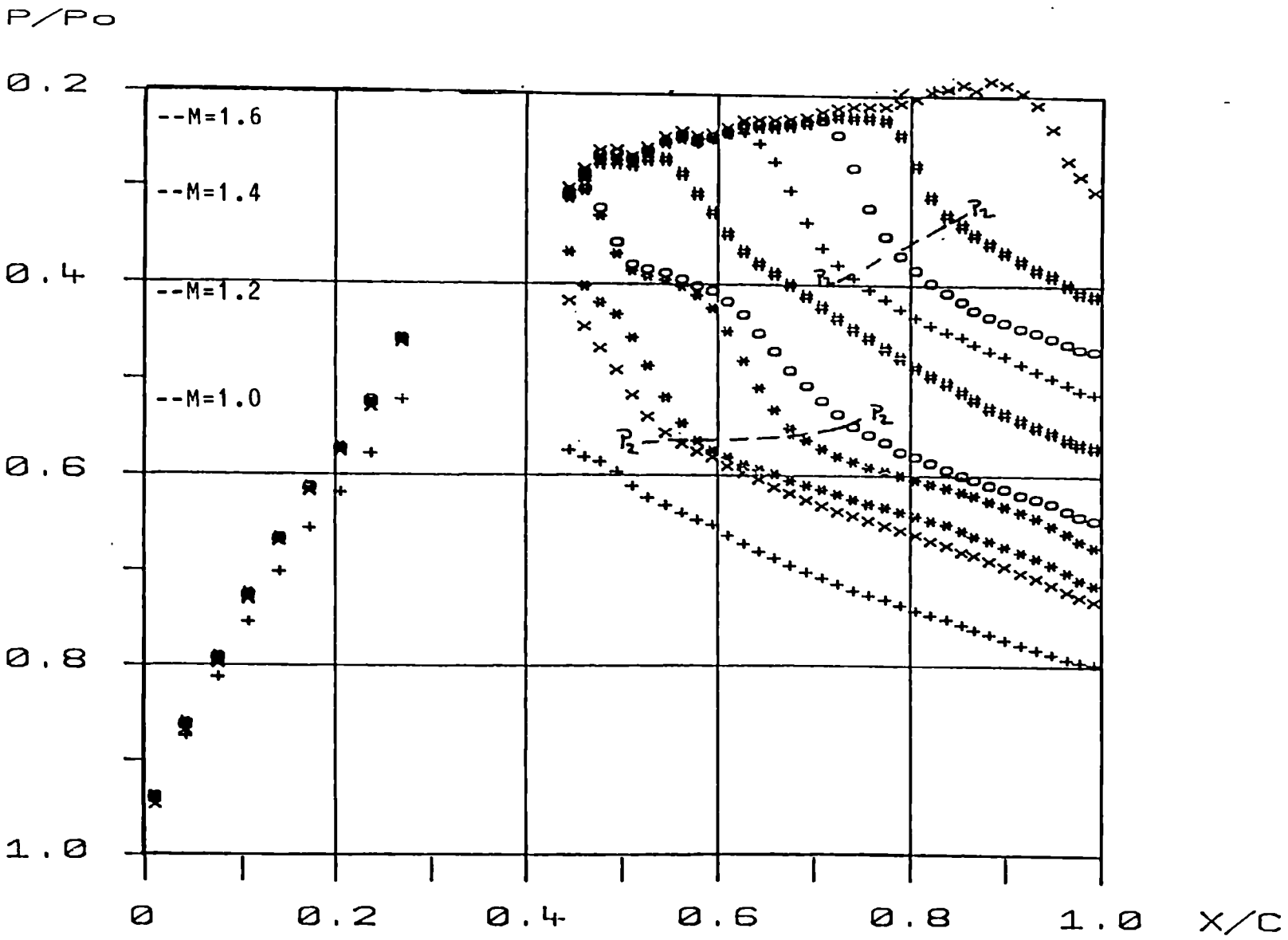

Figure 5.24 Experimental Pressure Distributions for the 14% Bump with Small Air Jet Vortex Generators ($\emptyset$=30°, P_b/P_o=1.6).

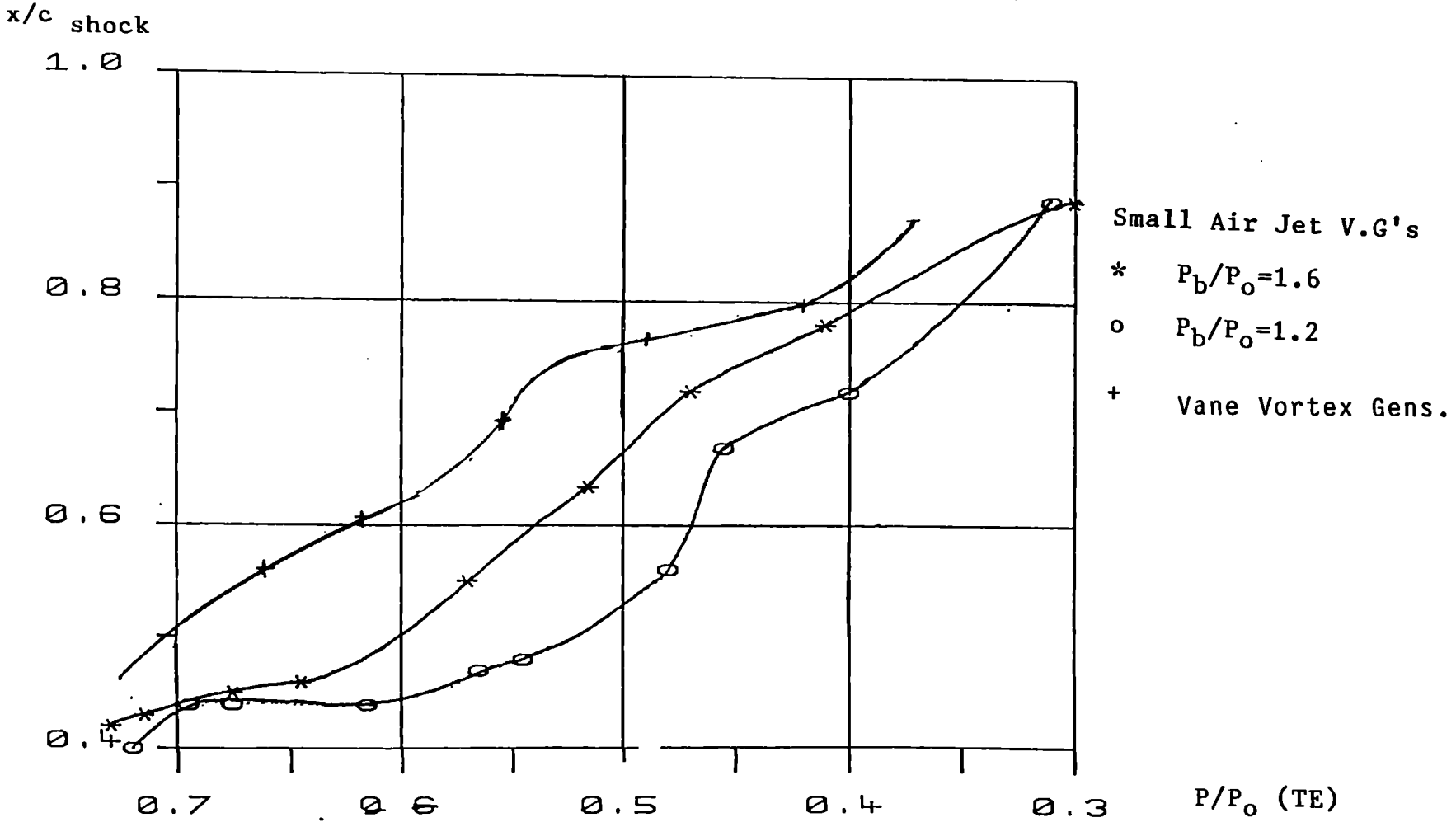

Figure 5.25 Comparison of the Loci of Shock Position Against Trailing Edge Pressure for the 14% Bump.

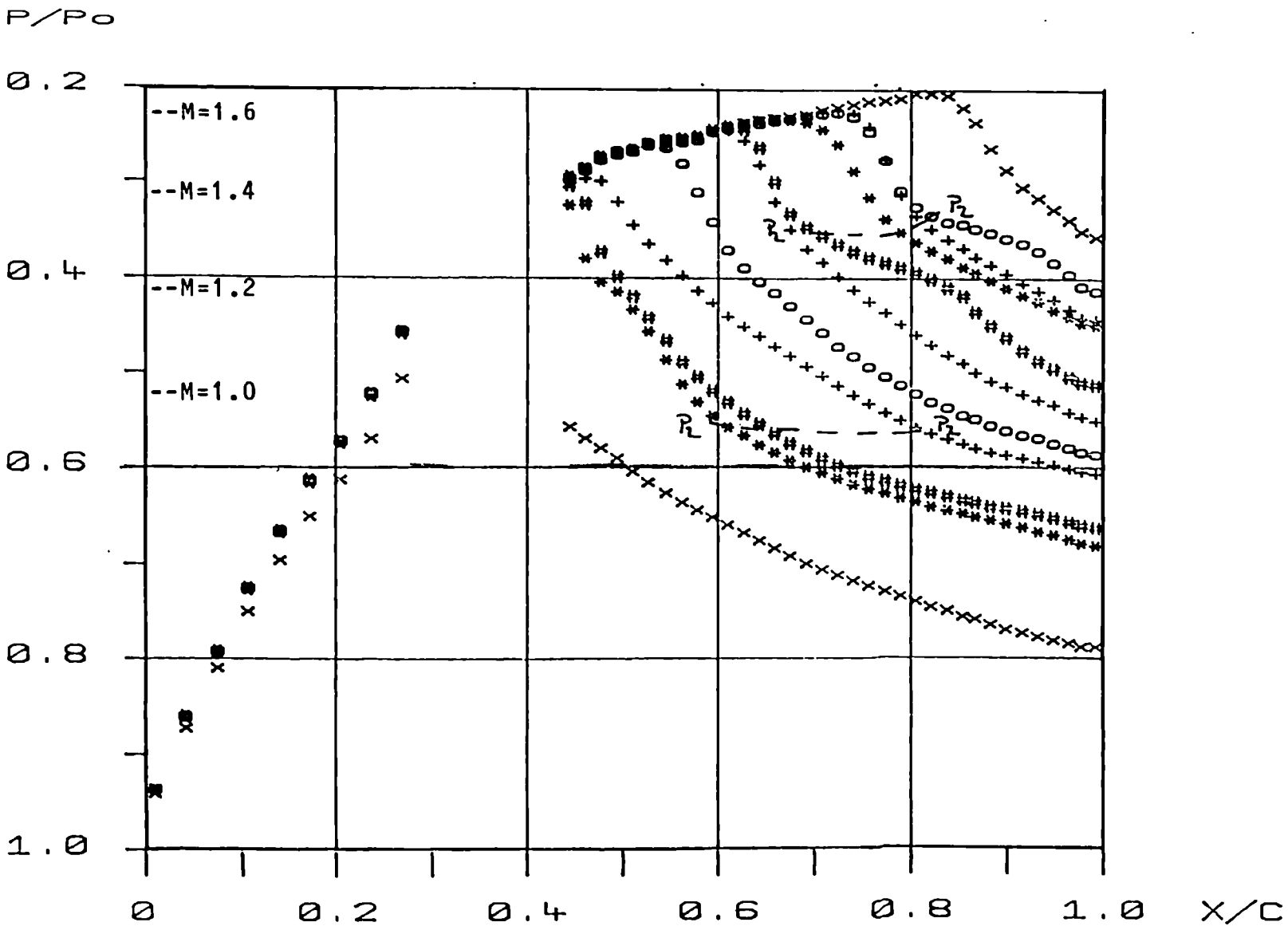

Figure 5.26 Experimental Pressure Distributions for the 14% Bump with Small Air Jet Vortex Generators (ϕ=45°, P_b/P_o=1.2).

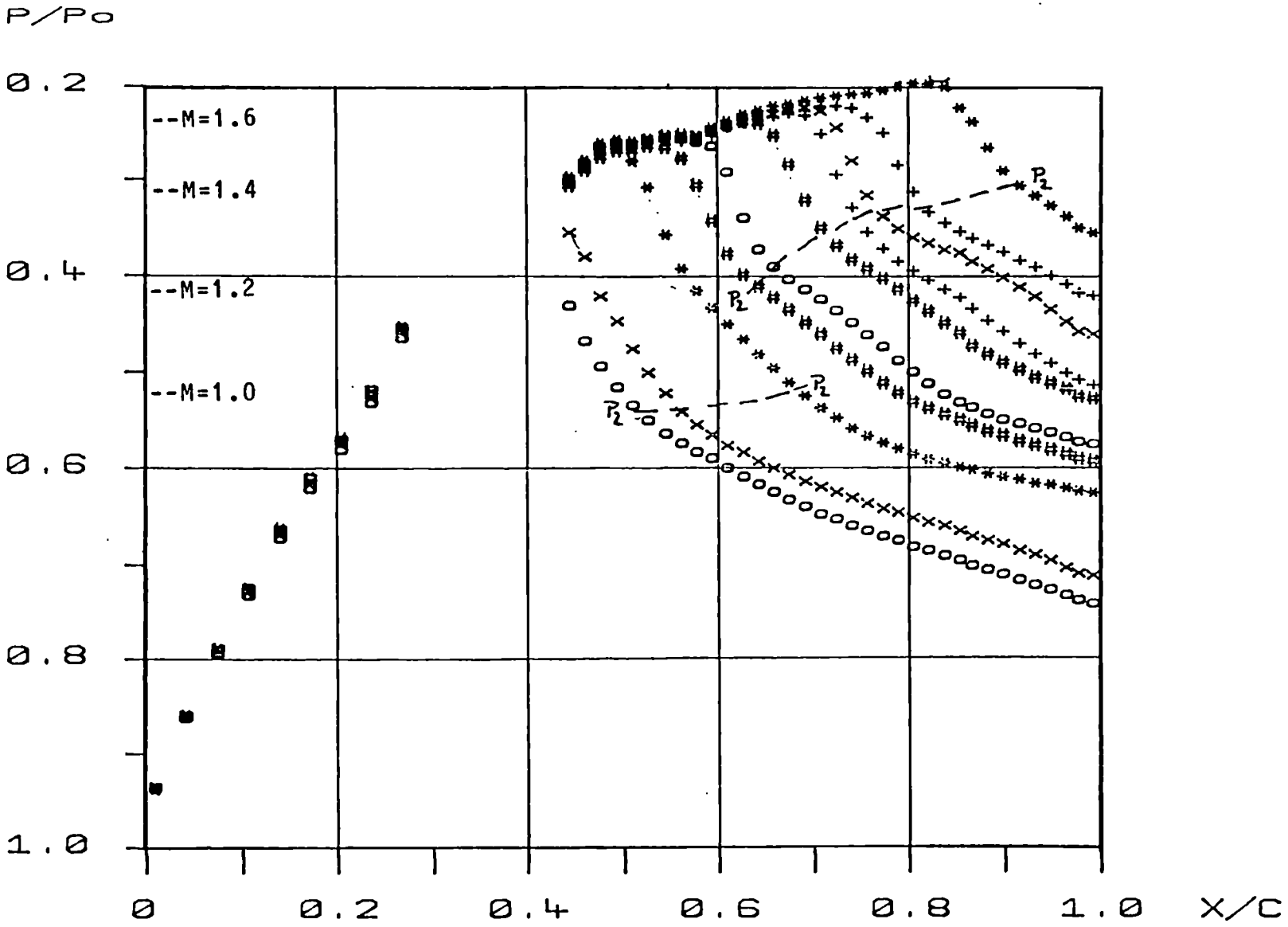

Figure 5.27 Experimental Pressure Distributions for the 14% Bump with Small Air Jet Vortex Generators ($\emptyset$=45°, P_b/P_o=1.6).

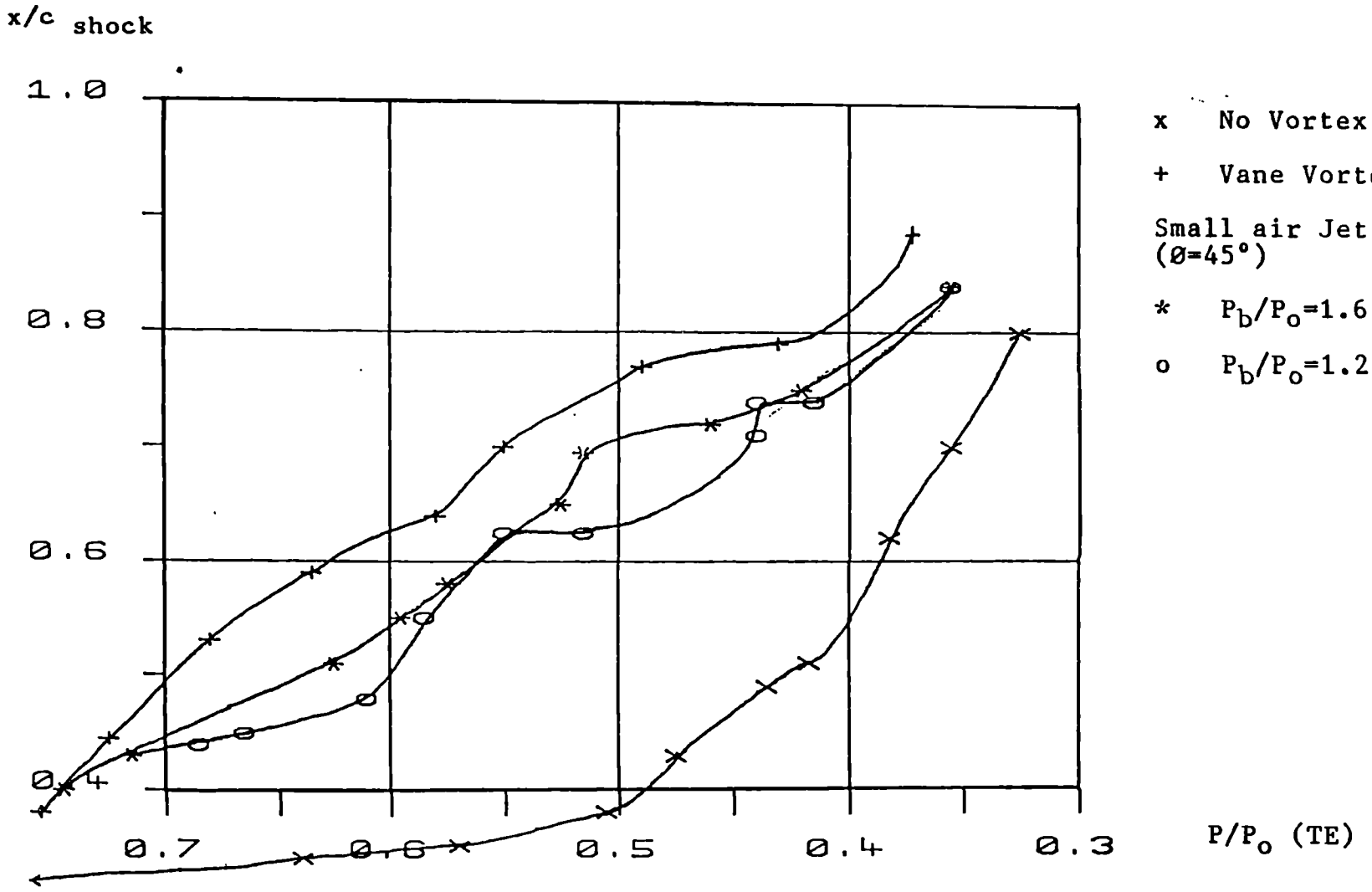

Figure 5.28 Comparison of the Loci of Shock Position Against Trailing Edge Pressure for the 14% Bump.

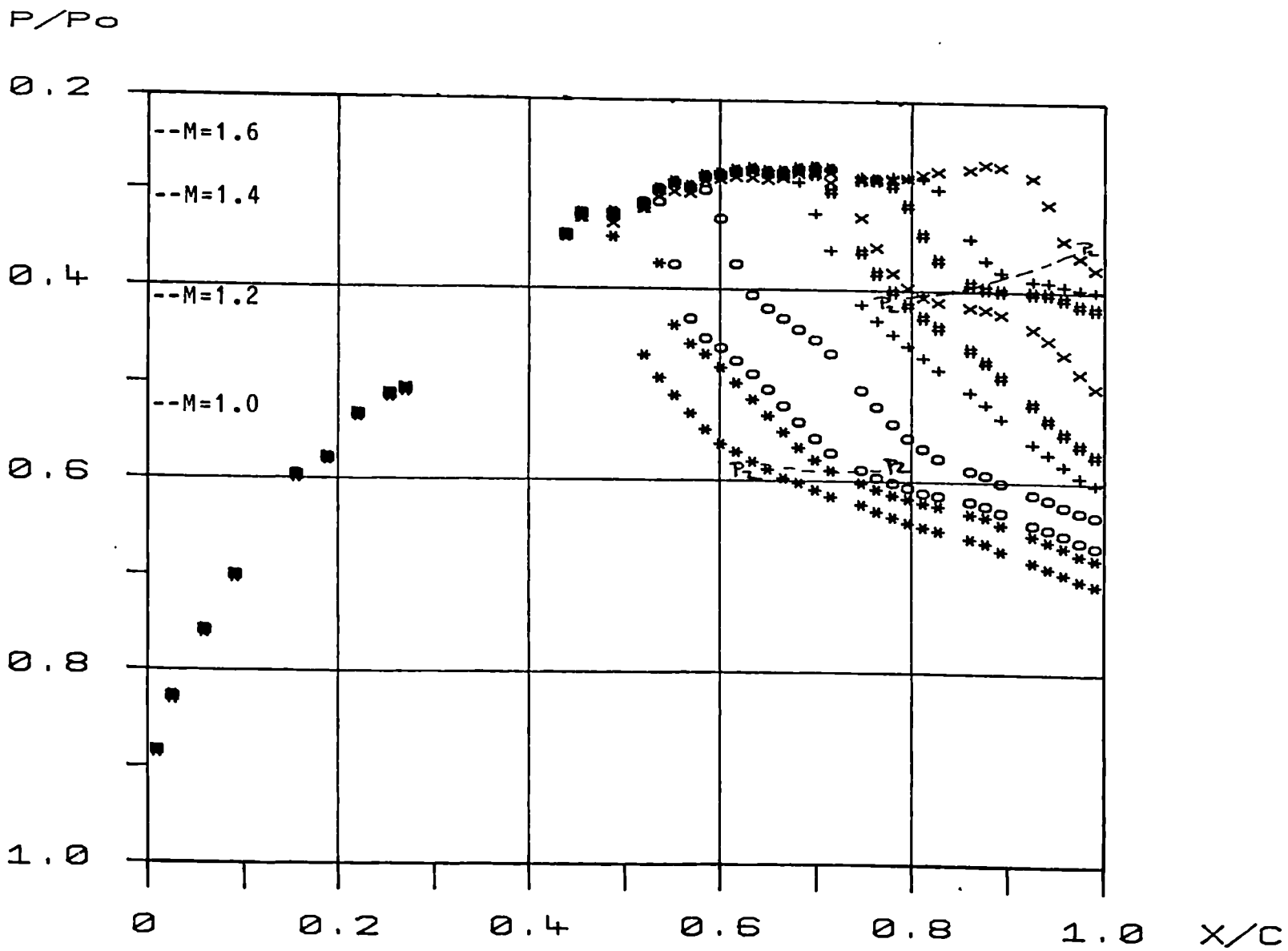

Figure 5.29 Experimental Pressure Distributions for the 10% Bump with Large Air Jet Vortex Generators (θ=60°, P_b/P_o=1.0).

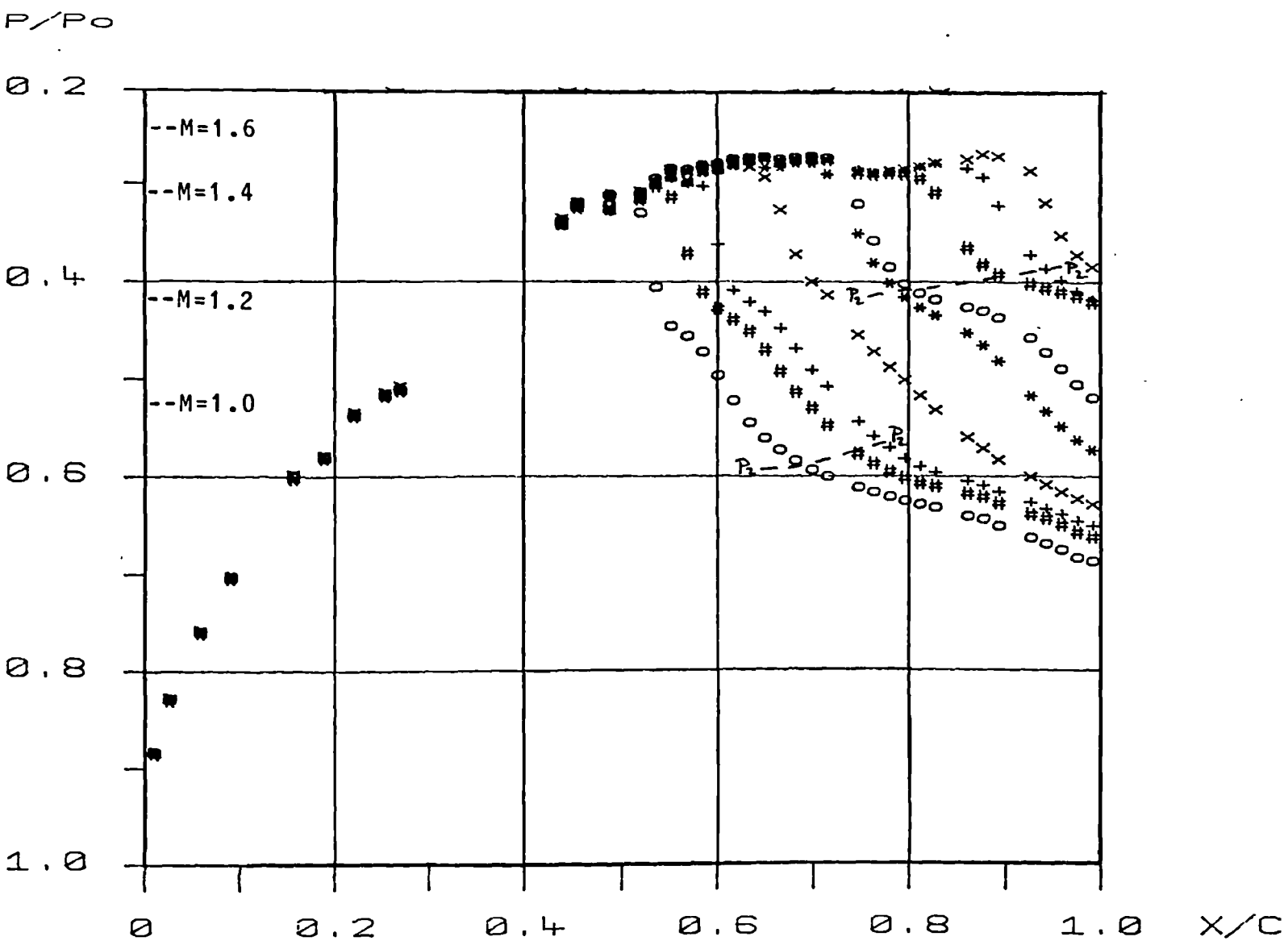

Figure 5.30 Experimental Pressure Distributions for the 10% Bump with Large Air Jet Vortex Generators (θ=60°, P_b/P_o=1.2).

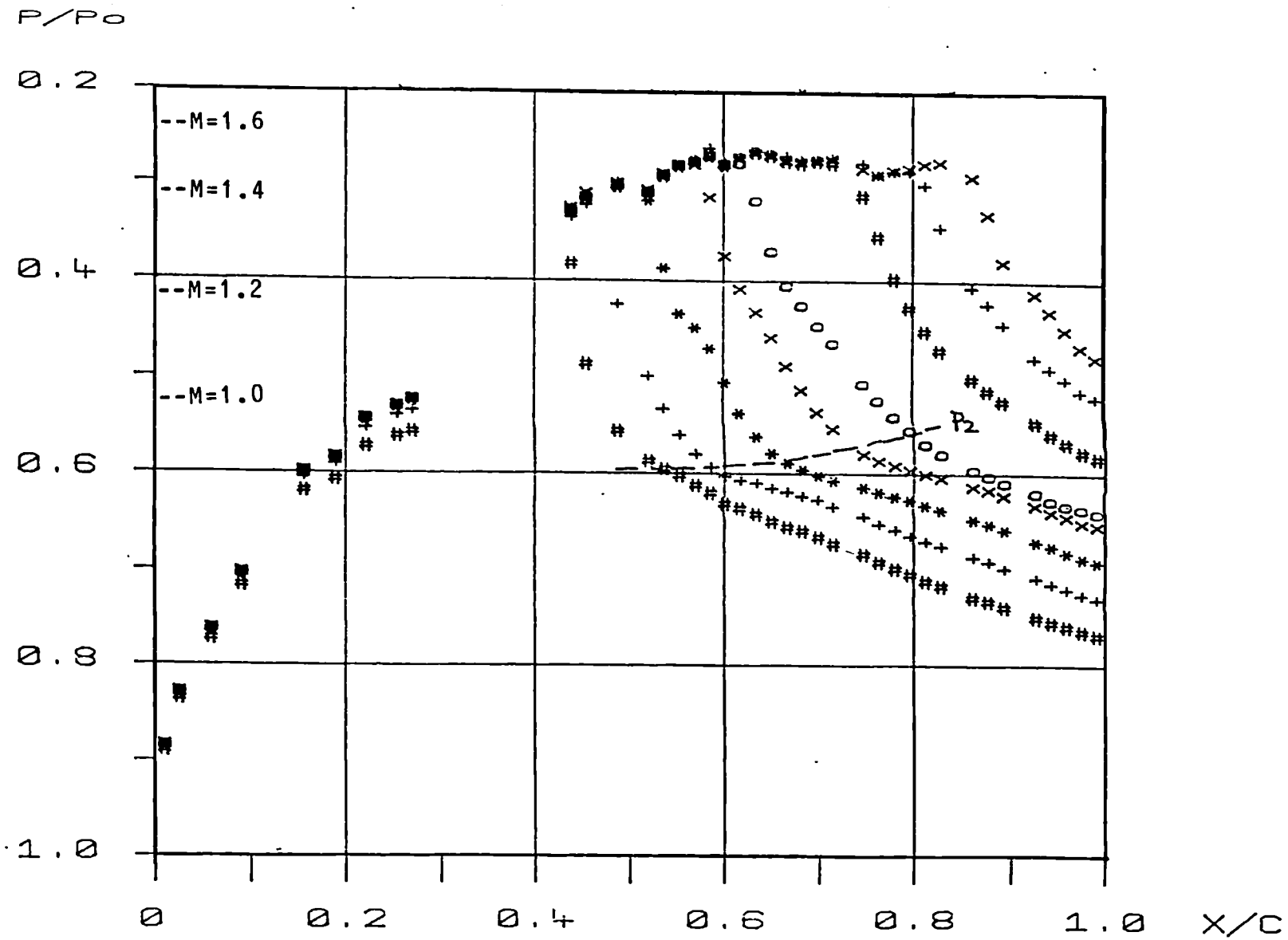

Figure 5.31 Experimental Pressure Distributions for the 10% Bump with Large Air Jet Vortex Generators (θ=60°, P_b/P_o=1.8).

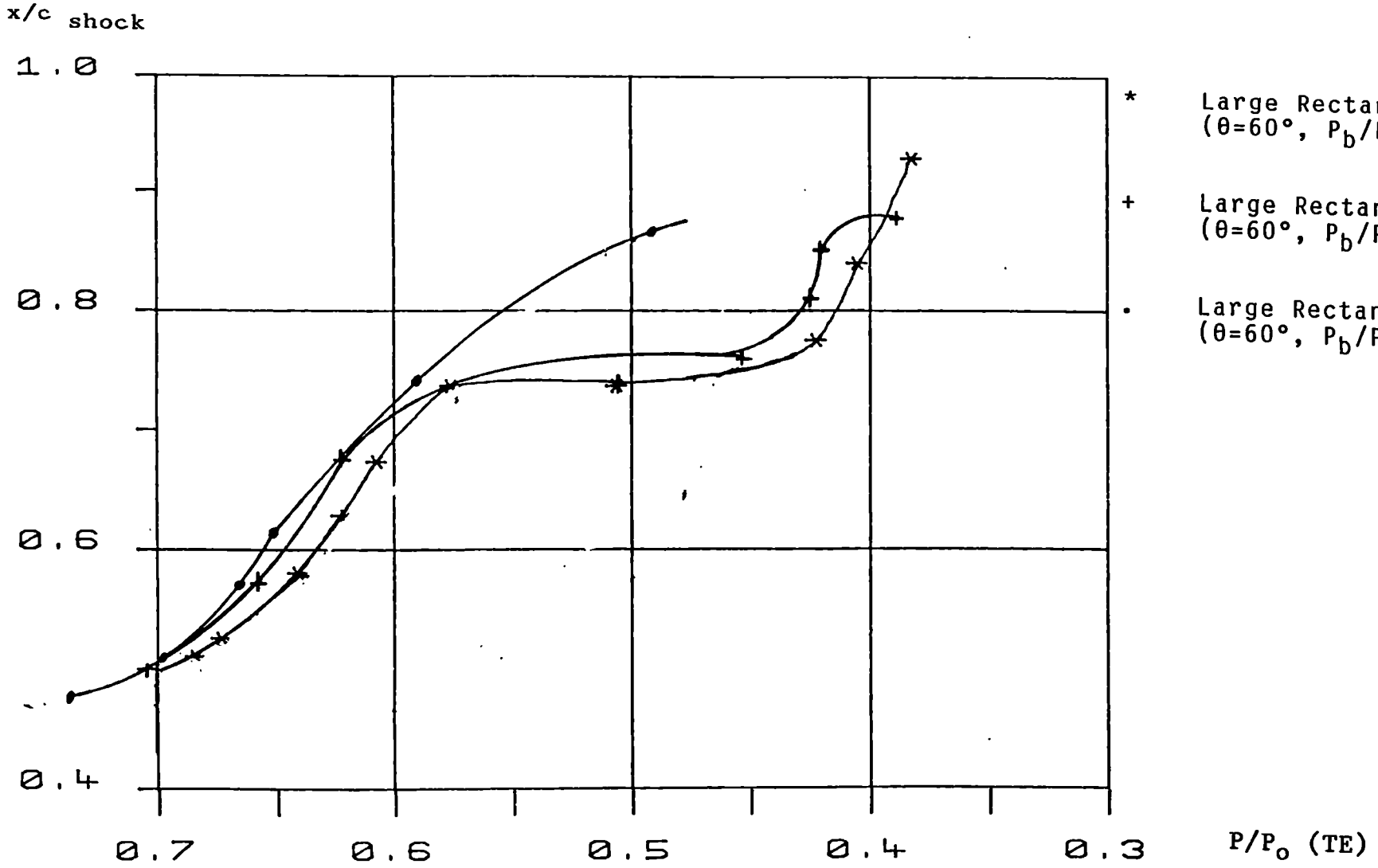

Figure 5.32 Comparison of the Loci of Shock Position Against Trailing Edge Pressure for the 10% Bump.

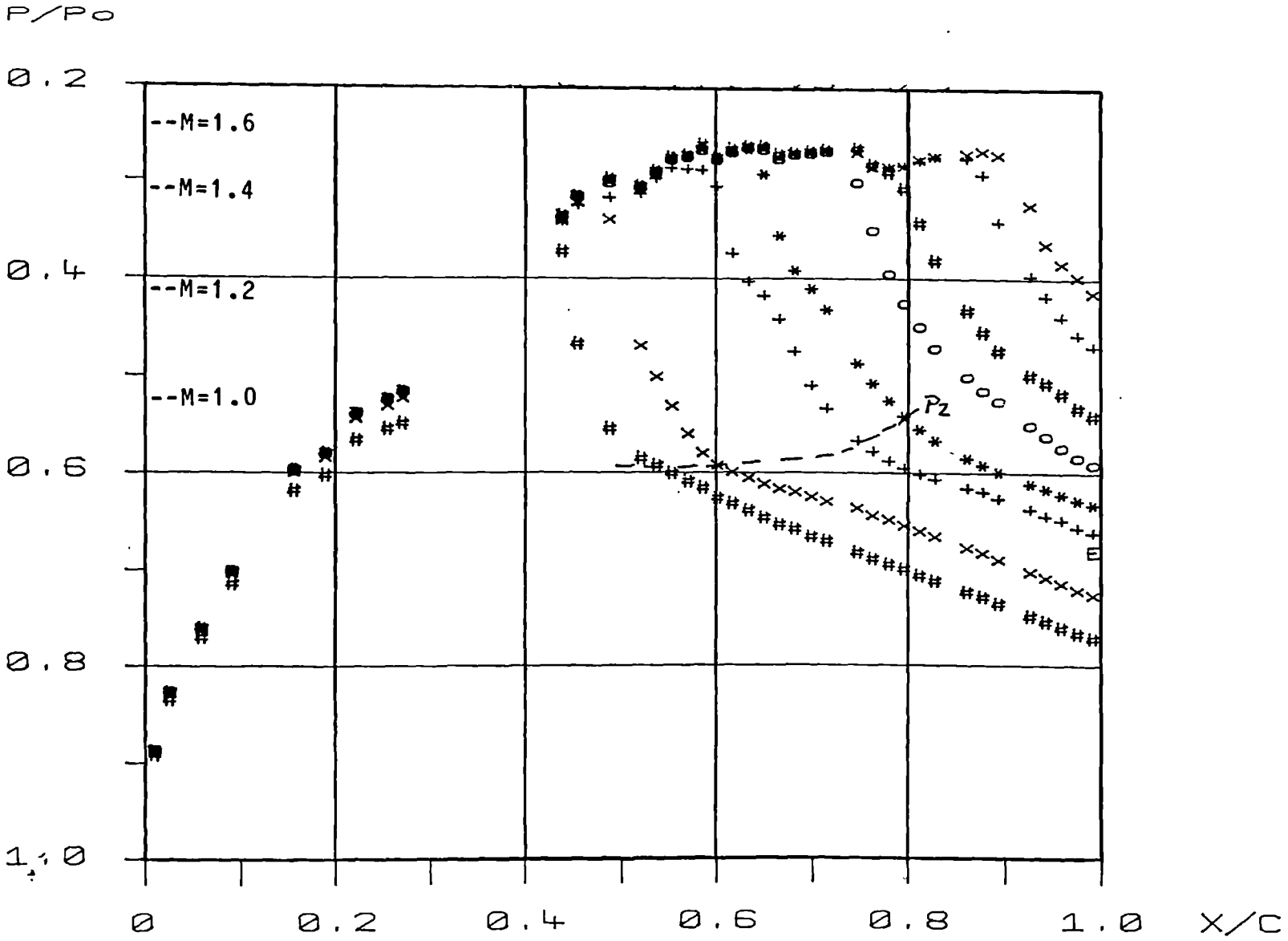

Figure 5.33 Experimental Pressure Distributions for the 10% Bump with Large Air Jet Vortex Generators (θ=45°, P_b/P_o=1.8).

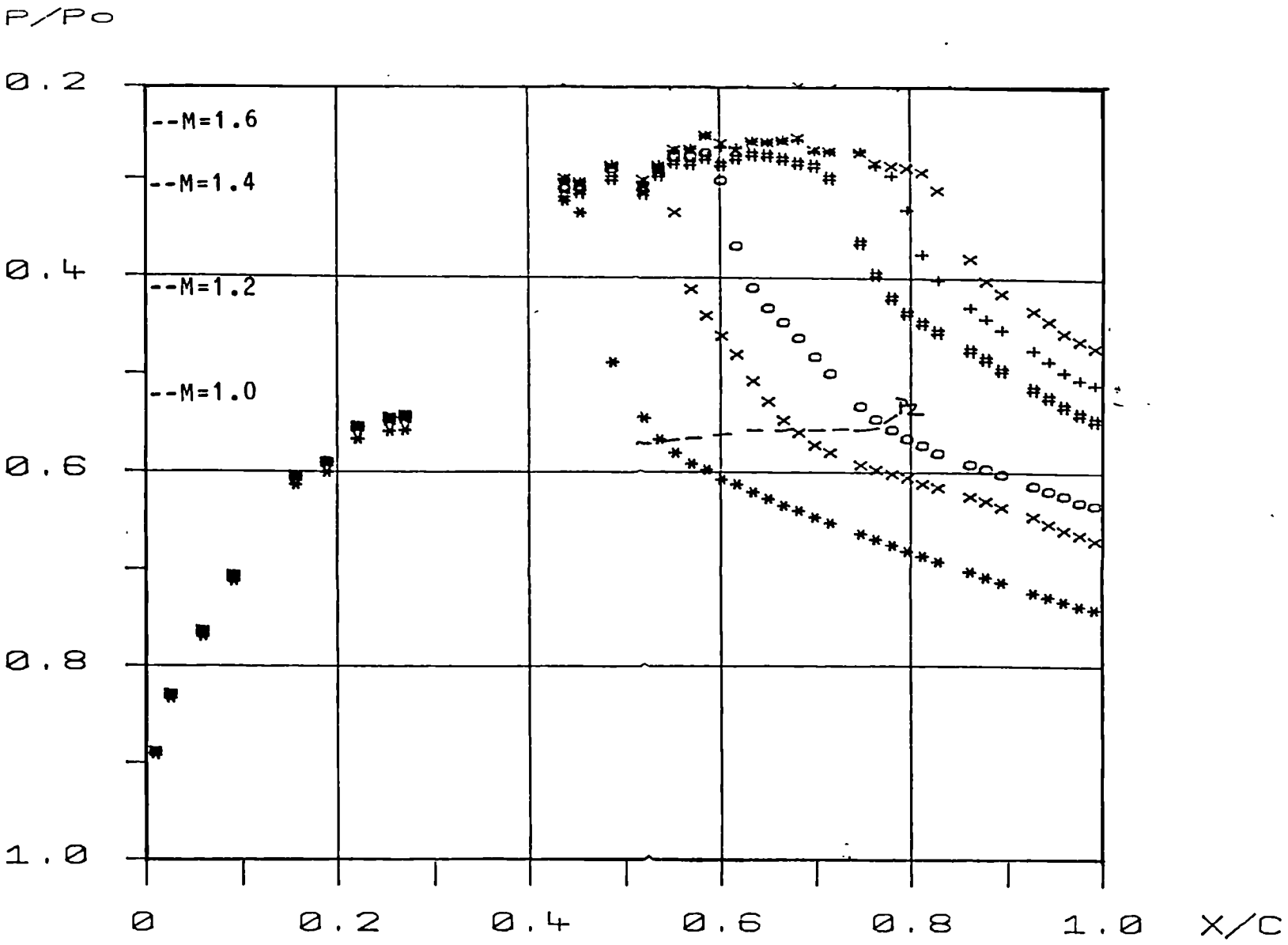

Figure 5.34 Experimental Pressure Distributions for the 10% Bump with Large Air Jet Vortex Generators (θ=75°, P_b/P_o=1.8).

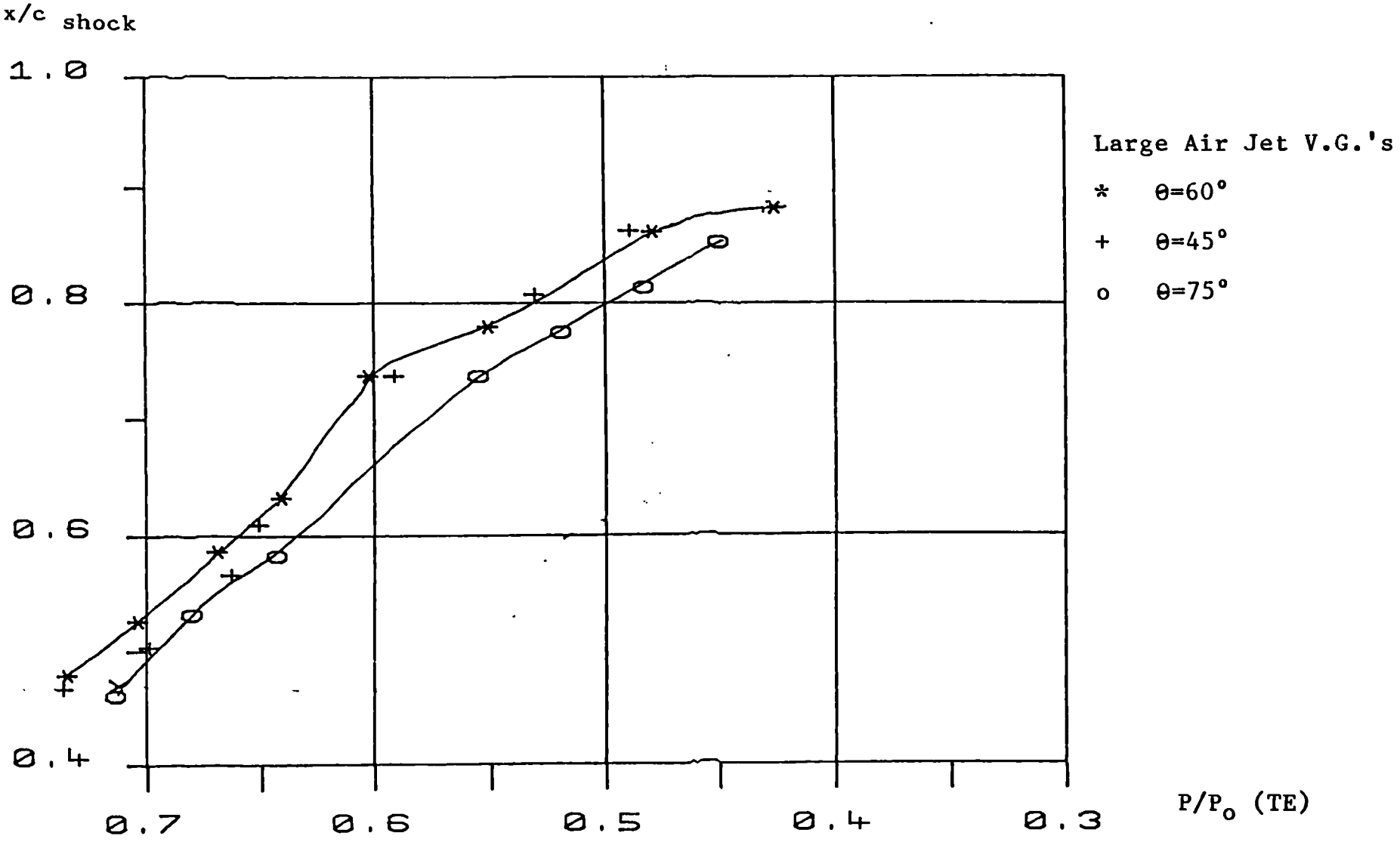

Figure 5.35 Comparison of the Loci of Shock Position Against Trailing Edge Pressure for the 10% Bump.

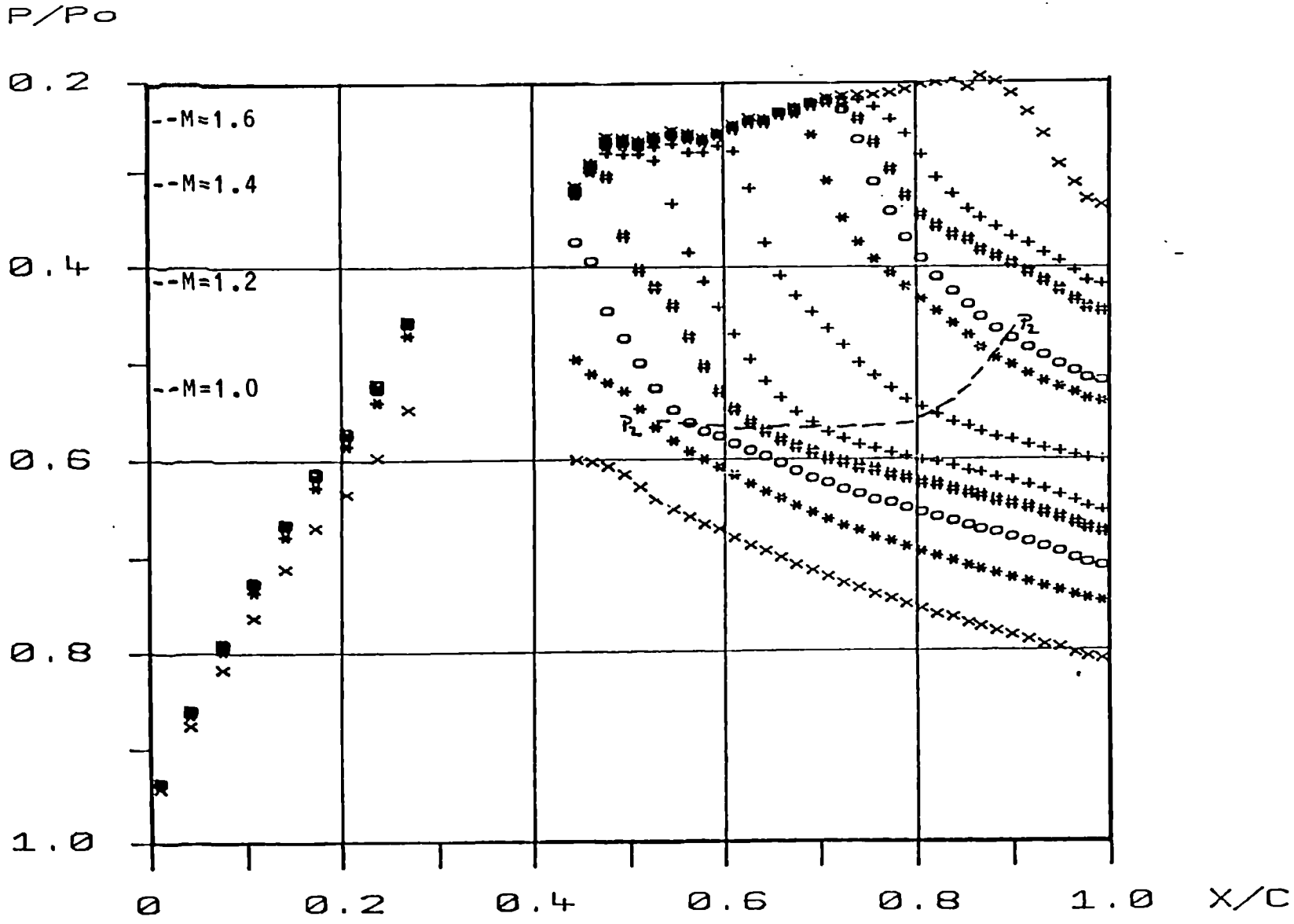

Figure 5.36 Experimental Pressure Distributions for the 14% Bump with Large Air Jet Vortex Generators (θ=60°, P_b/P_o=1.2).

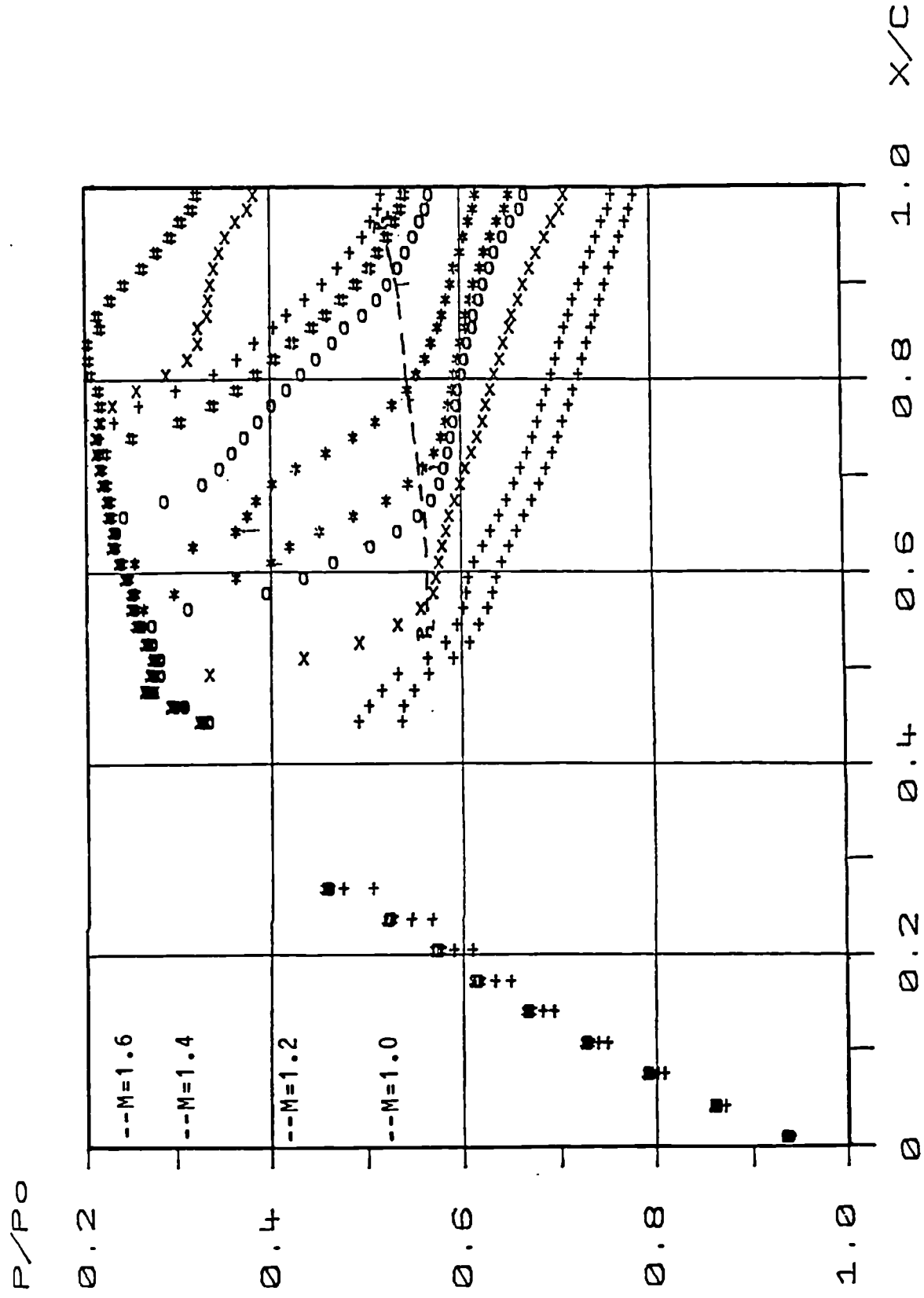

Figure 5.37 Experimental Pressure Distributions for the 14% Bump with Large Air Jet Vortex Generators (θ=60°, P_b/P_o=1.5).

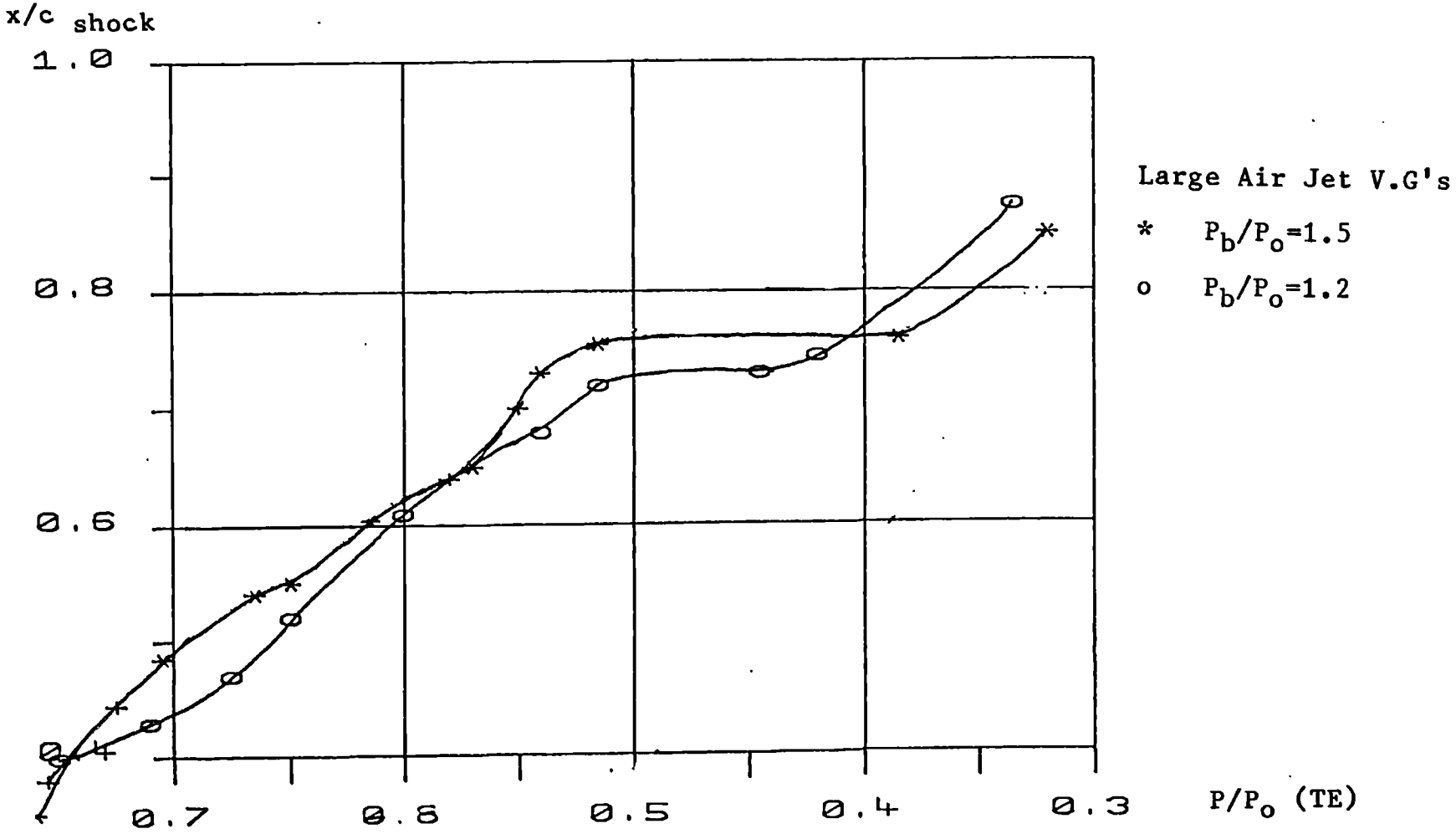

Figure 5.38 Comparison of the Loci of Shock Position Against Trailing Edge Pressure for the 14% Bump.

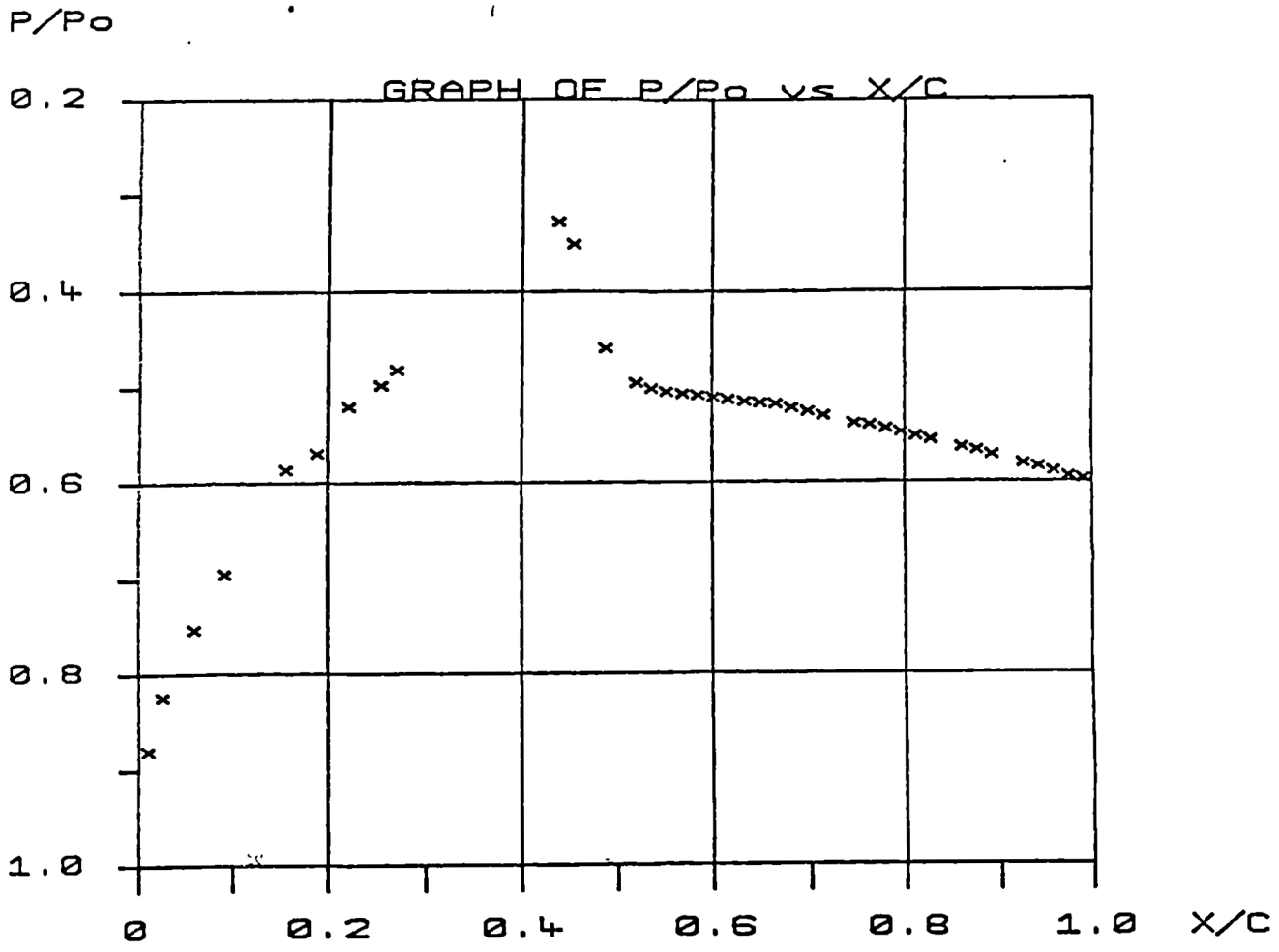

Figure 5.39 Experimental Pressure Distribution with Corresponding Schlieren Image for the 10% Bump with No Vortex Generators.

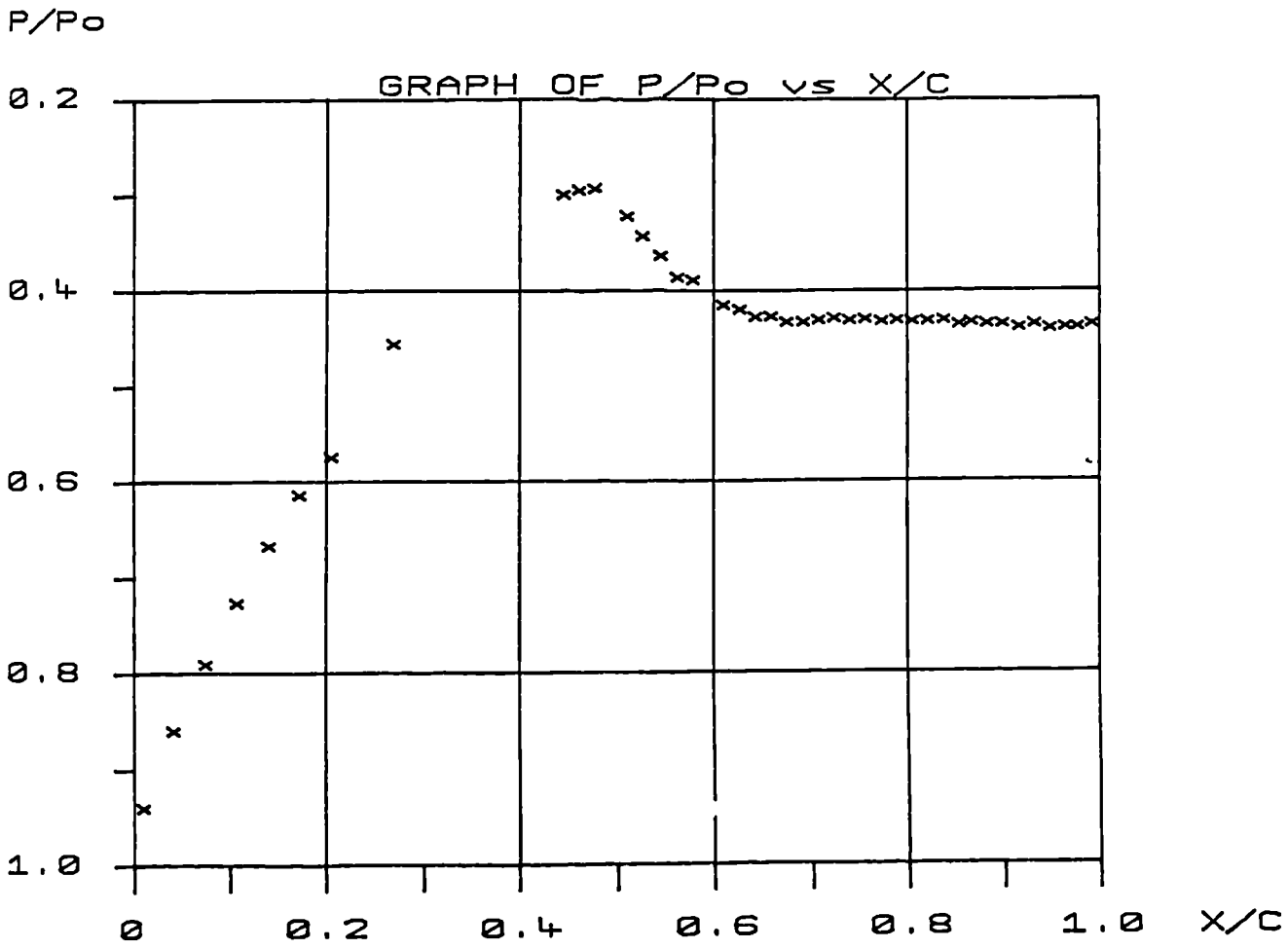

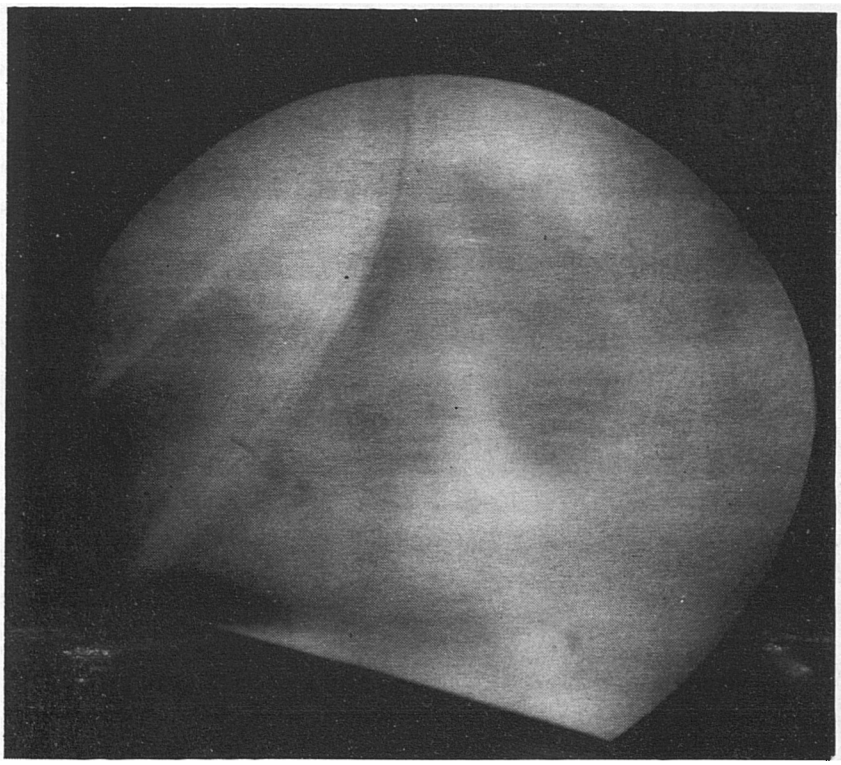

Figure 5.40 Experimental Pressure Distributions with Corresponding Schlieren Image for the 14% Bump with No Vortex Generators.

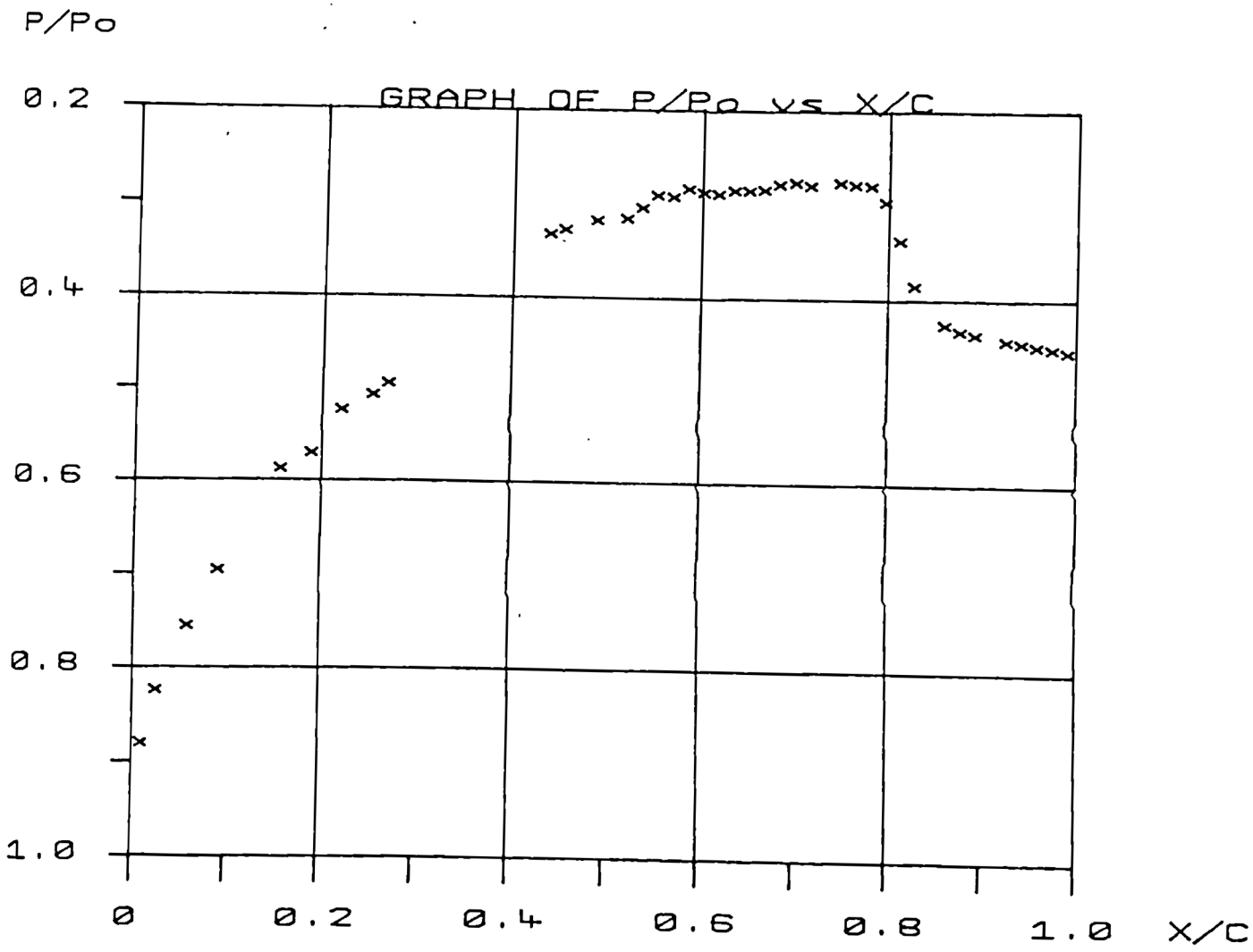

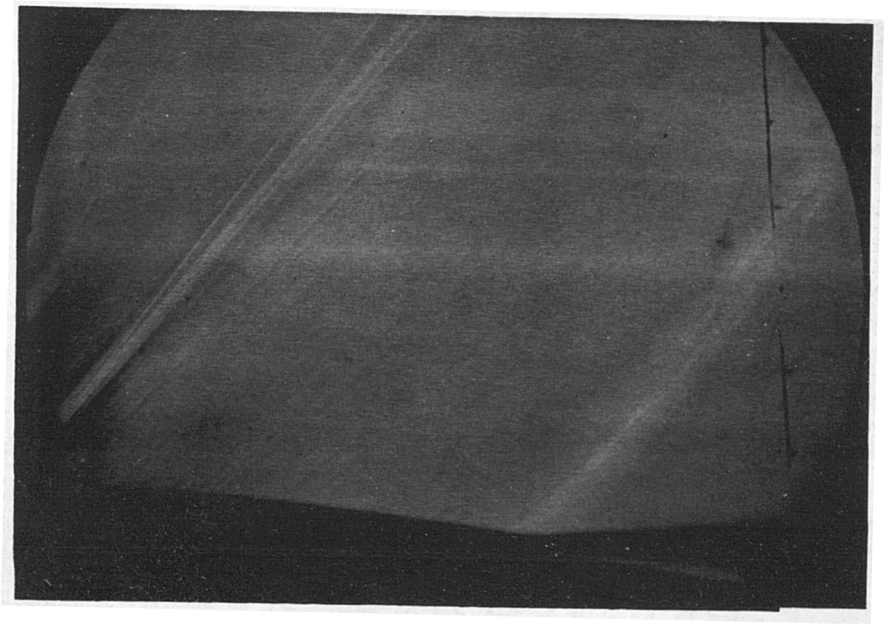

Figure 5.41 Experimental Pressure Distribution with Corresponding Schlieren Image for the 10% Bump with No Vortex Generators.

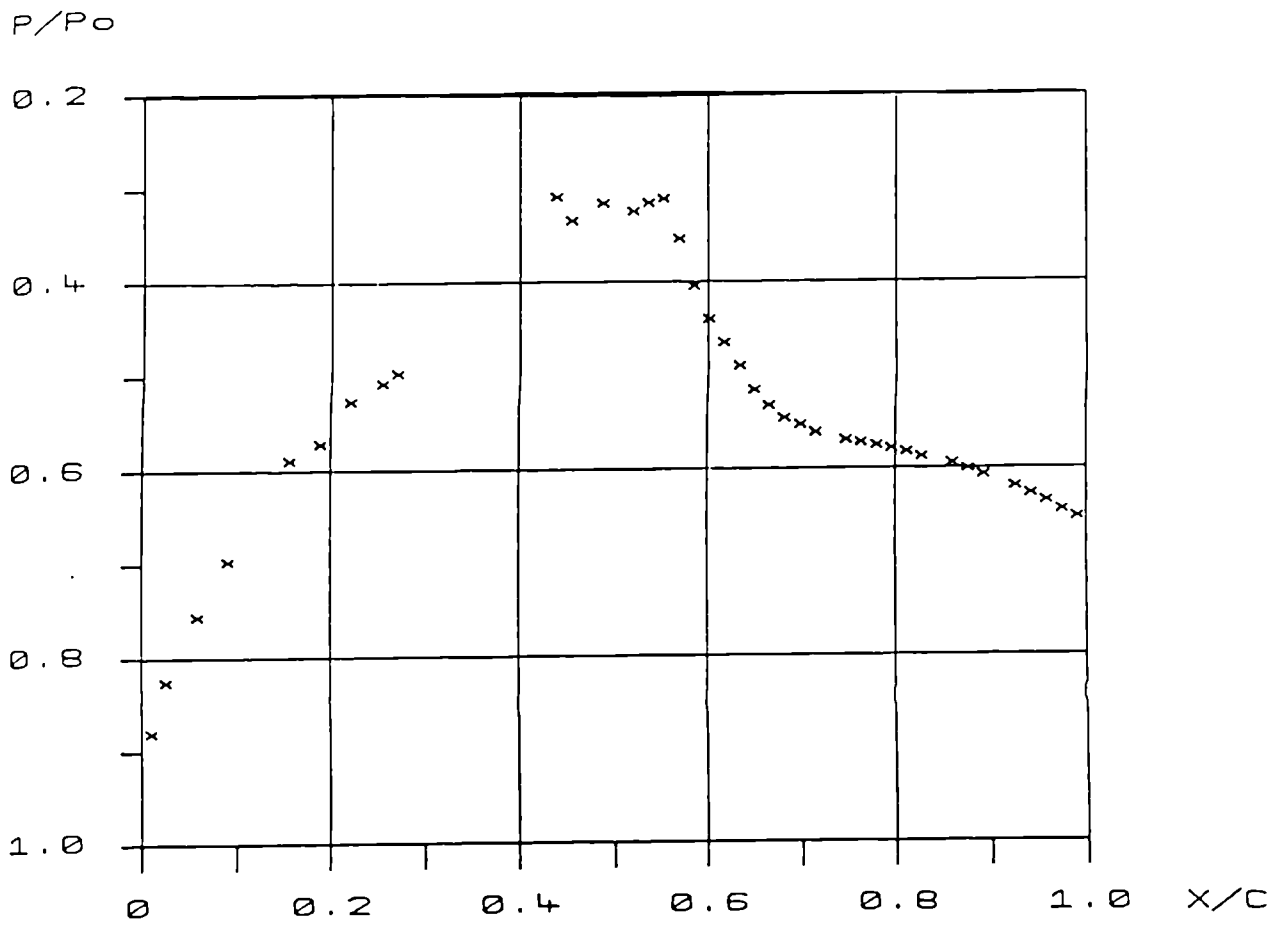

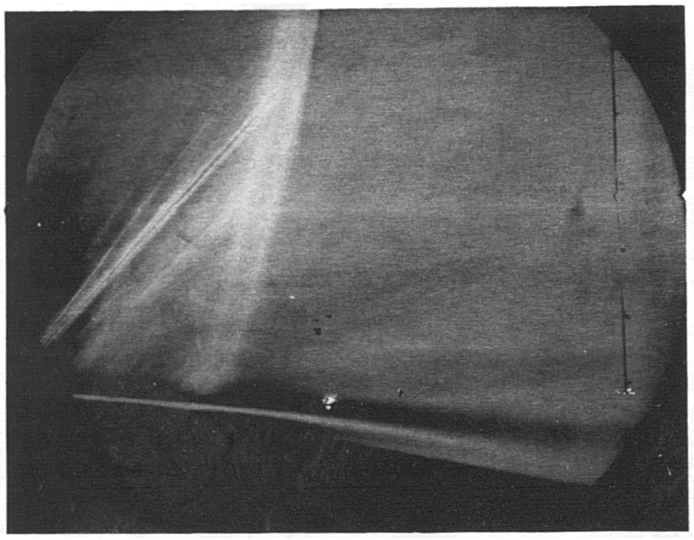

Figure 5.43 Experimental Pressure Distribution with *Corresponding* Schlieren Image for the 10% Bump with Vane Vortex Generators.

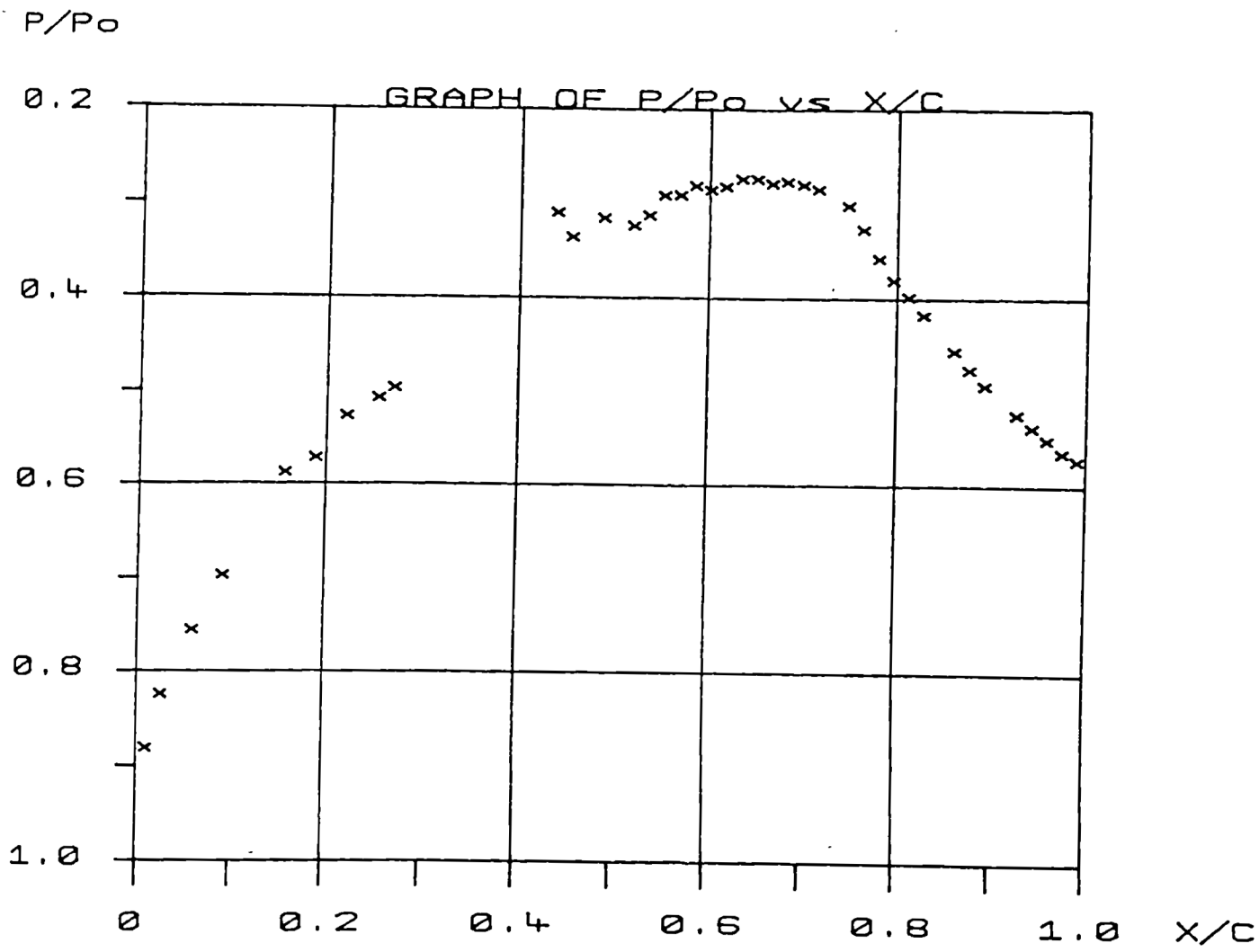

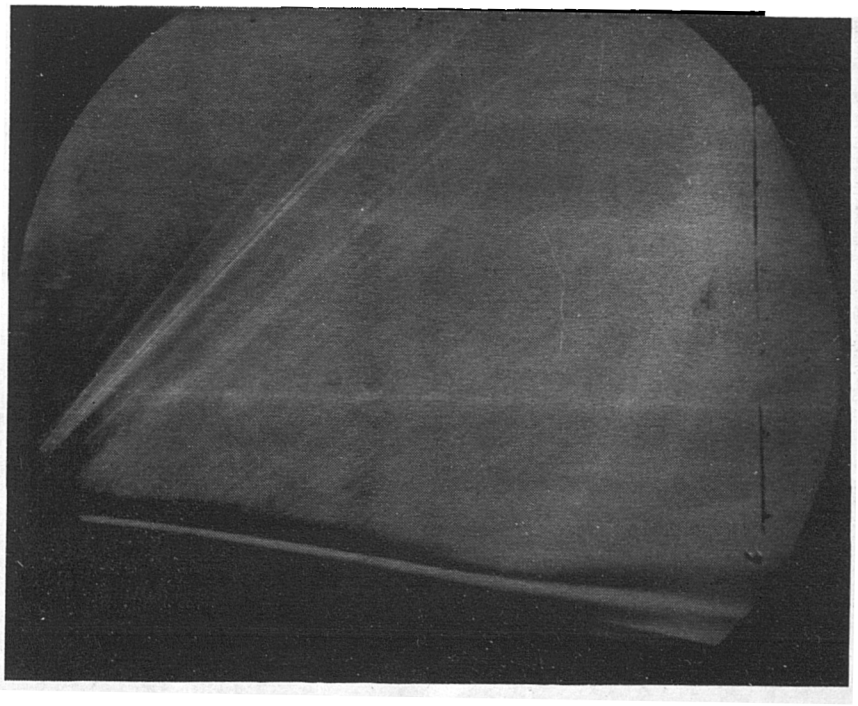

Figure 5.44 Experimental Pressure Distribution with Corresponding Schlieren Image for the 10% Bump with Vane Vortex Generators.

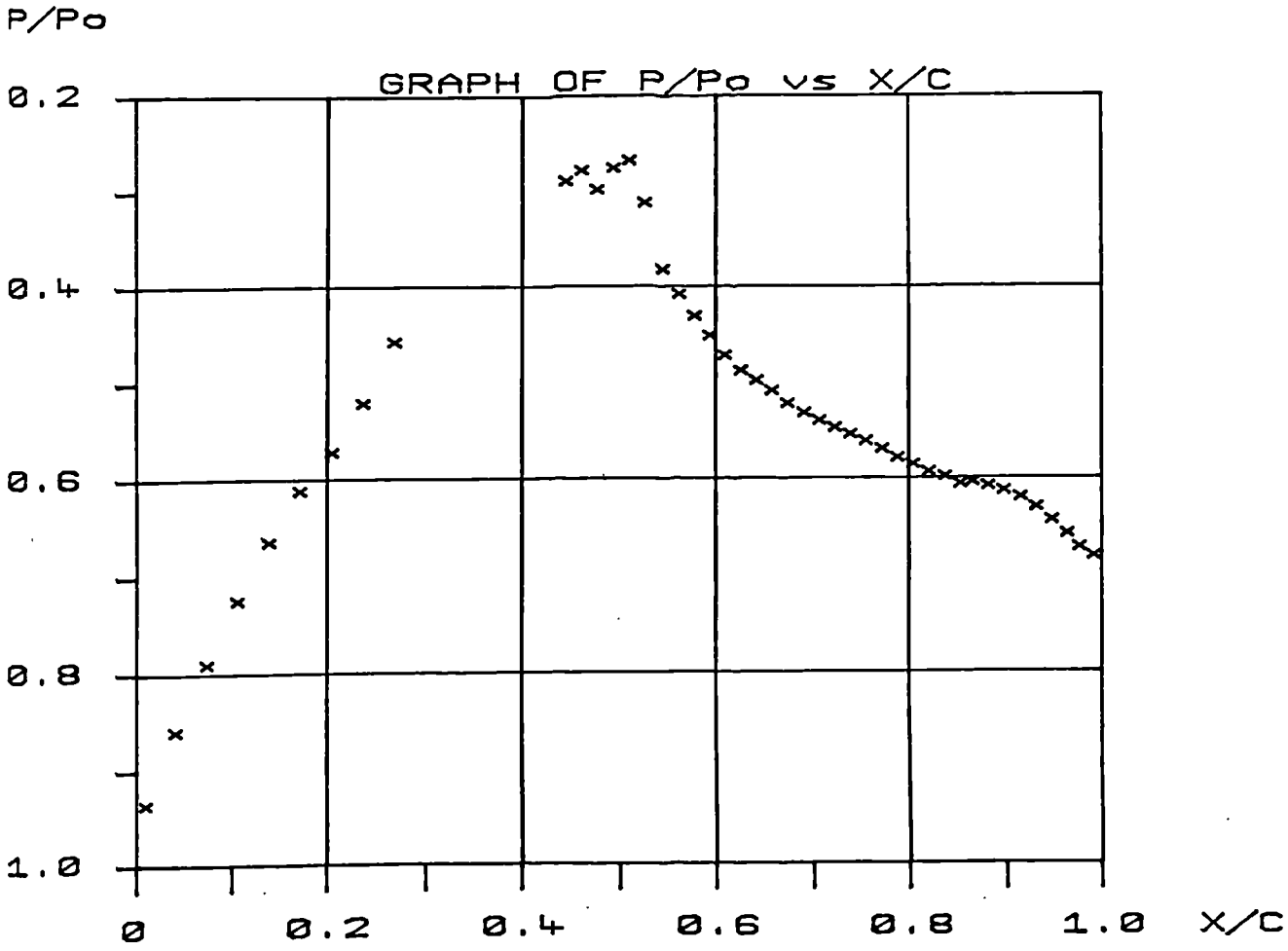

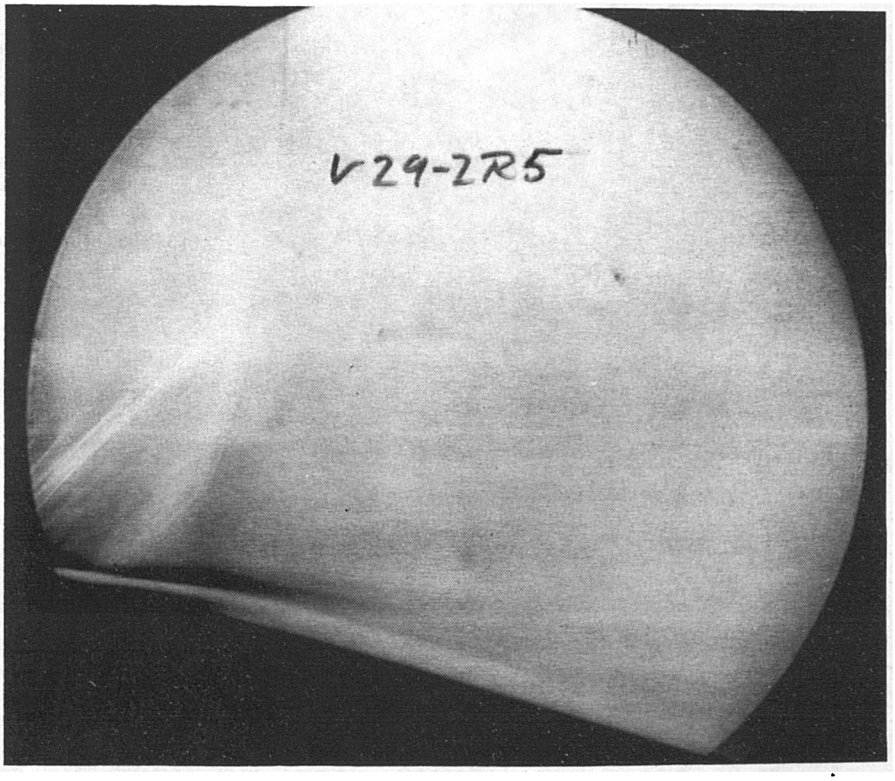

Figure 5.45 Experimental Pressure Distributions with Corresponding Schlieren Image for the 14% Bump with Vane Vortex Generators.

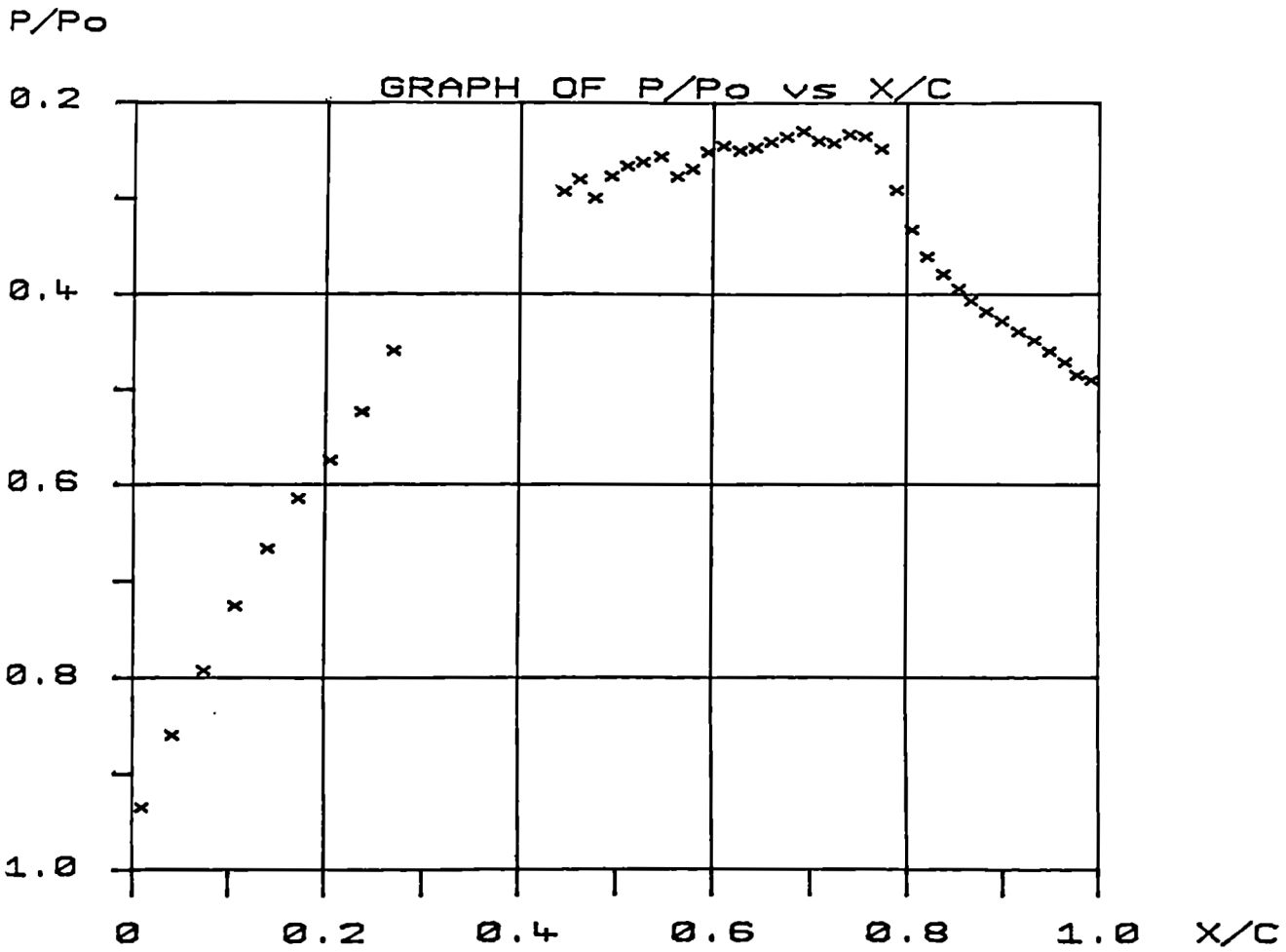

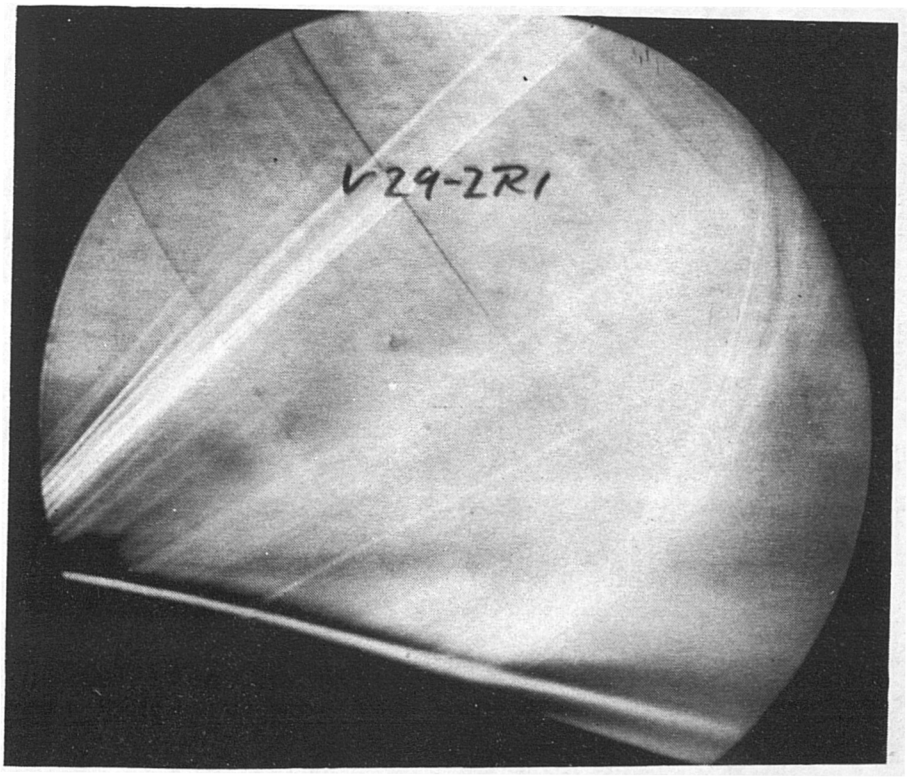

Figure 5.46 Experimental Pressure Distributions with Corresponding Schlieren Image for the 14% Bump with Vane Vortex Generators

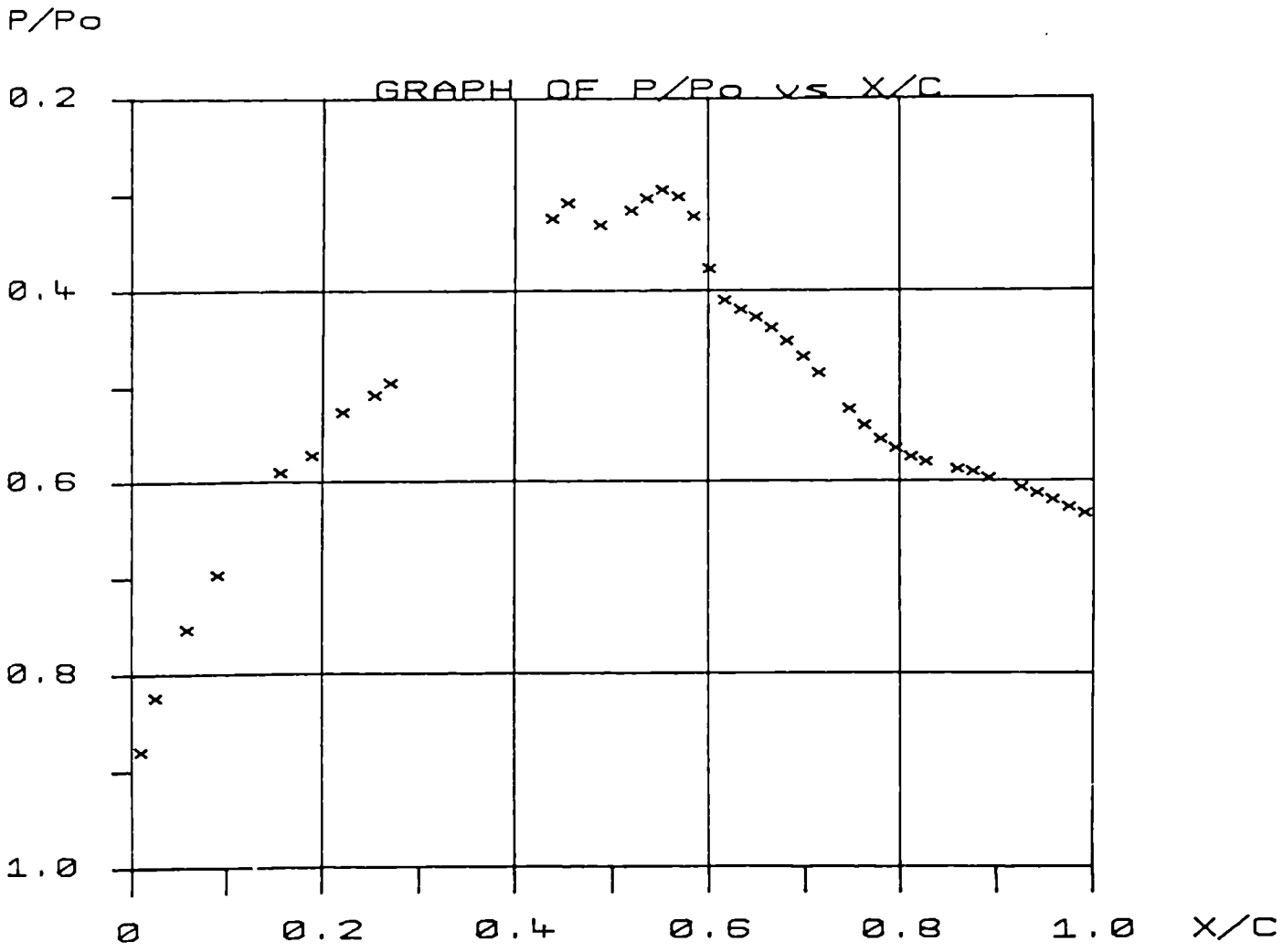

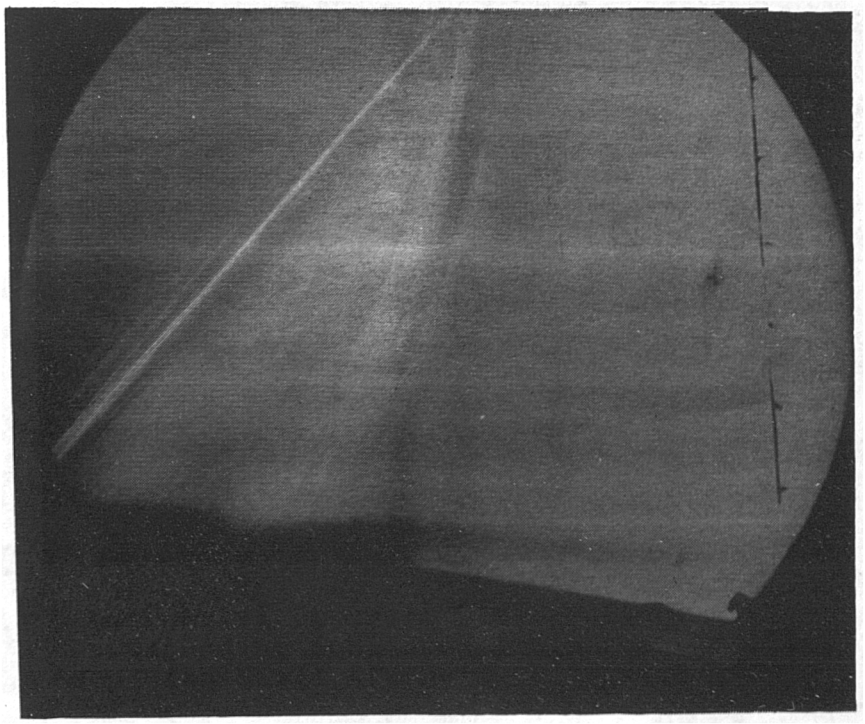

Figure 5.47 Experimental Pressure Distributions with Corresponding Schlieren Image for the 10% Bump with Small Air Jets (P_b/P_o=1.2

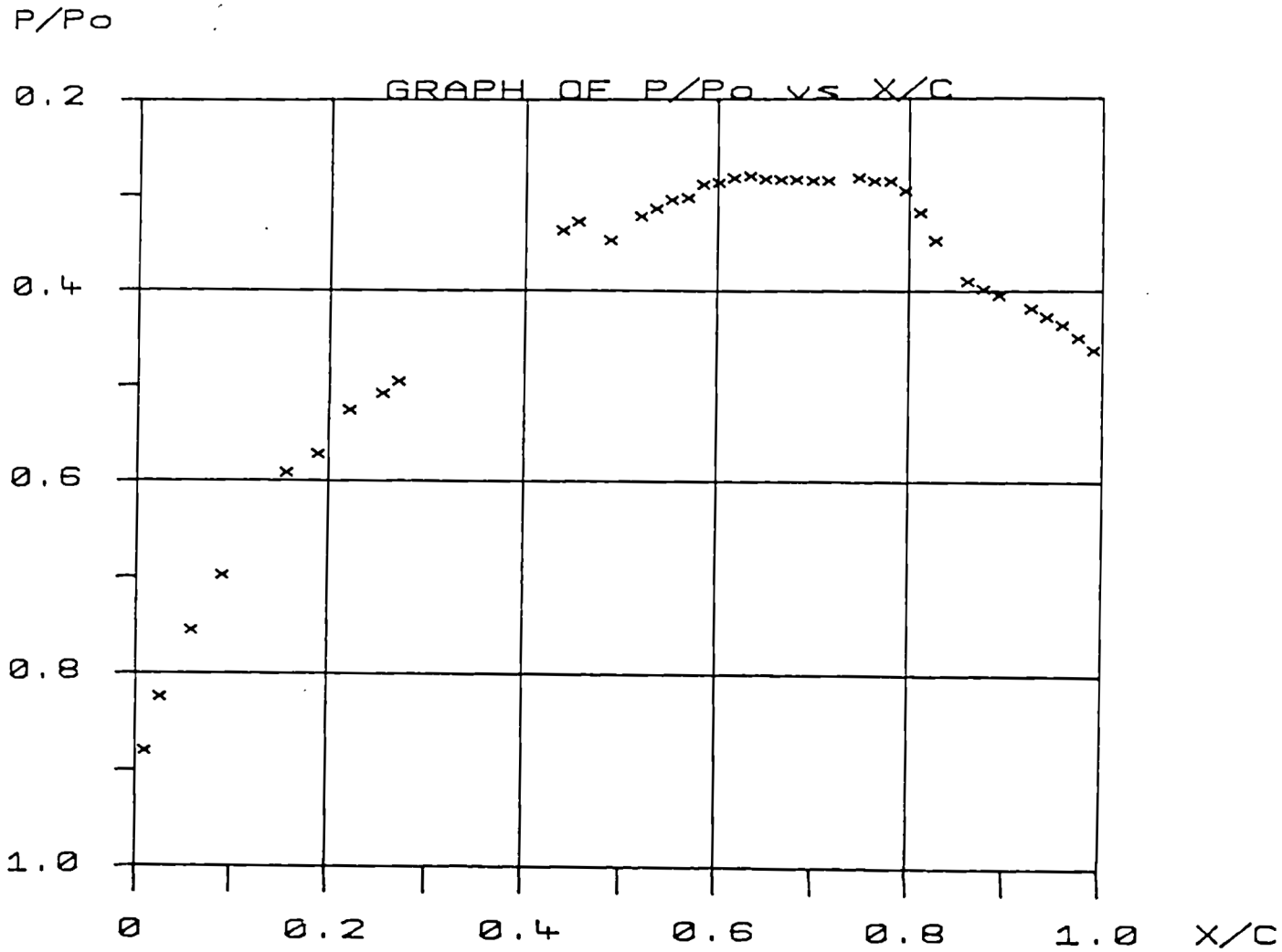

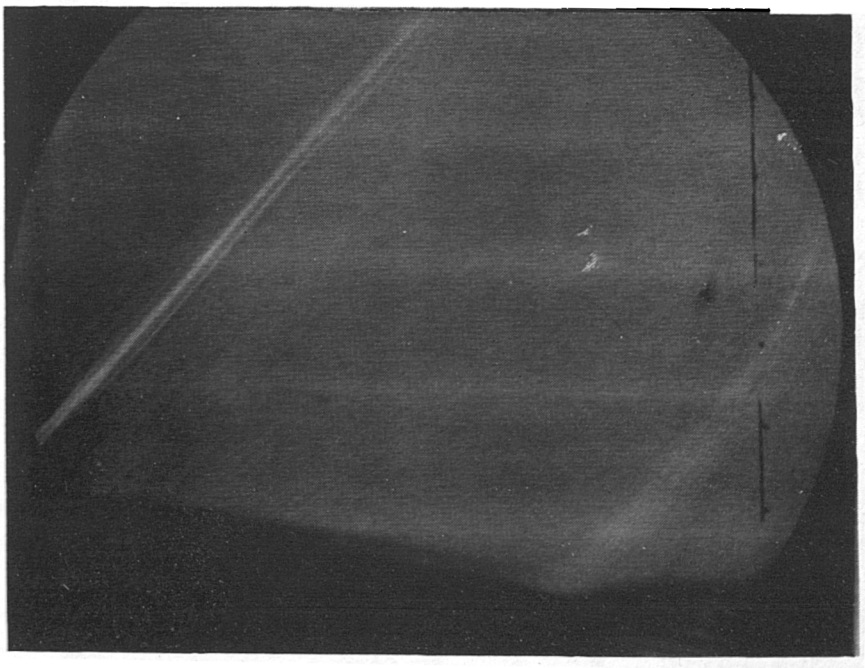

Figure 5.48 Experimental Pressure Distributions with Corresponding Schlieren Image for the 10% Bump with Small Air Jets (P_b/P_o=1.2)

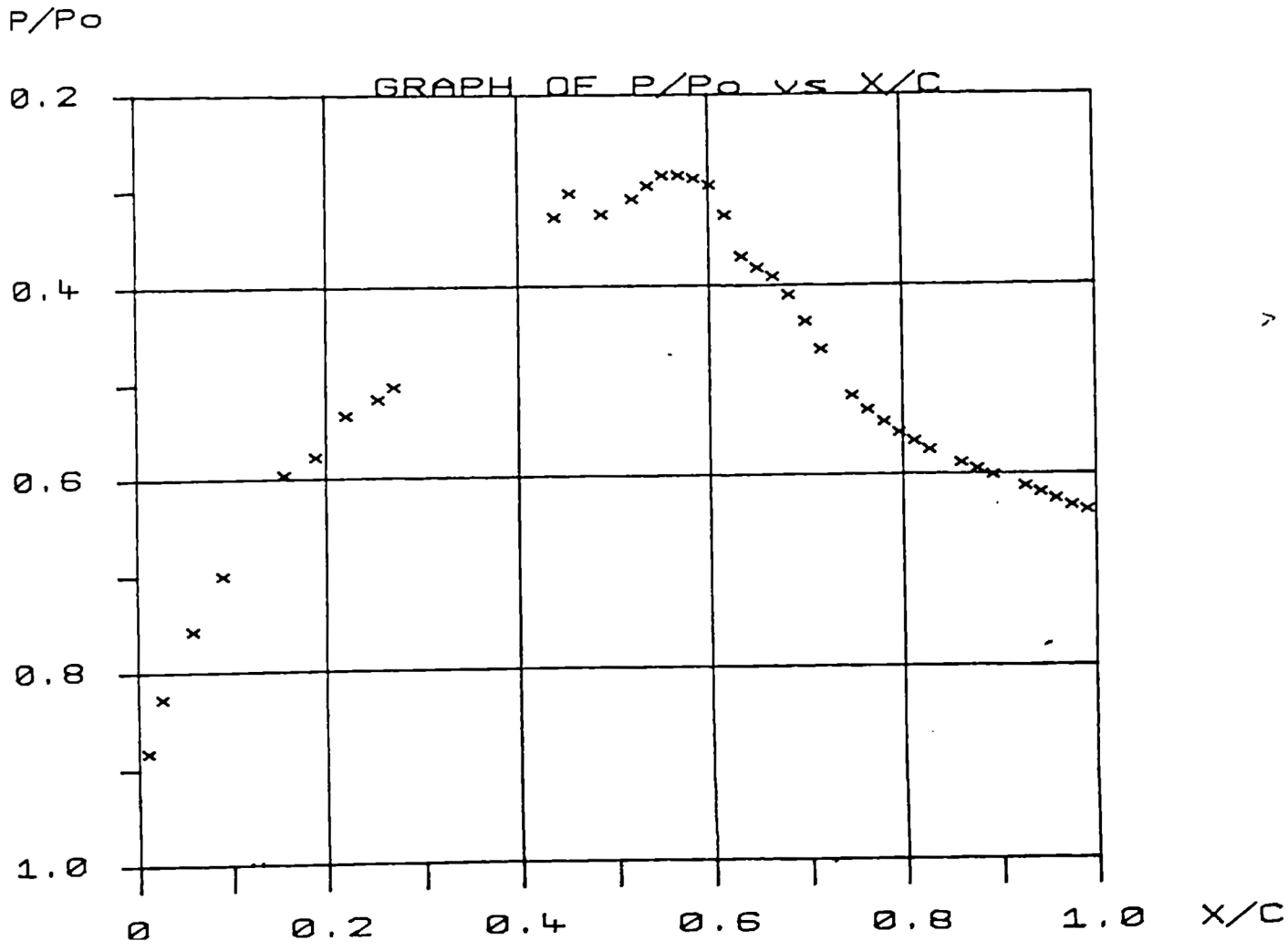

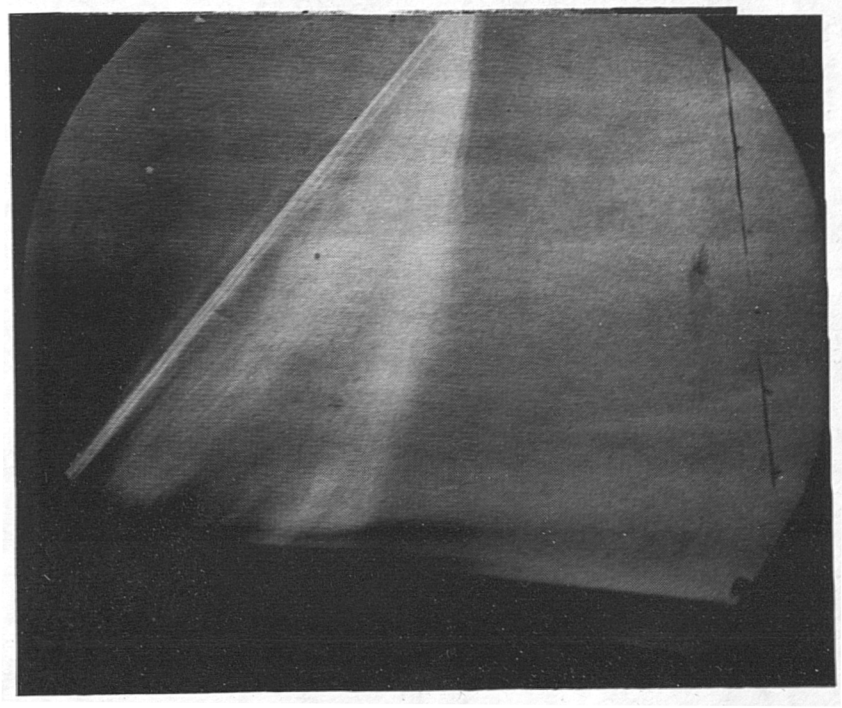

Figure 5.49 Experimental Pressure Distributions with Corresponding Schlieren Image for the 10% Bump with Small Air Jets (P_b/P_o=1.6

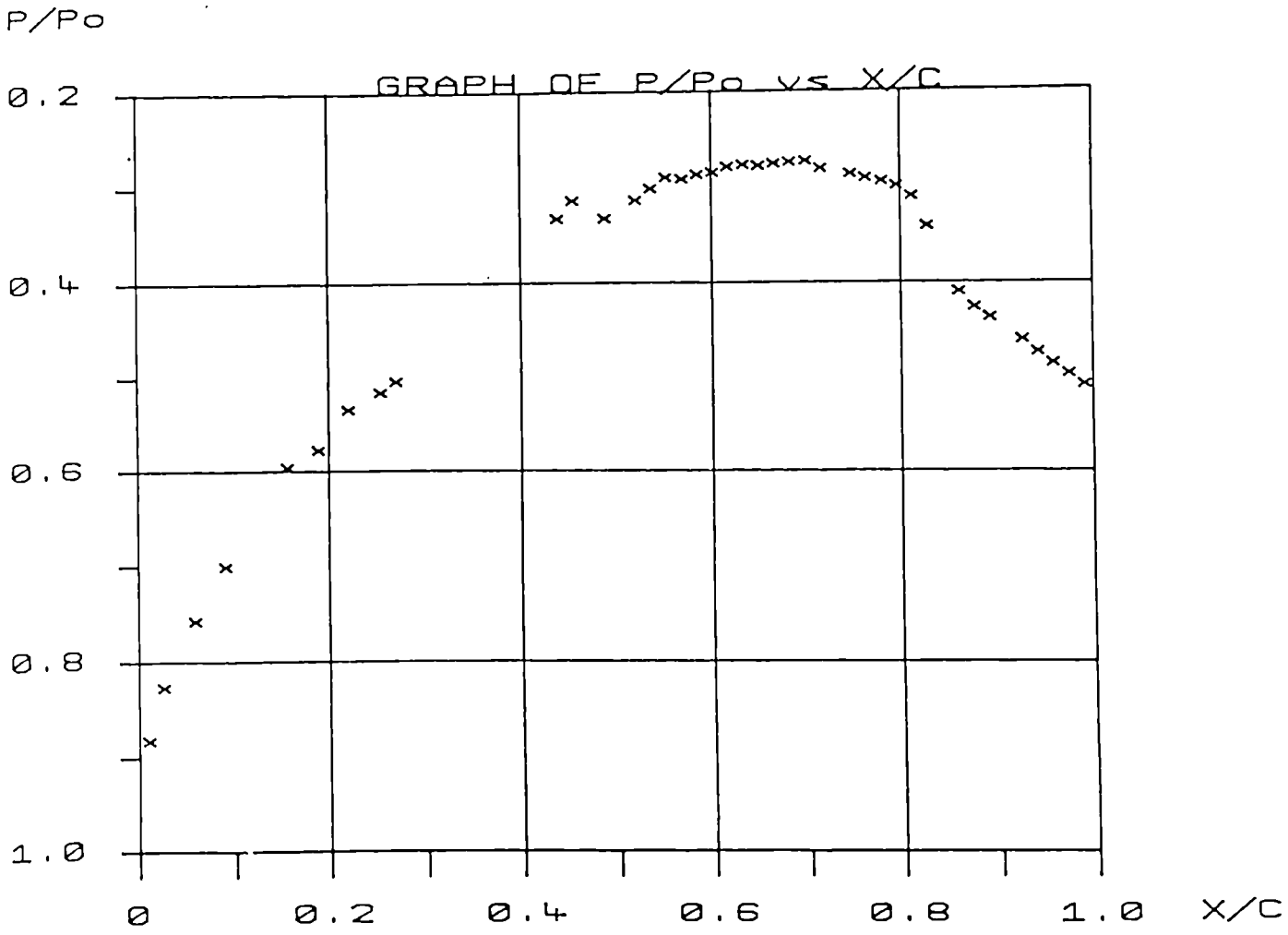

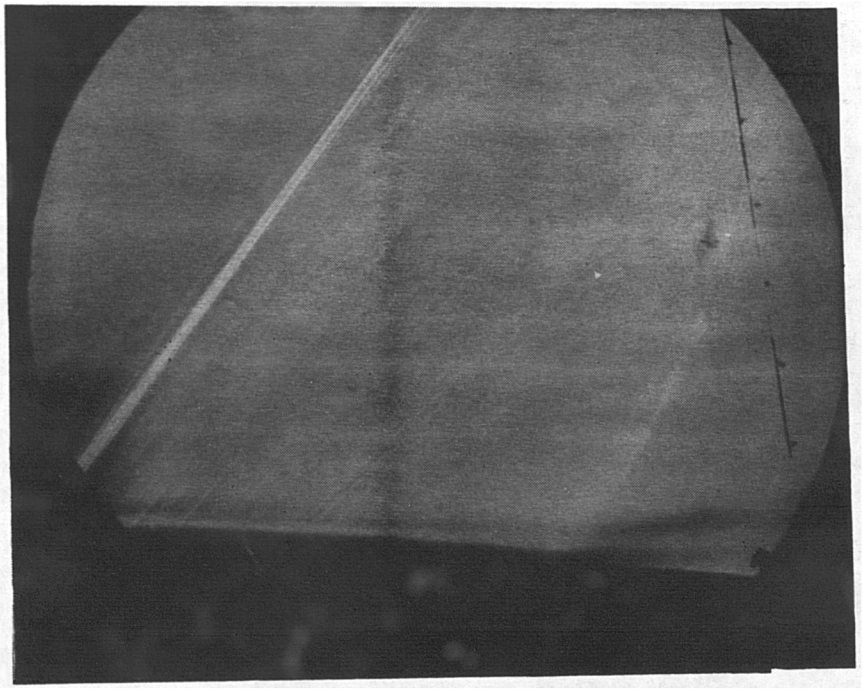

Figure 5.50 Experimental Pressure Distributions with Corresponding Schlieren Image for the 10% Bump with Small Air Jets (P_b/P_o=1.6

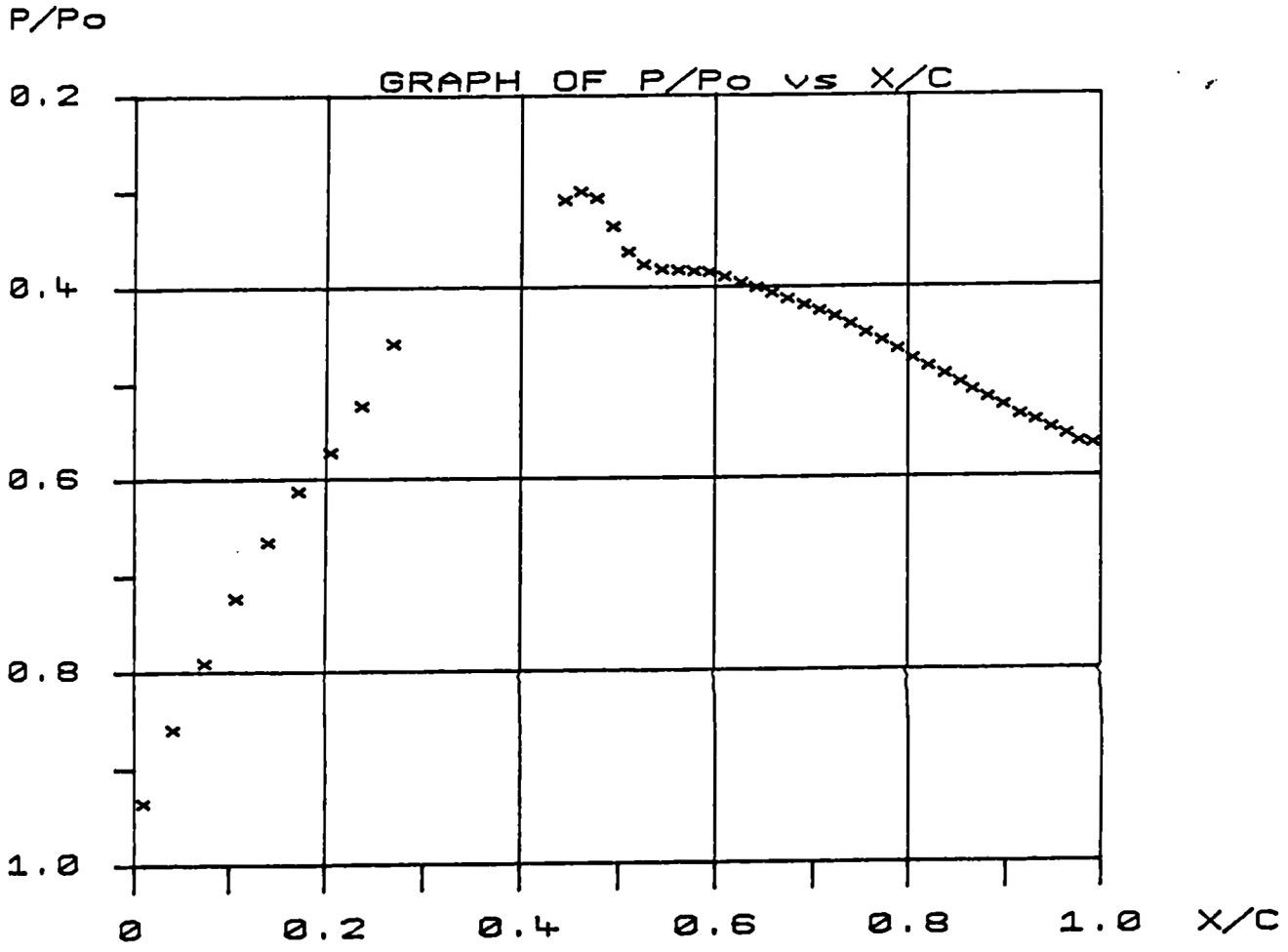

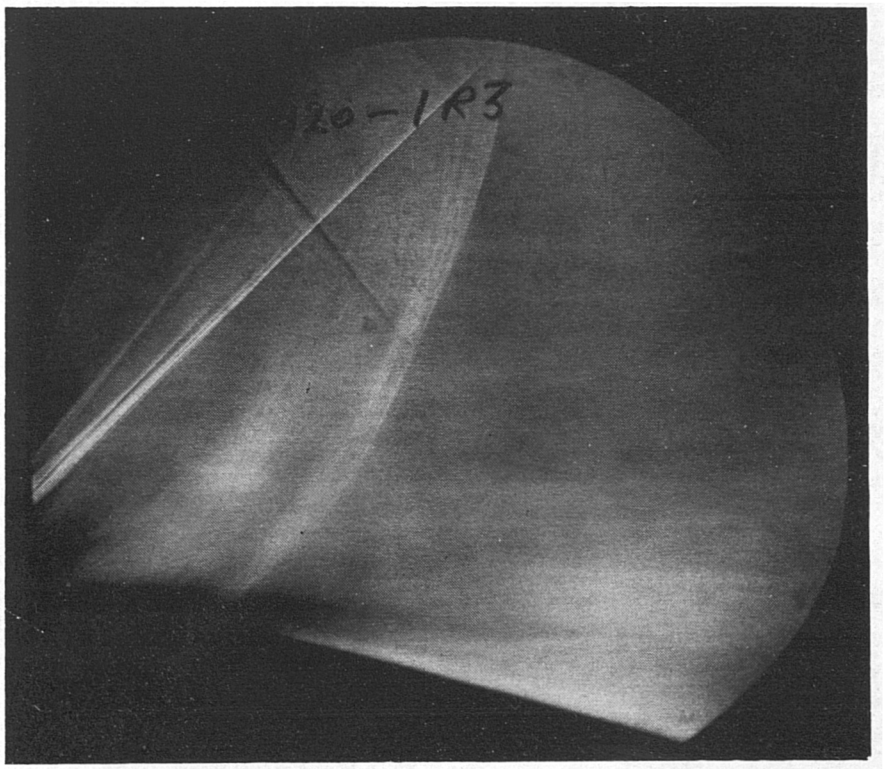

Figure 5.51 Experimental Pressure Distributions with Corresponding Schlieren Image for the 14% Bump with Small Air Jets (ϕ=30°, P_b/P_o=1.2).

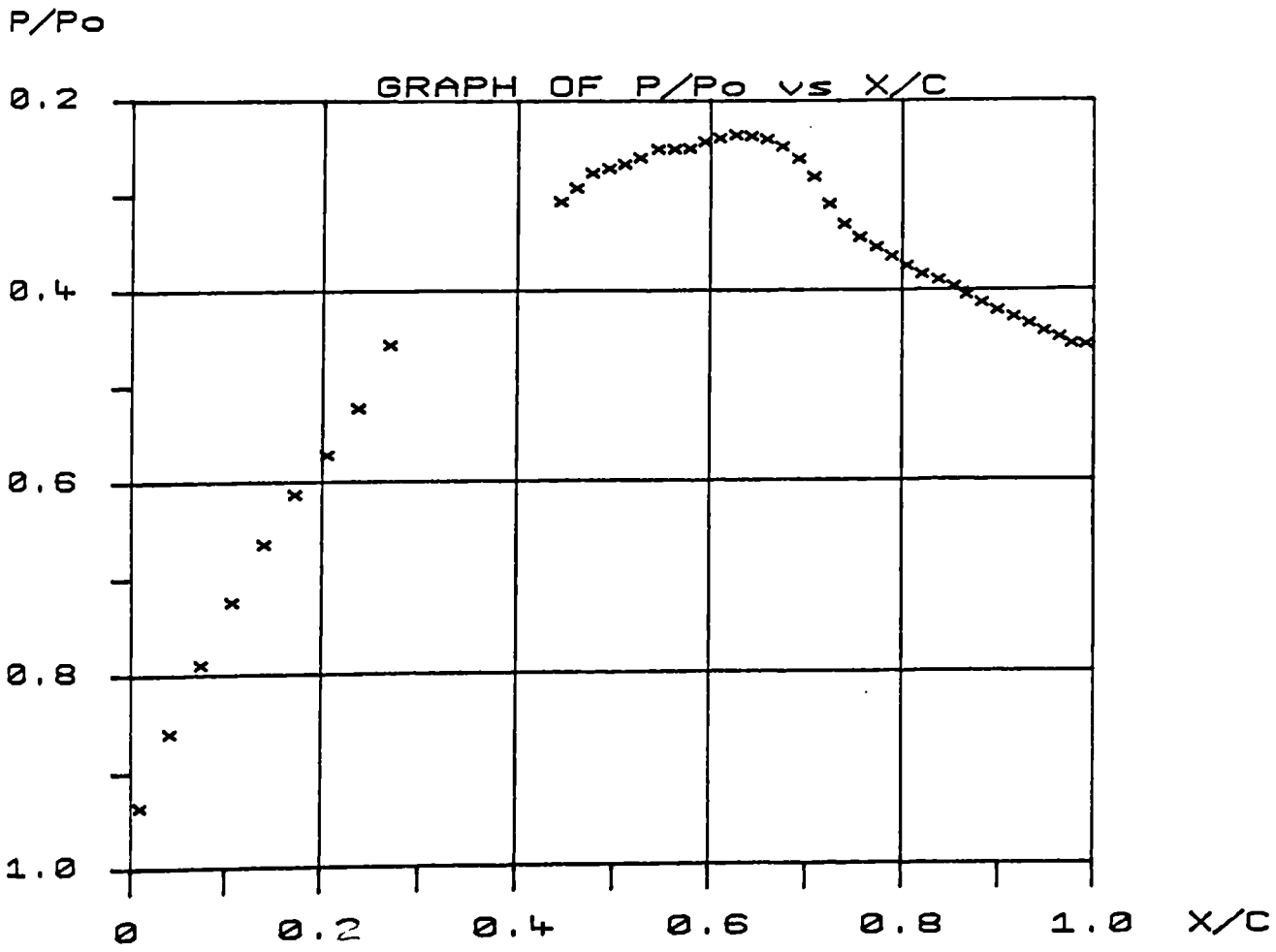

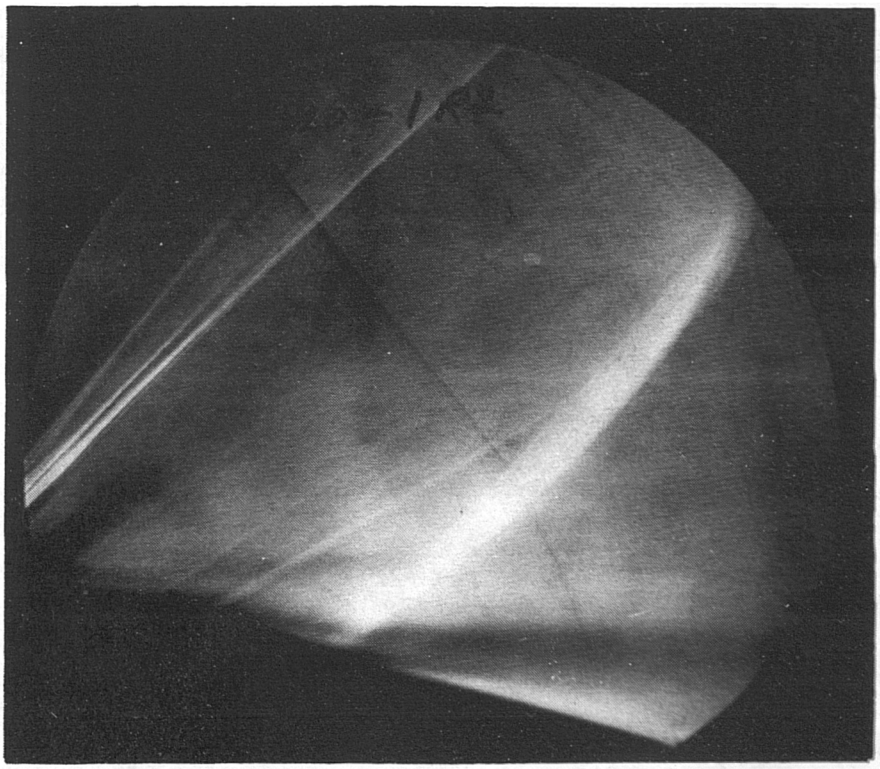

Figure 5.52 Experimental Pressure Distributions with Corresponding Schlieren Image for the 14% Bump with Small Air Jets (ϕ=30°, P_b/P_o=1.2).

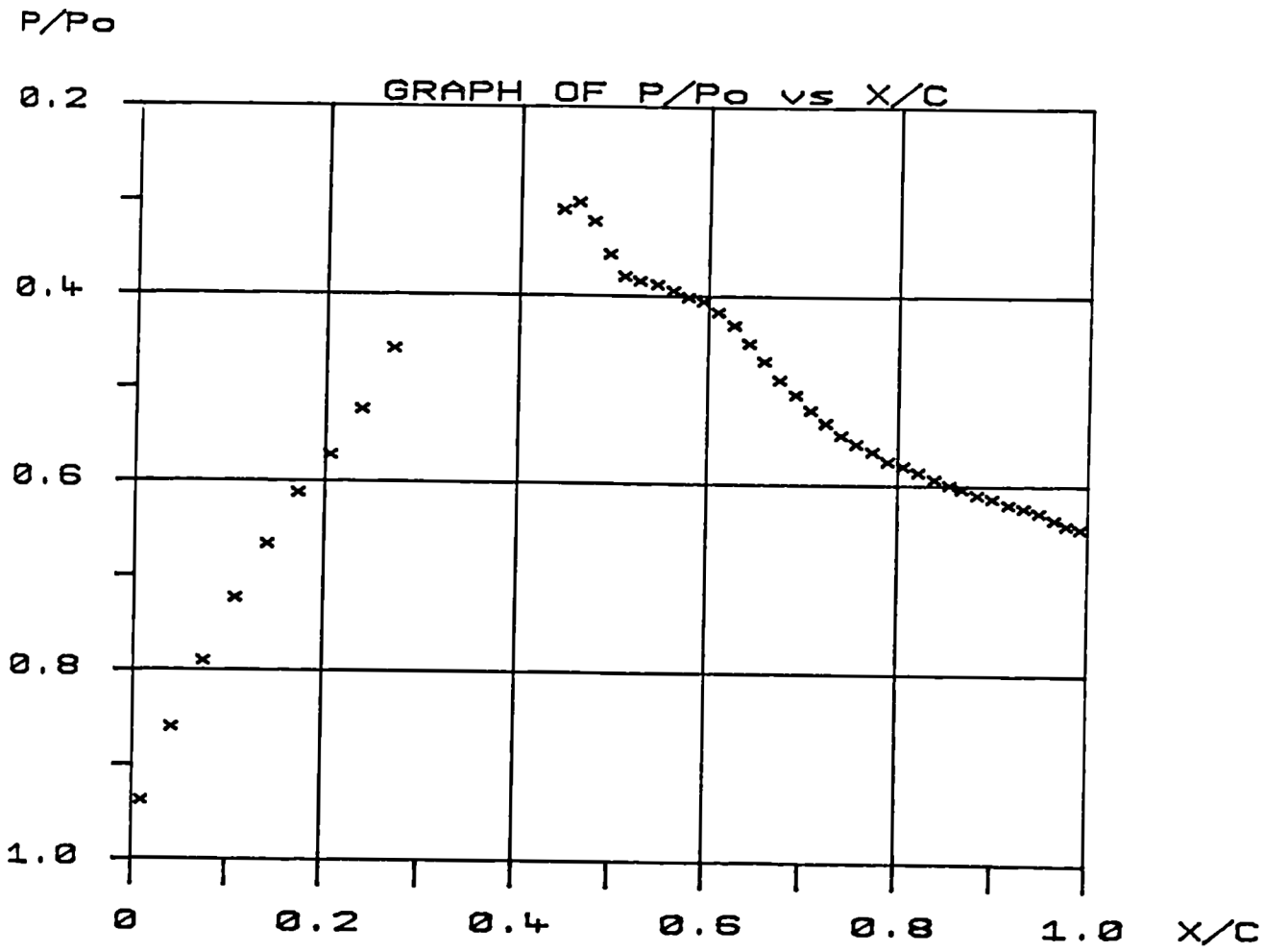

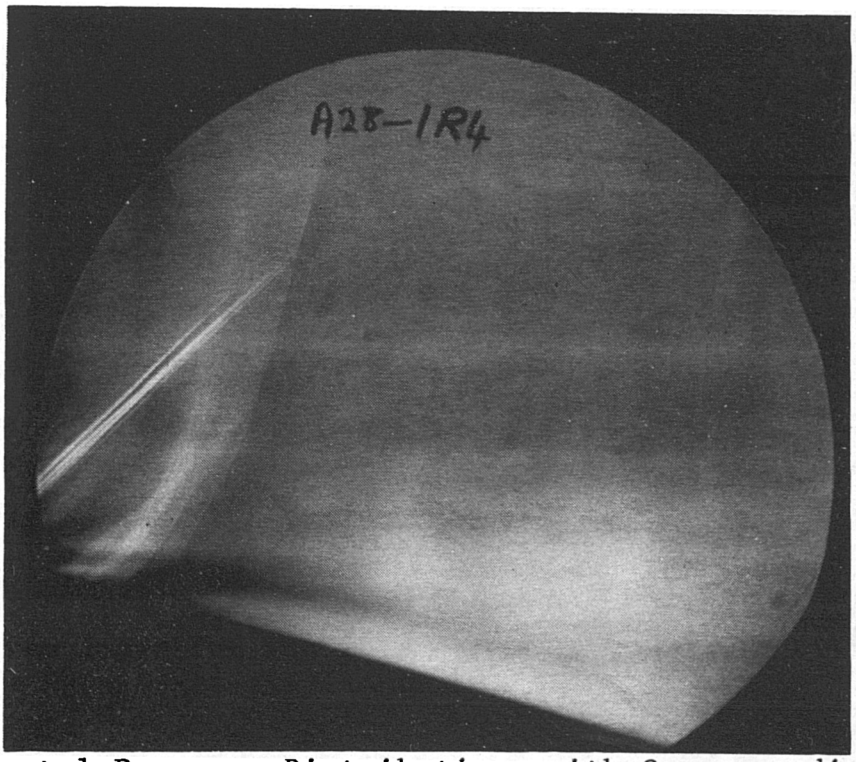

Figure 5.53 Experimental Pressure Distributions with Corresponding Schlieren Image for the 14% Bump with Small Air Jets (ϕ=30°, P_b/P_o=1.6).

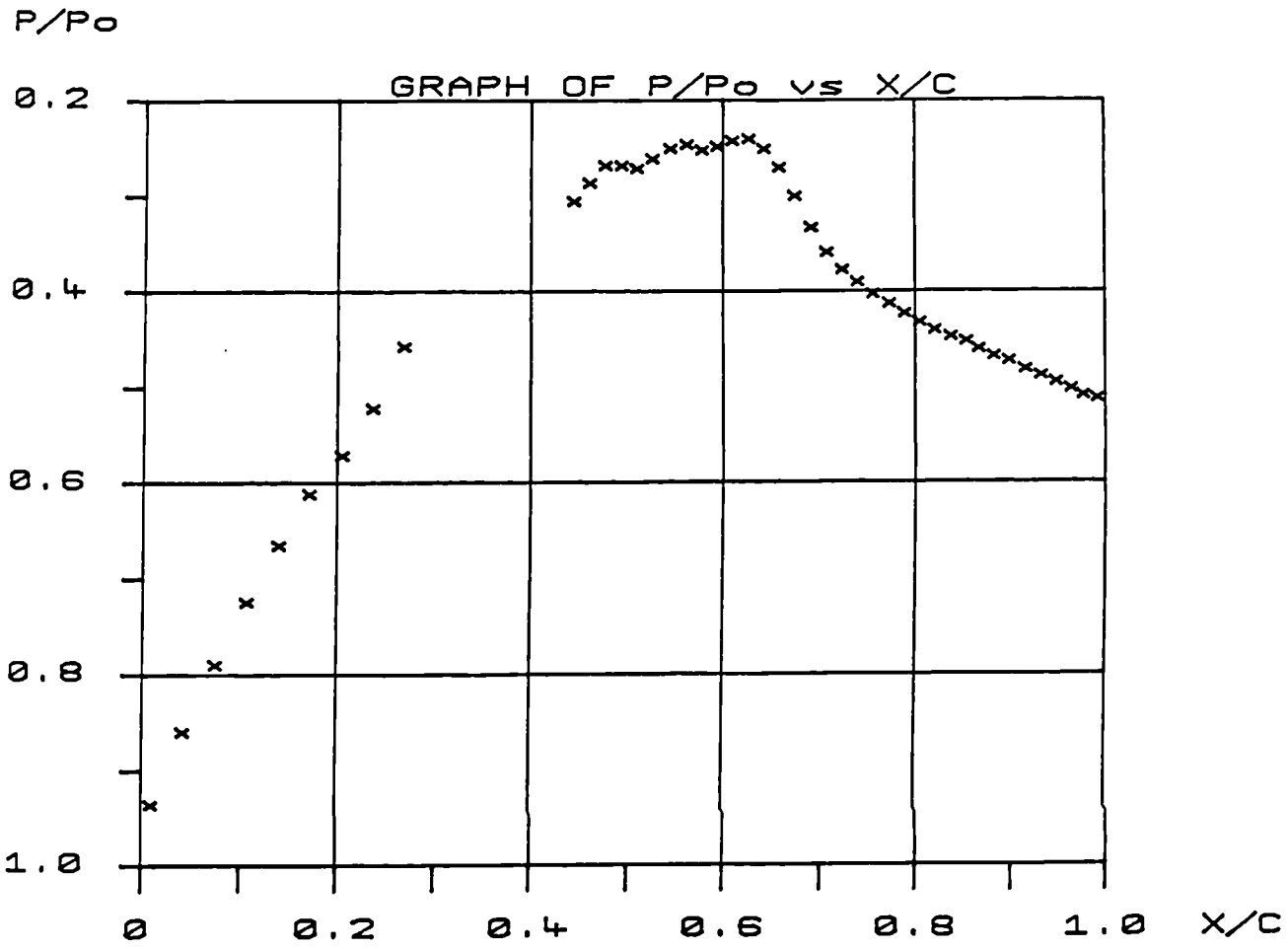

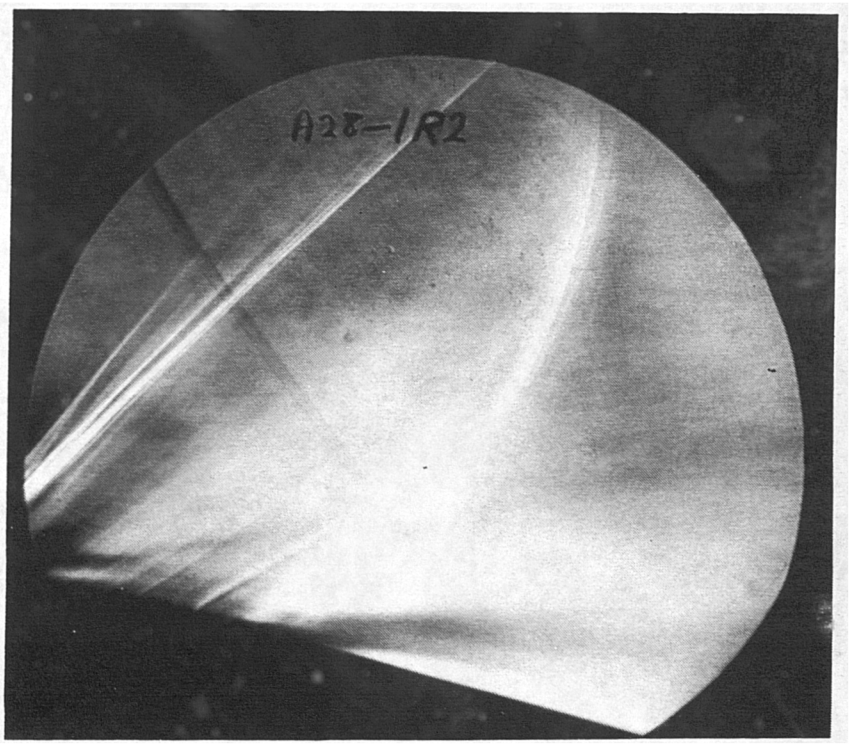

Figure 5.54 Experimental Pressure Distributions with Corresponding Schlieren Image for the 14% Bump with Small Air Jets (ϕ=30°, P_b/P_o=1.6).

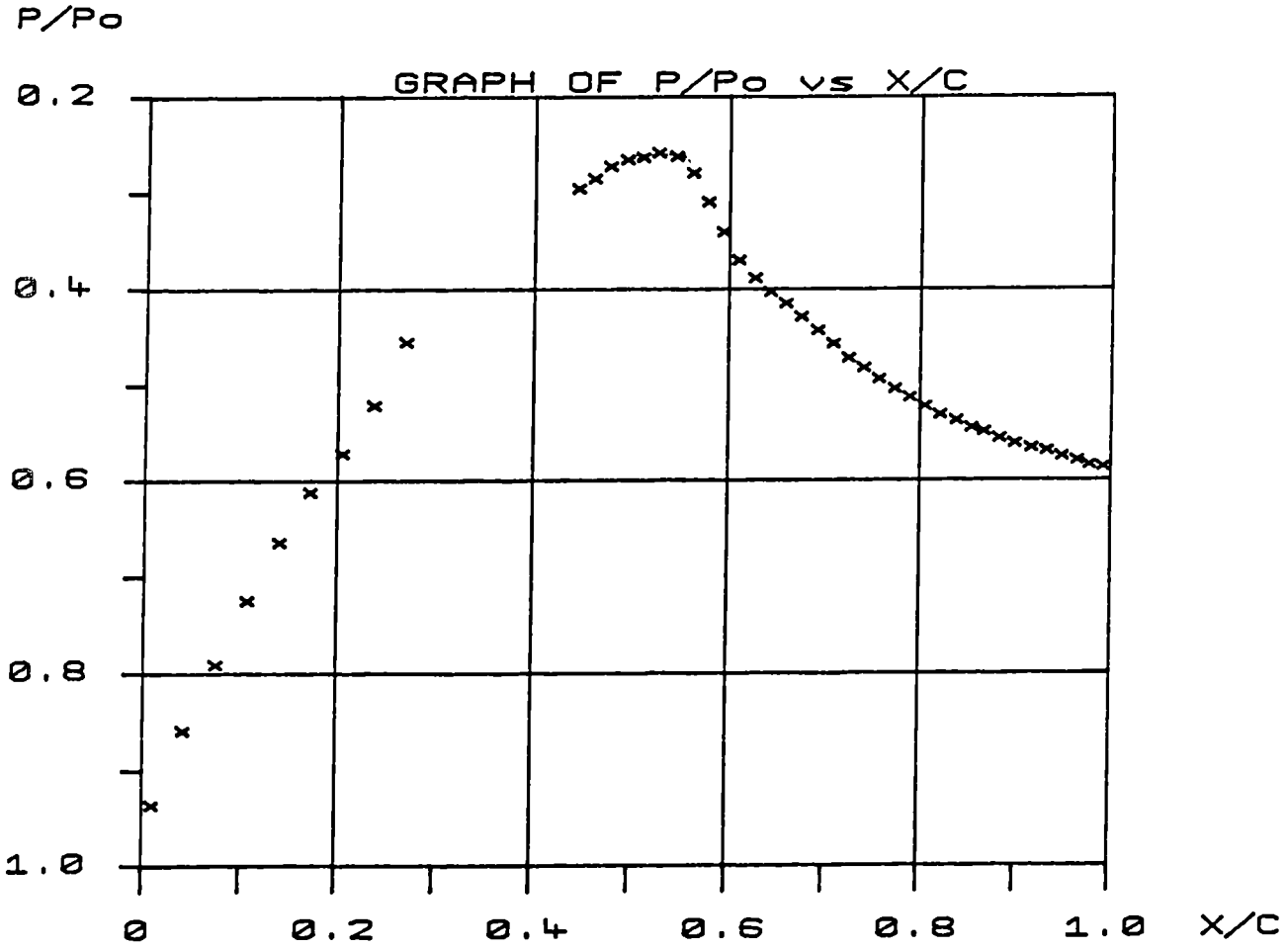

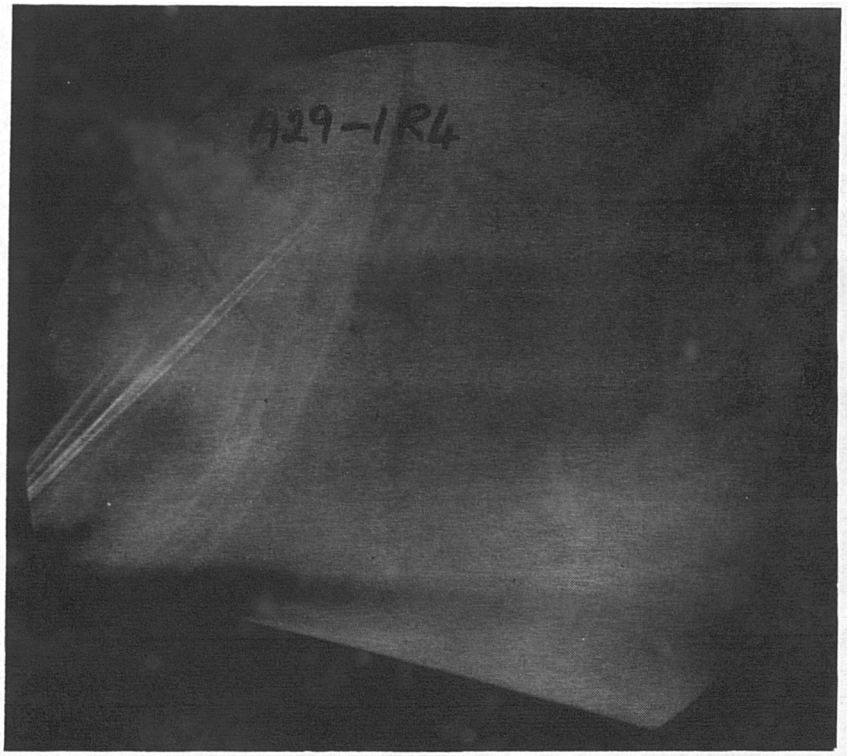

Figure 5.55 Experimental Pressure Distributions with Corresponding Schlieren Image for the 14% Bump with Small Air Jets (ϕ=45°, P_b/P_o=1.2).

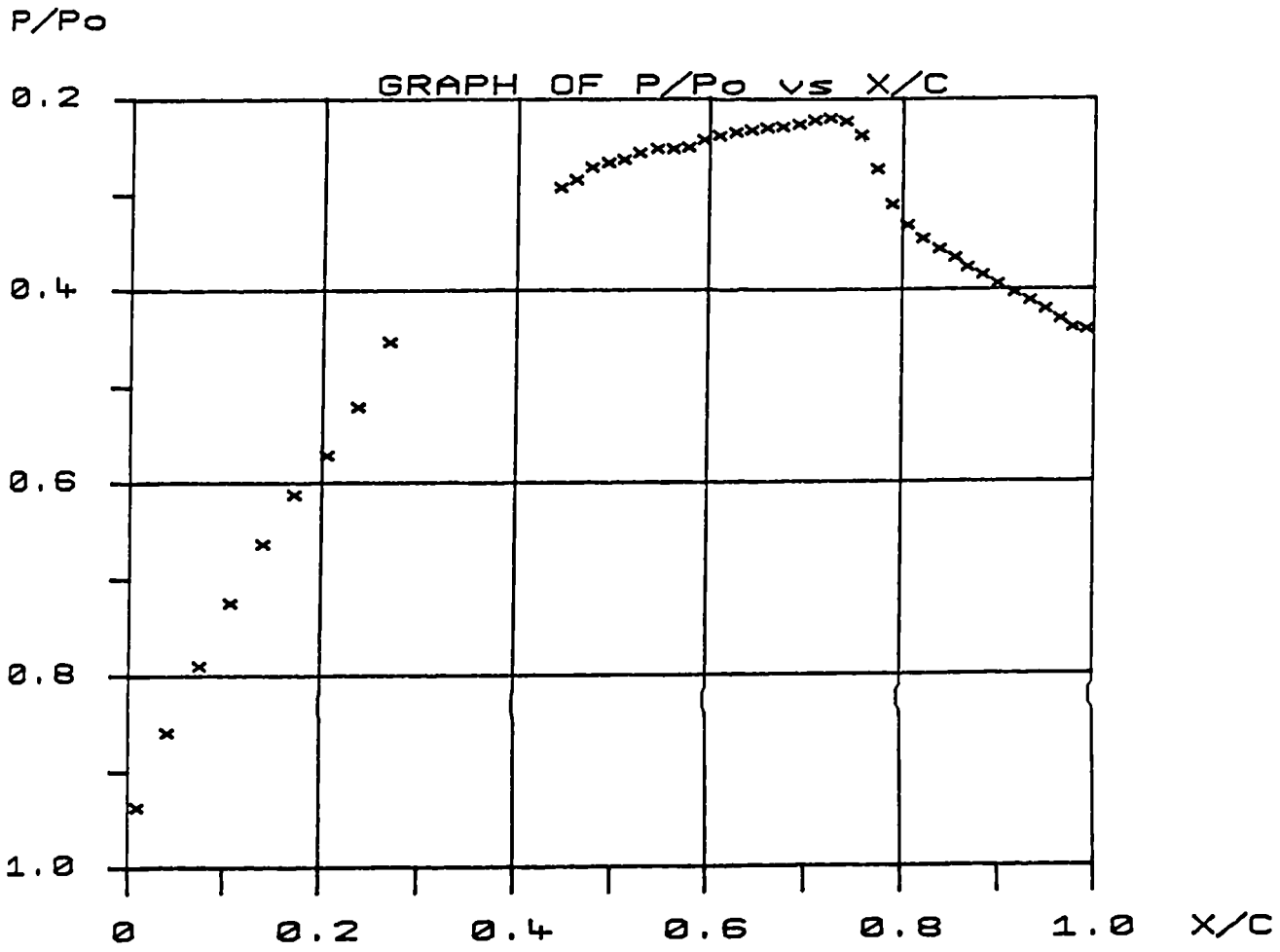

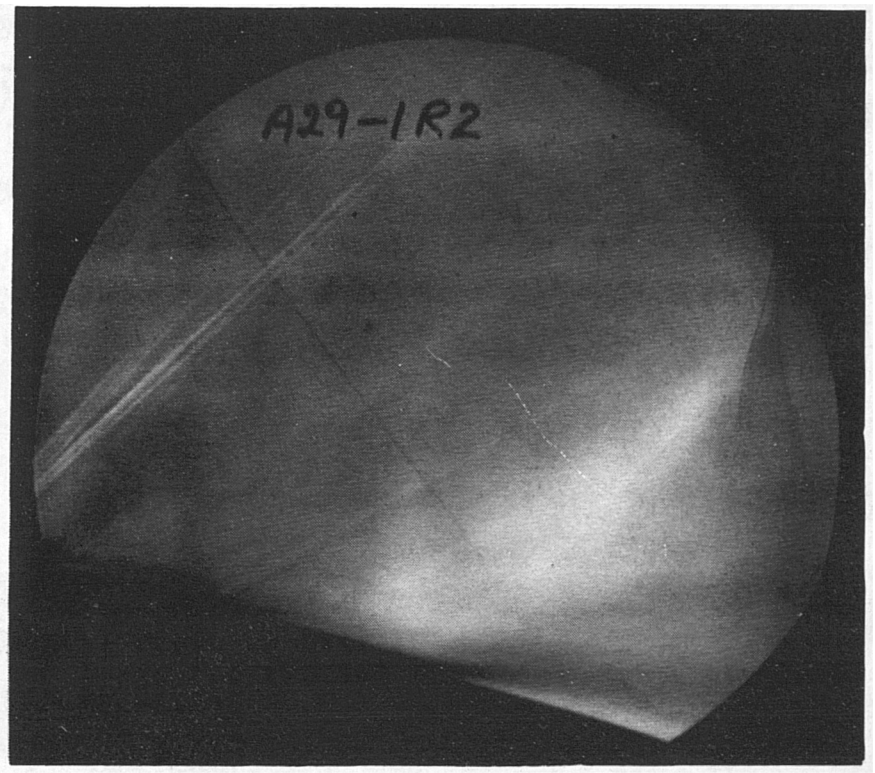

Figure 5.56 Experimental Pressure Distributions with Corresponding Schlieren Image for the 14% Bump with Small Air Jets (ϕ=45°, P_b/P_o=1.2).

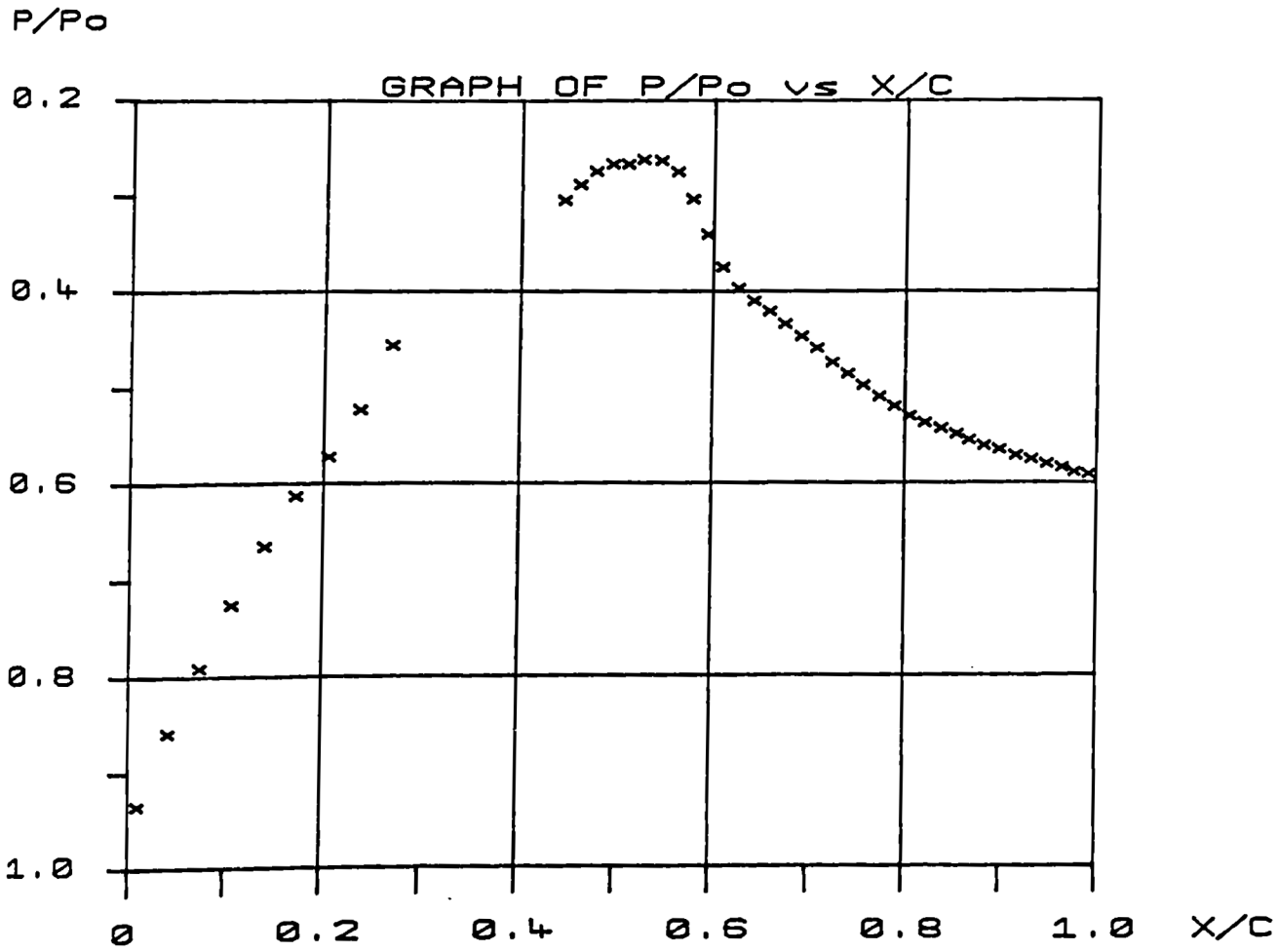

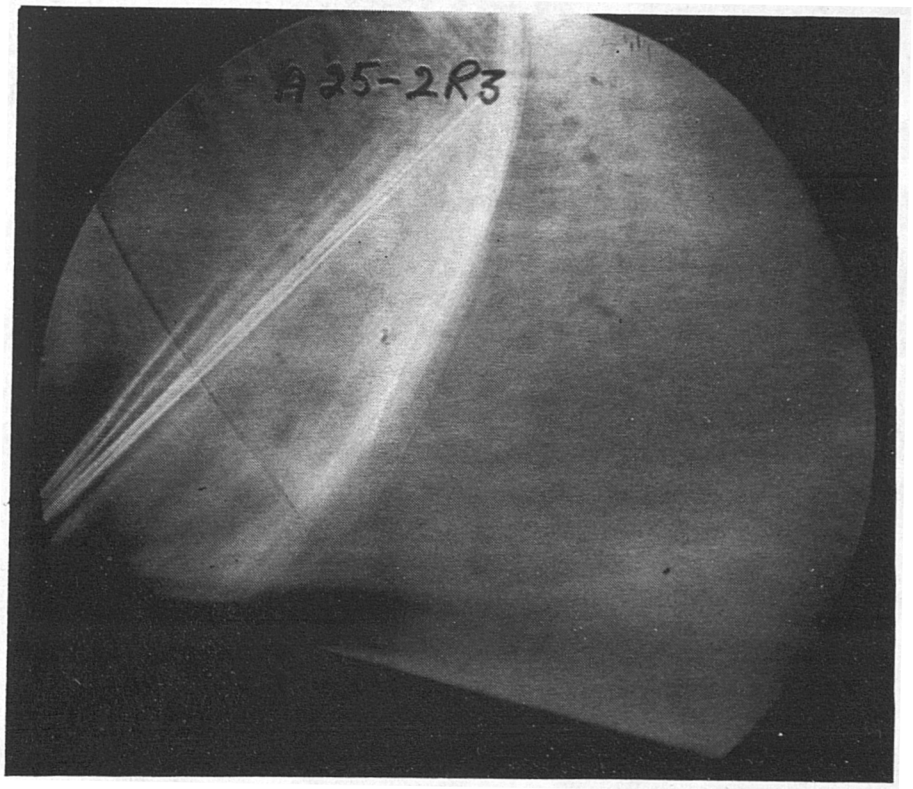

Figure 5.57 Experimental Pressure Distributions with Corresponding Schlieren Image for the 14% Bump with Small Air Jets (ϕ=45°, P_b/P_o=1.6).

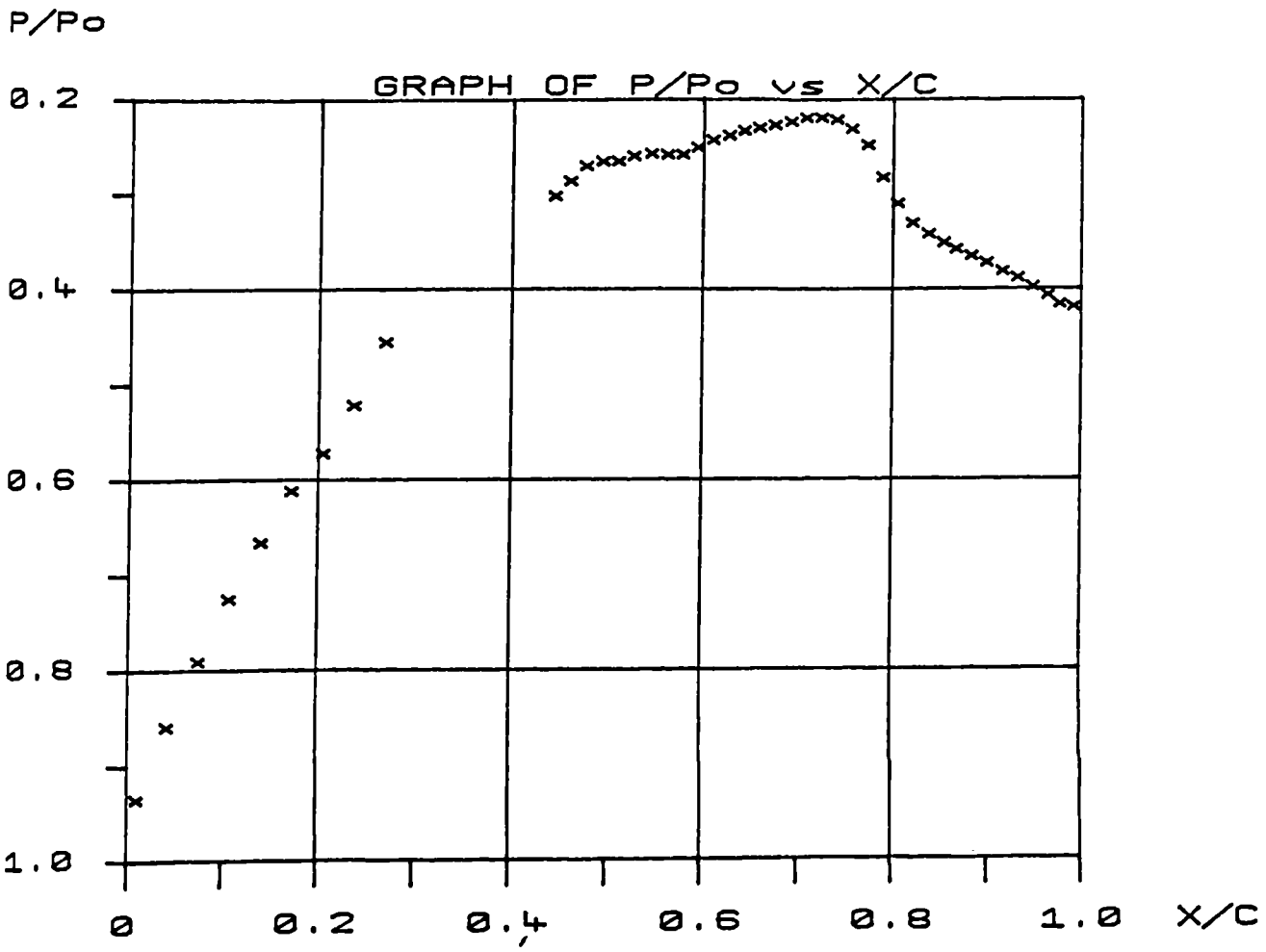

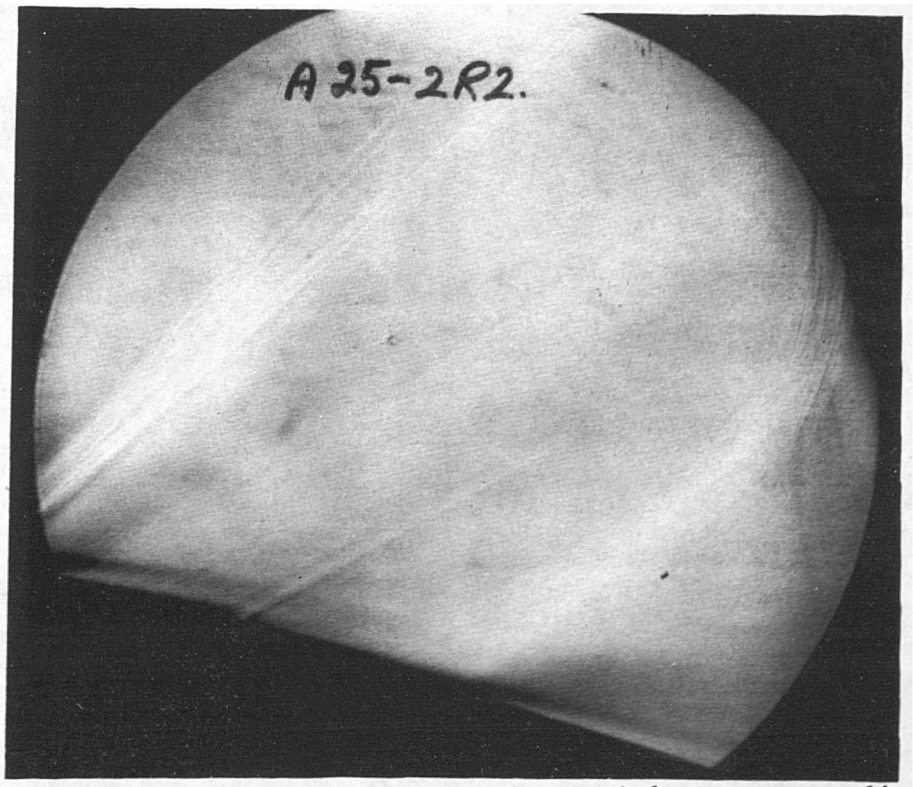

Figure 5.58 Experimental Pressure Distributions with Corresponding Schlieren Image for the 14% Bump with Small Air Jets (ϕ=45°; P_b/P_o=1.6).

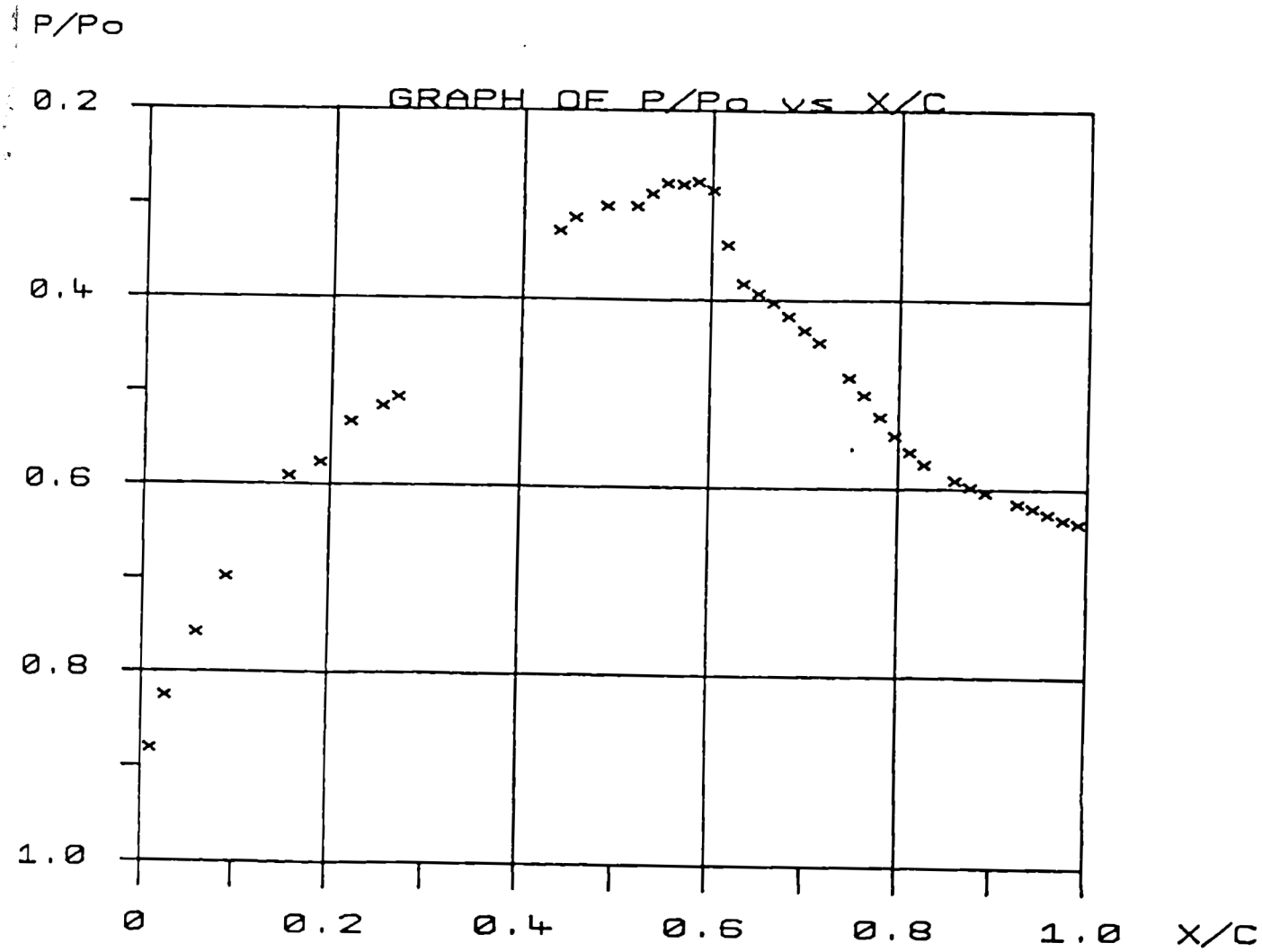

Figure 5.59 Experimental Pressure Distributions with Corresponding Schlieren Image for the 10% Bump with Large Air Jets (θ=60°, P_b/P_o=1.2).

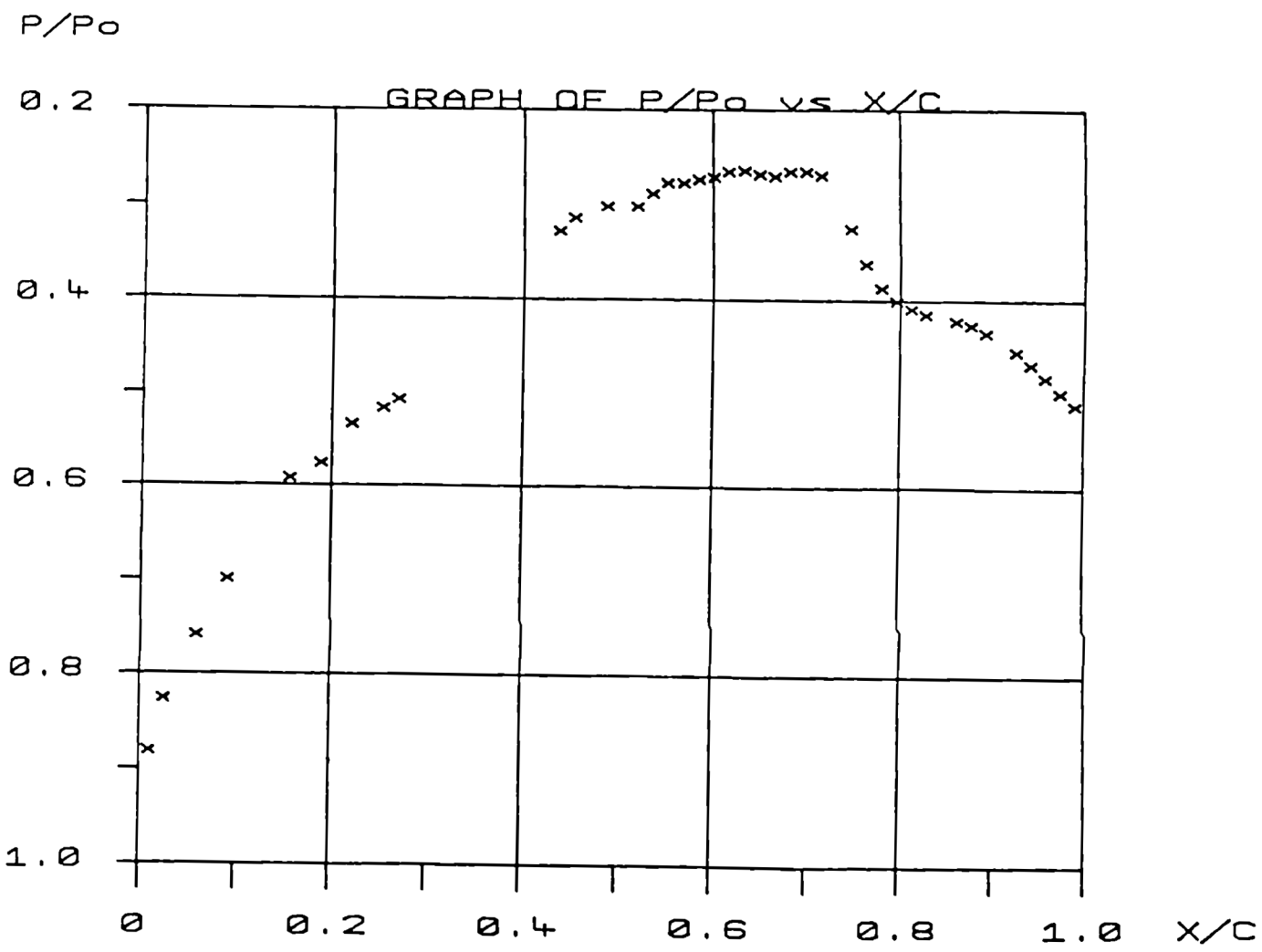

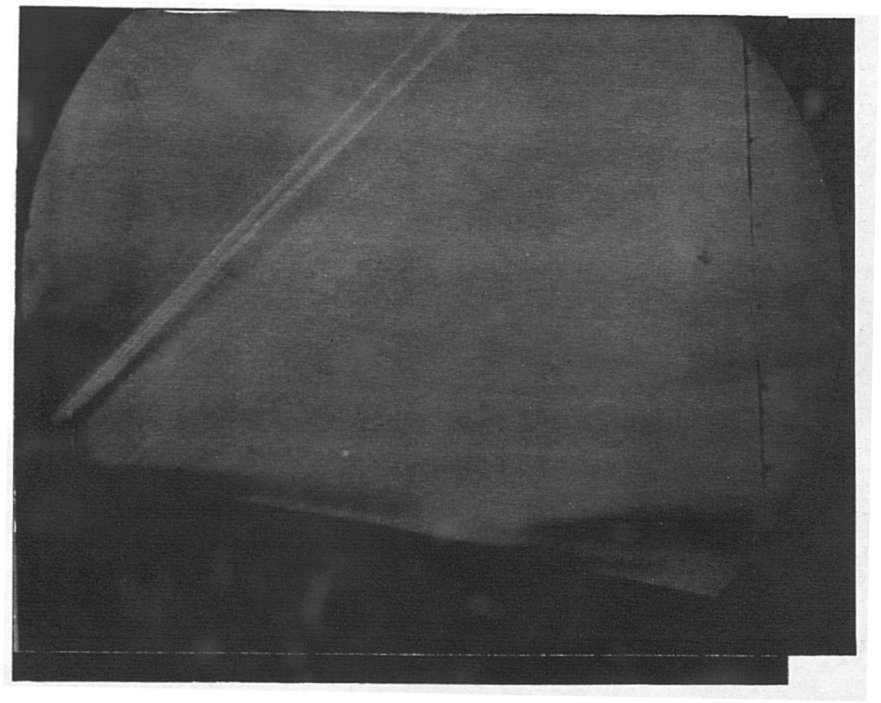

Figure 5.60 Experimental Pressure Distributions with Corresponding Schlieren Image for the 10% Bump with Large Air Jet (θ=60°, P_b/P_o=1.2).

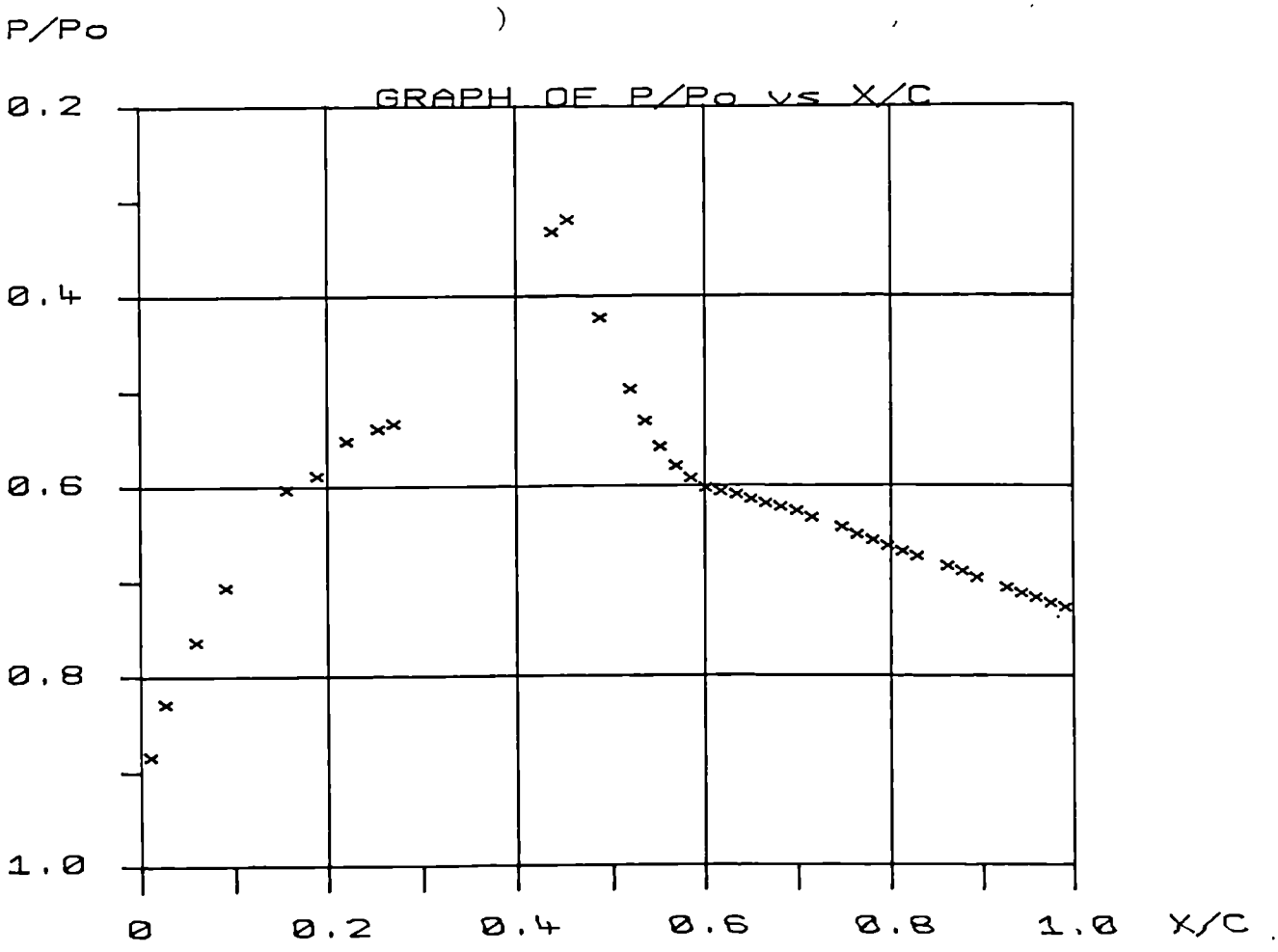

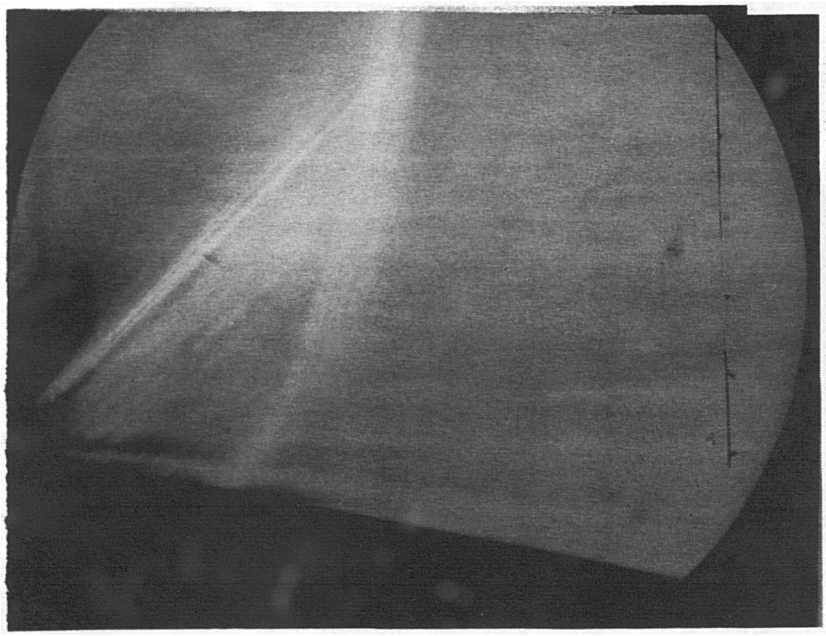

Figure 5.61 Experimental Pressure Distributions with Corresponding Schlieren Image for the 10% Bump with Large Air Jets (θ=60°, P_b/P_o=1.8).

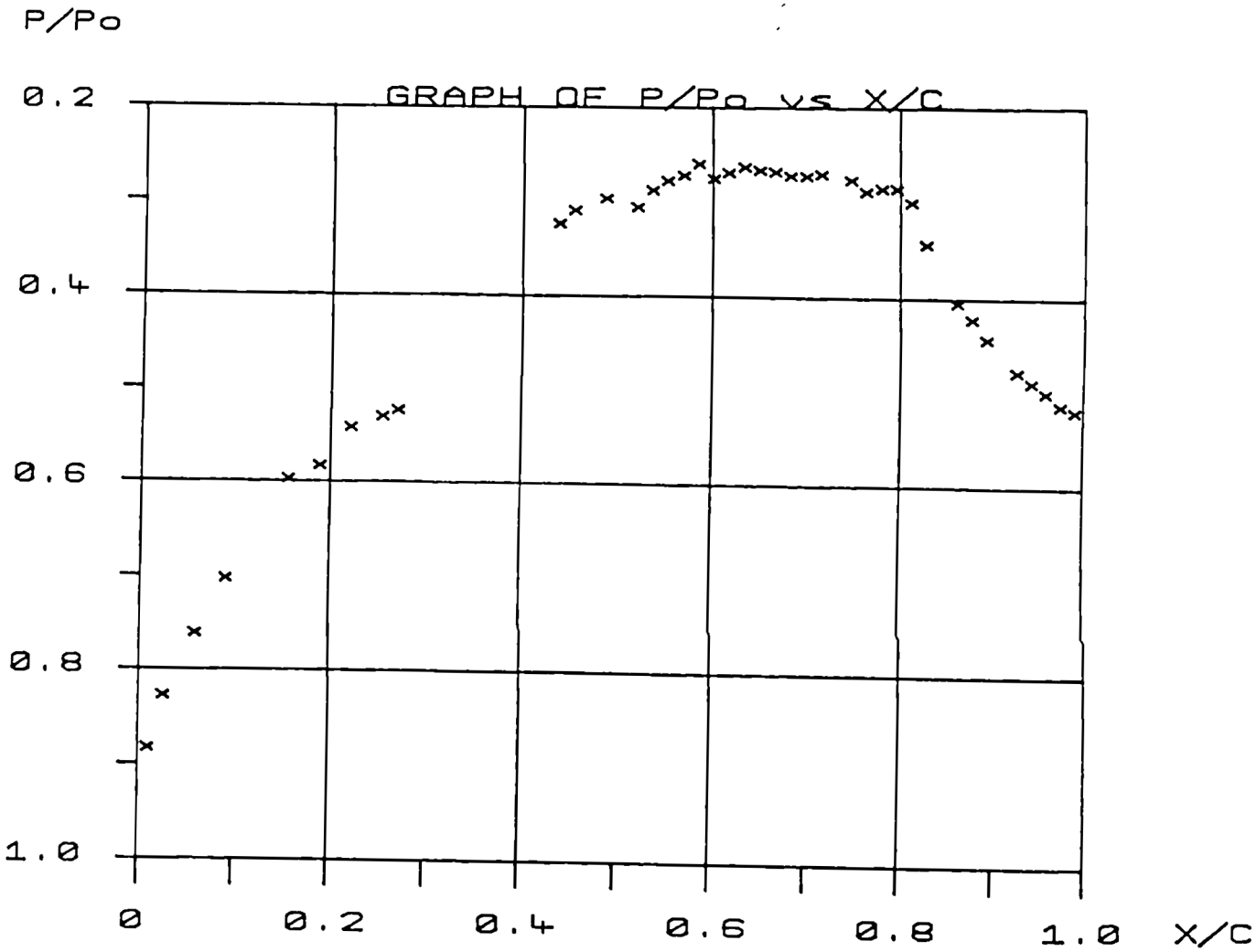

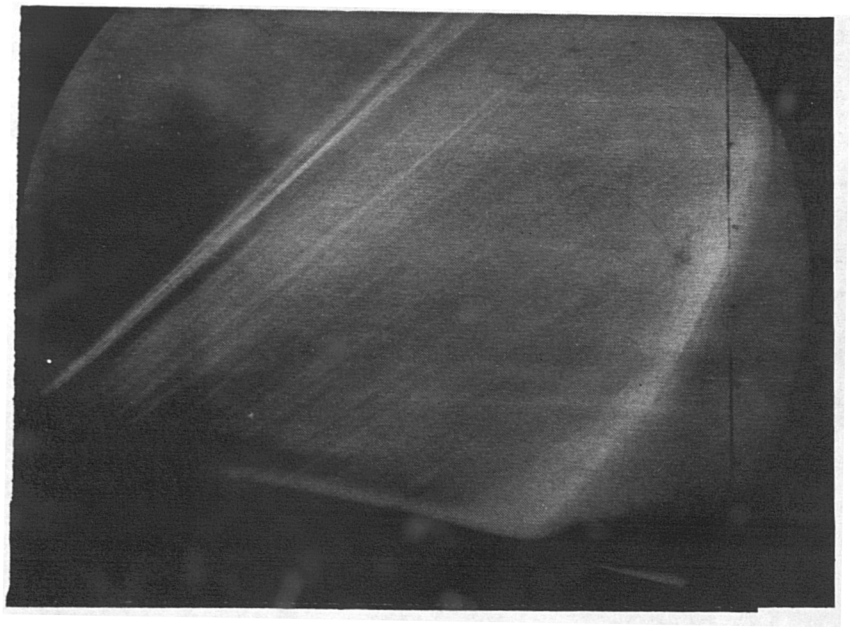

Figure 5.62 Experimental Pressure Distributions with Corresponding Schlieren Image for the 10% Bump with Large Air Jets ($\theta=60°, P_b/P_o=1.8$).

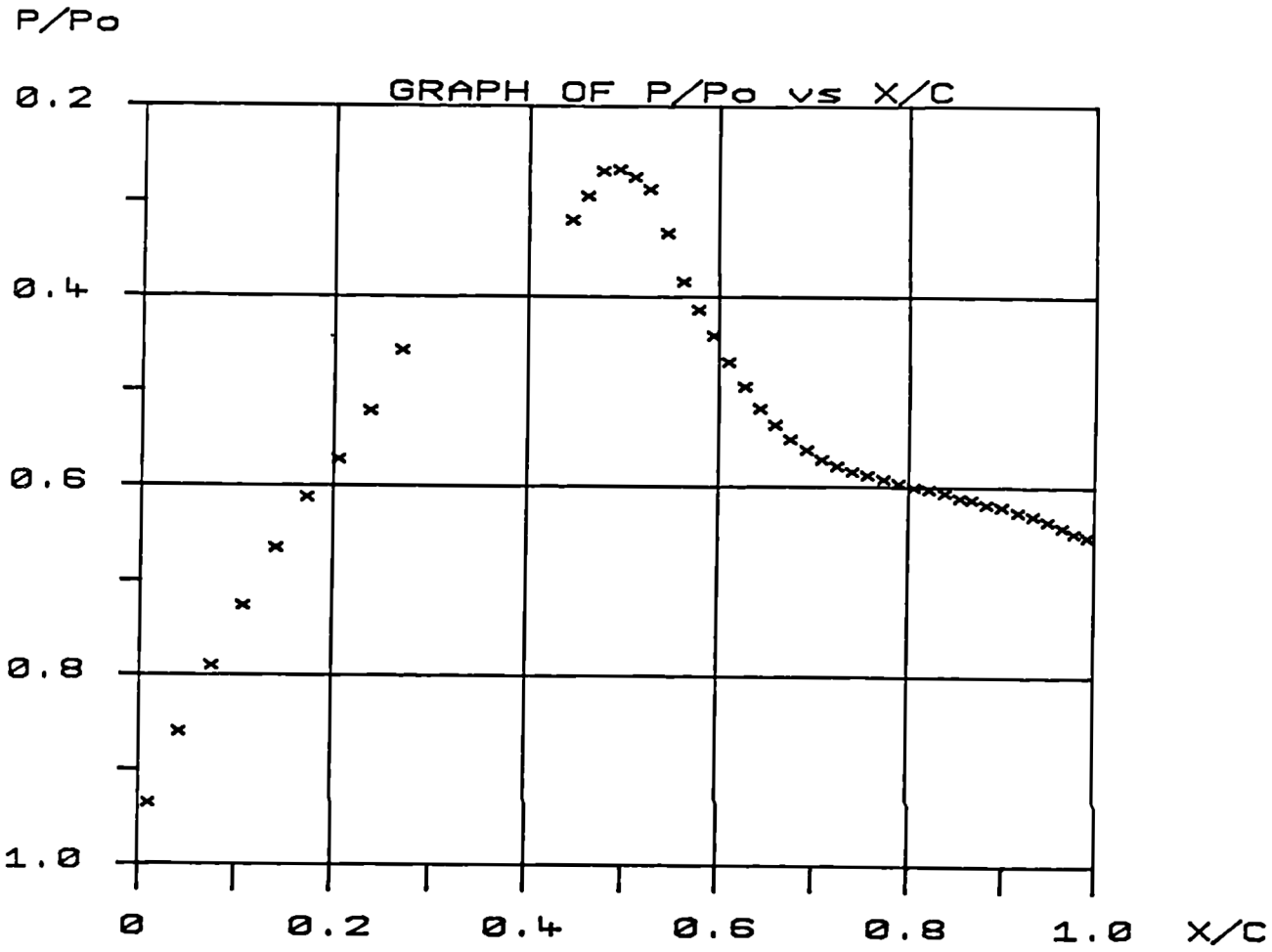

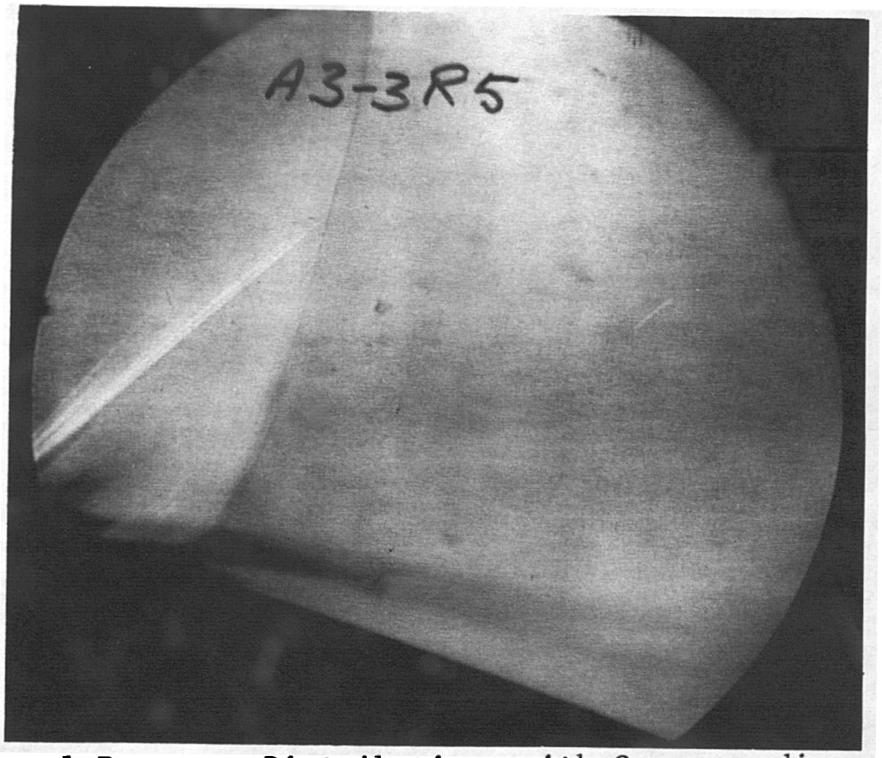

Figure 5.63 Experimental Pressure Distributions with Corresponding Schlieren Image for the 14% Bump with Large Air Jets (θ=60°, P_b/P_o=1.2).

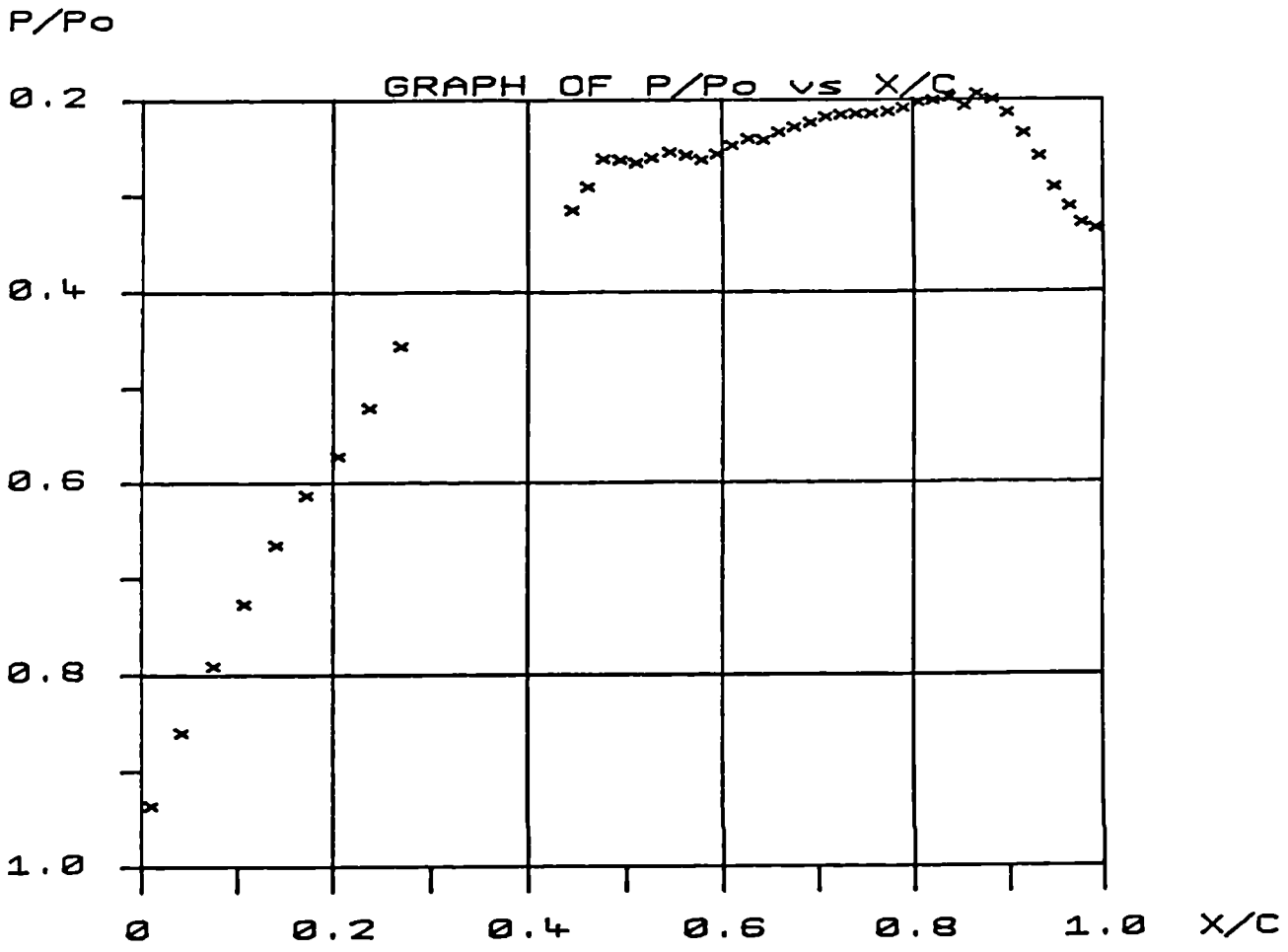

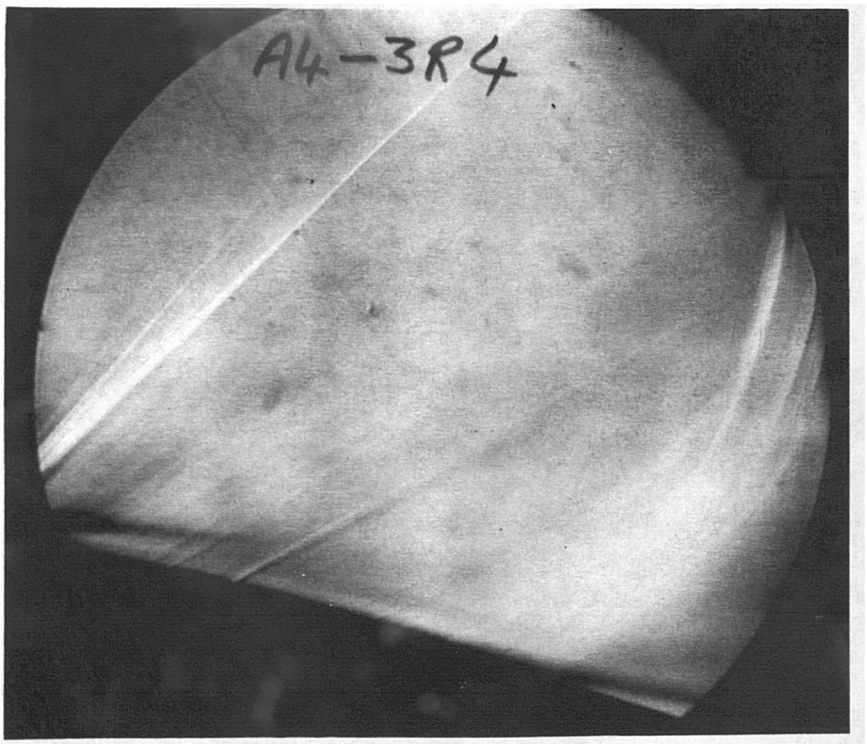

Figure 5.64 Experimental Pressure Distributions with Corresponding Schlieren Image for the 14% Bump with Large Air Jets (θ=60°, P_b/P_o=1.2).

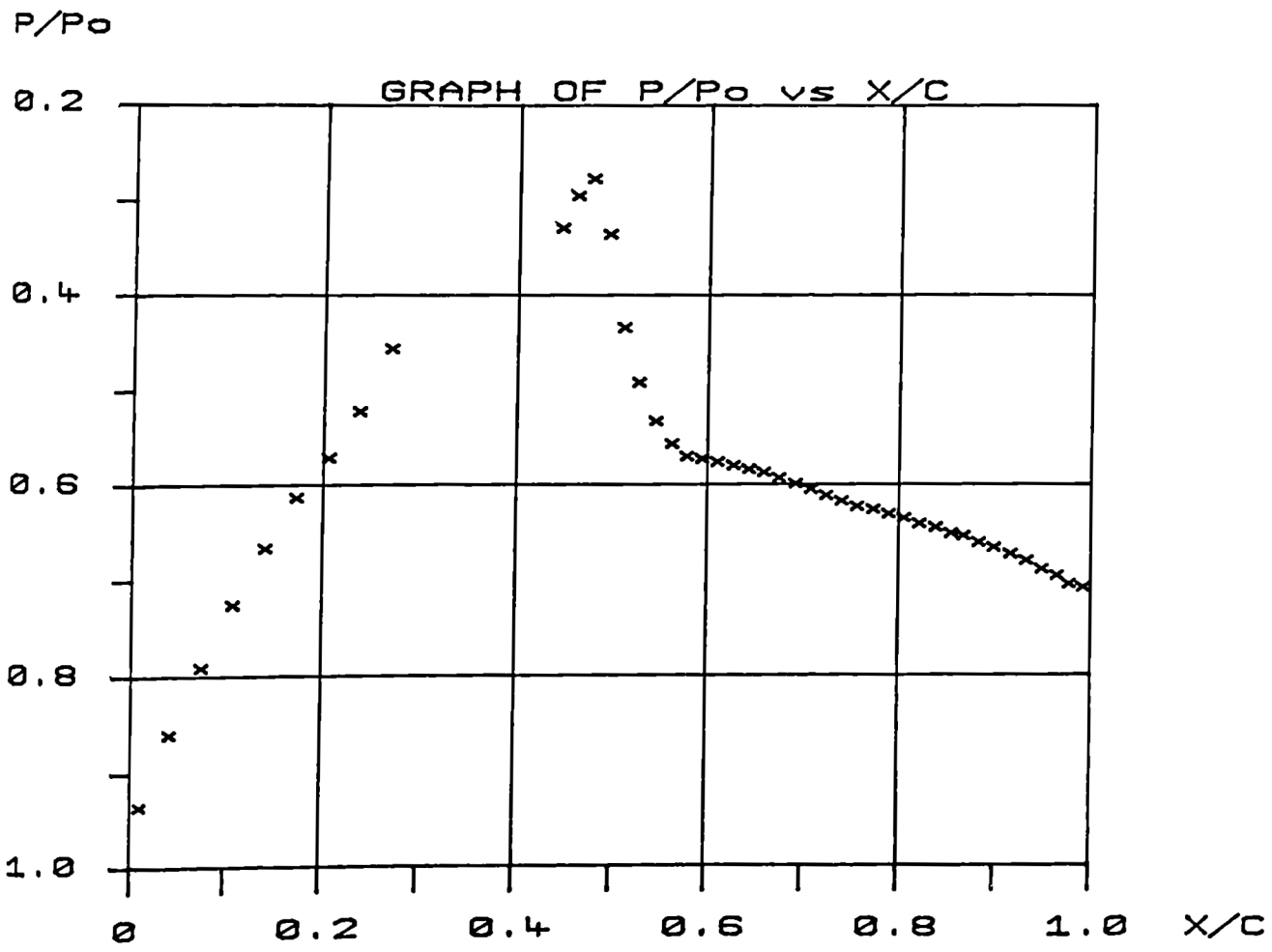

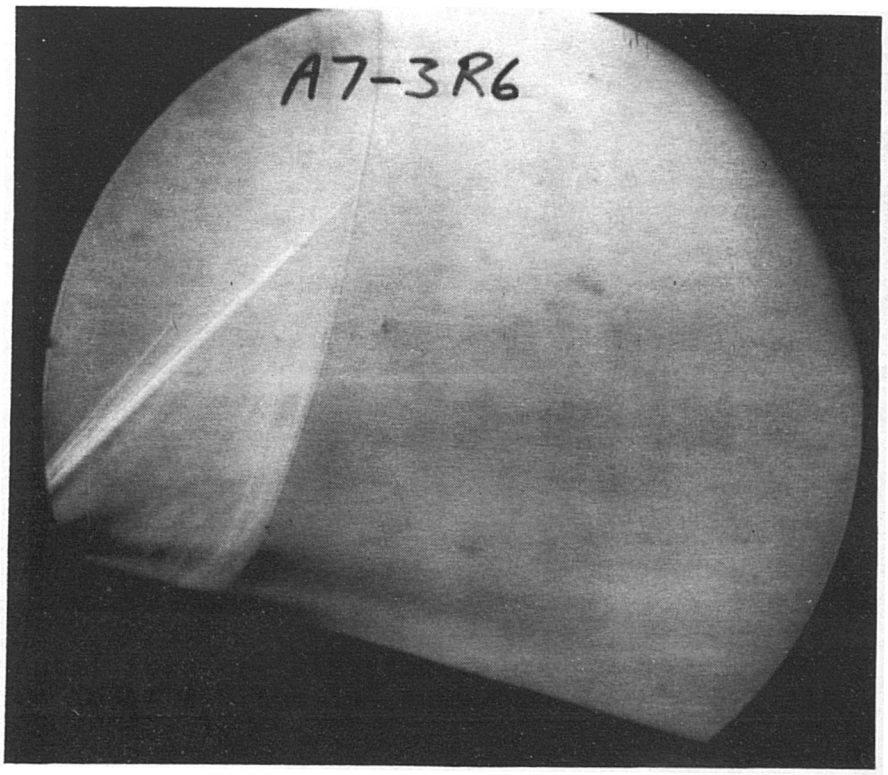

Figure 5.65 Experimental Pressure Distributions with Corresponding Schlieren Image for the 14% Bump with Large Air Jets (θ=60°, P_b/P_o=1.5).

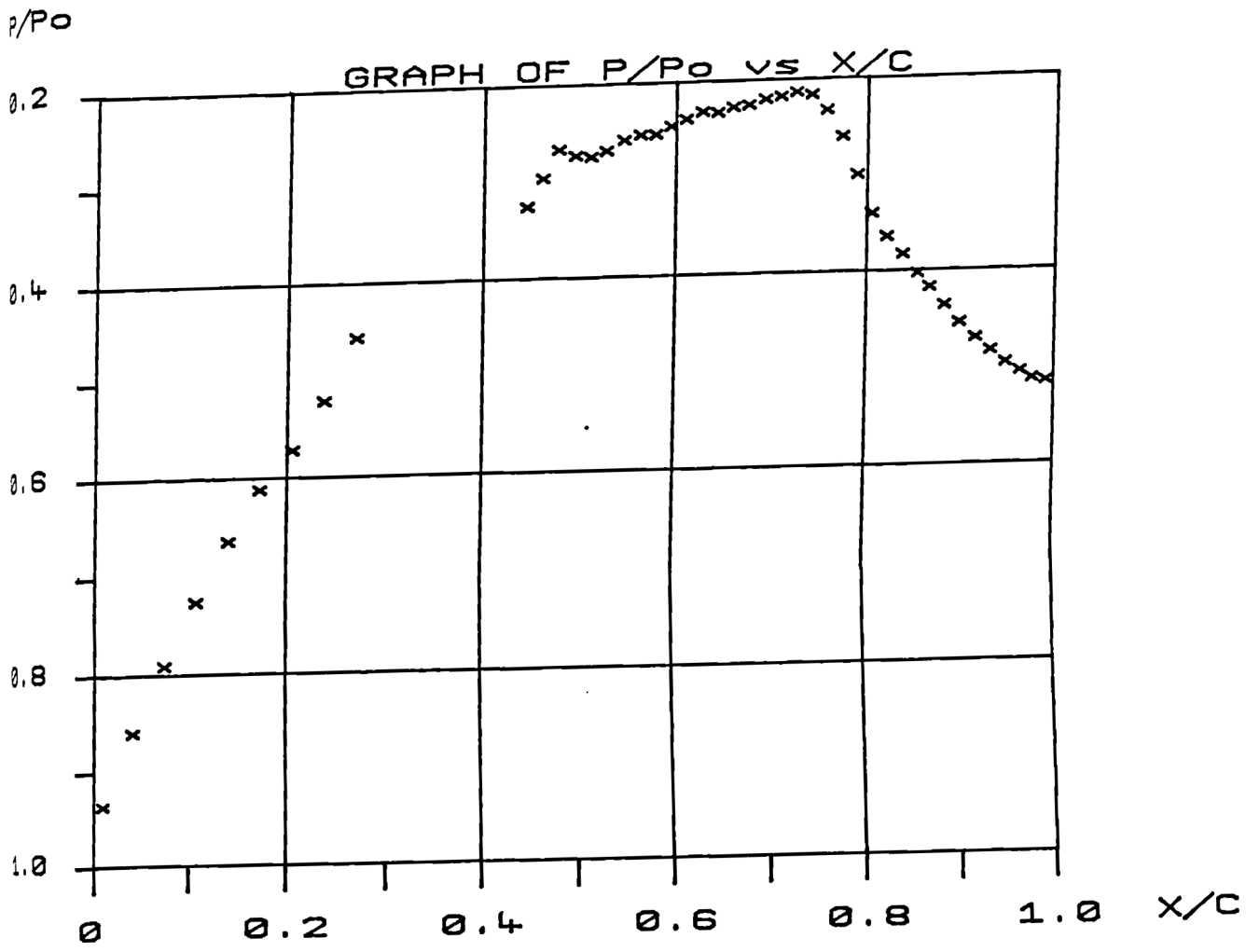

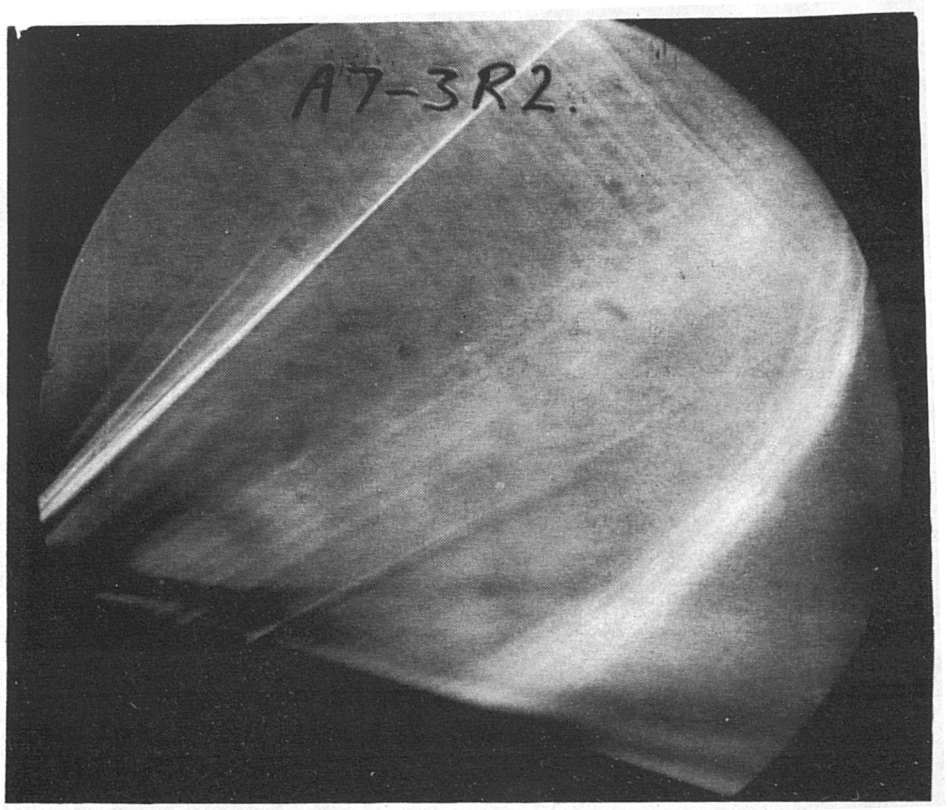

Figure 5.66 Experimental Pressure Distributions with Corresponding Schlieren Image for the 14% Bump with Large Air Jets (θ=60°, P_b/P_o=1.5).

(a) Attached Flow

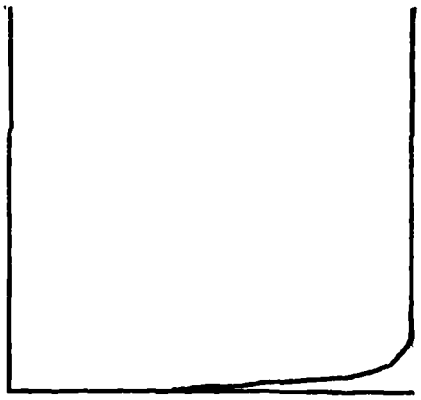

(b) Separated Flow

(c) Vortex Embedded in Attached Flow

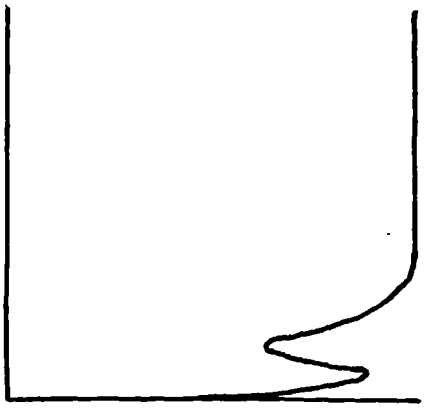

Figure 5.67 Typical Boundary Layer Profiles.

Figure 5.68 Boundary Layer Profiles With No Vortex Generators.

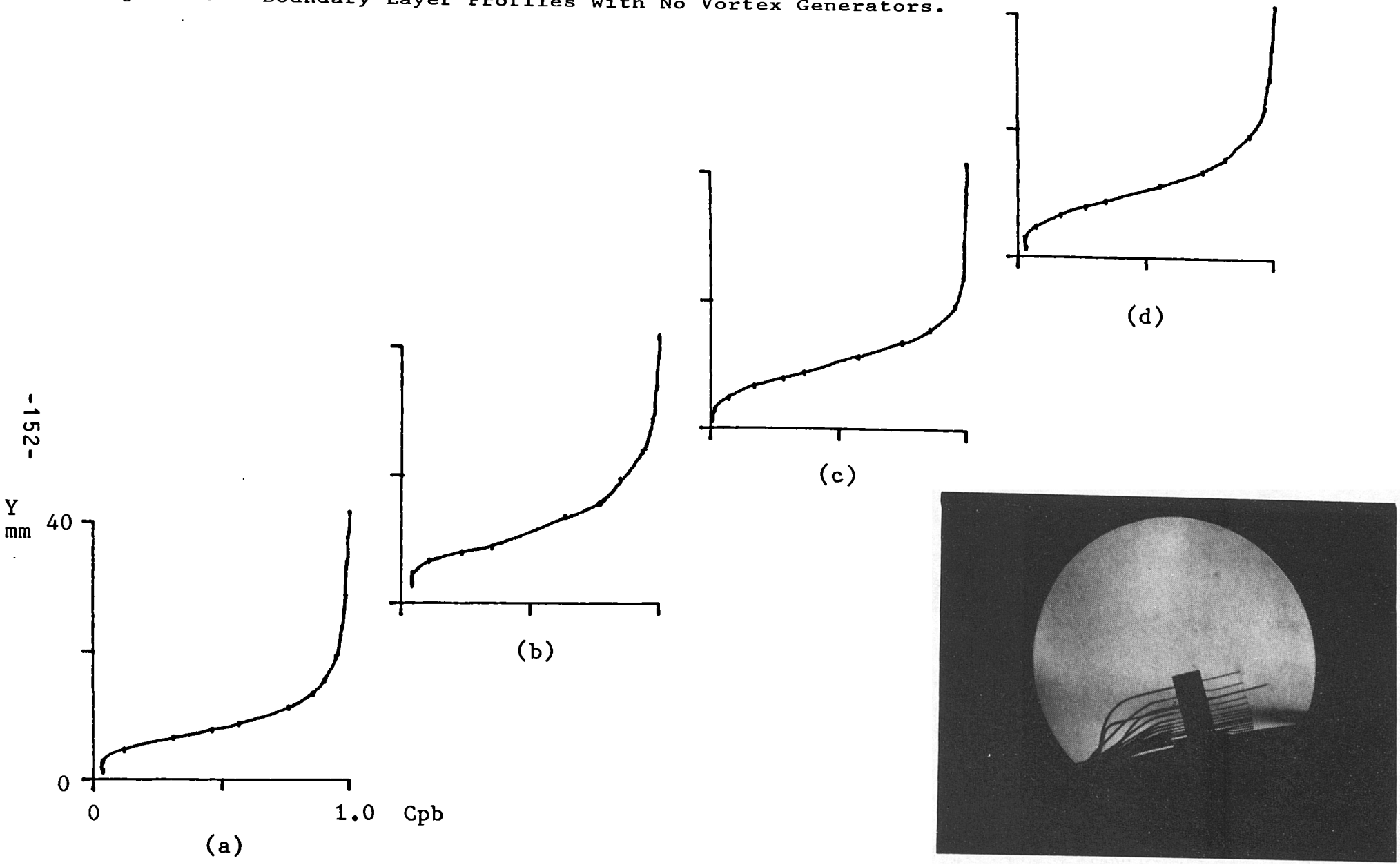

Figure 5.69 Boundary Layer Profiles With No Vortex Generators.

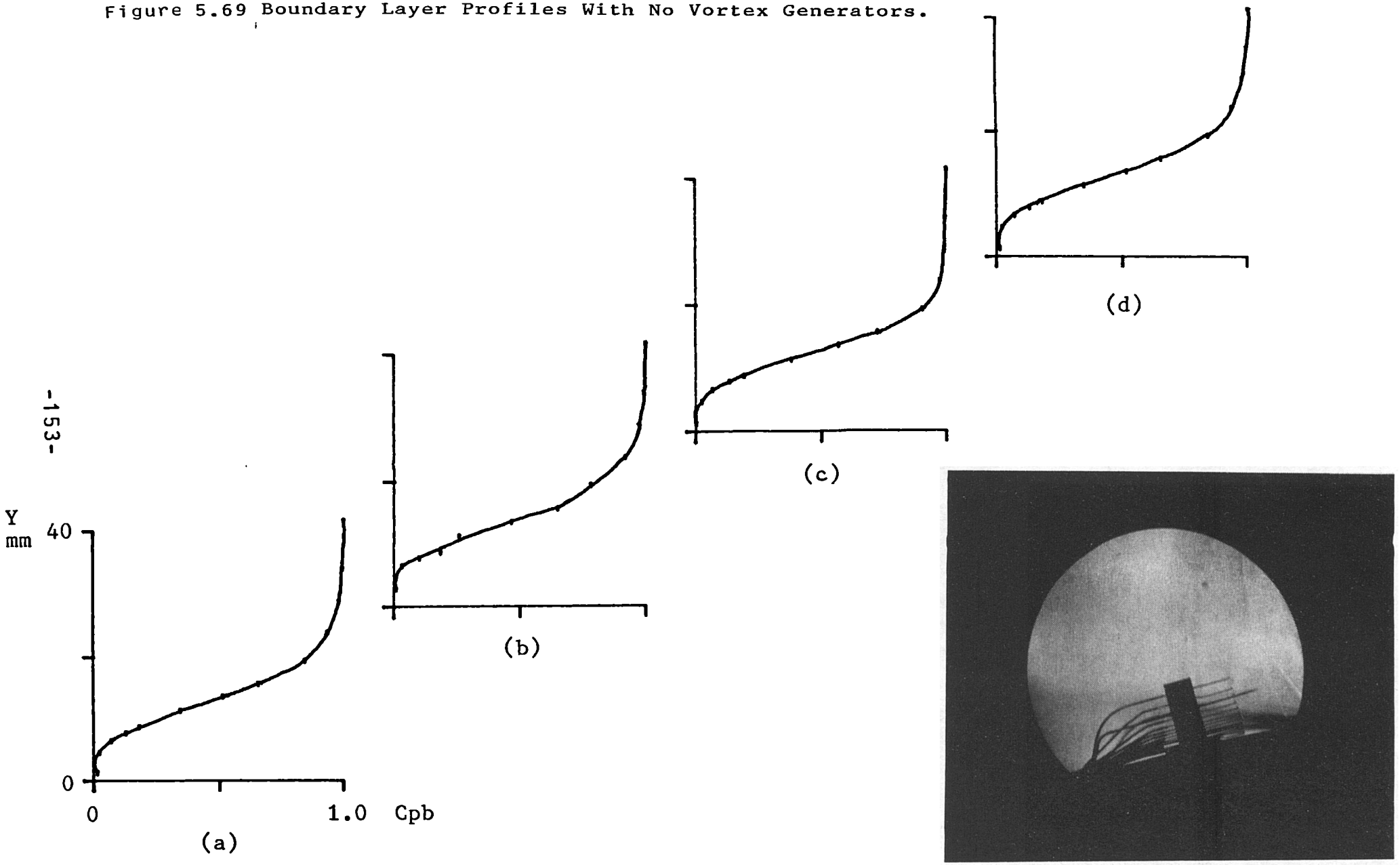

Figure 5.70 Boundary Layer Profiles With No Vortex Generators.

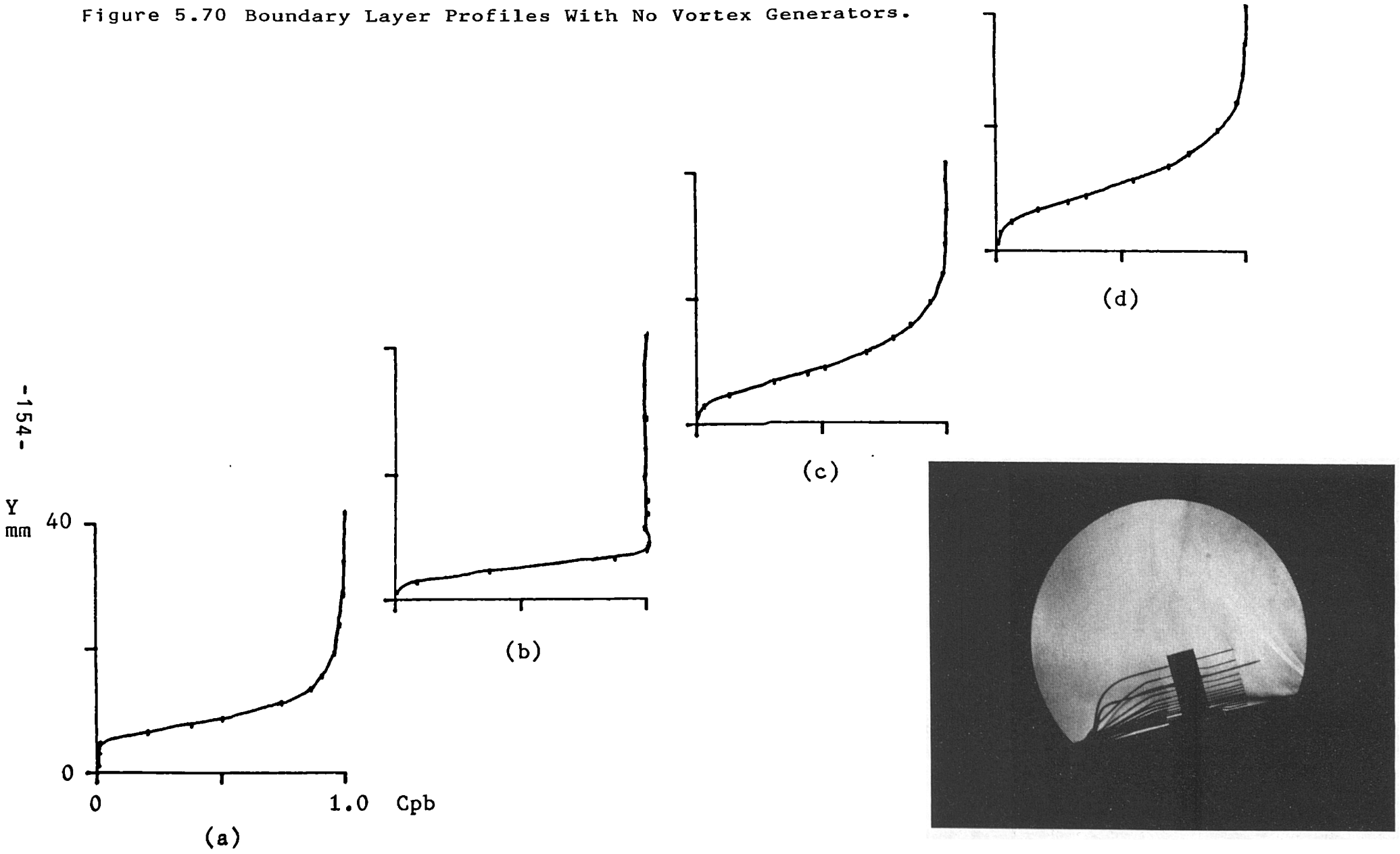

Figure 5.71 Boundary Layer Profiles With No Vortex Generators.

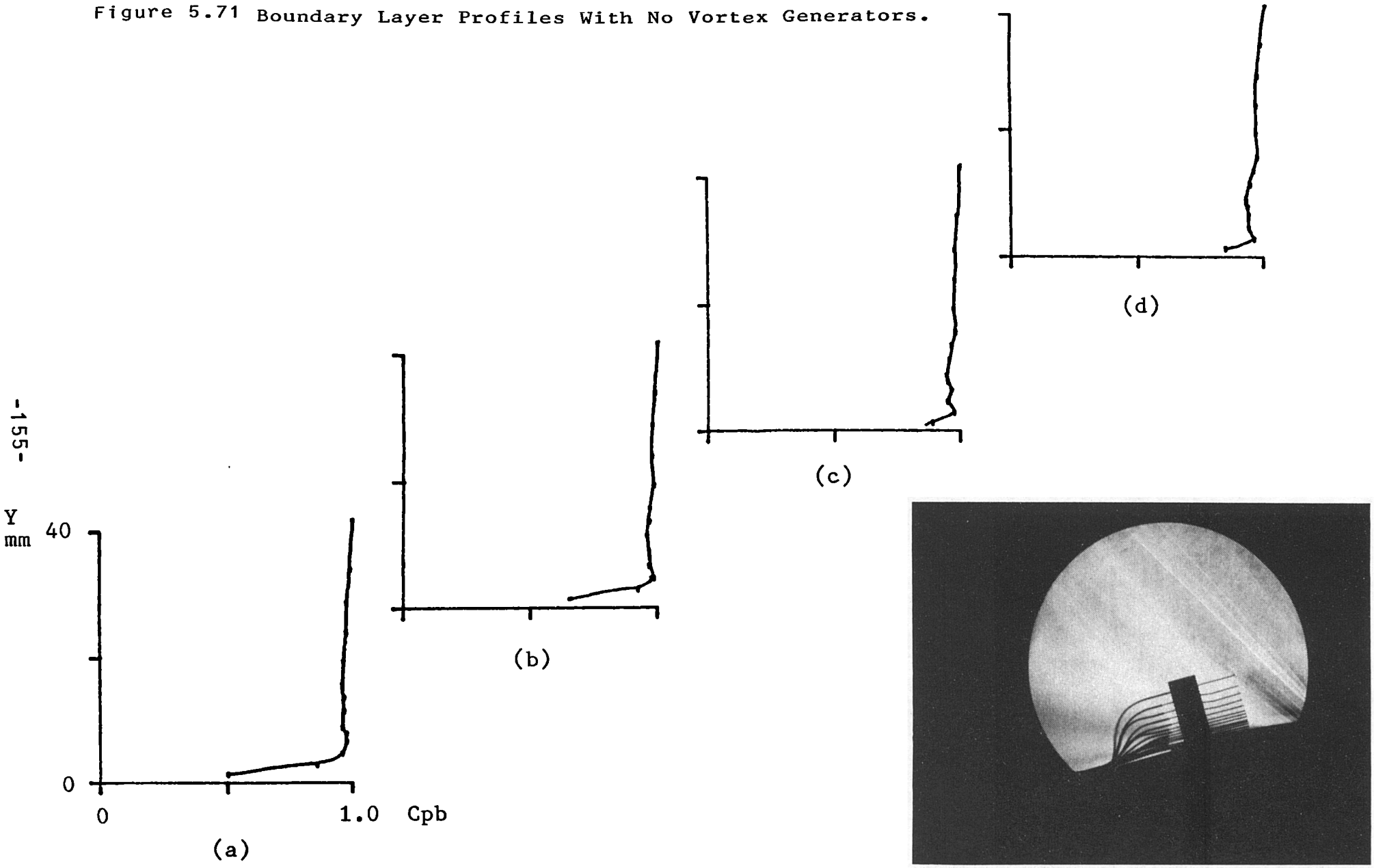

Figure 5.72 . Boundary Layer Profiles With Vane Vortex Generators.

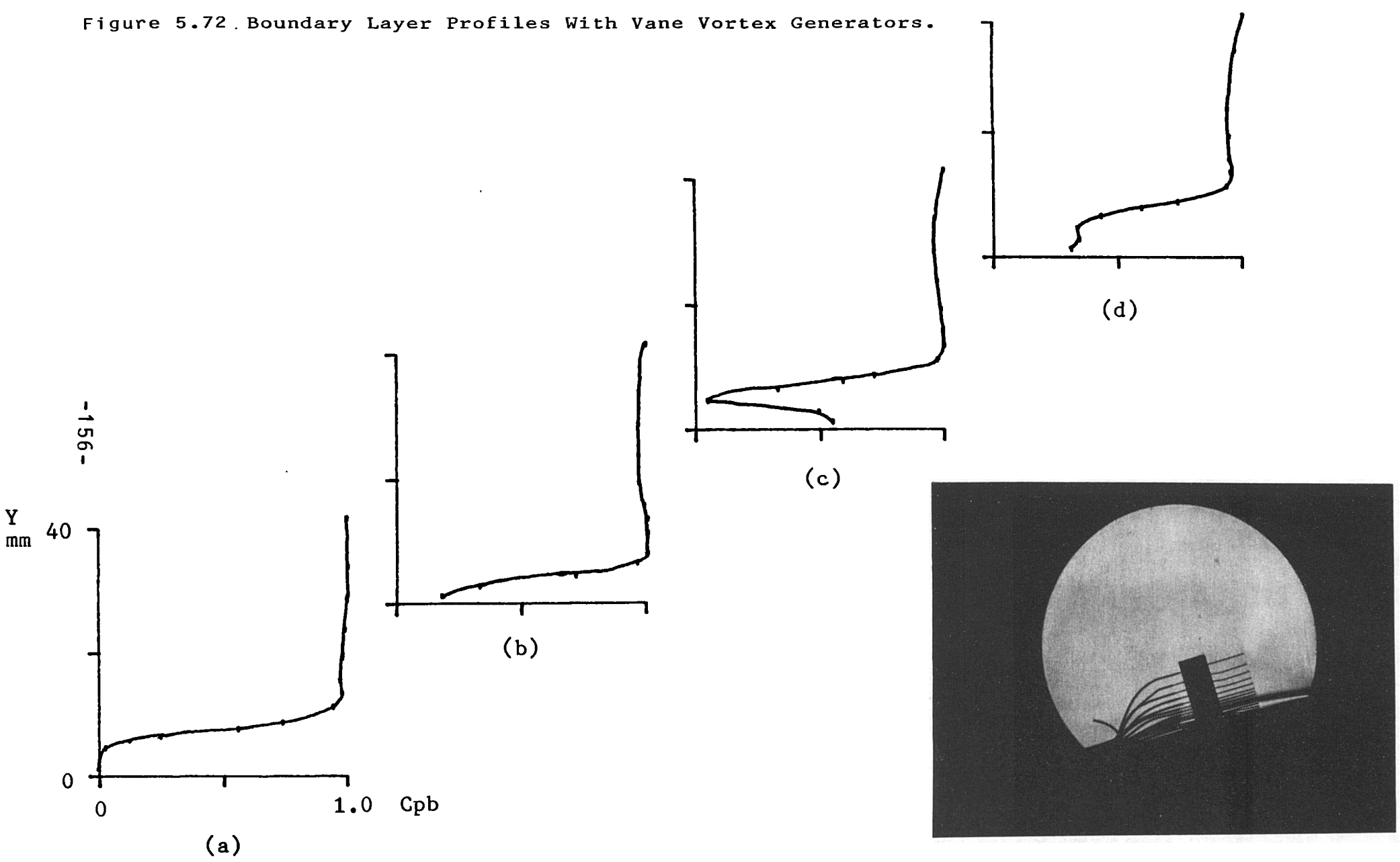

Figure 5.73 Boundary Layer Profiles With Vane Vortex Generators.

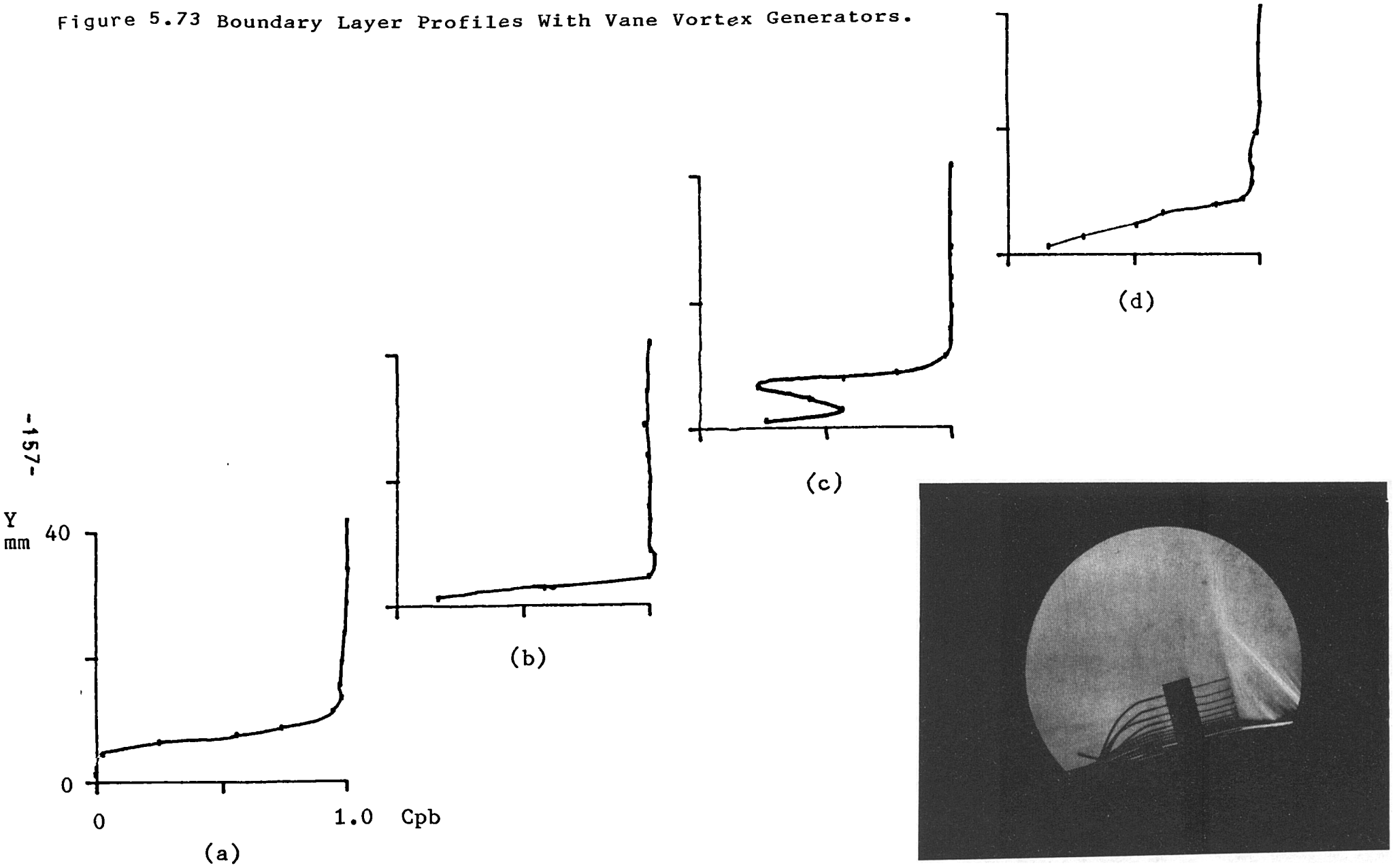

Figure 5.74 Boundary Layer Profiles With Vane Vortex Generators.

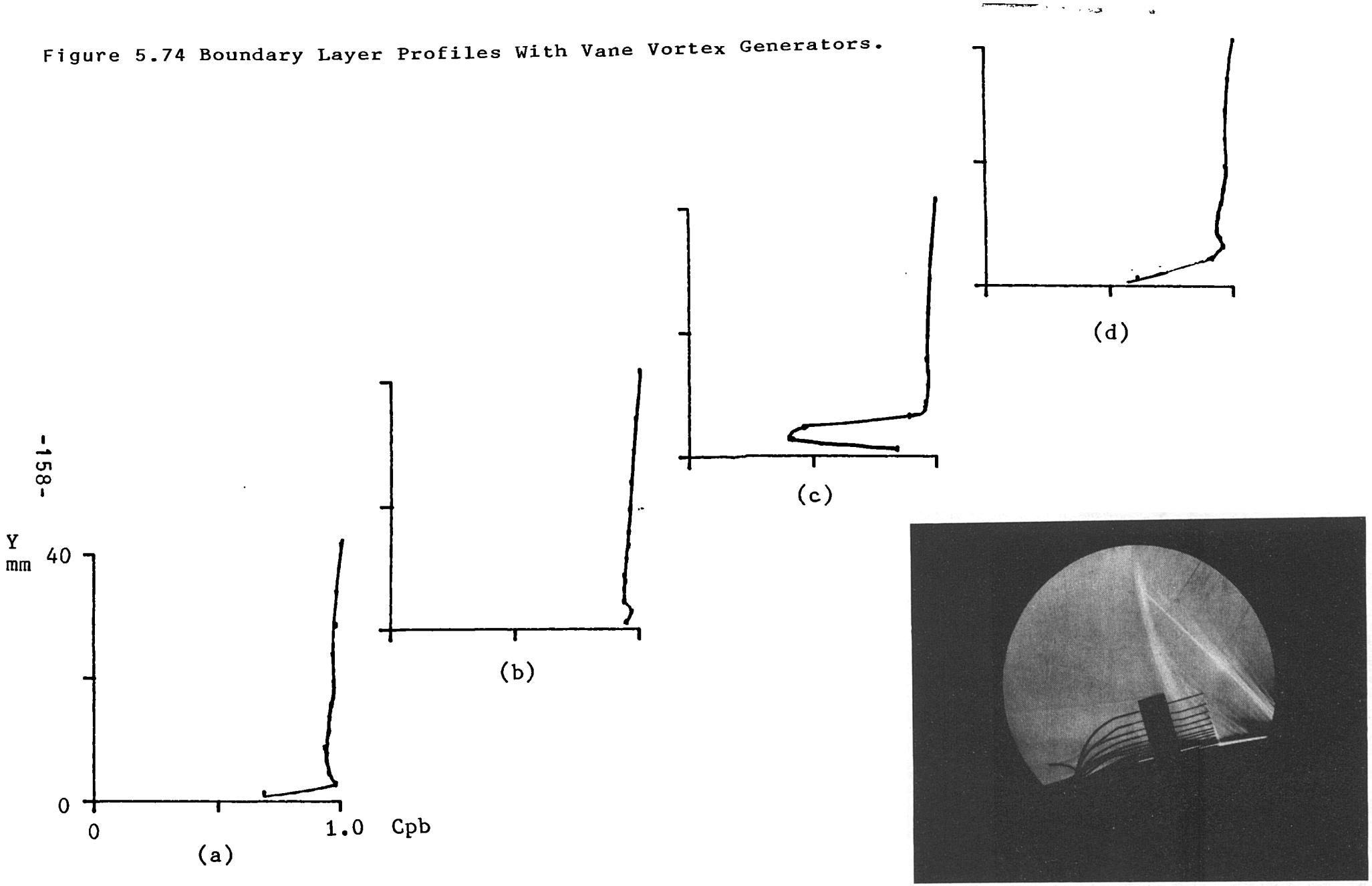

Figure 5.75 Boundary Layer Profiles With Vane Vortex Generators.

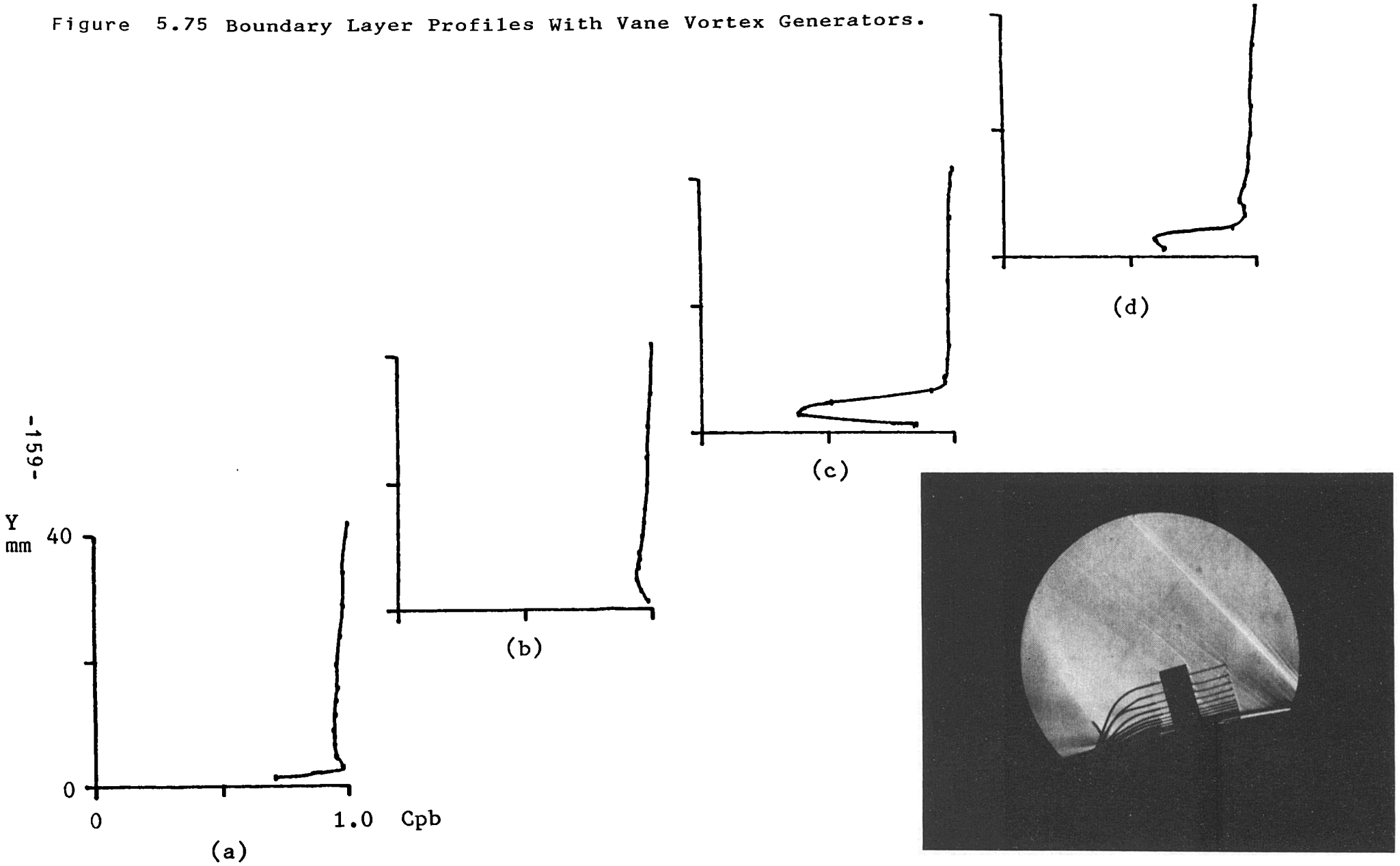

Figure 5.76 Boundary Layer Profiles With Small Air Jet Vortex Generators (P_b/P_o=1.2, Ø=30°).

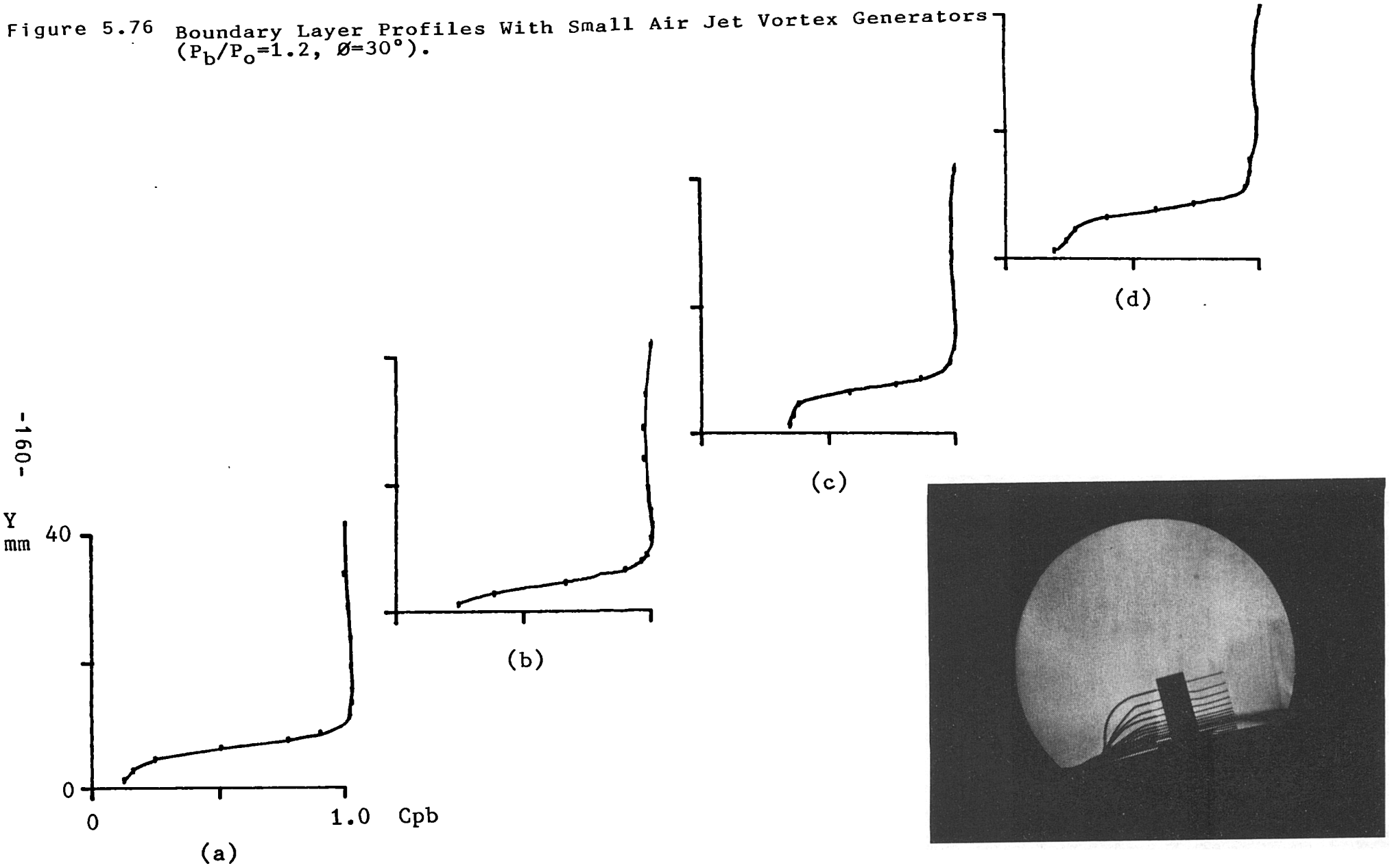

Figure 5.77 Boundary Layer Profiles With Small Air Jet Vortex Generators (P_b/P_o=1.2, ϕ=30°).

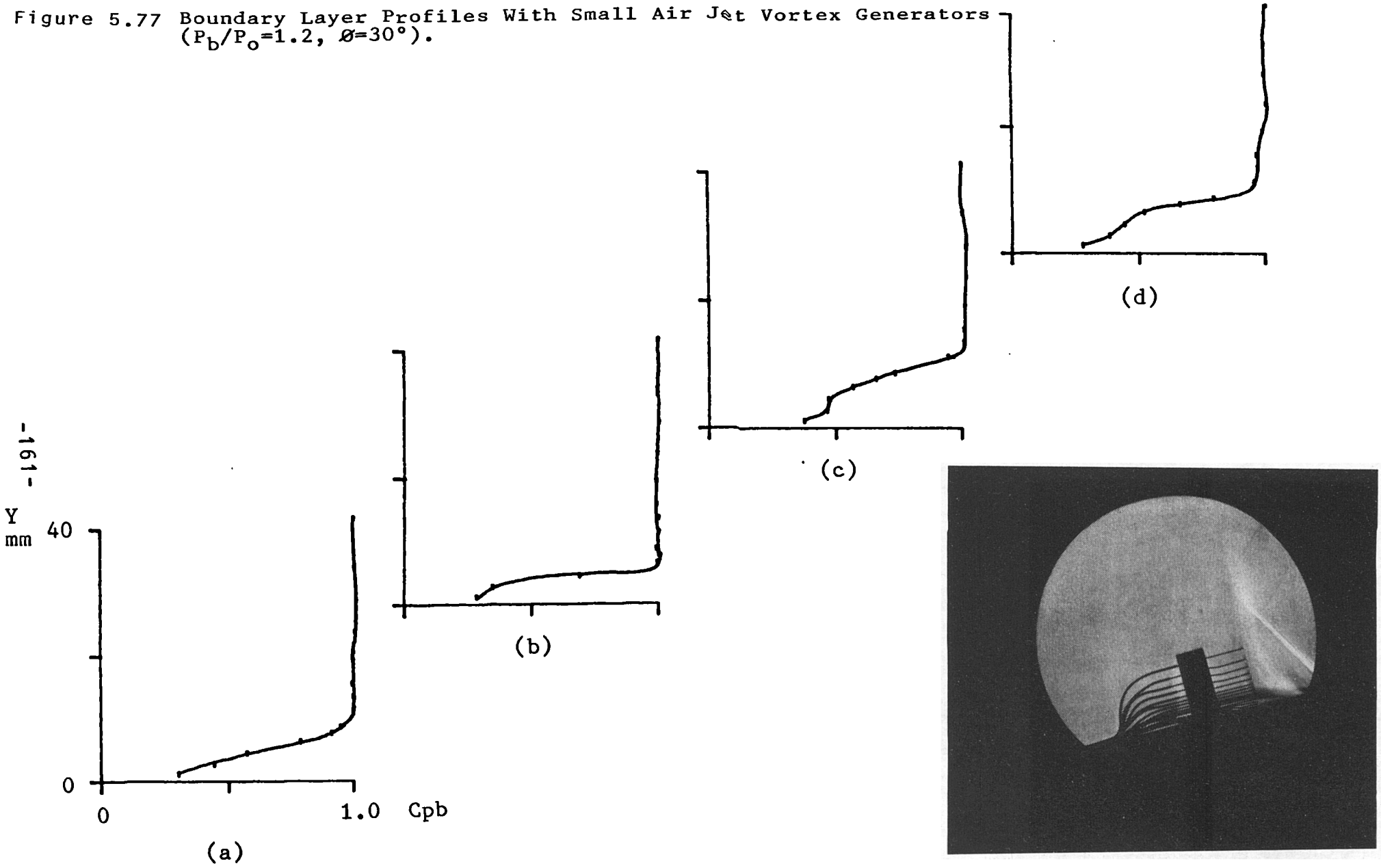

Figure 5.78 Boundary Layer Profiles With Small Air Jet Vortex Generators (P_b/P_o=1.2, ϕ=30°).

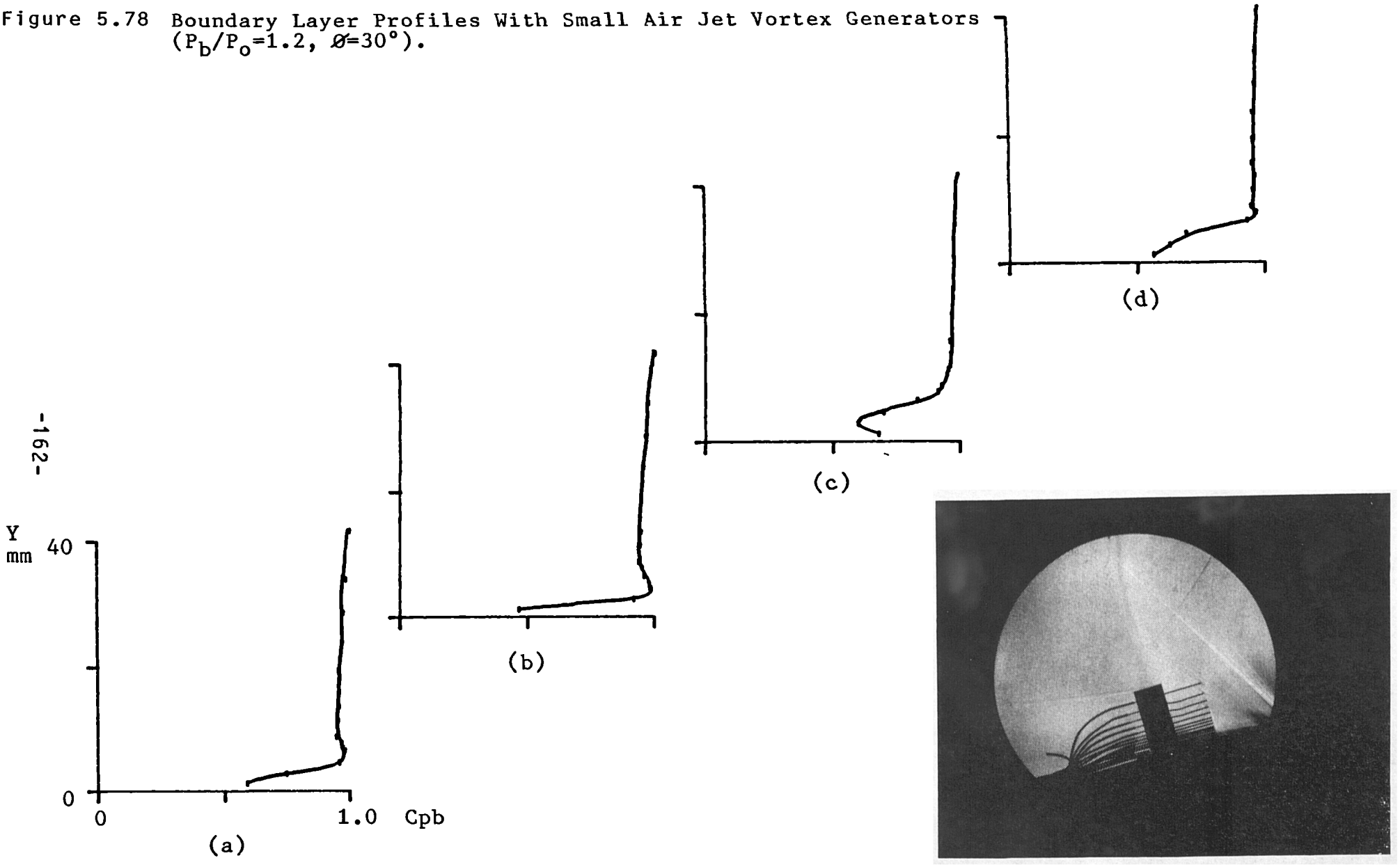

Figure 5.79 Boundary Layer Profiles With Small Air Jet Vortex Generators (P_b/P_o=1.2, ϕ=30°).

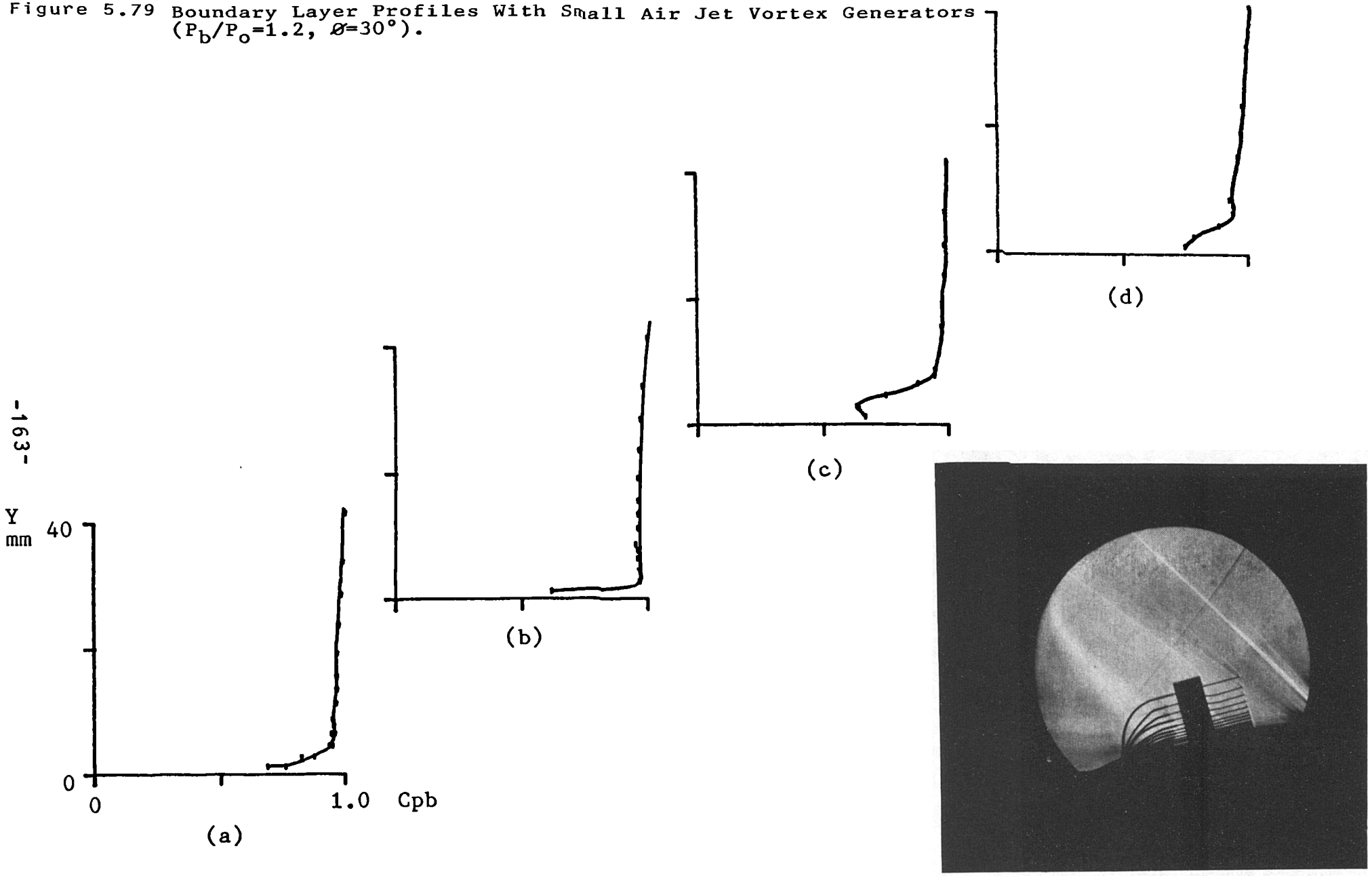

Figure 5.80 Boundary Layer Profiles With Small Air Jet Vortex Generators (P_b/P_o=1.6, ϕ=30°).

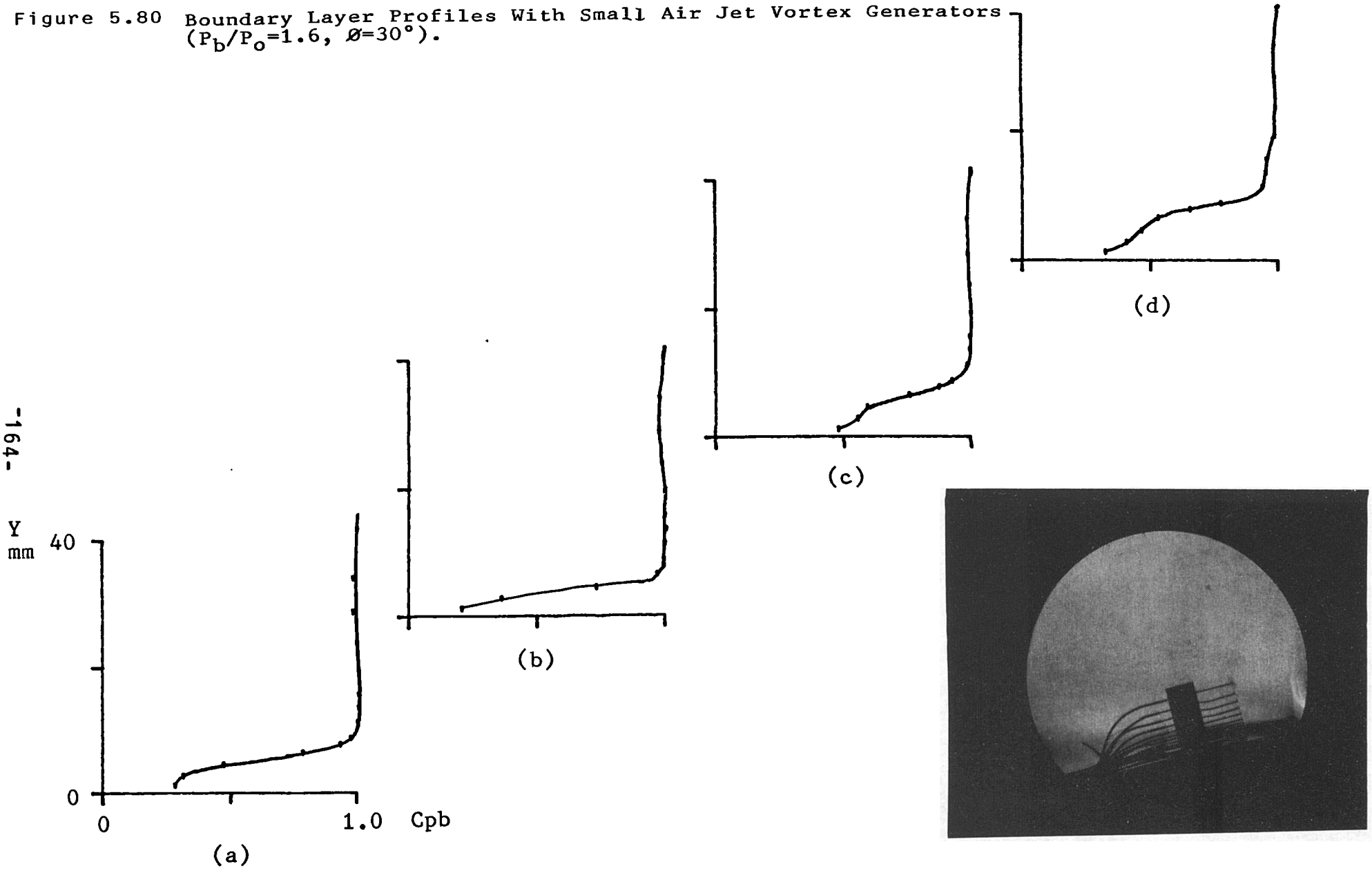

Figure 5.81 Boundary Layer Profiles With Small Air Jet Vortex Generators (P_b/P_o=1.6, Ø=30°).

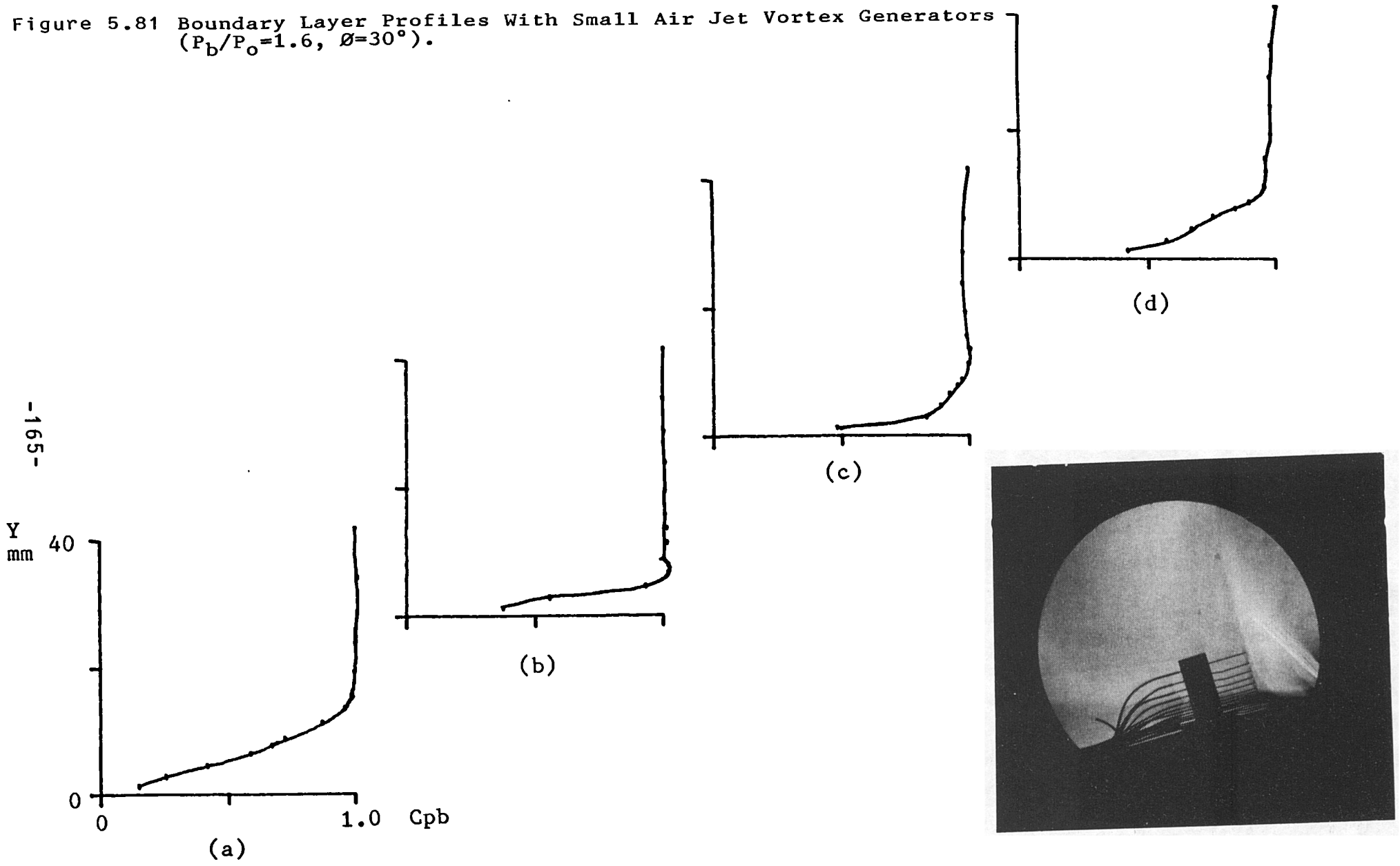

Figure 5.82 Boundary Layer Profiles With Small Air Jet Vortex Generators (P_b/P_o=1.6, Ø=30°).

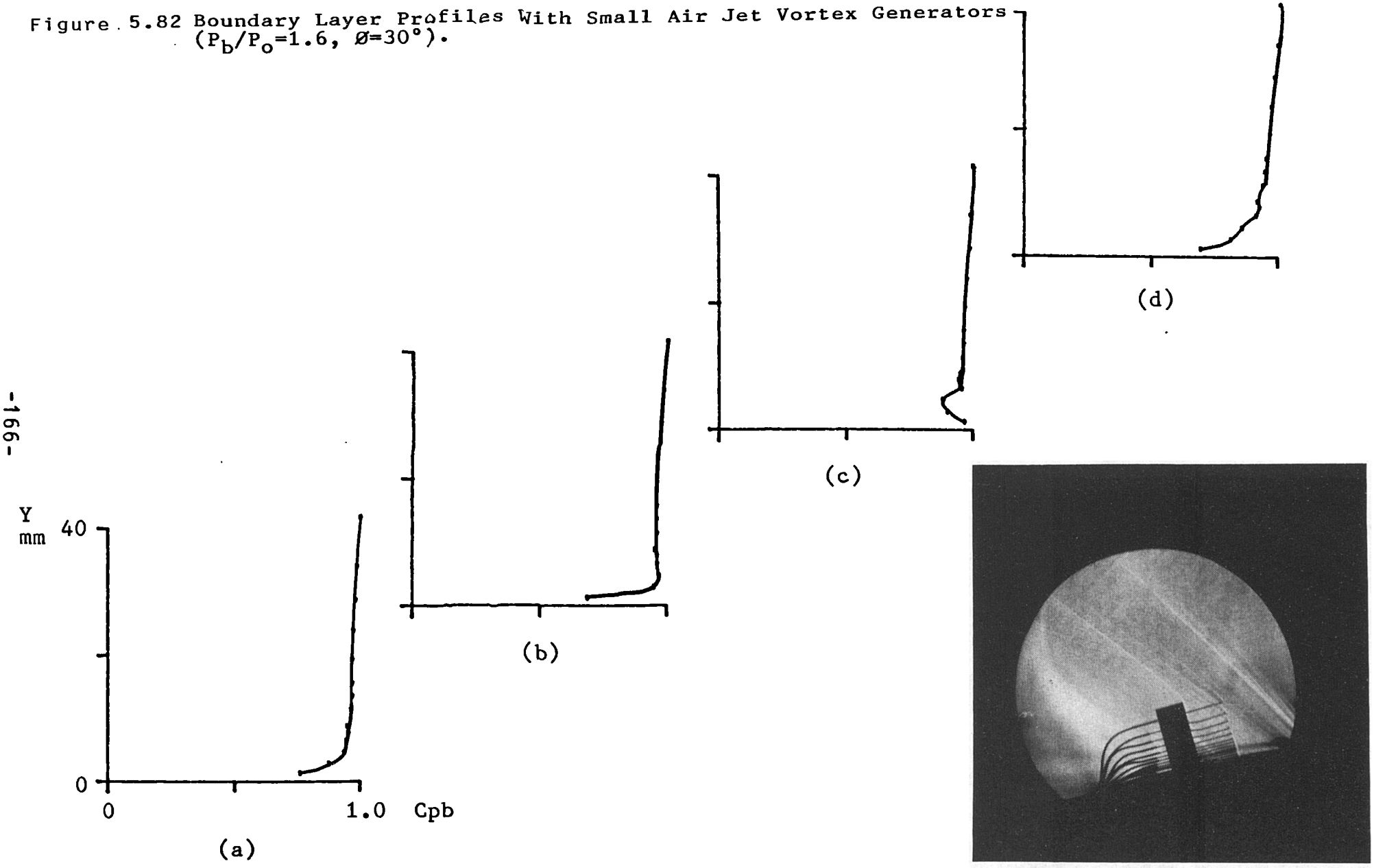

Figure 5.83 Boundary Layer Profiles With Small Air Jet Vortex Generators (P_b/P_o=1.6, ϕ=45°).

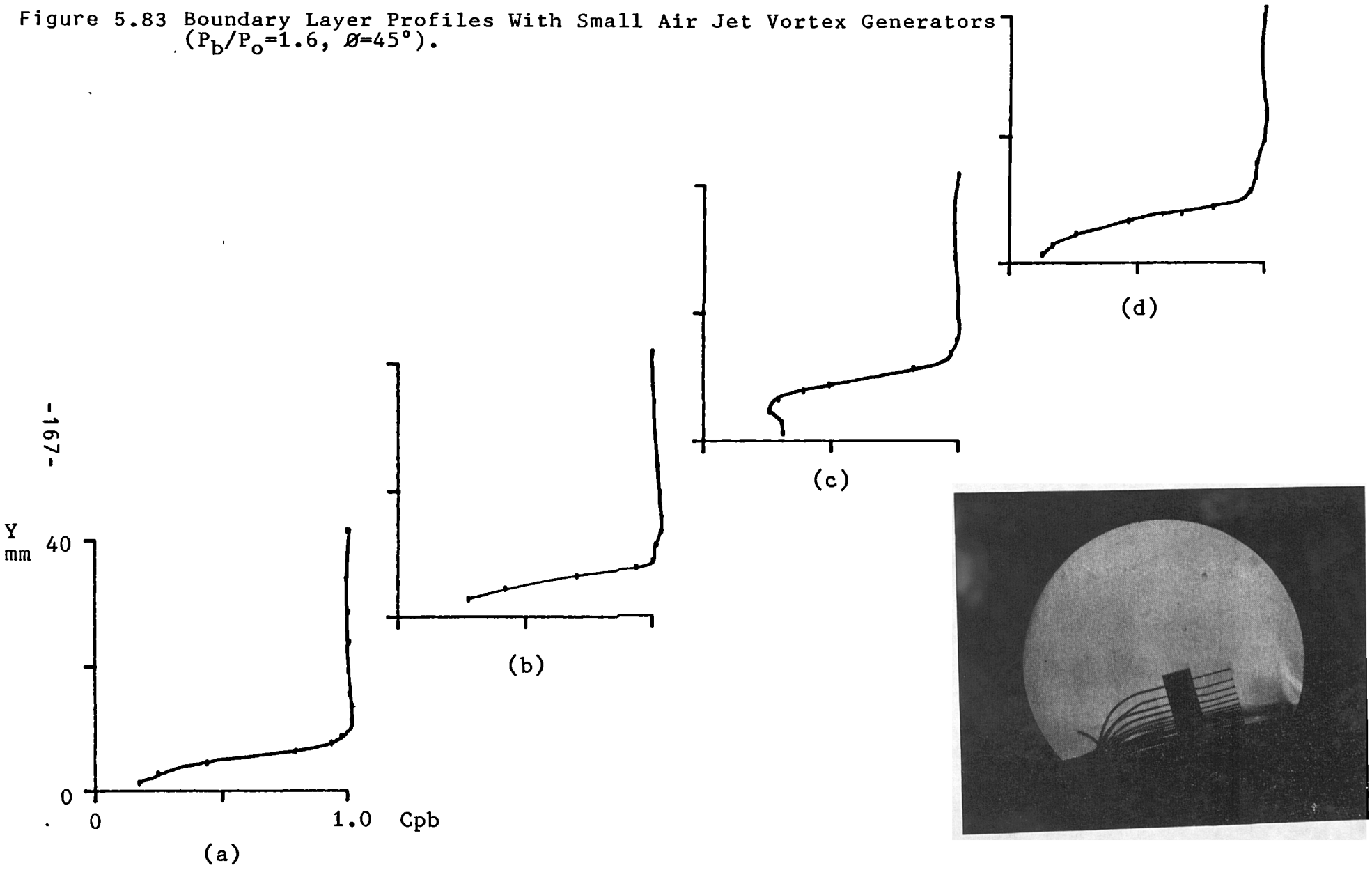

Figure 5.84 Boundary Layer Profiles With Small Air Jet Vortex Generators (P_b/P_o=1.6, Ø=45°).

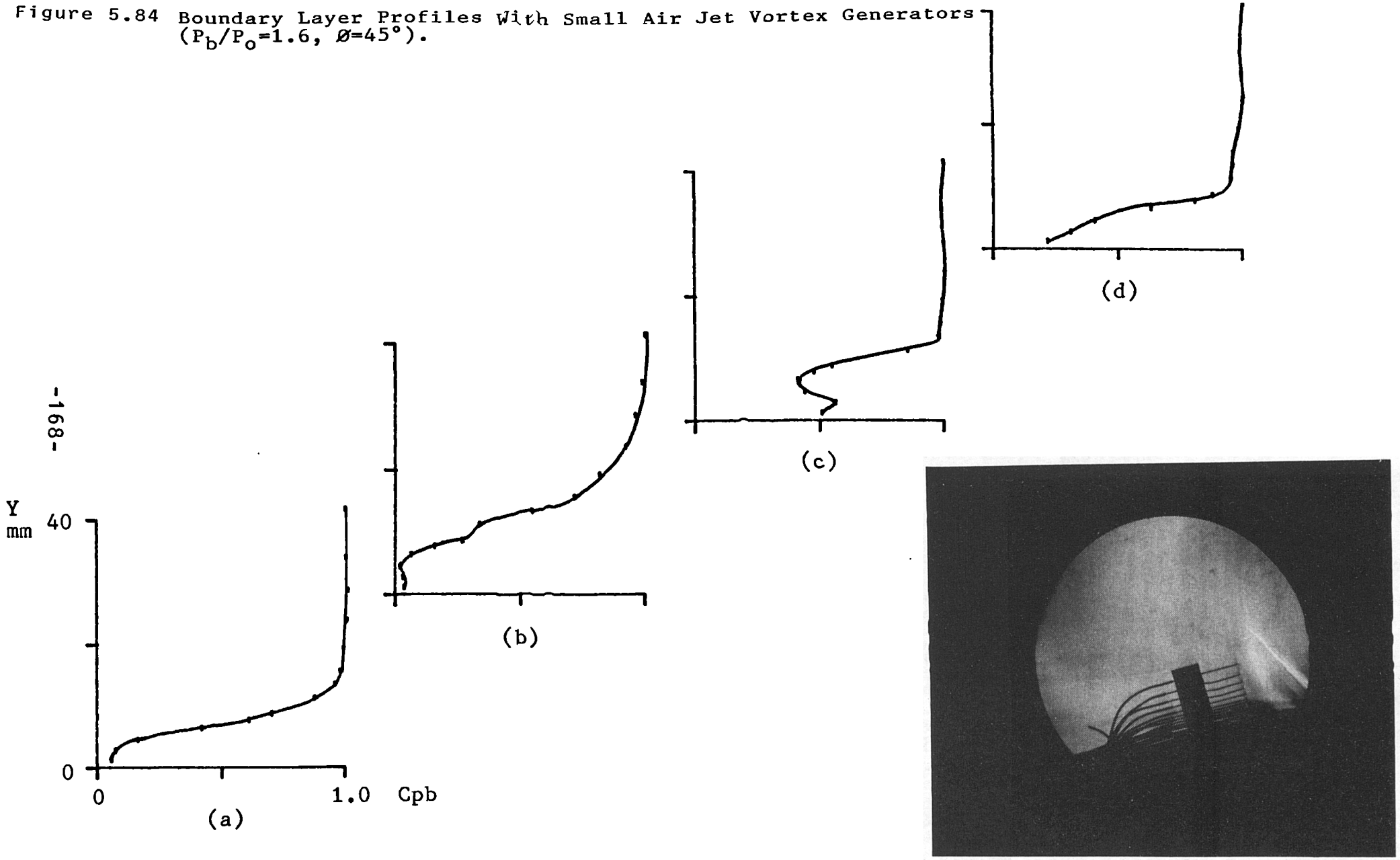

Figure 5.85 Boundary Layer Profiles With Small Air Jet Vortex Generators (P_b/P_o=1.6, Ø=45°).

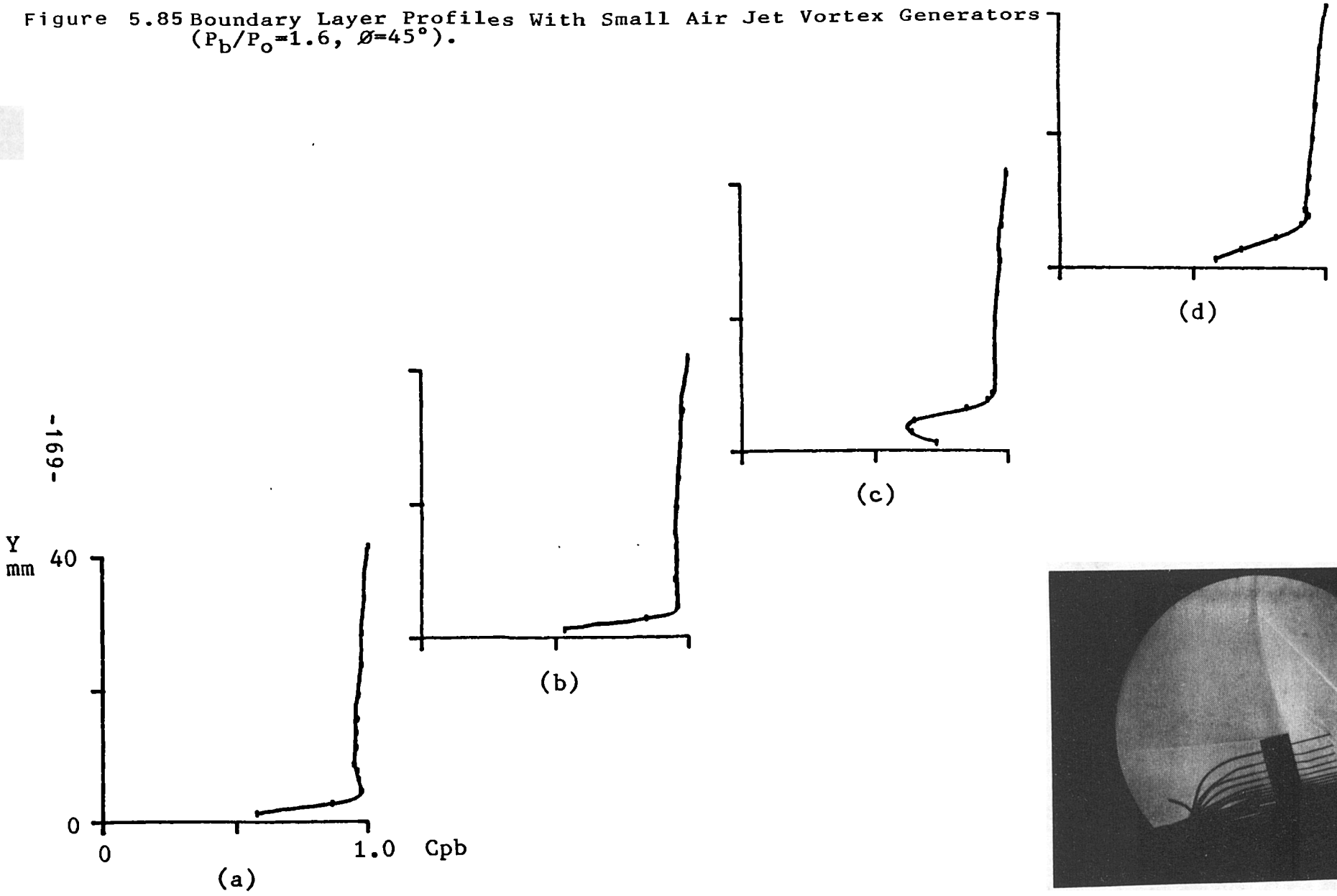

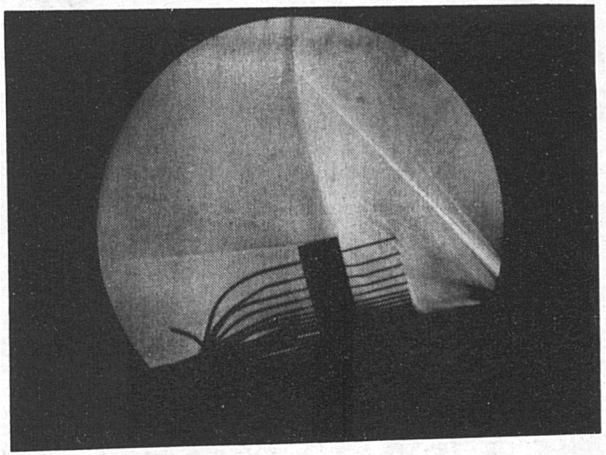

Figure 5.86 Boundary Layer Profiles With Small Air Jet Vortex Generators (P_b/P_o=1.6, ϕ=45°).

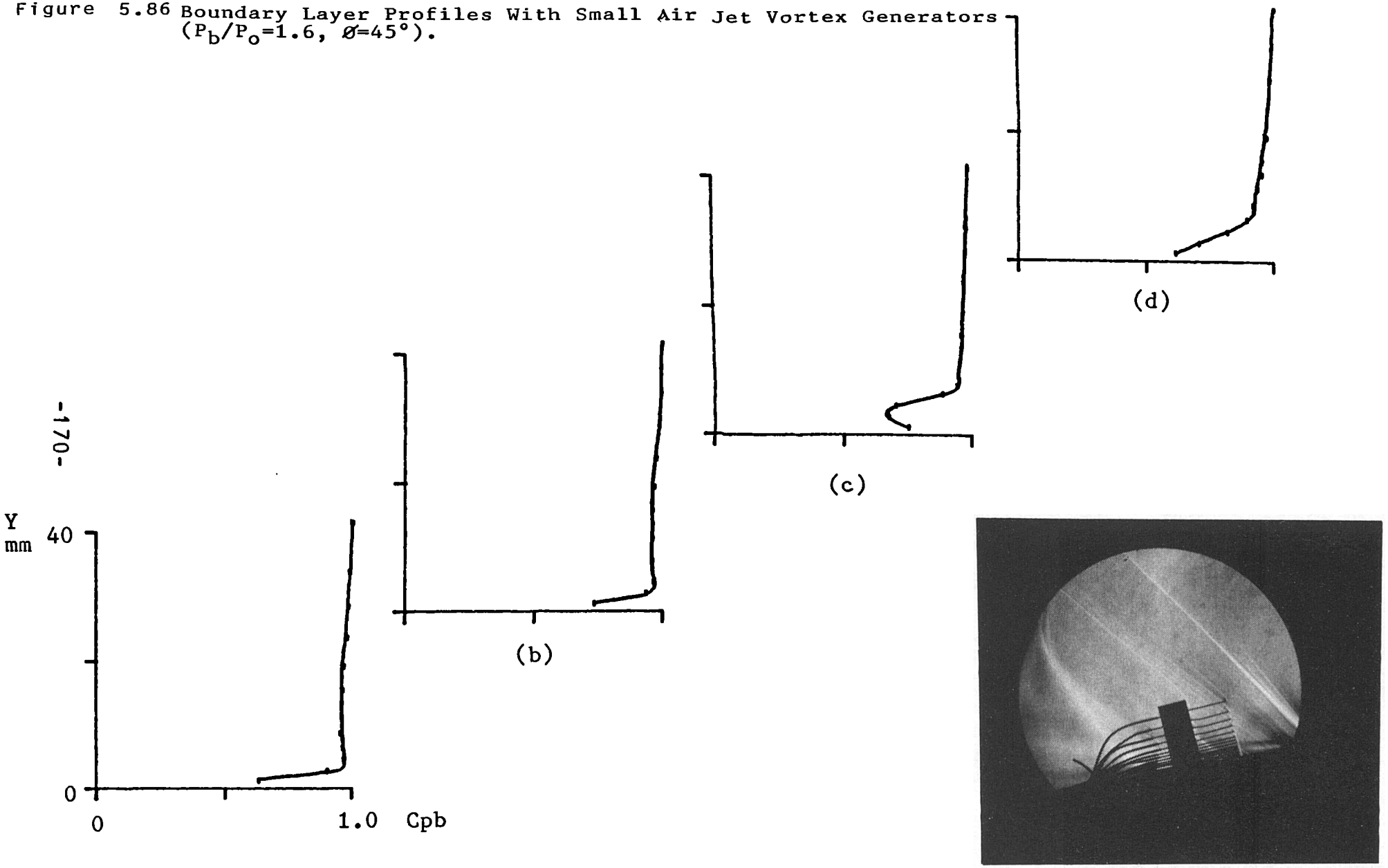

Figure 5.87 Boundary Layer Profiles With Large Air Jet Vortex Generators (P_b/P_o=1.2, θ=60°).

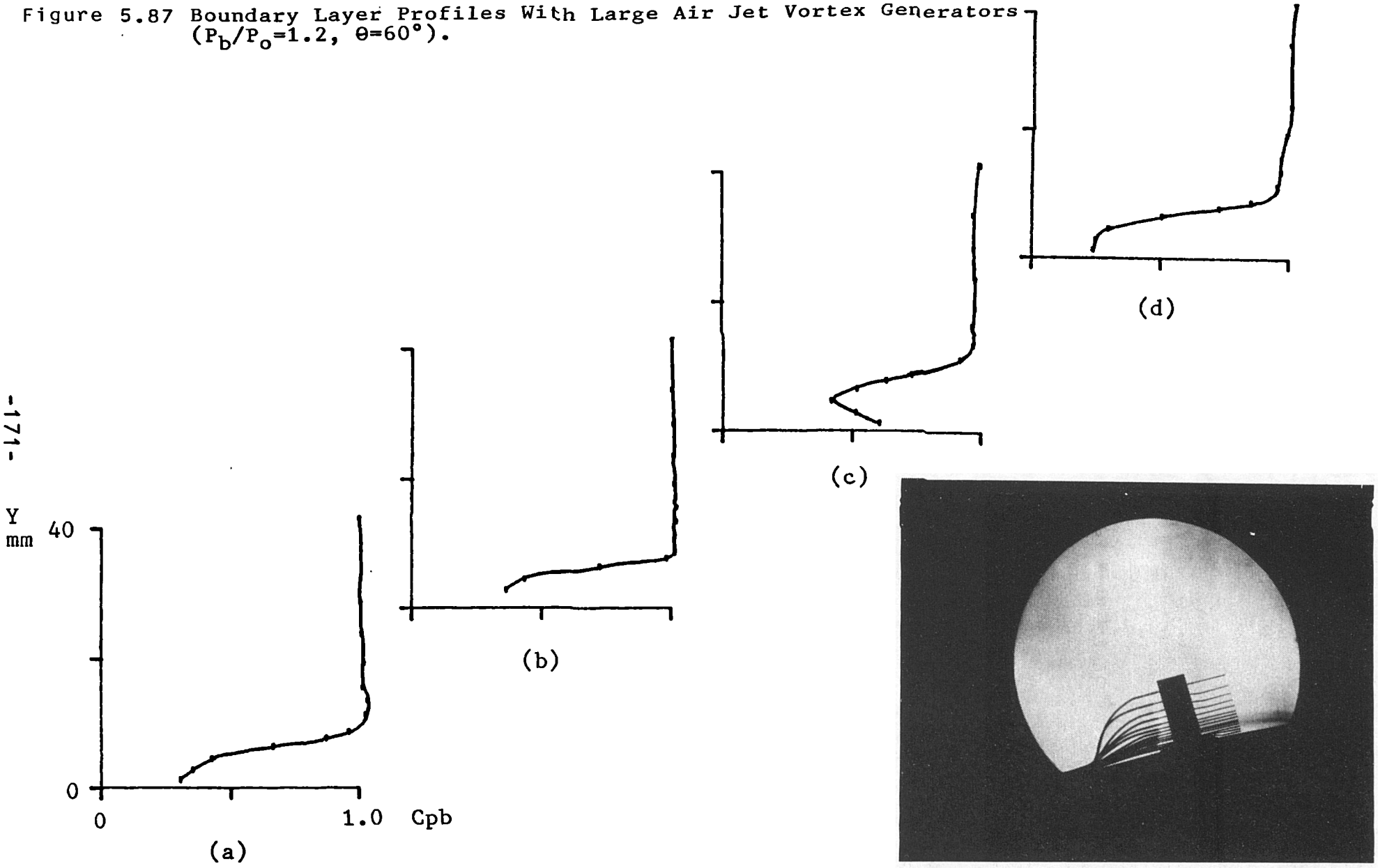

Figure 5.88 Boundary Layer Profiles With Large Air Jet Vortex Generators (P_b/P_o=1.2, θ=60°).

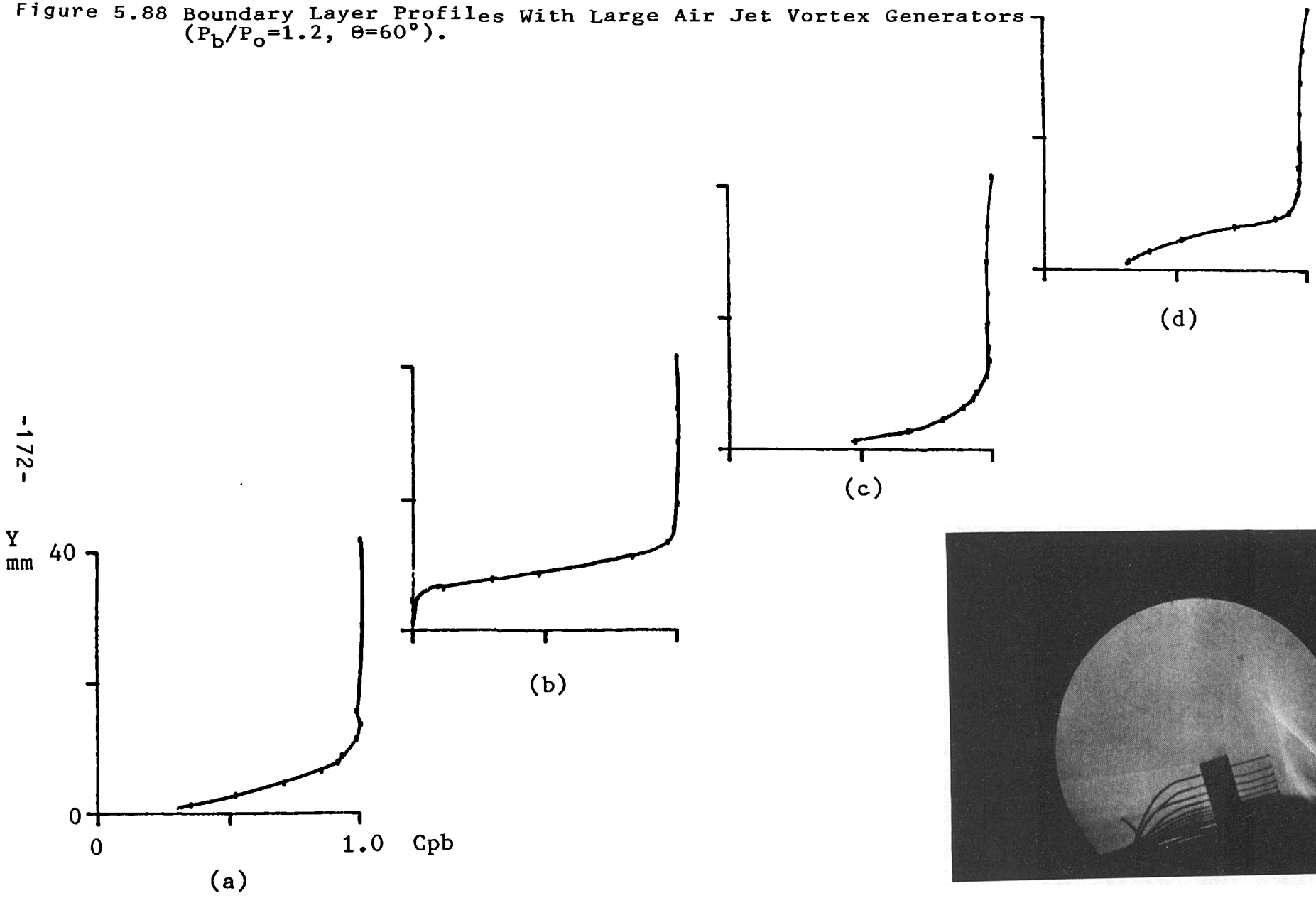

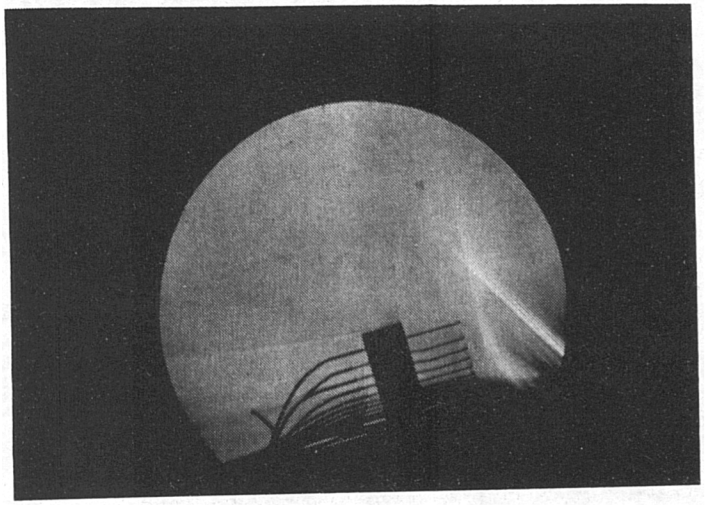

Figure 5.89 Boundary Layer Profiles With Large Air Jet Vortex Generators (P_b/P_o=1.2, θ=60°).

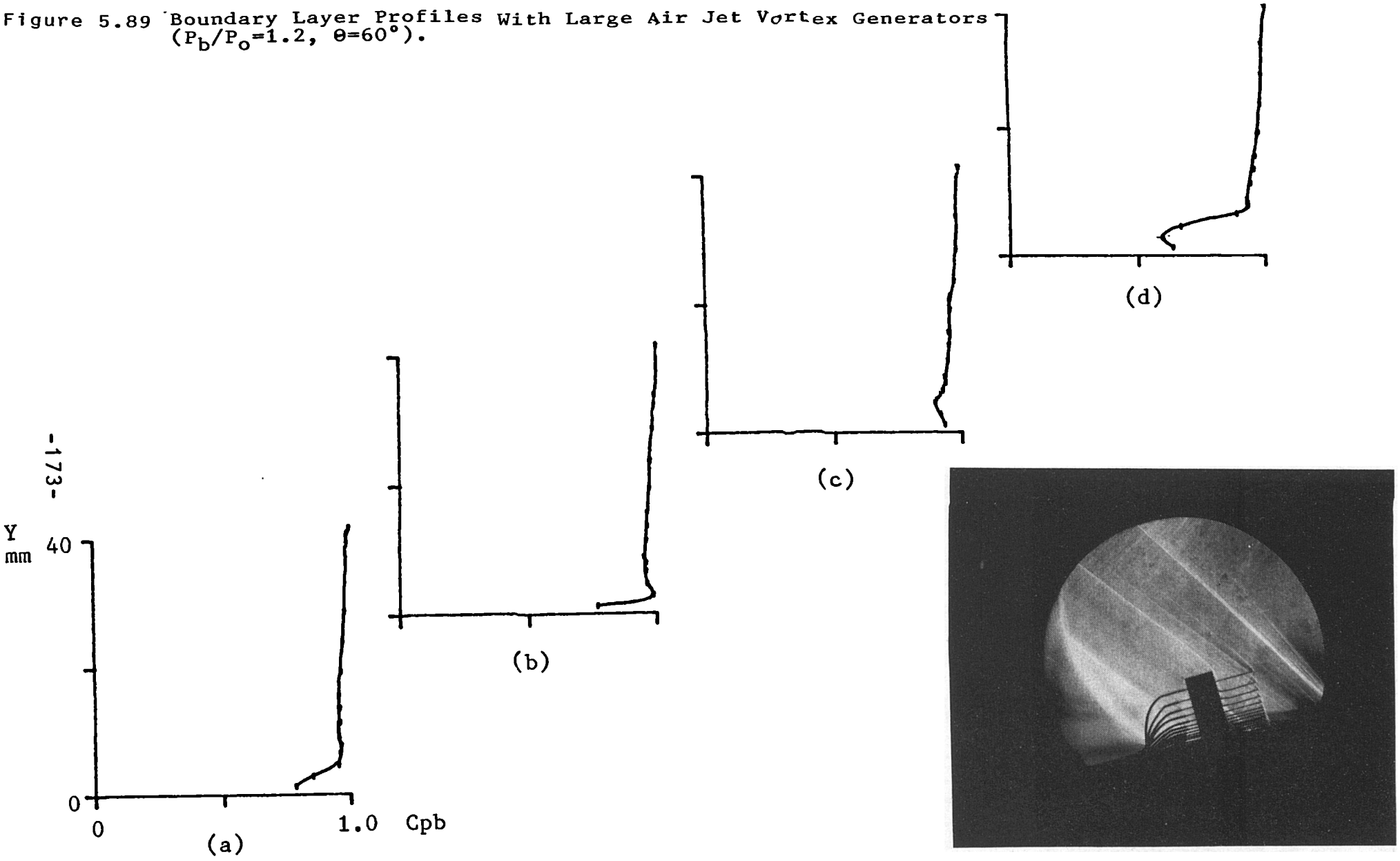

Figure 5.90 Boundary Layer Profiles With Large Air Jet Vortex Generators (P_b/P_o=1.5, θ=60°).

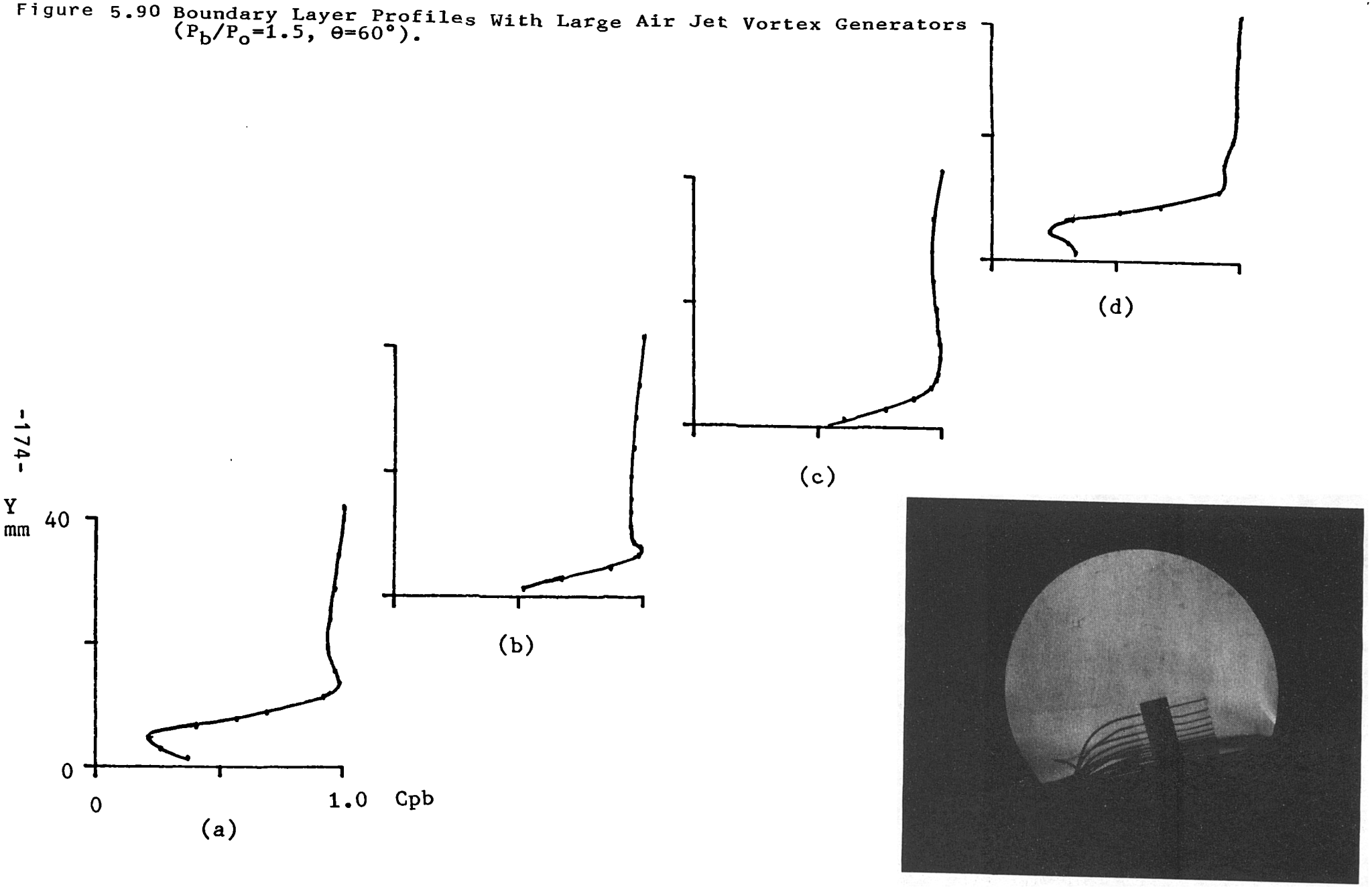

Figure 5.91 Boundary Layer Profiles With Large Air Jet Vortex Generators (P_b/P_o=1.5, θ=60°).

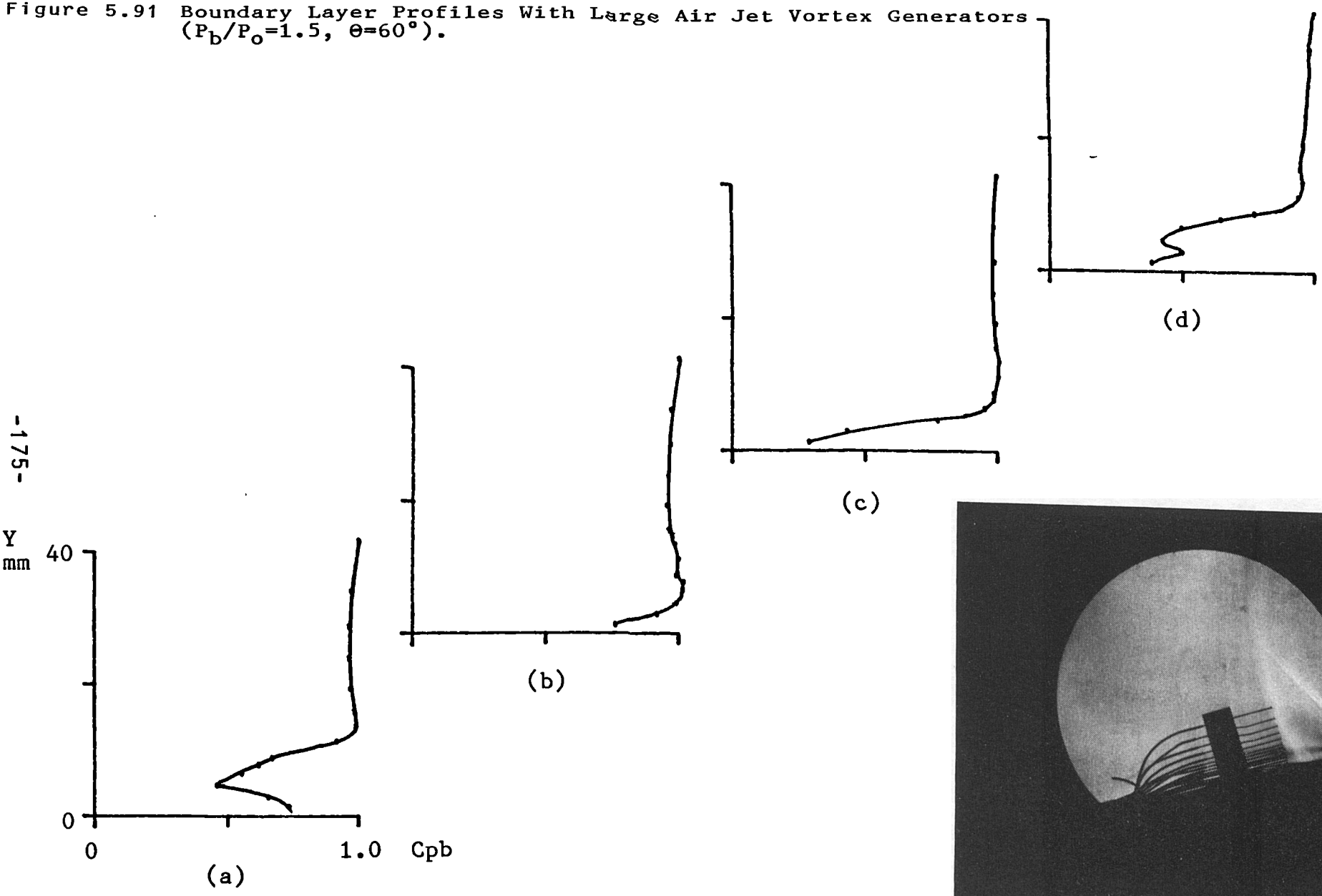

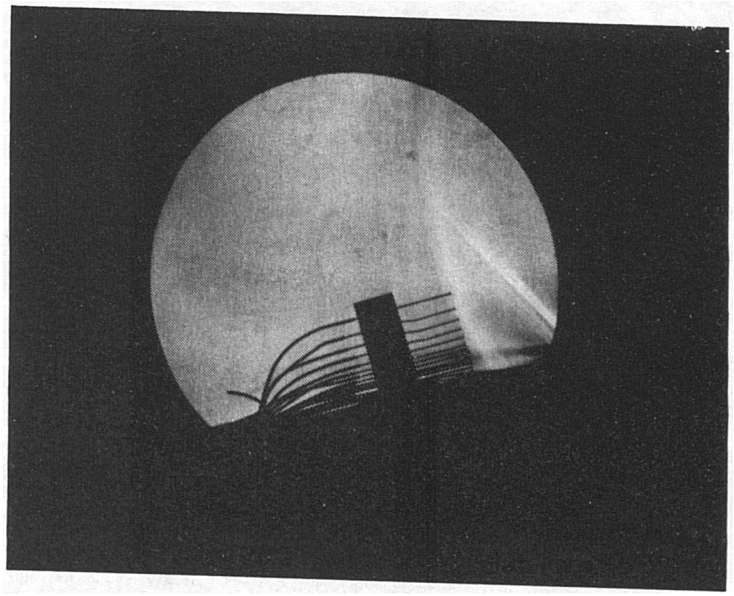

Figure 5.92 Boundary Layer Profiles With Large Air Jet Vortex Generators (P_b/P_o=1.5, θ=60°).

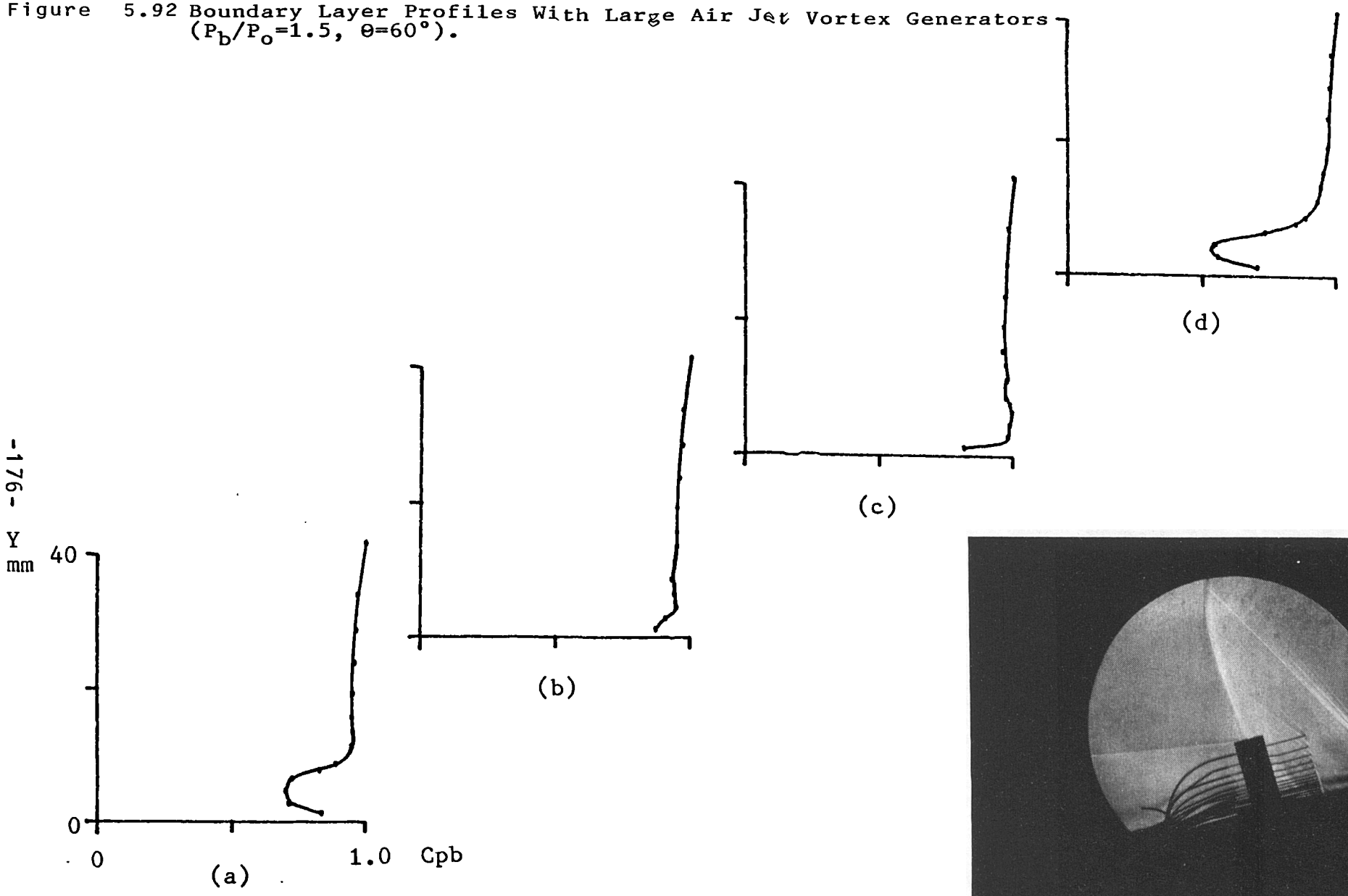

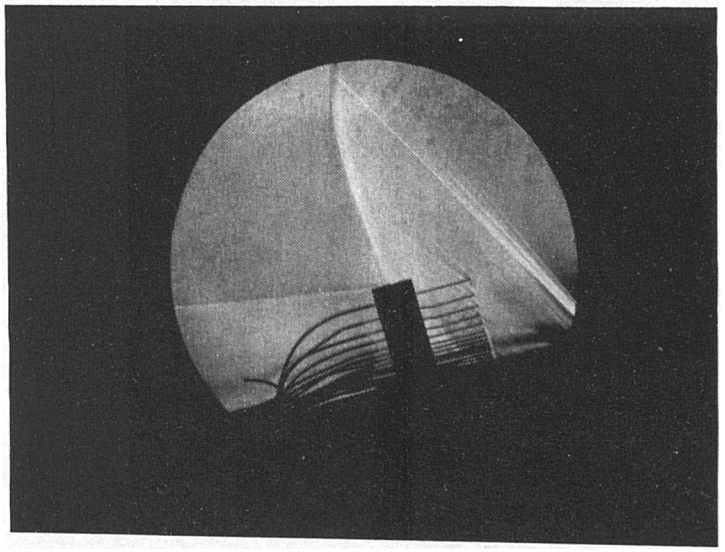

Figure 5.93 Boundary Layer Profiles With Large Air Jet Vortex Generators (P_b/P_o=1.5, θ=60°).

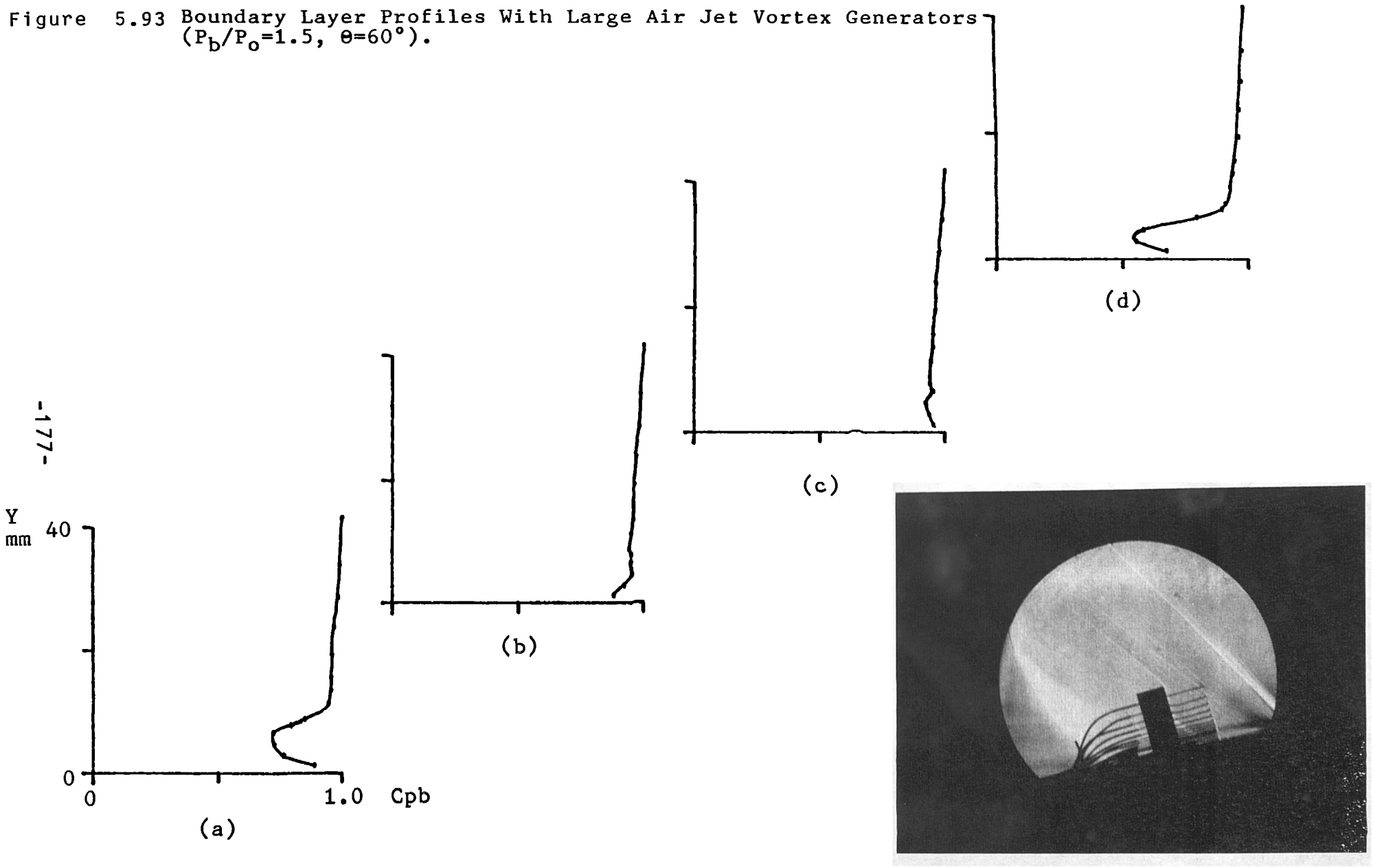

6.0 DISCUSSION OF RESULTS

This chapter discusses the method by which air jet vortex generators produce vortices, and develops an understanding of the effects of the various parameters involved. Also, the ability of air jet vortex generators to delay the onset of shock induced boundary layer separation is compared with that of vane vortex generators. The design implications of these findings are presented in this chapter, together with recommendations for further work.

6.1 Establishing the Bench Mark

In order to establish a bench mark against which to test air jet vortex generator designs, three bumps of varying thickness to chord ratios were tested. With no vortex generator devices fitted the results show that shock induced boundary layer separation was present on all three bumps (see Figures 5.7 to 5.10). The separation can be seen to be of Type A (Reference 4) and the shock pause is clearly indicated by the progressive flattening of the downstream pressure recovery while the shock positions remain constant.

The separation is more severe as the thickness of the bumps is increased from 8%, through 10%, to 14%. This is shown in Figure 6.1 where it can be seen that the pressure recoveries through the shocks are reduced as the thickness to chord ratio is increased (compare P_2 loci for the three bumps). Figure 6.2 shows the loci of shock position against trailing edge pressure for the three bumps, it can be seen that a more exacting test for the vortex generators is achieved by progressively increasing the thickness to chord ratio. Local Mach numbers ahead of the

shock were in the region of 1.40, 1.48 and 1.64 for the 8%, 10% and 14% bumps respectively.

In order to set a datum of control effectiveness, a set of nine co-rotating vane vortex generators were tested on all three bumps. The height, pitch and incidence of the vanes were selected according to Pearcey's guidelines mentioned in section 3.1.2 and detailed in Reference 1.

The results for the vane vortex generators were presented in chapter 5 (Figure 5.11 to 5.14) and showed that, where the bumps previously exhibited significant amounts of shock induced boundary layer separation, the addition of vane vortex generators has delayed the onset of this separation. This is shown by the increase in the shock downstream pressures P_2 (see Figures 6.3 to 6.5). The increase in trailing edge pressure recovery (P_{TE}/P_0) for a range of shock positions can be seen in Figures 6.6 to 6.8 where the absence of a shock pause is also noticeable. Further evidence of the ability of the vane vortex generators to delay the onset of shock induced boundary layer separation can be obtained by comparing schlieren photographs (compare Figure 6.9 with Figure 6.10). The boundary layer can be seen to be separated in the absence of vane vortex generators. The effect of the vane vortex generators can also be seen by comparing the boundary layer profiles in Figures 6.11 and 6.12 where the separated flow is clearly evident for the case without the generators.

Hence, it has been demonstrated that significant shock induced boundary layer separation was present on all three bumps and the vane vortex generators successfully delayed the onset and/or reduced the severity of the onset of this

separation. Therefore it was judged that these bumps would prove to be a good test of the ability of air jet vortex generators to delay the onset of separation and that the vanes would be a suitable datum against which to compare their effectiveness.

6.2 Air Jet Vortex Generators

Air jet vortex generators were originally investigated by Wallis (2). Results showed that their effectiveness in delaying shock induced boundary layer separation was not as good as vane type vortex generators. More recent low speed wind tunnel tests (Reference 3) indicated that the strength of the vortex could be increased considerably by using rectangular jet exits with a downstream component, rather than the round exits blowing across the freestream as used by Wallis.

It was felt that in order to evaluate the effectiveness of air jet vortex generators it would necessary to understand the mechanism by which an air jet forms a vortex, and to establish the influence of various design parameters on vortex size, strength and position. The following parameters were investigated using a combination of high speed wind tunnel tests and flow visualisation in a water channel:

- exit shape
- exit size
- jet direction
- jet inclination
- blowing pressure.

6.2.1 Method of Vortex Formation

The flow visualisation tests carried out in the water channel showed that the fluid issuing from the jet exit formed the vortex core, and the vortex itself is established by the mainstream flow wrapping itself around this core. This interaction was illustrated in Figure 5.1. Just upstream of the jet the mainstream is forced to divert as part of the flow follows the jet direction and part is diverted away from the jet. Immediately downstream of the exit, the diverted flow is entrained towards the jet and passes beneath it wrapping itself around the jet to form a vortex. It is the cross flow between the jet flow and the mainstream entrained beneath it which is responsible for the circulation required to generate the vortex. Hence, the properties of the jet will have a significant influence on the size, strength and position of the resulting vortex. The influence of the various jet parameters are dealt with in the following sections.

6.2.2 Influence of Exit Length

It was observed in the flow visualisation tests that, for a jet configuration which produced a vortex, any increase in the length (l) of the jet exit resulted in an increase in the diameter of the vortex. The reason for this increase in diameter is probably associated with the method by which the jet forms a vortex. As previously mentioned, the jet flow forms the core of the vortex and if the length of the jet is increased the core size must also increase. Since the vortex is formed as a result of the mainstream flow wrapping itself around this core any increase in core size results in an increase in the diameter of the vortex which is formed.

This increase in vortex diameter as a result of an increase in jet exit length was also observed in the high speed wind tunnel tests. The schlieren image of a row of vortices appears as a pale and dark band above the dark boundary layer and the diameter of the vortex has been defined as the width of the band (see Section 5.2). The schlieren image of vortices produced by the small and large jets ($\emptyset$=30° and θ=60°) are presented in Figures 6.13 and 6.14 respectively. Comparing Figure 6.13 with 6.14 it can clearly be seen that the diameter of the vortex has increased as a result of increasing the length of the jet exit.

Further evidence can be obtained by comparing the boundary layer profiles for the two cases. Figure 6.15 shows the boundary layer profiles obtained when the small jet exits were used and profile (c) shows the pressure drop associated with the vortex. Similarly, Figure 6.16 shows the boundary layer profiles when the large air jets were used and profile (a) shows the vortex. The diameter of the vortex has been loosely defined as the extent of the pressure drop region (see section 5.3) and based on this assumption it can be seen by comparing Figure 6.15 with 6.16 that increasing the length of the jet exit results in vortices of larger diameter. As previously mentioned, the boundary layer profile may not cut the vortex at its centre so relative sizes from profile to profile must be treated with caution.

The influence of exit length on vortex strength is dependant on the blowing pressure which is dealt with in Section 6.2.5. But briefly, as the jet exit length is increased it is proposed that for a constant blowing pressure (increased mass flow rate) a corresponding increase in vortex strength will be obtained.

Summarising, it can be said that the diameter of the vortex is proportional to the jet exit length and for a constant blowing pressure the vortex strength will also increase as the exit length increases.

6.2.3 Influence of Jet Direction

Experiments carried out by Freestone (3) in a low speed wind tunnel have shown that a significant increase in vortex strength could be achieved by giving the jets a small downstream component. Similar investigations carried out in these high speed tests for jet directions between 45° and 90° resulted in a variation in their effectiveness in delaying the onset of shock induced boundary layer separation.

The proposed model for vortex formation showed that it is the cross flow of the mainstream passing beneath the jet flow which is responsible for the initiation of the vortex. Figure 6.17 shows the influence of this cross flow for various jet direction. It can be seen that for $\theta=0°$ their would be very little effective cross flow and as a result a pair of weak counter rotating vortices are formed. For $\theta=90°$, where the relative angle between the mainstream flow and the jet flow is a maximum, tests have shown that there is very little vortex strength. This is because, although the mainstream flow is diverted by a large amount the entrainment of this flow beneath the jet flow is weak and hence there is again very little cross flow or vortex strength. The 'optimum' jet direction must therefore lie somewhere between these two extremes where there is both an initial diversion of the mainstream flow and a strong entrainment of the flow beneath the jet.

Tests in the water channel showed that a lower blowing pressure was required to instigate the formation of a vortex as the jet was given a downstream component (see Figure 5.2). The best jet direction appeared to be 45° because any further increase in the downstream component beyond 45° resulted in an increase in the critical blowing pressure. The high speed wind tunnel tests confirmed that θ=45° is the better angle (see Section 6.3.3).

6.2.4 Influence of Jet inclination

Although jet inclination was not investigated in the water channel tests, the proposed model indicates that a minimum inclination is required to allow the freestream flow to pass beneath the jet flow, and hence form a vortex (see Figure 5.1). The wind tunnel results have shown that increasing the inclination of the jet, from $\emptyset$=30° to $\emptyset$=45°, results in an increase in the strength and diameter of the vortex. This increase in strength and diameter can be seen by comparing the boundary layer profiles for small jets inclined at 30° and 45°. Figure 6.15 shows the profiles for the jets inclined at 30° and profile (c) shows the pressure drop associated with the vortex. The boundary layer profiles associated with the jet exits inclined at 45° are presented in Figure 6.18 and again profile (c) shows the vortex. Comparing profile (c) in Figure 6.15 with that in Figure 6.18 it can be seen that the pressure drop associated with the vortex is more pronounced when the jet exits were inclined at 45°. As mentioned in Section 5.3 the strength and diameter of a vortex can be related to the extent of the pressure drop. Hence it can be said that the jet exits inclined at 45° produce vortices of increased strength and diameter.

Further evidence to support this finding can be obtained by comparing the schlieren photographs for the two cases (compare Figures 6.19 with 6.20). The schlieren image of the vortices produced by the jet exits inclined at 45° are slightly wider and more prominent than image produced by the jet exits inclined at 30°. The wider image can be associated with a vortex of increased diameter and the more prominent image can be interpreted as an increase in vortex strength.

A reasonable explanation for this proposed increase in vortex strength and diameter is that the jet inclination determines the height at which the jet penetrates into the mainstream. Therefore, as the jet inclination is increased the distance between the jet flow and the model surface increases allowing the mainstream air to be entrained more efficiently beneath the jet (see Figure 5.1). It is also reasonable to assume that increasing the inclination of the jet exit will result in the vortex centre forming further away from the surface. Hence, there must also exist a maximum inclination angle beyond which the vortex would form outside the boundary layer. A vortex formed outside the boundary layer would have less influence on the characteristics of the boundary layer profile and therefore will have no beneficial effect in delaying the onset of shock induced separation.

6.2.5 Influence of Blowing Pressure

The effect of varying blowing pressure was investigated in the water channel tests and it was found that a critical blowing pressure existed, for a given jet configuration, below which a vortex was not formed. Increasing the blowing pressure, beyond this critical value, resulted in

a vortex of increased strength. This increase in strength was evident by the fact that the rotational speed of the flow around the vortex was greater.

A reasonable hypothesis for this behaviour could be that an increase in blowing pressure results in an increase in jet velocity (V) and therefore an increase in the differential pressure between the jet flow and the local mainstream (Ue). The increased pressure differential makes the entrainment of the mainstream flow (see Figure 5.1) more vigorous which results in the increase in the rotation speed of the flow around the vortex and hence an increase in the strength of the vortex.

This increase in strength was observed in the boundary layer investigation where the drop in pressure associated with the vortex was clearly more pronounced for the higher blowing pressures (compare Figures 6.21 with 6.22). Also, comparing the schlieren photographs associated with these boundary layer profiles it can be seen that the vortex image associated with the higher blowing pressure is more distinct and therefore can be interpreted as having an increased vortex strength.

6.3 Qualitative Assessment of the Effectiveness of Air Jet Vortex Generators.

The effectiveness in delaying the onset of significant effects of shock induced boundary layer separation of the various air jet vortex generators is described and compared with vane vortex generators in the following section. The observations made from the water channel and

high speed tests are used to explain some of the important features.

6.3.1 Round Air Jet Vortex Generators

Round air jet vortex generators which were designed to be similar to those used by Wallis (2) (see Section 3.3) were tested on the 8% bump. The jet exits were inclined to the surface at 45° (ϕ=45°) and initially directed at 90° (θ=90°) to the freestream. The blowing pressure used in these tests was P_b/P_o=1.0. Figure 6.23 shows that in terms of pressure recovery at the trailing edge, these round air jets were effective in delaying the onset of significant effects of separation, but were not as effective as the vane vortex generators.

Changing the jet direction to 60° resulted in an increase in the effectiveness, especially for shock positions downstream of 65% chord (see Figure 6.24). In section 6.2.3 it was proposed that giving the jet exits a small downstream component would result in the formation of a vortex of increased strength. It is reasonable to assume that vortices of increased strength are more effective in delaying the onset of shock induced boundary layer separation since the momentum transfer will be greater. Based on this assumption the increase in strength accounts for the increased effectiveness. This jet configuration was still not as good as the vane type generators.

6.3.2 Small Rectangular Air Jet Vortex Generators

Small rectangular air jet vortex generators with jet exits inclined at 30° to the surface and directed at 60° to the freestream were tested on all three bumps. In addition, the effect of increasing the jet inclination to 45° was investigated on the 14% bump.

Figure 6.25 shows that for a blowing pressure of $P_b/P_o=1.0$ the small rectangular air jet vortex generators ($\emptyset=30°$ and $\theta=60°$) were more effective than the round air jets ($\emptyset=45°$ and $\theta=60°$). The round jets and the small rectangular jets had comparable jet exit areas. It has been proposed in section 6.2.2 that for a given jet area an increase in the length of the jet exit will result in an increase in the diameter of the resulting vortex. The small rectangular jets therefore produce vortices of larger diameter than the round jets and since the blowing pressures were equal the vortices would be of increased strength. The increased effectiveness is partially due to the increased vortex strength but more importantly the ratio between the spacing to diameter of the vortices has decreased.

As mentioned in Section 2.3 the spacing to height ratio for vane vortex generators producing co-rotating vortices is a dominant factor in their ability to delay the onset of shock induced boundary layer separation. The height of the vane determines the diameter of the resulting vortex. For air jet vortex generators it appears that the length of the jet exit governs the vortex diameter. It is proposed that the spacing to diameter ratio of the vortices produced by the round jets is above a maximum value. For the small rectangular jets this ratio is

reduced and hence the effectiveness in delaying the onset of shock induced separation is improved.

Comparing the effectiveness of the small rectangular air jets with vane type generators it can be seen from Figure 6.26 that a blowing pressure of $P_b/P_o=1.2$ was required for these small jets to be more effective than the vanes. As proposed in section 6.2.5, the effect of increasing blowing pressure is to form vortices of increased strength. This increased strength accounts for the improved effectiveness.

The small jets ($\emptyset=30°$ and $\theta=60°$) were also tested on the 10% and 14% bumps. The effect of increasing the blowing pressure was again seen to increase effectiveness in delaying the onset of significant effects of shock induced boundary layer separation (see Figure 6.27 and 6.28).

From the families of pressure distributions for these small jets (Figure 6.29 and 6.30) it can be seen that for shock positions near the generators the pressure rise occurred in two stages indicated by a separation and almost immediate reattachment. For shock positions further aft, the two stages merged into one. The pressure distributions showed that this 'dog leg' pressure rise through the shock has little effect on the overall pressure recovery at the trailing edge. In practice however, the boundary layer height at the trailing edge will probably increase as a result of this 'dog leg' pressure rise. Therefore it might be desirable to design the generators so that this form of pressure rise does not occur.

The effect of changing the jet inclination from 30° to 45° was investigated on the 14% bump using the small air vortex generators. The families of pressure distributions for blowing pressure (P_b/P_o) of 1.2 and 1.6 can be seen in Figures 6.31 and 6.32 respectively. The results showed that the jet exits inclined at 45° to the surface were more effective in delaying the onset of significant effects of shock induced boundary layer separation than those with $\varnothing$=30° but were still not as effective as the vane type generators (see Figure 6.33). More importantly, Figure 6.34 shows that the 'dog leg' pressure rises were much less pronounced when the jet exits were inclined at 45°.

A probable explanation for the 'dog leg' pressure distributions could be that the spacing between small jet exits inclined at 30° is large relative to the diameter of the vortices produced. Hence, as discussed in Section 2.3 their influence on the boundary layer will be limited. As these vortices progress downstream through the adverse pressure gradient their diameter increases (reference 16) and the ratio between spacing and vortex diameter decreases. At some point downstream this ratio passes the critical value and the vortices begin to influence the boundary layer and help reattach or delay the onset of separation.

It is important to note that the initial strength of the vortices produced by the small jets inclined at 30° was probably sufficient and if the initial spacing was reduced the 'dog leg' pressure distribution might not have occurred. Increasing the jet inclination to 45° resulted in a more efficient vortex formation giving a vortex of increased strength and diameter. The increased strength and more importantly the increased diameter accounts for

the less pronounced 'dog leg' pressure distributions when the jet exits were inclined at 45°.

Alternatively, the 'dog leg' pressure distribution could just be associated with three dimensional nature of the separation. This however is unlikely since the 'dog leg' pressure distribution was always in the same chordwise position when tests were repeated. If this phenomena had been associated with three dimensional effects then the 'dog leg' distributions would have been more random and would have occurred for several jet or vane configurations.

6.3.3 Large Rectangular Air Jet Vortex Generators

Large air jet vortex generators were tested on the 10% and 14% bumps. Various blowing pressures between P_b/P_o=1.0 and 1.8 were investigated. In addition the effect of varying jet direction between θ=45° and 75° was also investigated.

Using the large air jets (ϕ=30° and θ=60°) on the 10% bump with a blowing pressure of P_b/P_o=1.8, the pressure recovery at the trailing edge was found to be higher, for the full range of shock positions, than those found using the vane vortex generators (see Figure 6.35). Lowering the blowing pressure to P_b/P_o=1.2 and 1.0 it can be seen in Figure 6.36 that for shock positions forward of 75% chord these large air jets were as effective as vane vortex generators. For shock positions downstream of 75% chord their effectiveness fell off to zero as a severe shock pause was noted. Similar results were obtained for tests carried out on the 14% bump.

A possible reason for this shock pause for shock positions downstream of 75% chord can be found by examining the results obtained from the boundary layer investigation. The diameter of the vortices produced by the large air jets was bigger than that produced by the vanes or small air jet vortex generators (compare boundary layer profiles in Figures 6.37, 6.38 and 6.39). As previously mentioned the diameter of a vortex increases as it progress downstream through an adverse pressure gradient (reference 16). For the small air jet vortex generators the reason for the 'dog leg' pressure distribution was said to be because the vortex spacing to diameter ratio was too large. In the case of the large air jets it is possible that this ratio is too small.

Initially, the spacing between the vortices produced by the large air jets is above the minimum value at the generator position but as the vortices translate downstream through the adverse pressure gradient they increases in diameter. At 75% chord the vortices have increased in diameter to the extent that their spacing is no longer above the minimum value and they interfere with each other. At this point the vortices have little effect on the boundary layer and the flow separates as it passes through the shock resulting in the observed shock pause.

The vortices produced by increasing the blowing pressure to P_b/P_o=1.8 are of increased strength and therefore do not decay (increase in diameter) as rapidly as the vortices produced using the lower blowing pressures (Reference 16). Hence their spacing remains above the minimum required, and they are effective in delaying the onset of shock induced boundary layer separation for shock positions right back to the trailing edge.

The large rectangular air jets were tested over a range of jet directions and from Figure 6.40 it can be seen that maximum effectiveness is achieved at $\theta=45°$, although there is little difference between the effectiveness at $\theta=45°$ and $\theta=60°$. There is however a significant reduction in effectiveness at $\theta=75°$. The reason for this reduction in effectiveness is probably due to a decrease in the strength of the vortices as the direction is varied between 45° and 75°. This decrease in strength was also observed in the water channel tests where it was proposed that the most effective jet direction for producing a vortex is about $\theta=45°$.

6.4 Design Implications

The findings discussed above indicate that when predicting the effectiveness of air jet vortex generators it is important to be able to estimate the size, position and strength of the vortices that the air jets will produce. Guidelines similar to those used in the design of vane vortex generators are essential if air jet vortex generators are to be used in practice. The work discussed in this thesis has given a first indication of the influence of the various jet exit parameters and based on these findings some initial guidelines are proposed. Further tests would be required beyond the guidelines suggested.

(i) In general, an increase in the length of a jet exit will result in a vortex of increased diameter and for a constant blowing pressure will result in a vortex of increased strength. Based on this initial work it is proposed that the ratio of the aerofoil chord to exit length should be between 25 and 50.

(ii) For efficient vortex formation and hence increased vortex strength, the jet direction should have a downstream component. A direction of about 45° was found to be the optimum angle.

(iii) A minimum jet inclination is required for vortex formation and it has been proposed that a maximum angle of inclination also exists. The work carried out in this thesis suggests that the inclination should lie between 30° and 45°. Between these limits the strength and diameter of the vortex can be increased by increasing the inclination.

(iv) A minimum blowing pressure is required to form a vortex and the results have showed that blowing pressures as low as P_b/P_o=1.0 are able to generate a vortex. In general, an increase in the blowing pressure results in an increase in vortex strength.

(v) As with vane vortex generators the spacing of the air jet vortex generators has been shown to be an important parameter. The spacing of air jet vortex generators should be a function of the jet exit length since it is the length that is the dominant parameter in determining the vortex diameter. From the tests carried it was shown that a row of small air jets vortex generators produced vortices with a spacing to diameter ratio which was on the upper limit for effective boundary layer control. On the other hand the row of large air jet vortex generators produced vortices with a spacing to diameter ratio which was on the lower limit as the vortices began to interfere with each other. Hence it is proposed that the spacing to exit length ratio (D/l) should be between 2 and 4 as this represents the large and small jet exits tested.

(vi) Although exit width (w) or exit aspect ratio (l/w) was not investigated a value of l/w between 5 and 10 is suggested.

6.5 Further Work

This thesis has shown that air jet vortex generators are able to delay the onset of significant effects of shock induced boundary layer separation. Further work is required however before they can be used in the design of real aircraft and some suggestions are made below.

(i) A detailed correlation between jet characteristics and vortex characteristics is required. Using such a correlation together with the knowledge gained from practical experience with vane type generators it will be possible to issue a set of detailed design guidelines to help in the design of air jet vortex generators.

(ii) A mathematical model of the method of vortex formation would help in improving the understanding of the effects of the air jet parameters.

(iii) An assessment of the practical problems associated with an air jet vortex generator system should be investigated. This could include a study into assessing whether ram air or engine bleed air is more effective bearing in mind that there will be a drag penalty associated with the ram air intake and there will be a loss in engine performance when bleed air is used. Also, the possibility of having an active systems where the blowing pressure is varied to suit the conditions could be investigated.

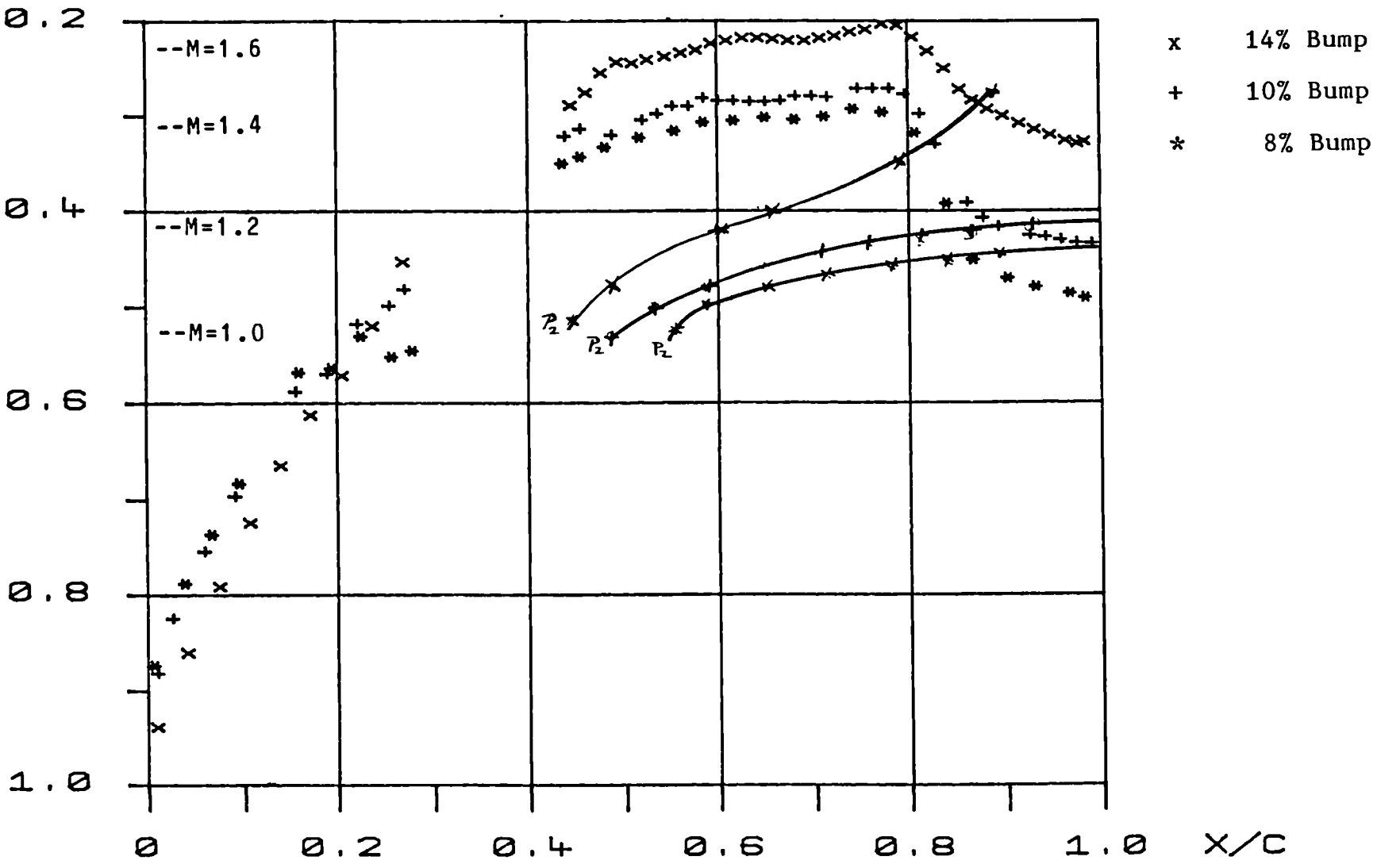

Figure 6.1 Comparison of the P_2 Loci on the Three Bumps with No Vortex Generators.

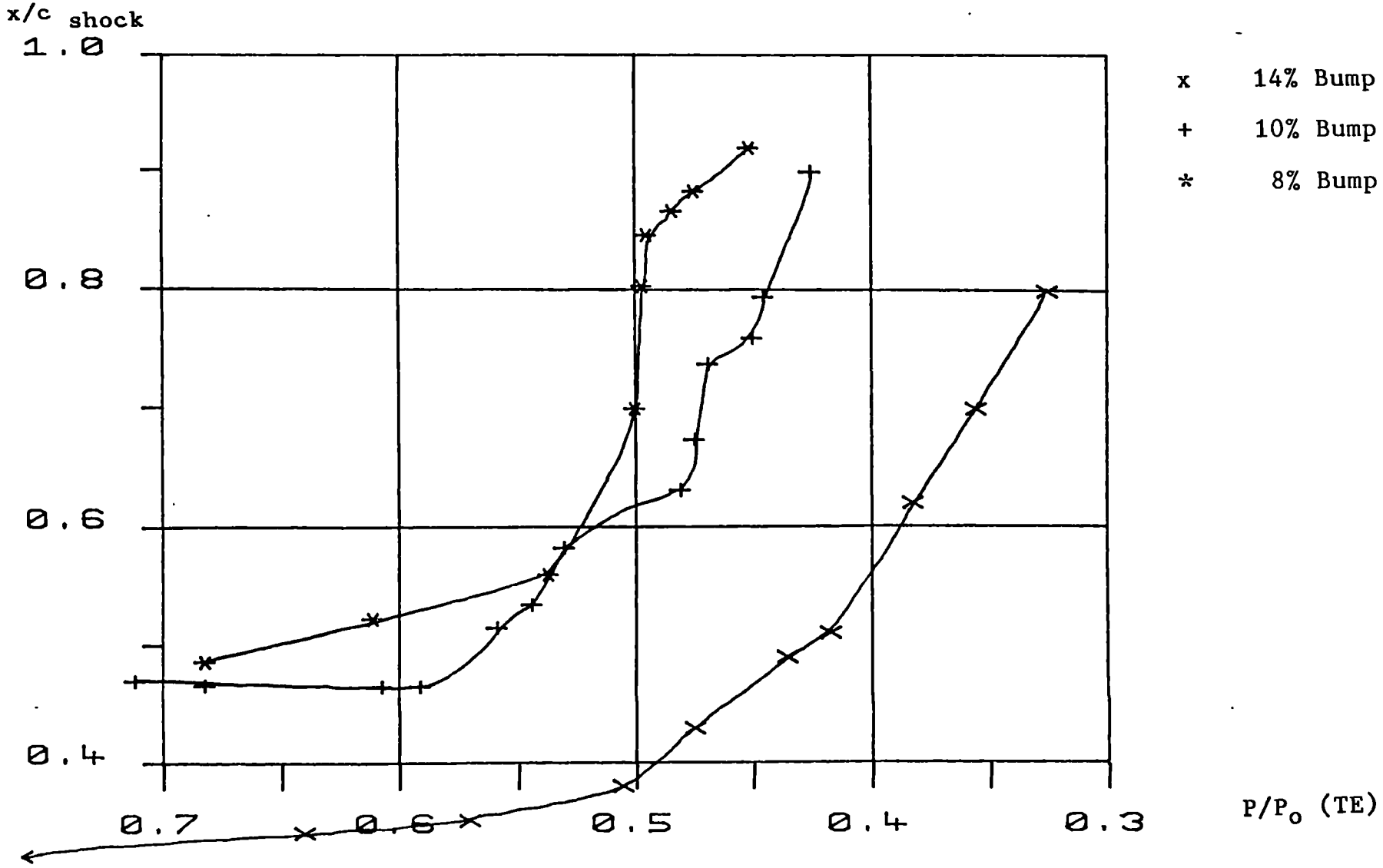

Figure 6.2 Comparison of the Loci of Shock Position Against Trailing Edge Pressure for the Three Bumps with No Vortex Generators.

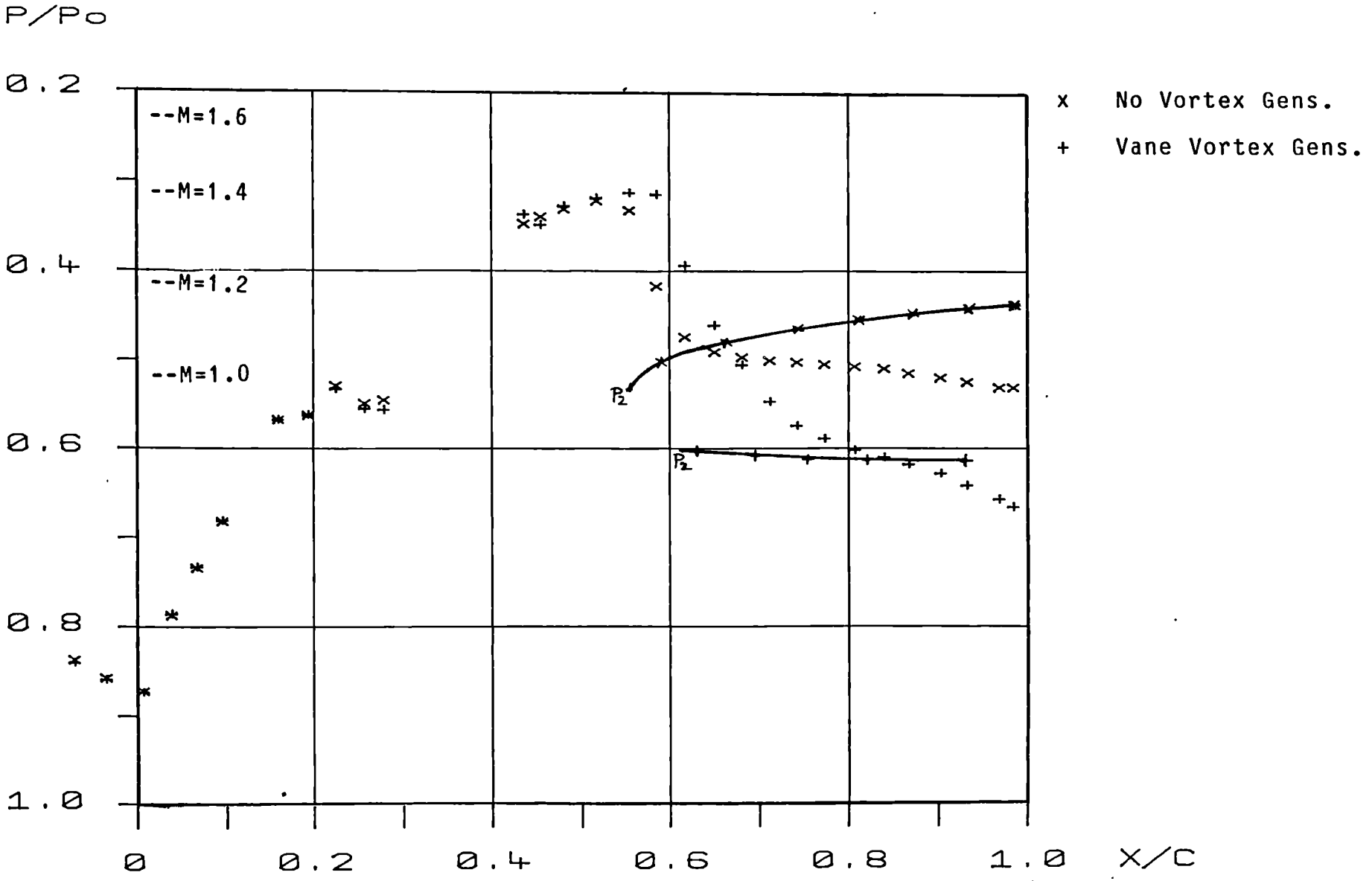

Figure 6.3 Comparison of the P_2 Loci on the 8% Bump with No Vortex Generators and Vane Vortex Generators.

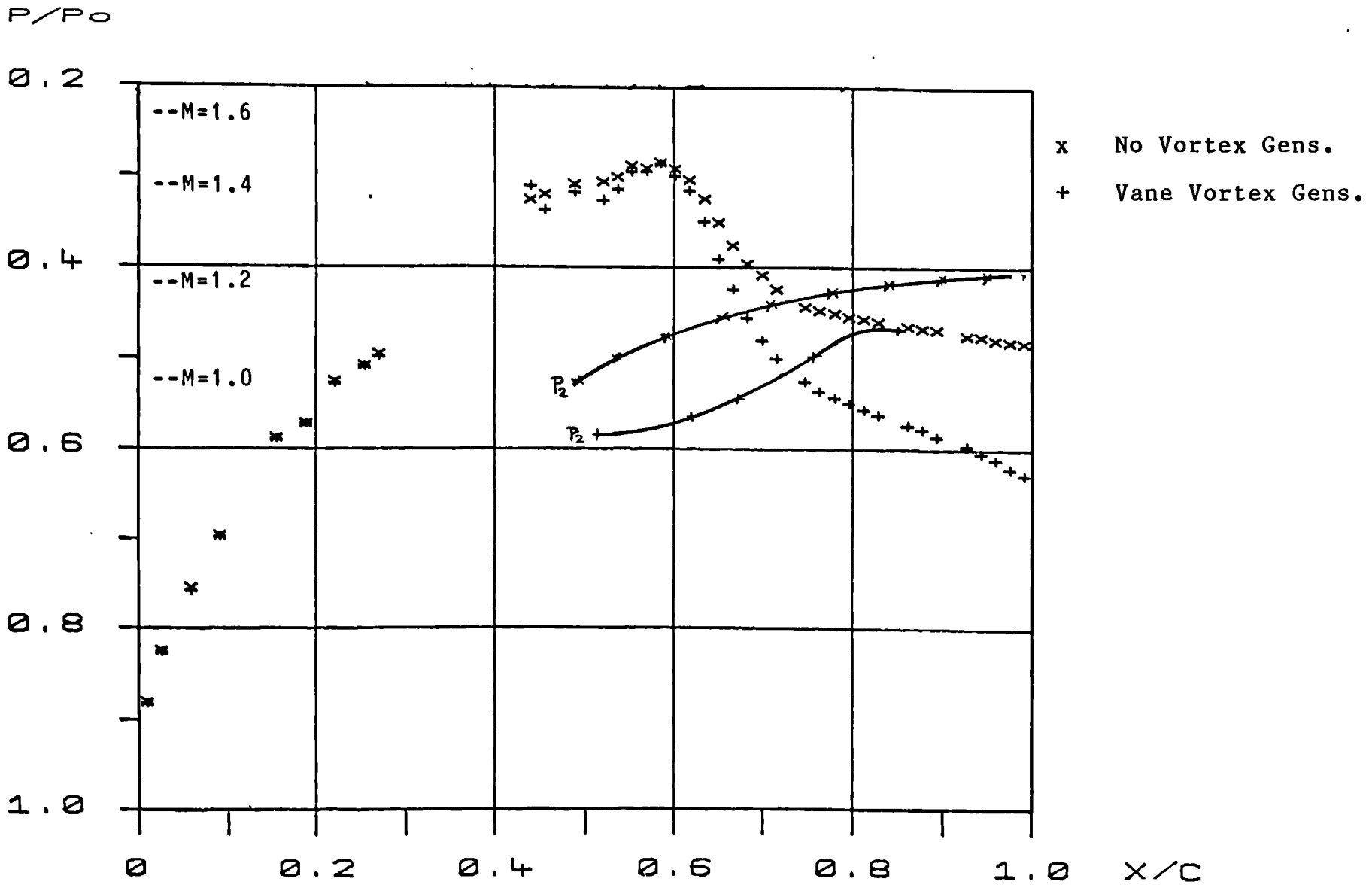

Figure 6.4 Comparison of the P_2 Loci on the 10% Bump with No Vortex Generators and Vane Vortex Generators.

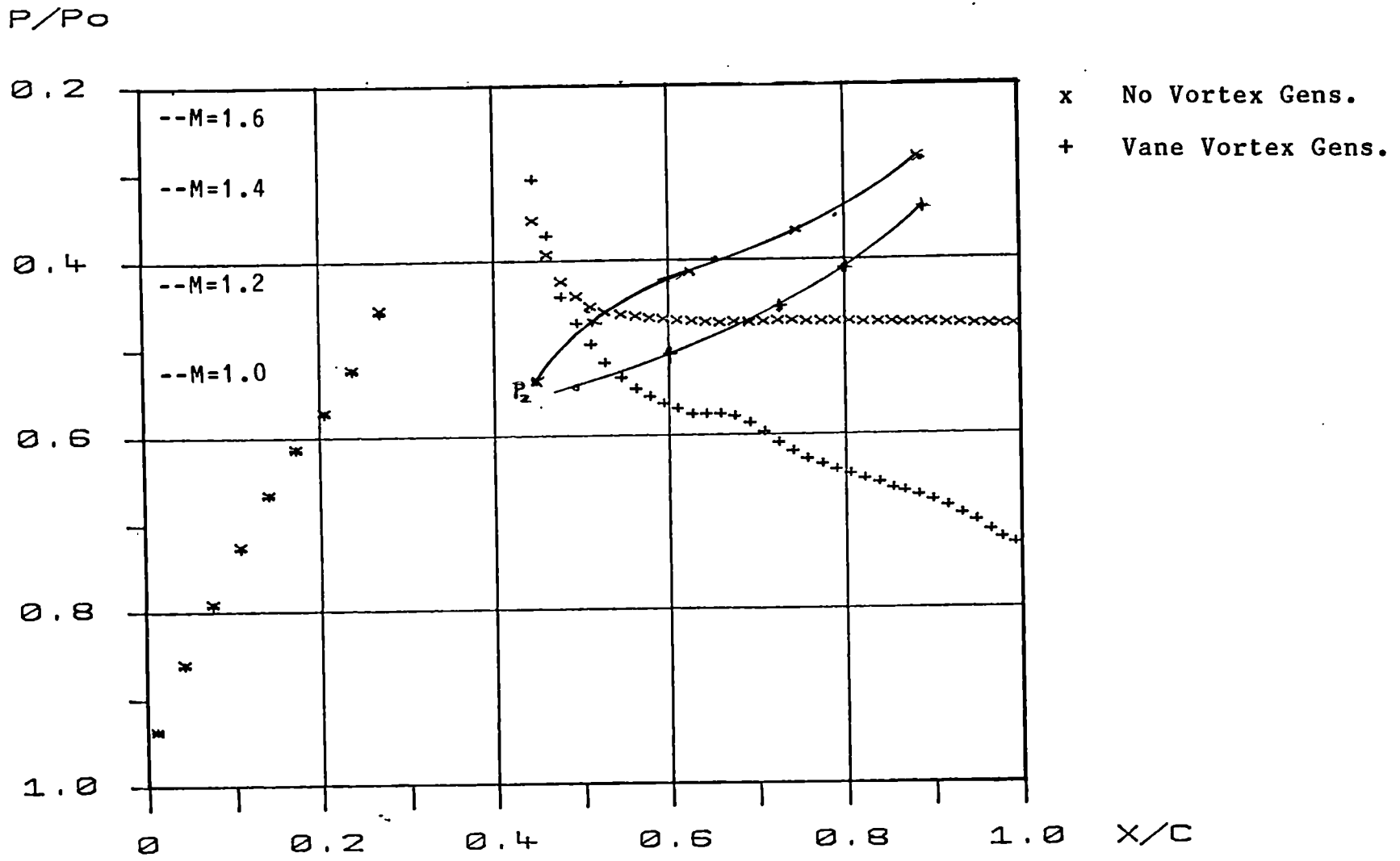

Figure 6.5 Comparison of the P_2 Loci on the 14% Bump with No Vortex Generators and Vane Vortex Generators.

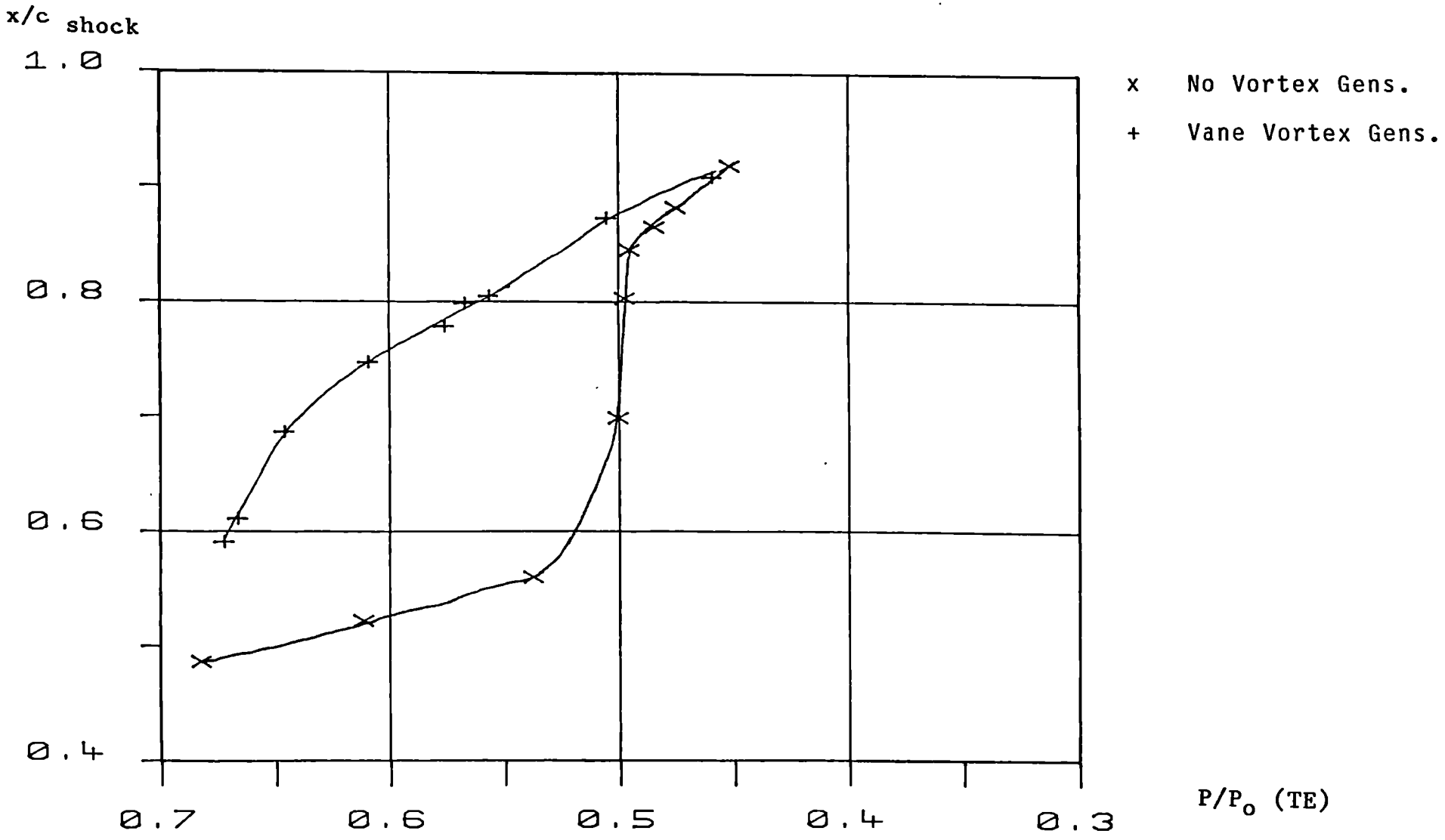

Figure 6.6 Comparison of the Loci of Shock Position Against Trailing Edge Pressure for the 8% Bump.

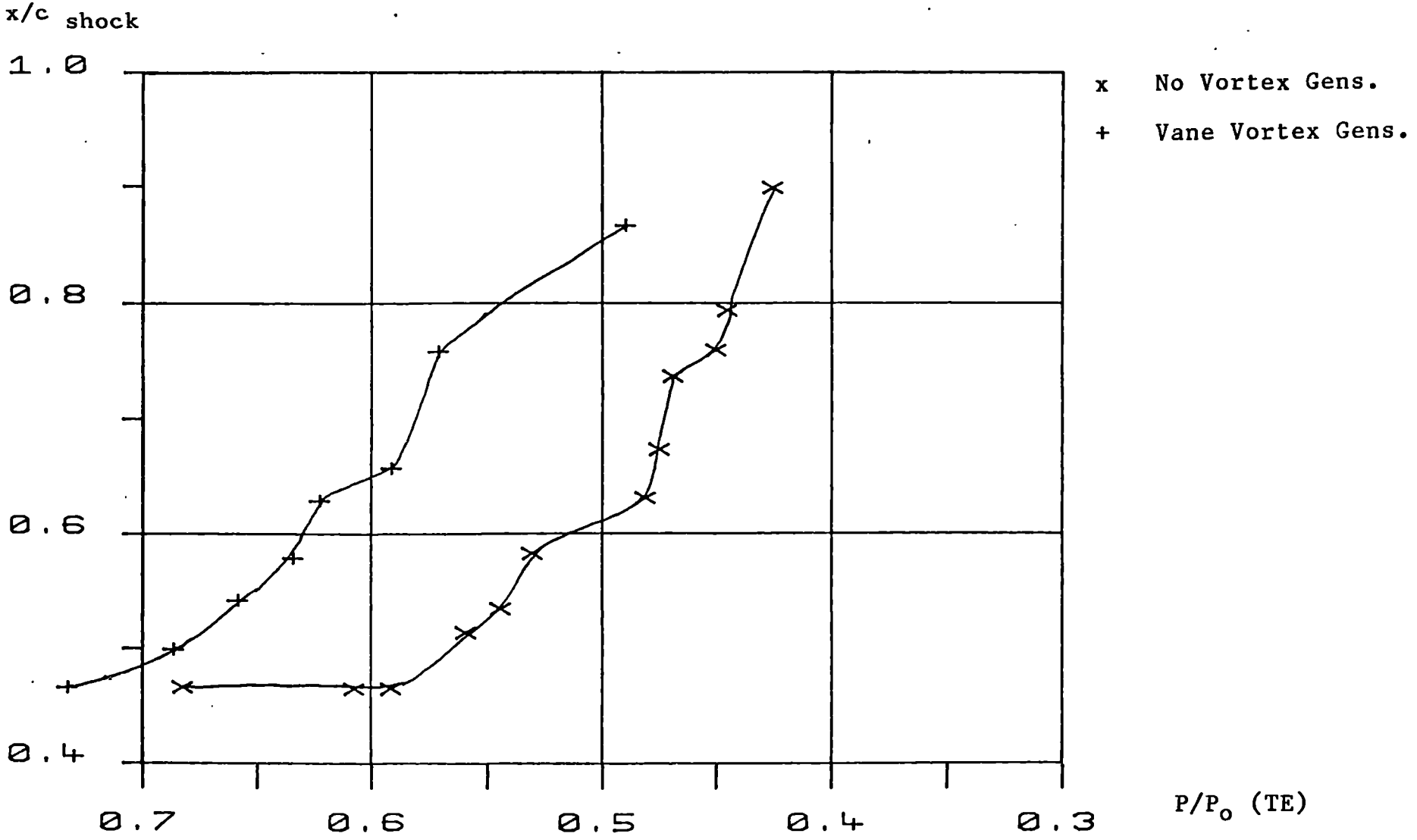

Figure 6.7 Comparison of the Loci of Shock Position Against Trailing Edge Pressure for the 10% Bump with and without Vortex Generators.

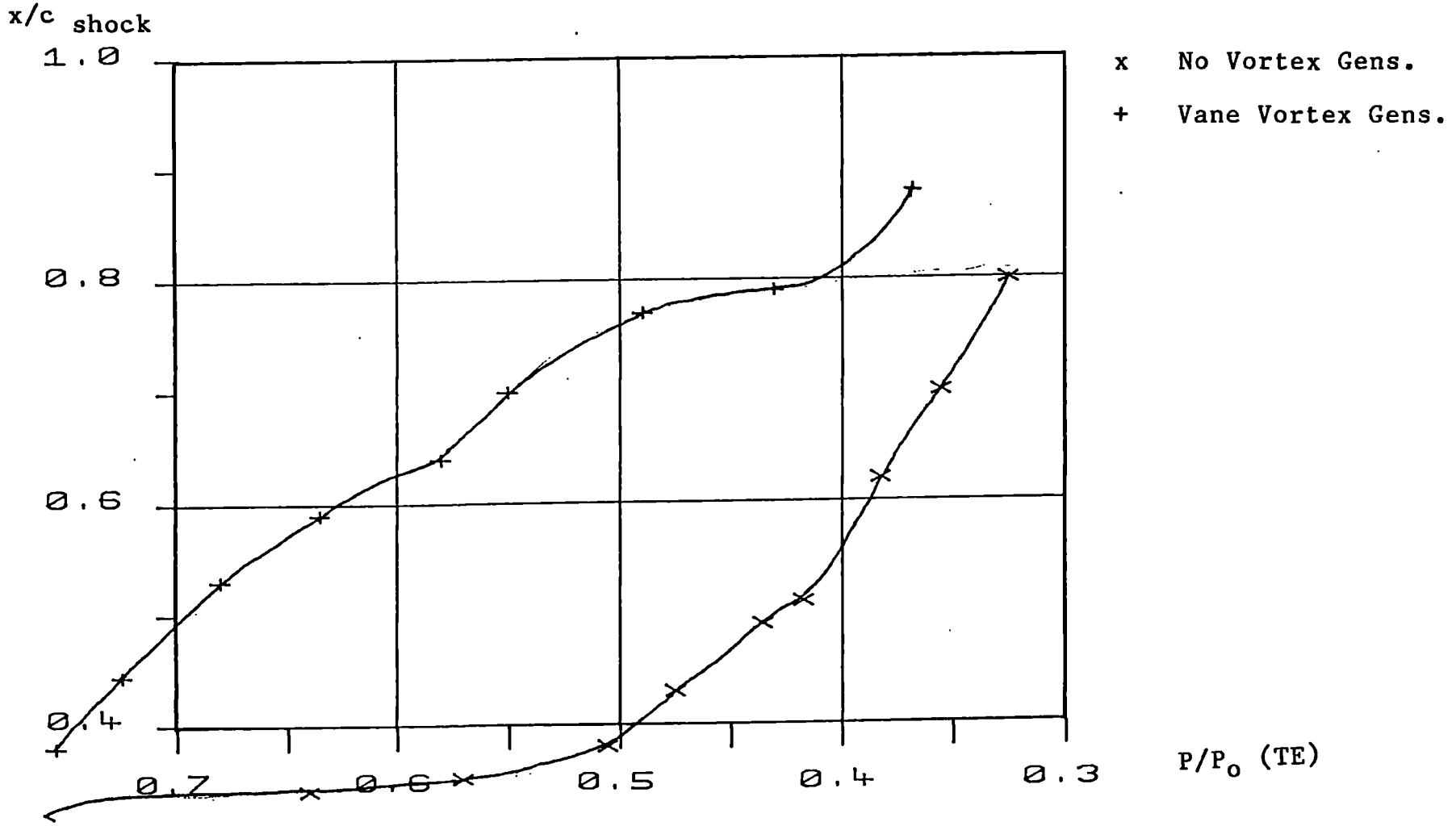

Figure 6.8 Comparison of the Loci of Shock Position Against Trailing Edge Pressure for the 14% Bump with and without Vortex Generators.

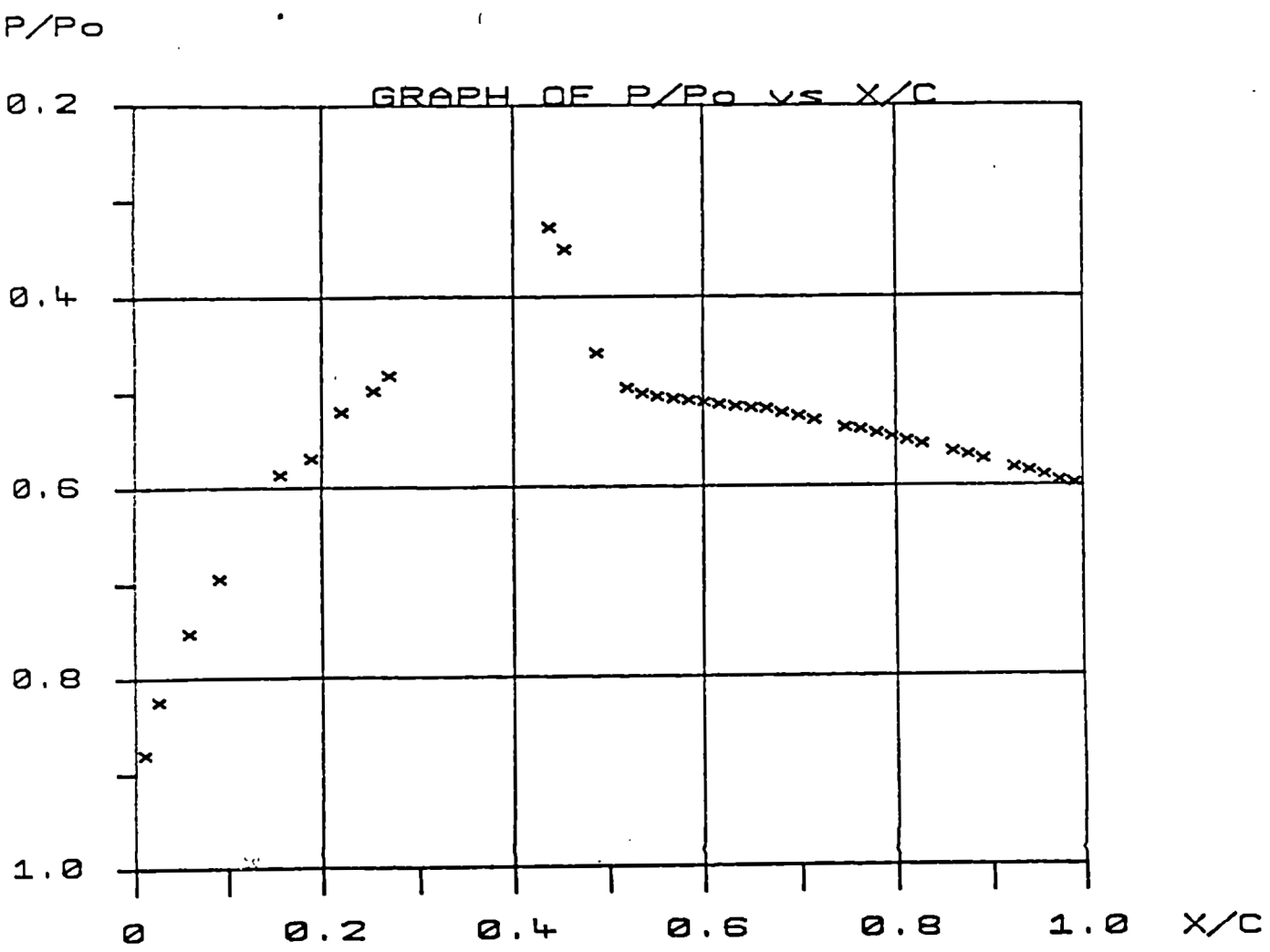

Figure 6.9 Experimental Pressure Distribution with Corresponding Schlieren Image for the 10% Bump with No Vortex Generators.

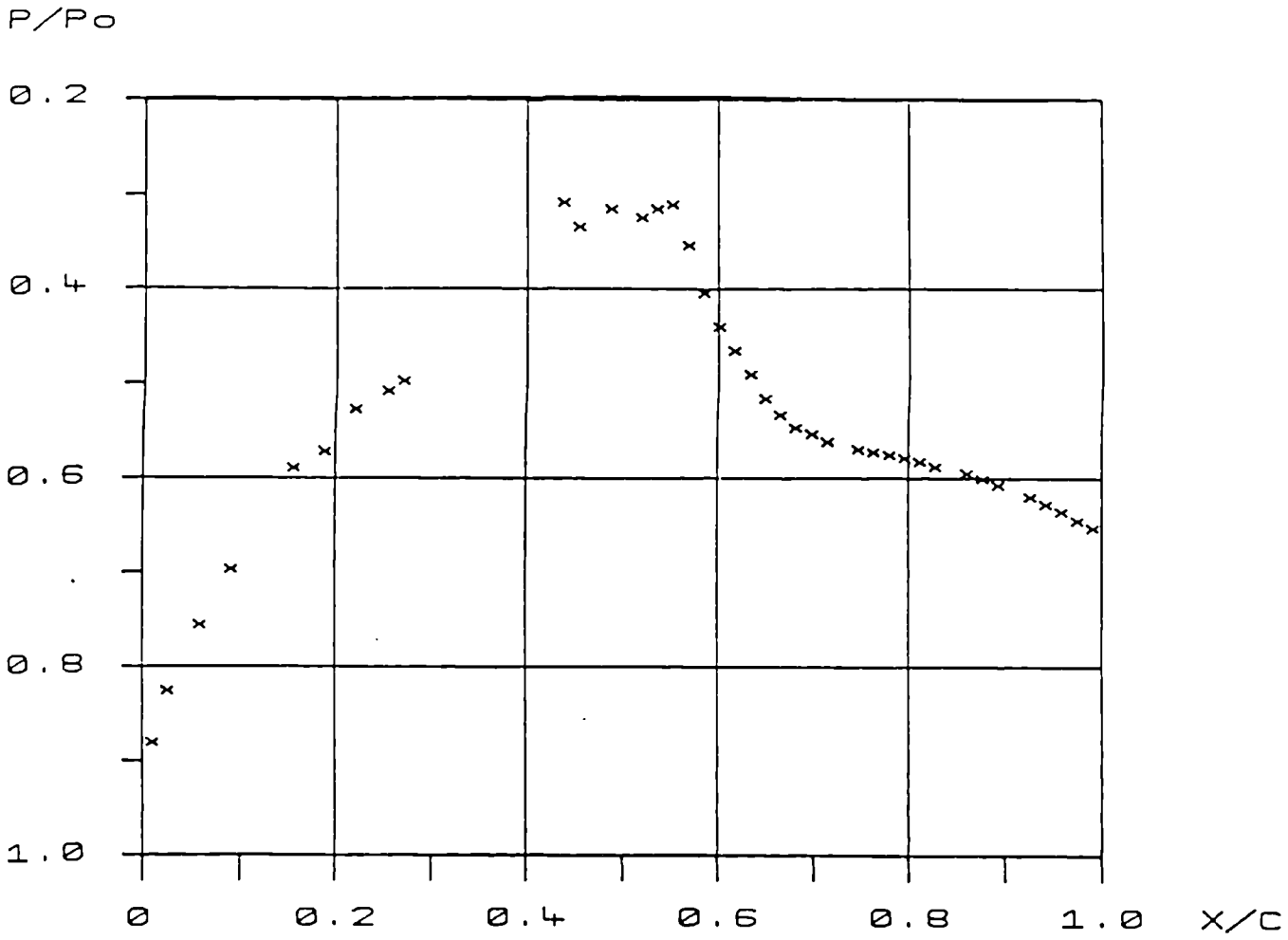

Figure 6.10 Experimental Pressure Distribution with Corresponding Schlieren Image for the 10% Bump with Vane Vortex Generators.

Figure 6.11 Boundary Layer Profiles With No Vortex Generators.

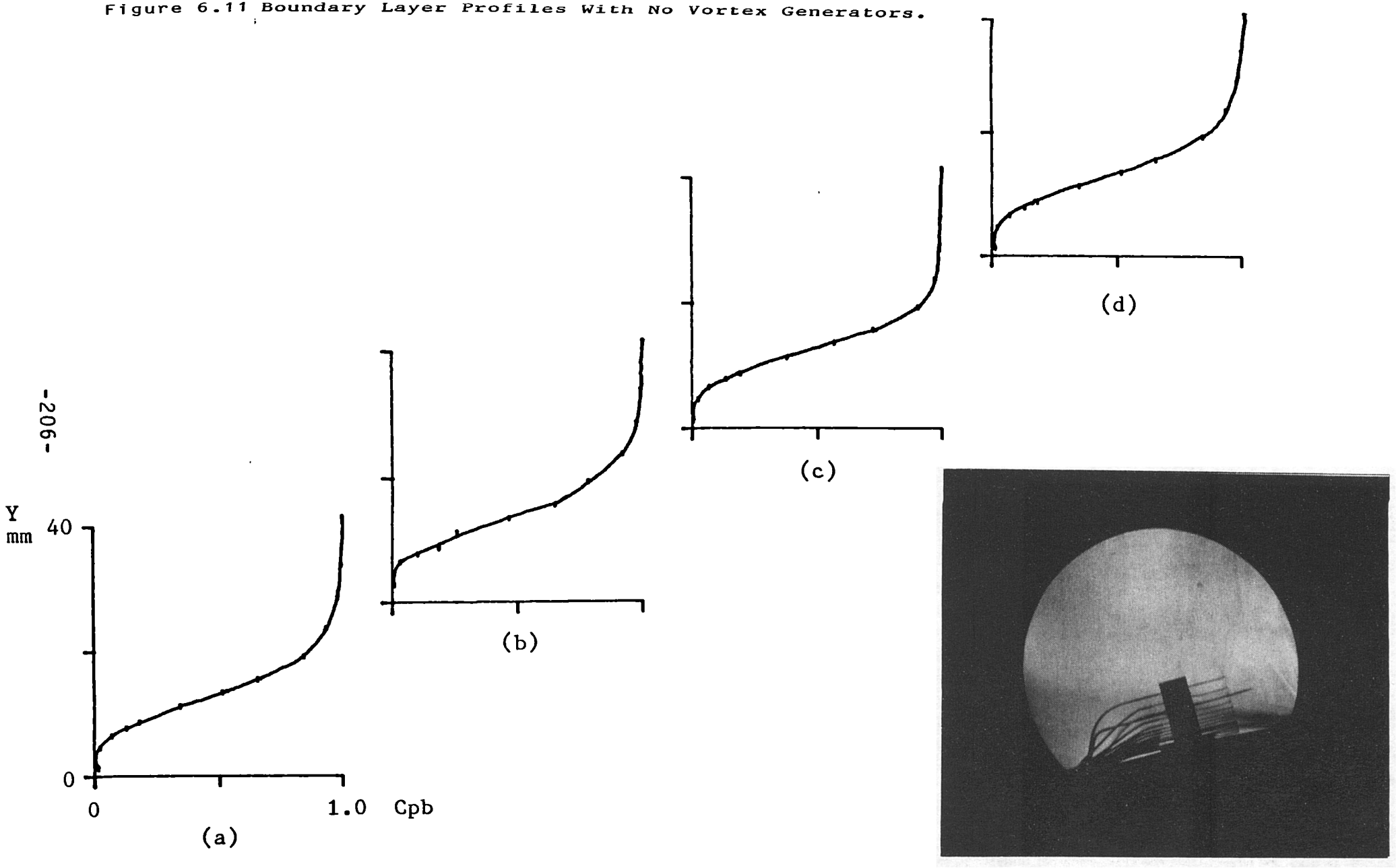

Figure 6.12 Boundary Layer Profiles With Vane Vortex Generators.

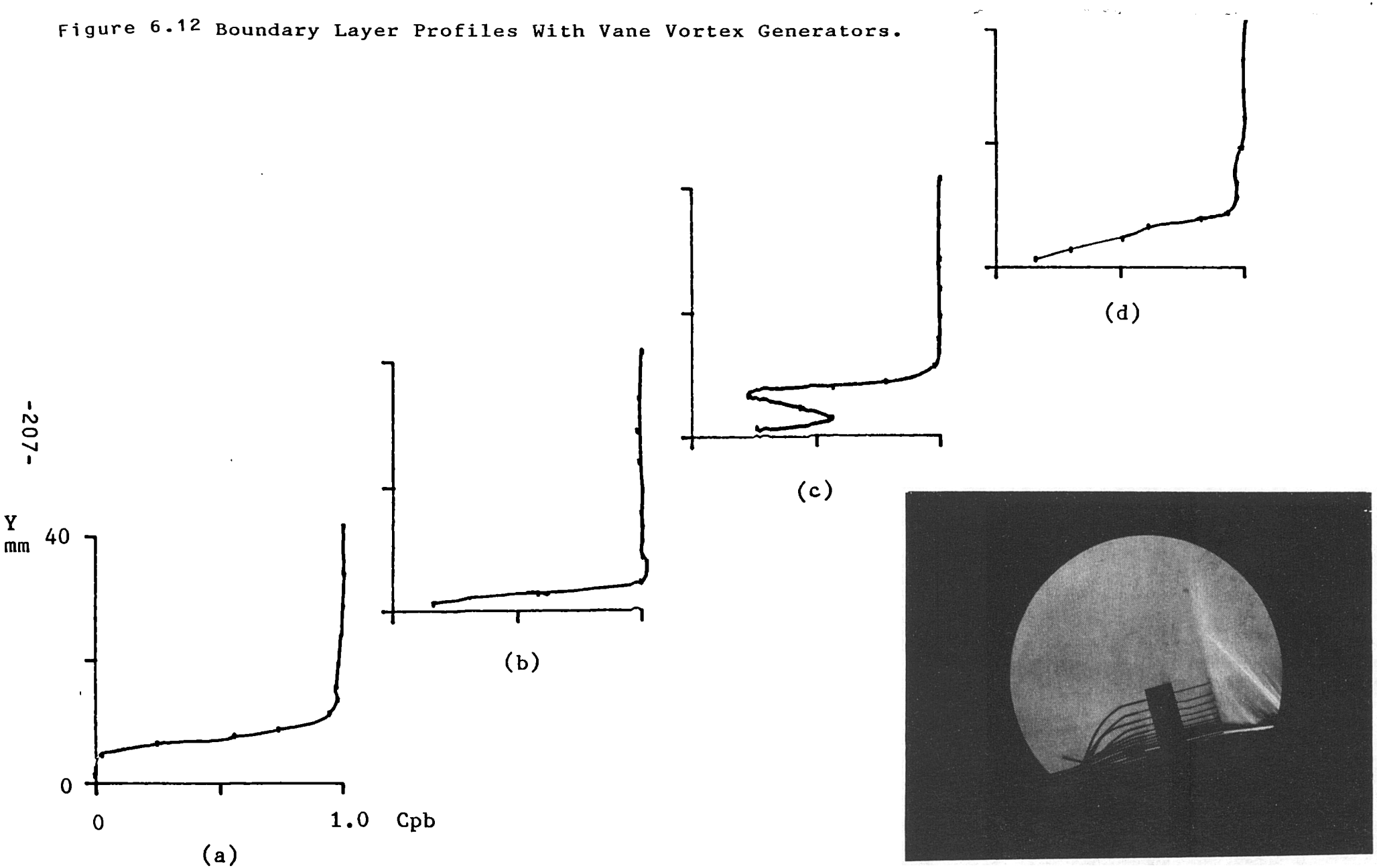

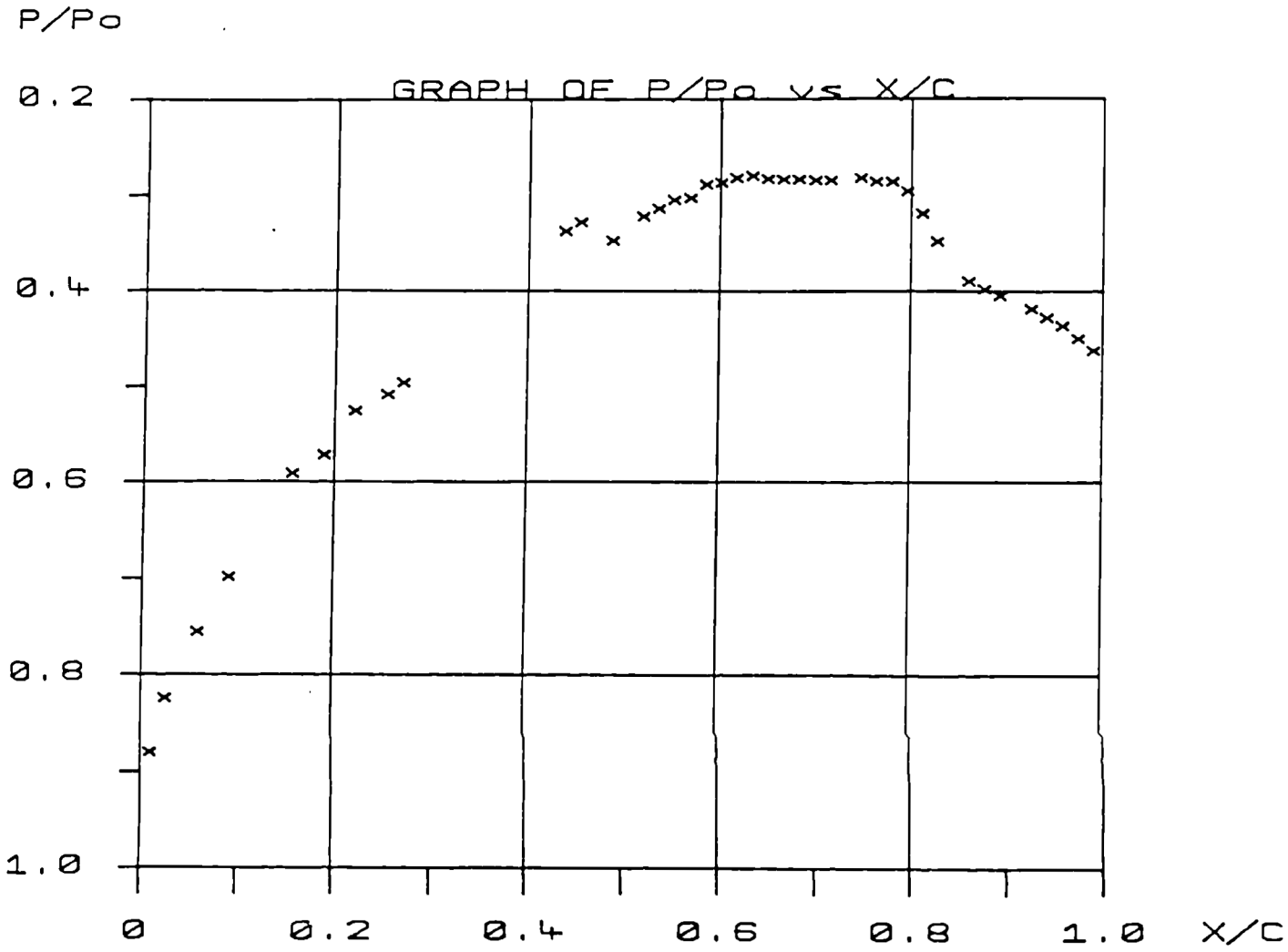

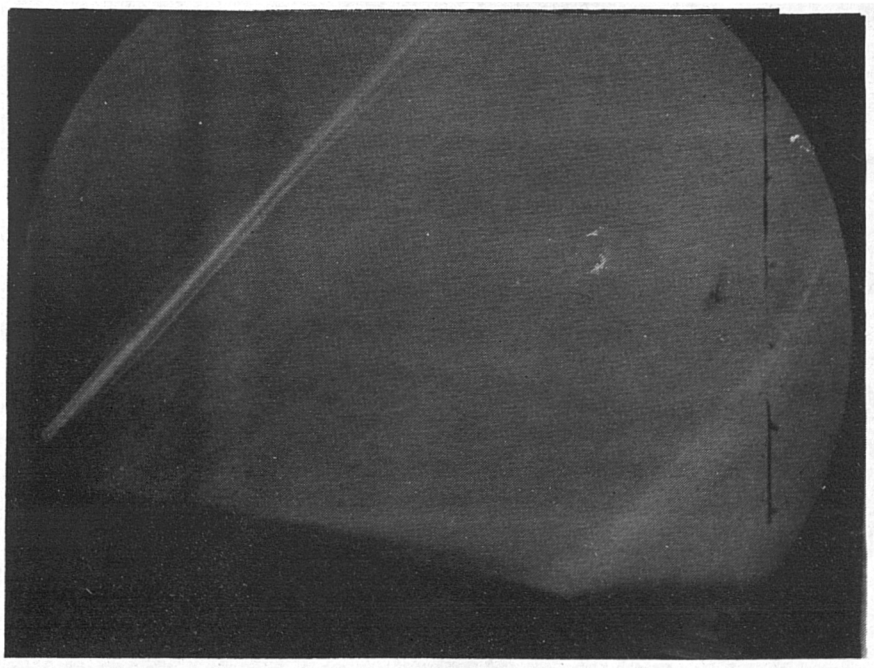

Figure 6.13 Experimental Pressure Distributions with Corresponding Schlieren Image for the 10% Bump with Small Air Jets (P_b/P_o=1.2)

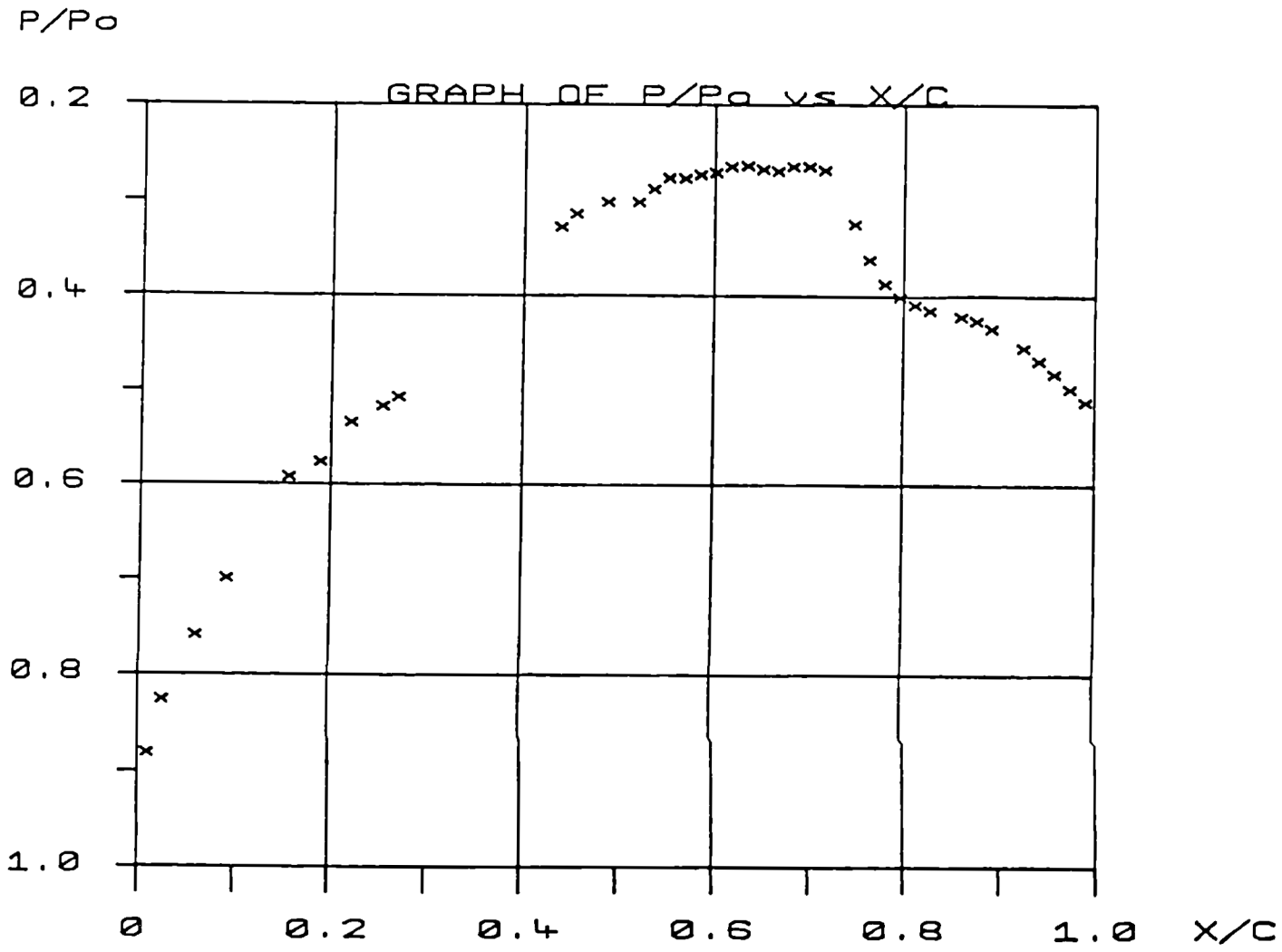

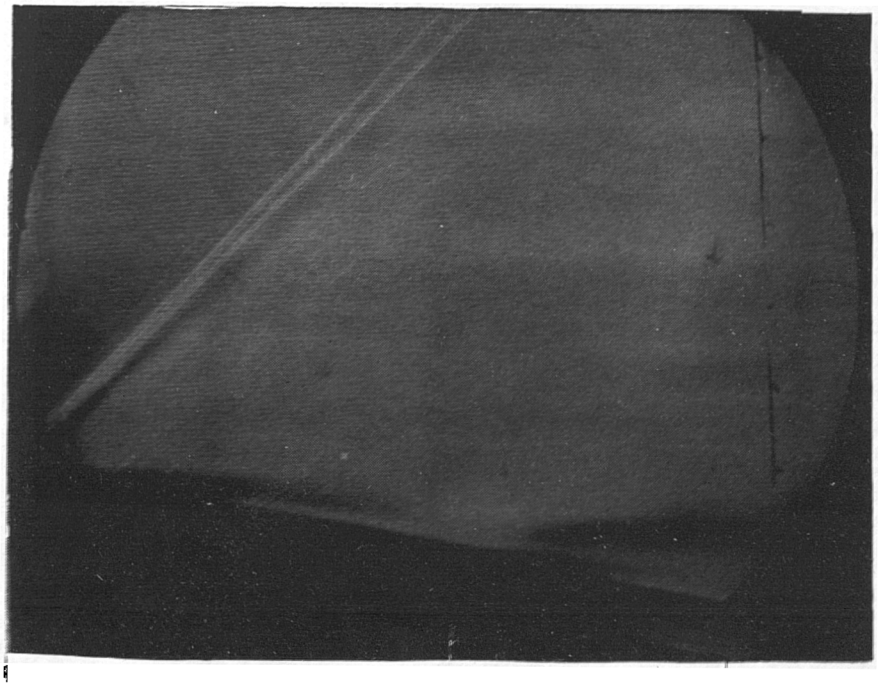

Figure 6.14 Experimental Pressure Distributions with Corresponding Schlieren Image for the 10% Bump with Large Air Jet (θ=60°, P_b/P_o=1.2).

Figure 6.15 Boundary Layer Profiles With Small Air Jet Vortex Generators (P_b/P_o=1.6, ø=30°).

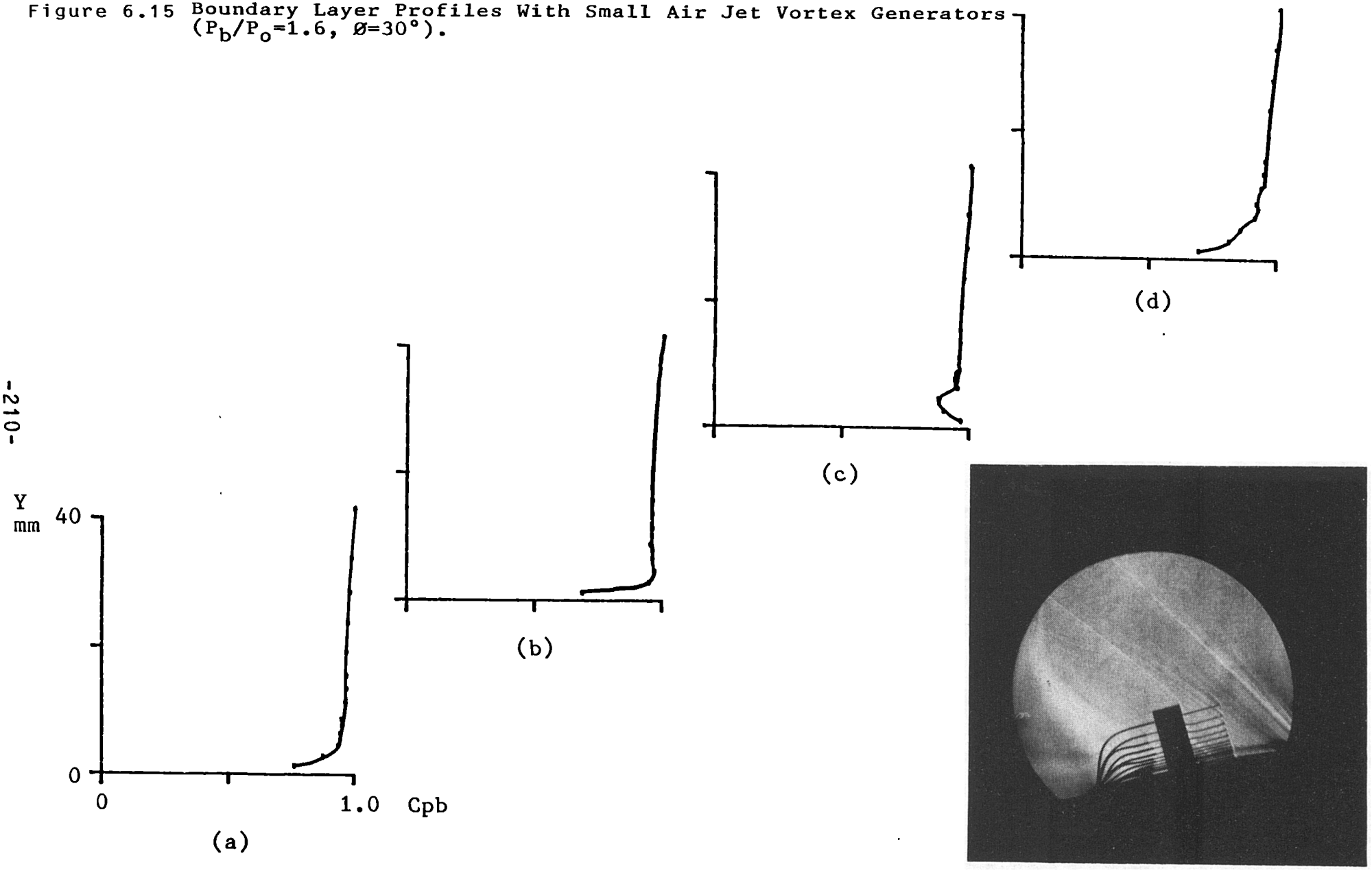

Figure 6.16 Boundary Layer Profiles With Large Air Jet Vortex Generators (P_b/P_o=1.5, θ=60°).

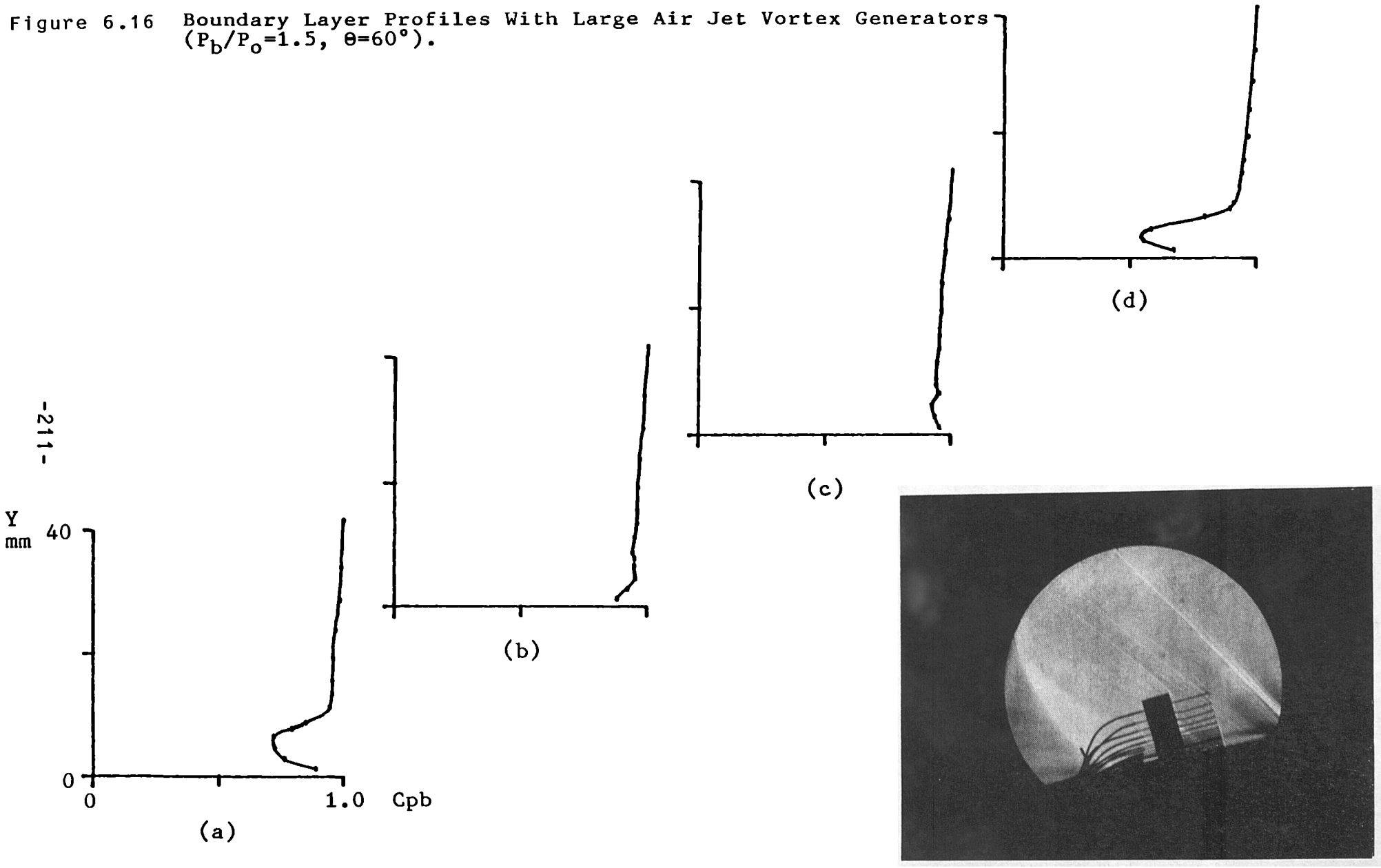

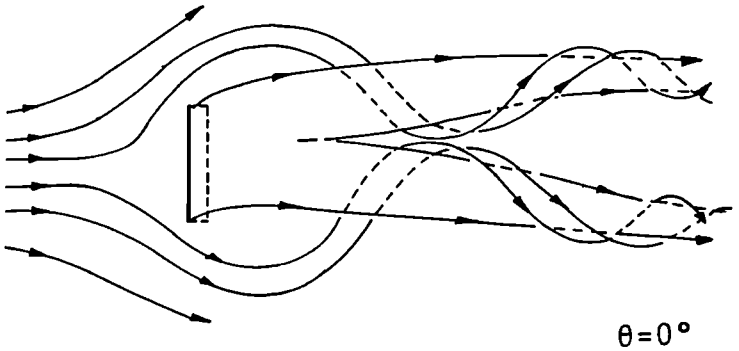

θ=0°

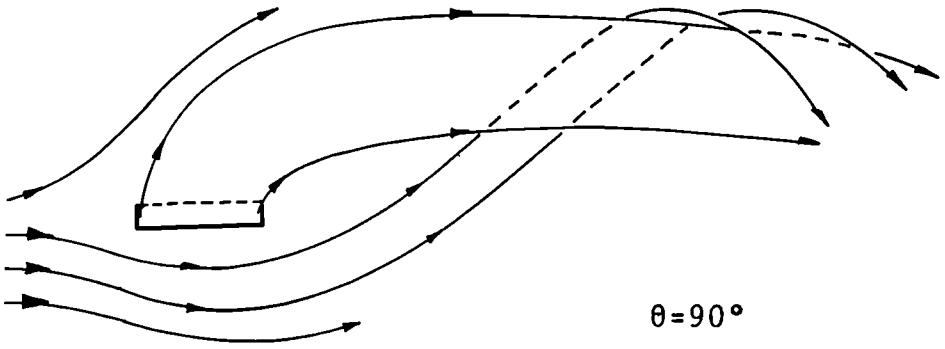

θ=90°

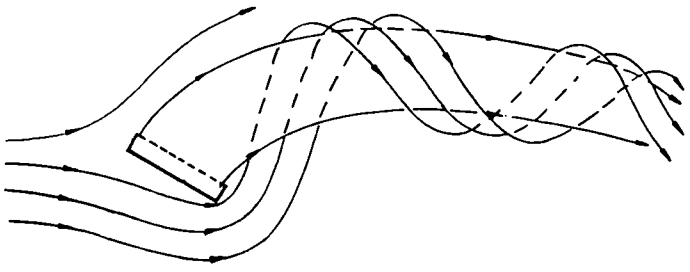

θ=45°

θ=Jet direction

Figure 6.17 Effect of Jet Direction on Vortex Formation

Figure 6.18 Boundary Layer Profiles With Small Air Jet Vortex Generators (P_b/P_o=1.6, Ø=45°).

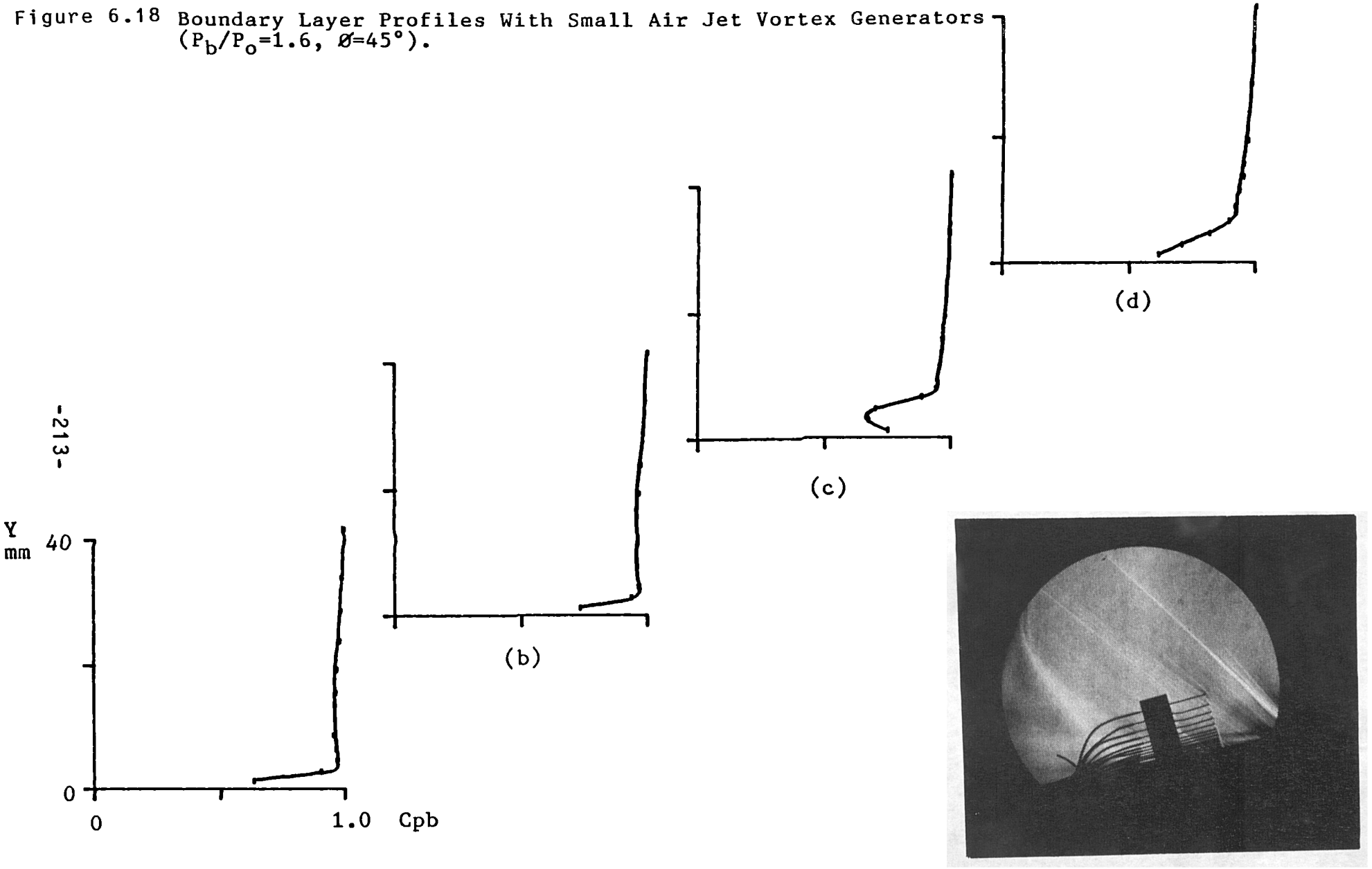

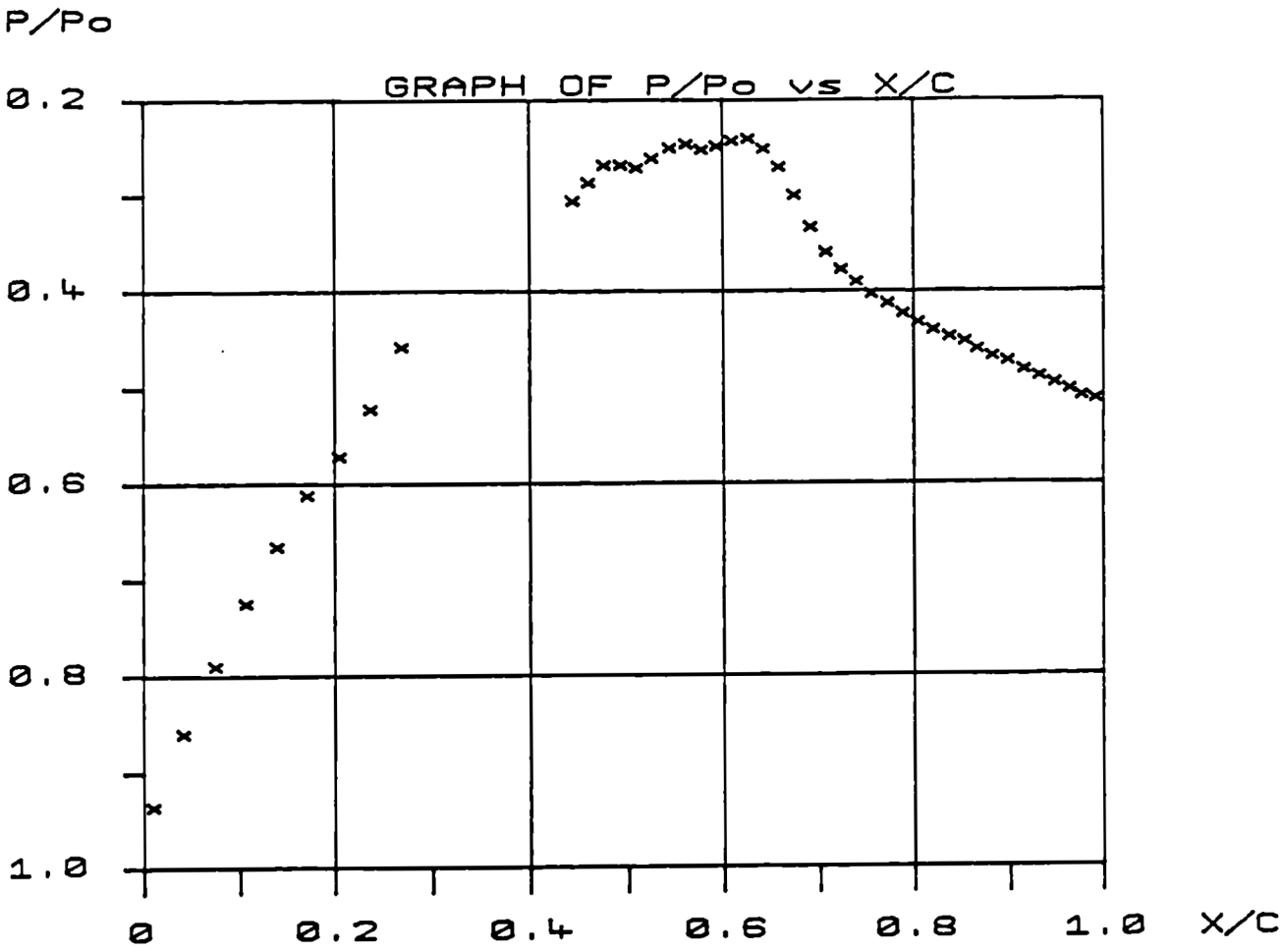

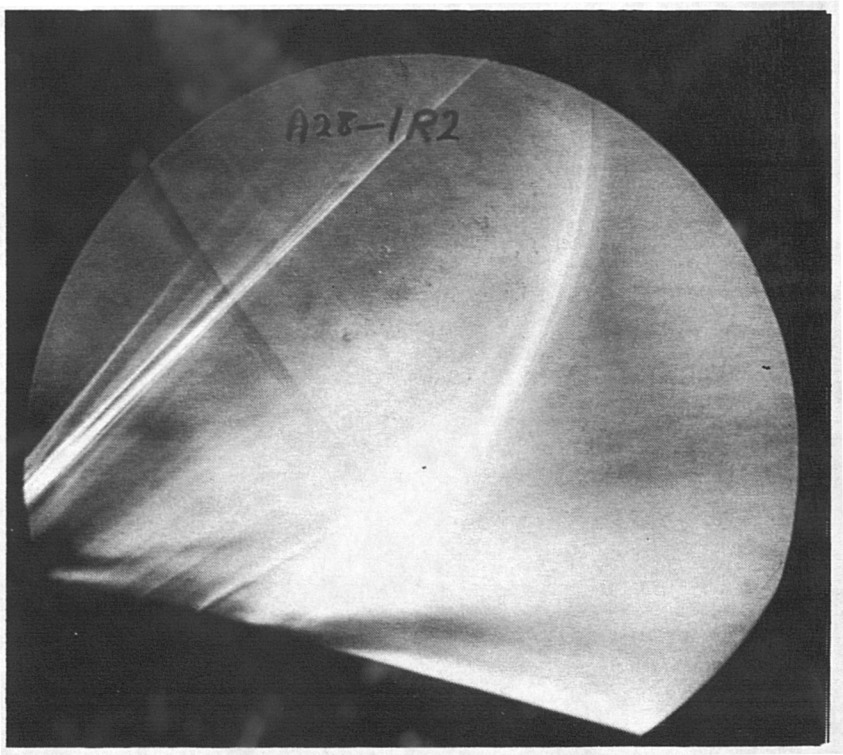

Figure 6.19 Experimental Pressure Distributions with Corresponding Schlieren Image for the 14% Bump with Small Air Jets (ϕ=30°, P_b/P_o=1.6).

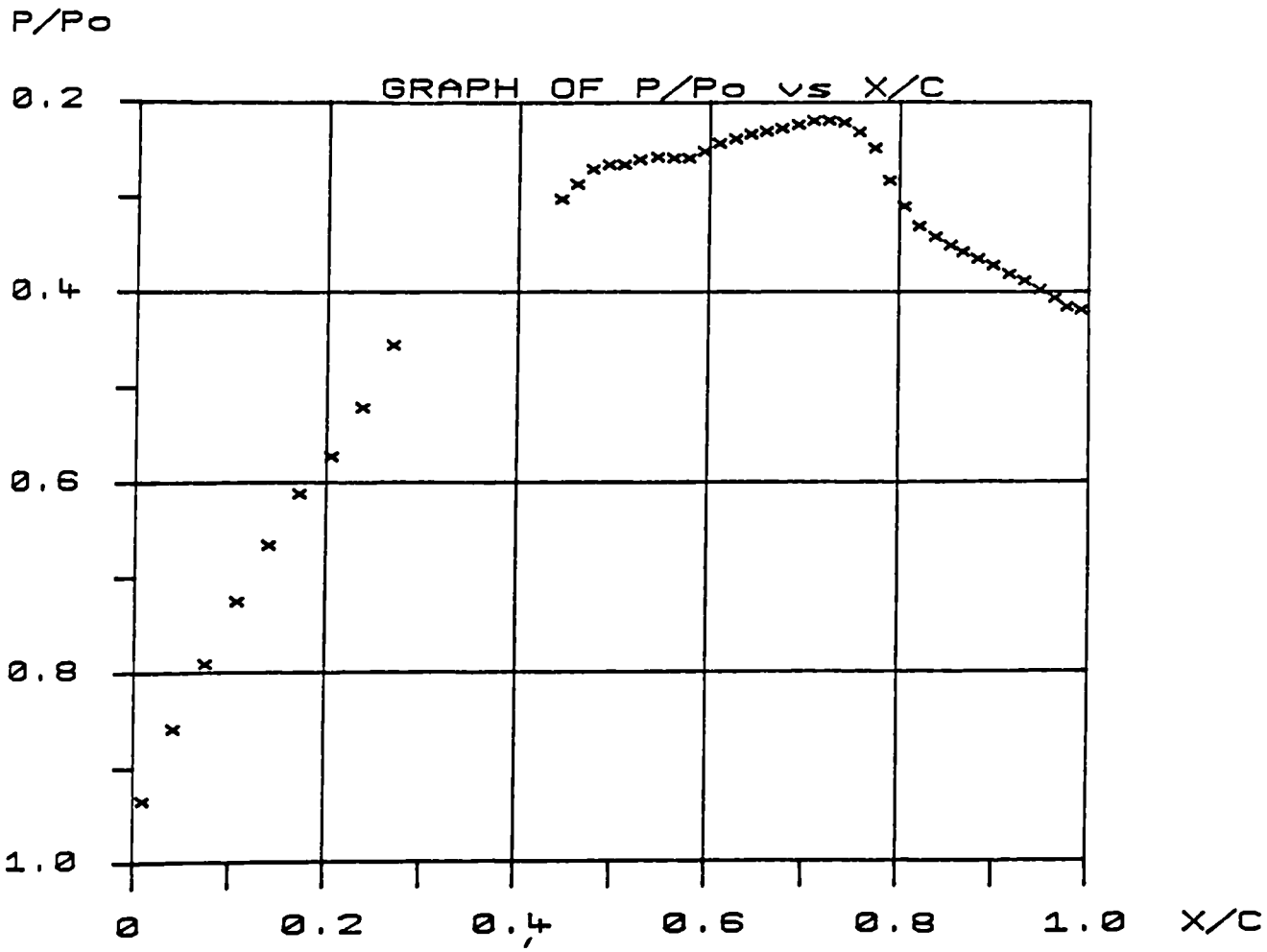

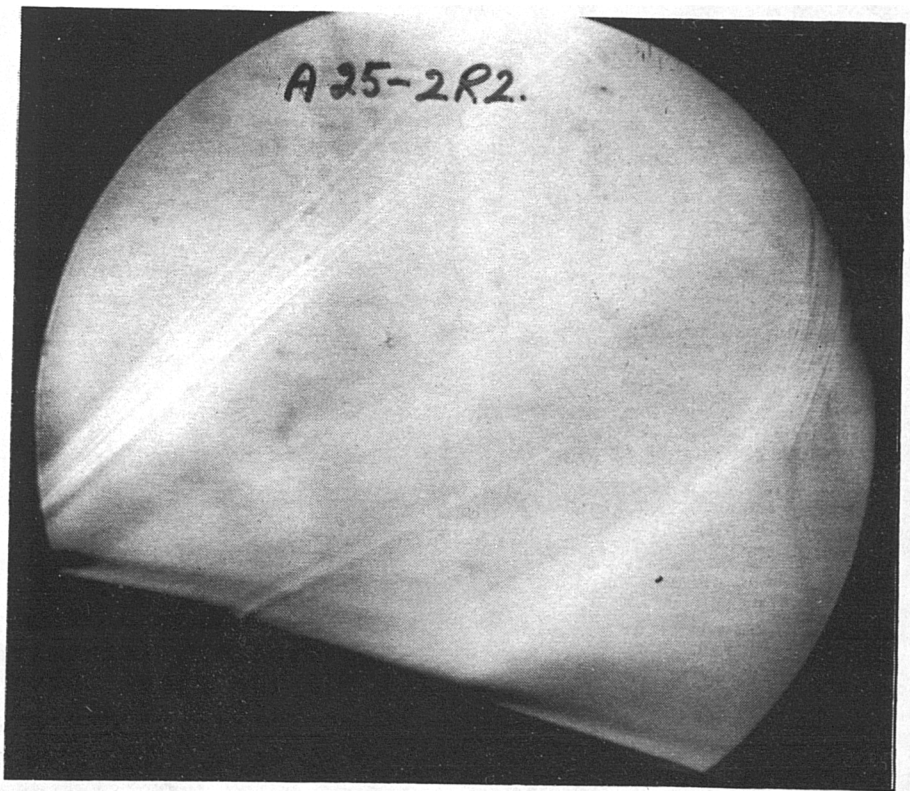

Figure 6.20 Experimental Pressure Distributions with Corresponding Schlieren Image for the 14% Bump with Small Air Jets ($\emptyset$=45°; P_b/P_o=1.6).

Figure 6.21 Boundary Layer Profiles With Large Air Jet Vortex Generators (P_b/P_o=1.2, θ=60°).

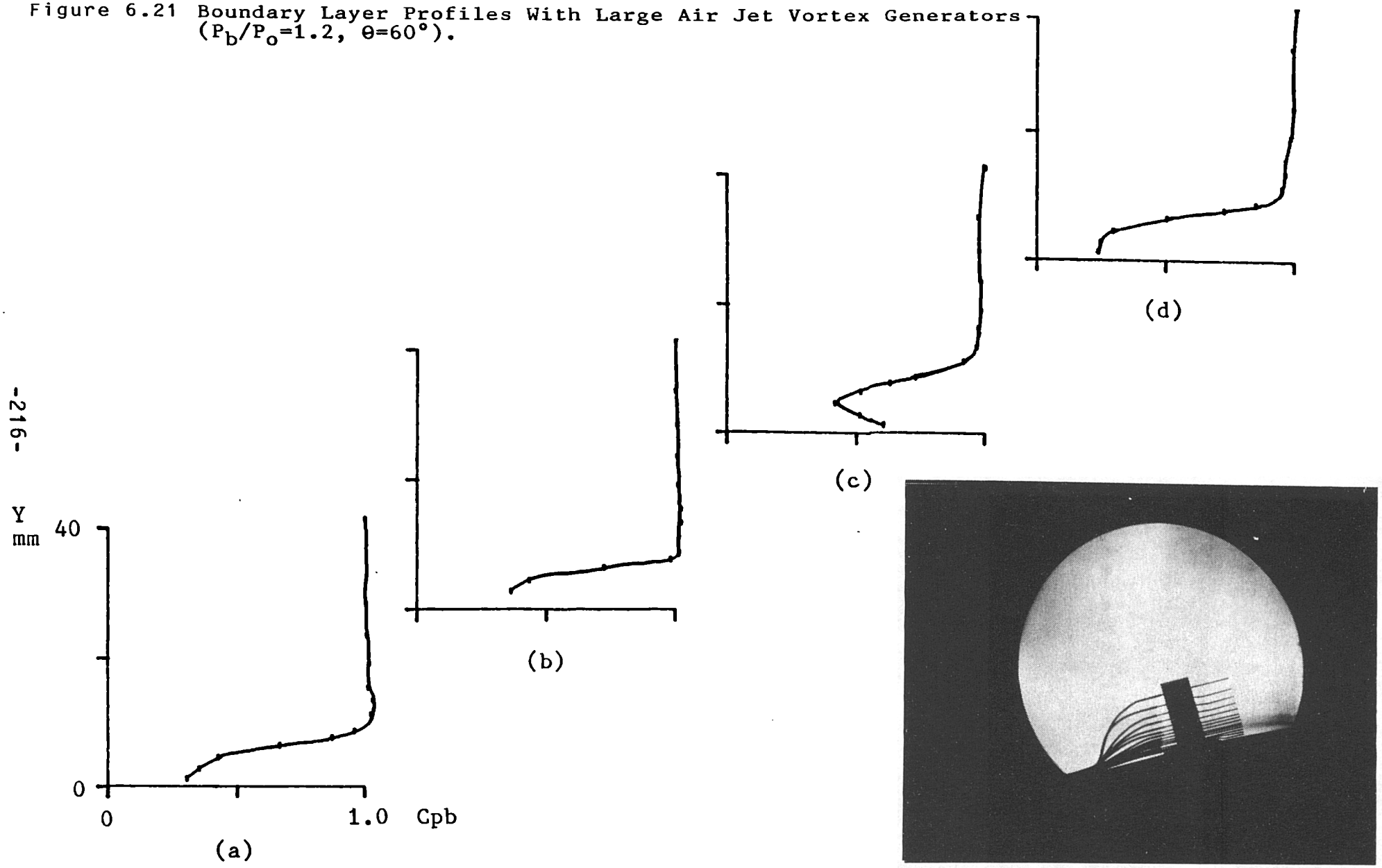

Figure 6.22 Boundary Layer Profiles With Large Air Jet Vortex Generators (P_b/P_o=1.5, θ=60°).

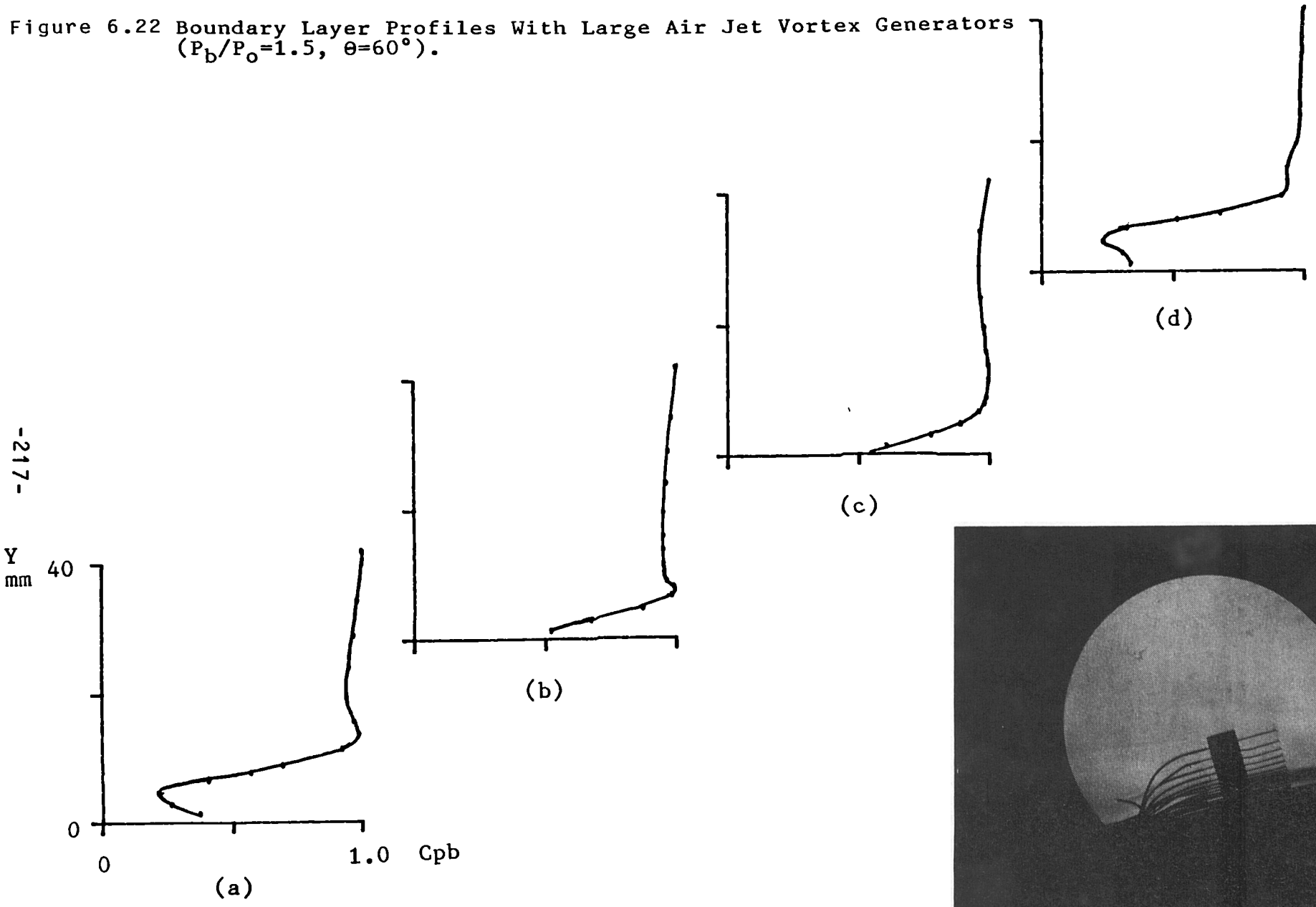

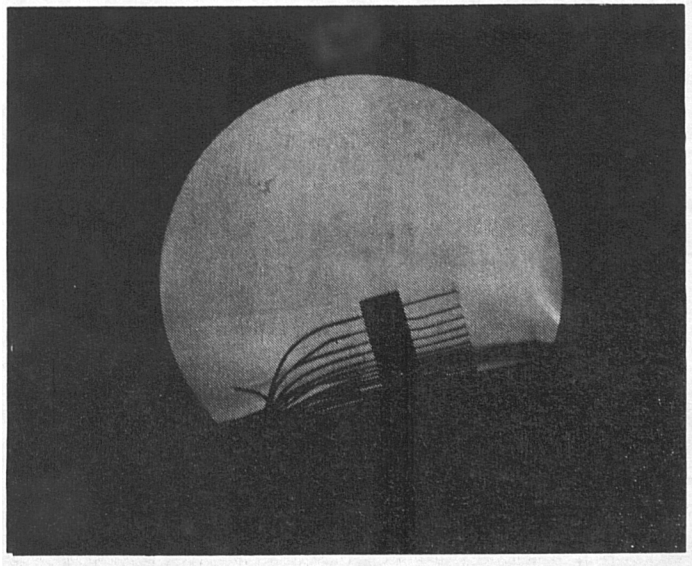

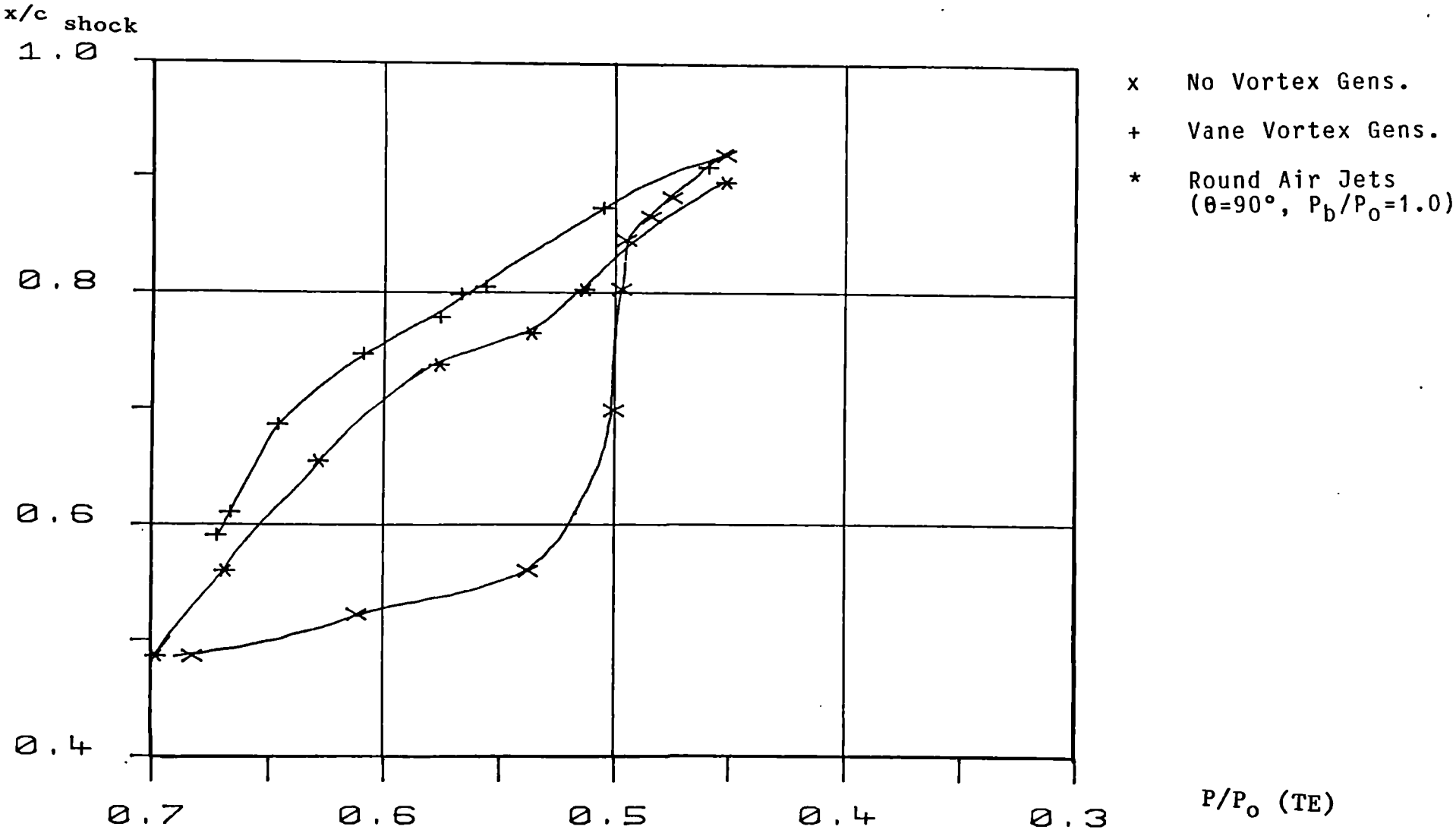

Figure 6.23 Comparison of the Loci of Shock Position Against Trailing Edge Pressure for the 8% Bump.

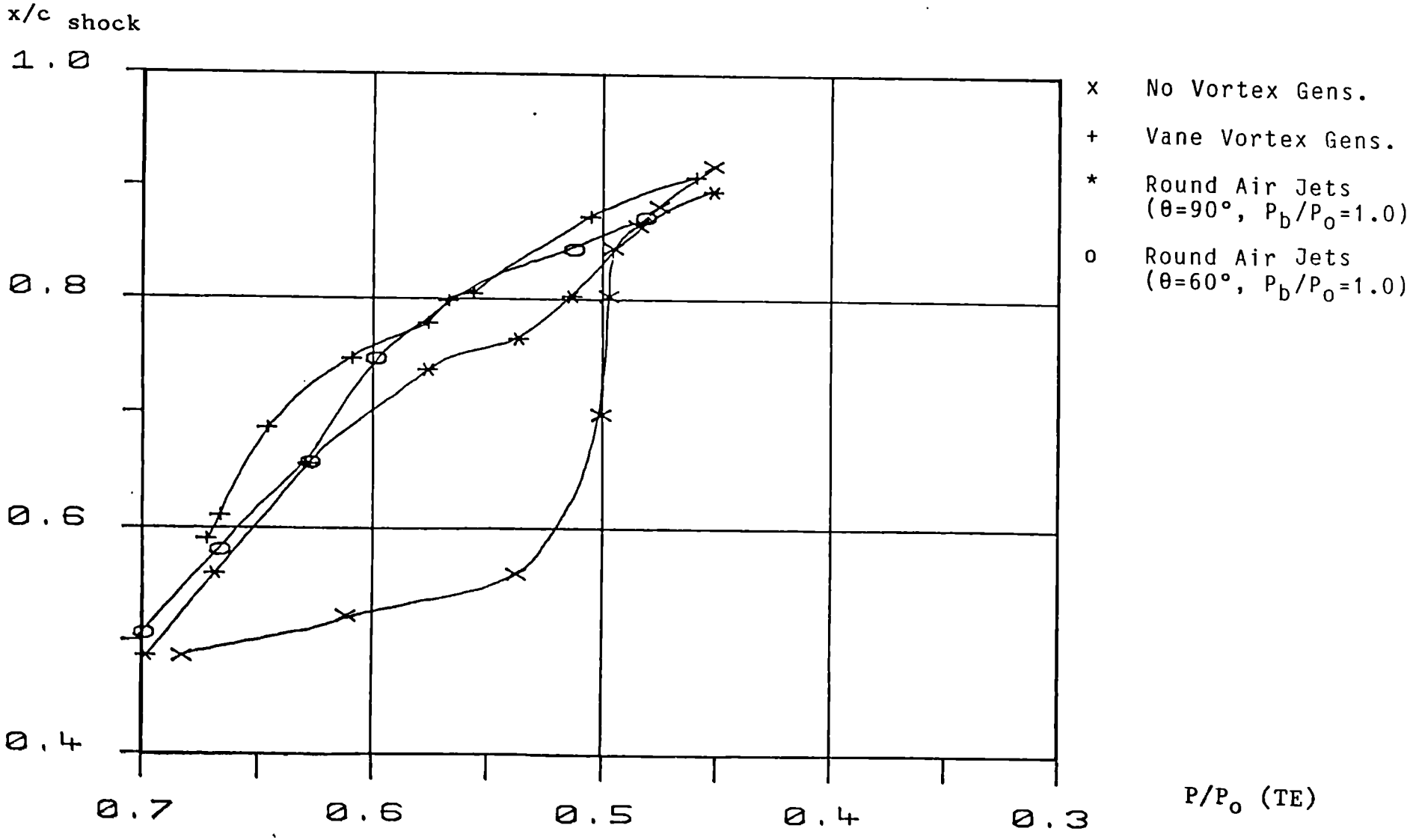

Figure 6.24 Comparison of the loci of Shock Position Against Trailing Edge Pressure for the 8% Bump.

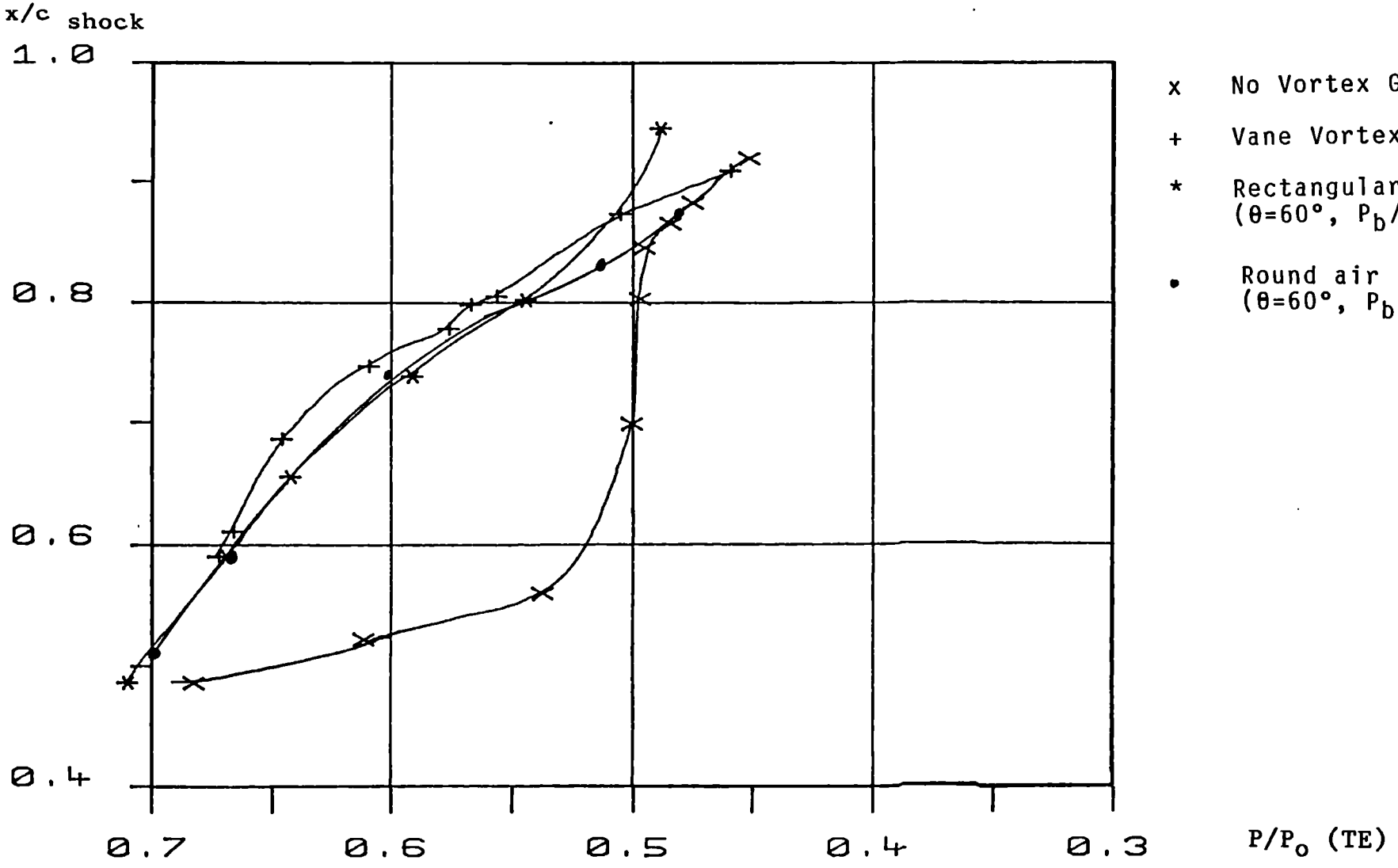

Figure 6.25 Comparison of the loci of Shock Position Against Trailing Edge Pressure for the 8% Bump.

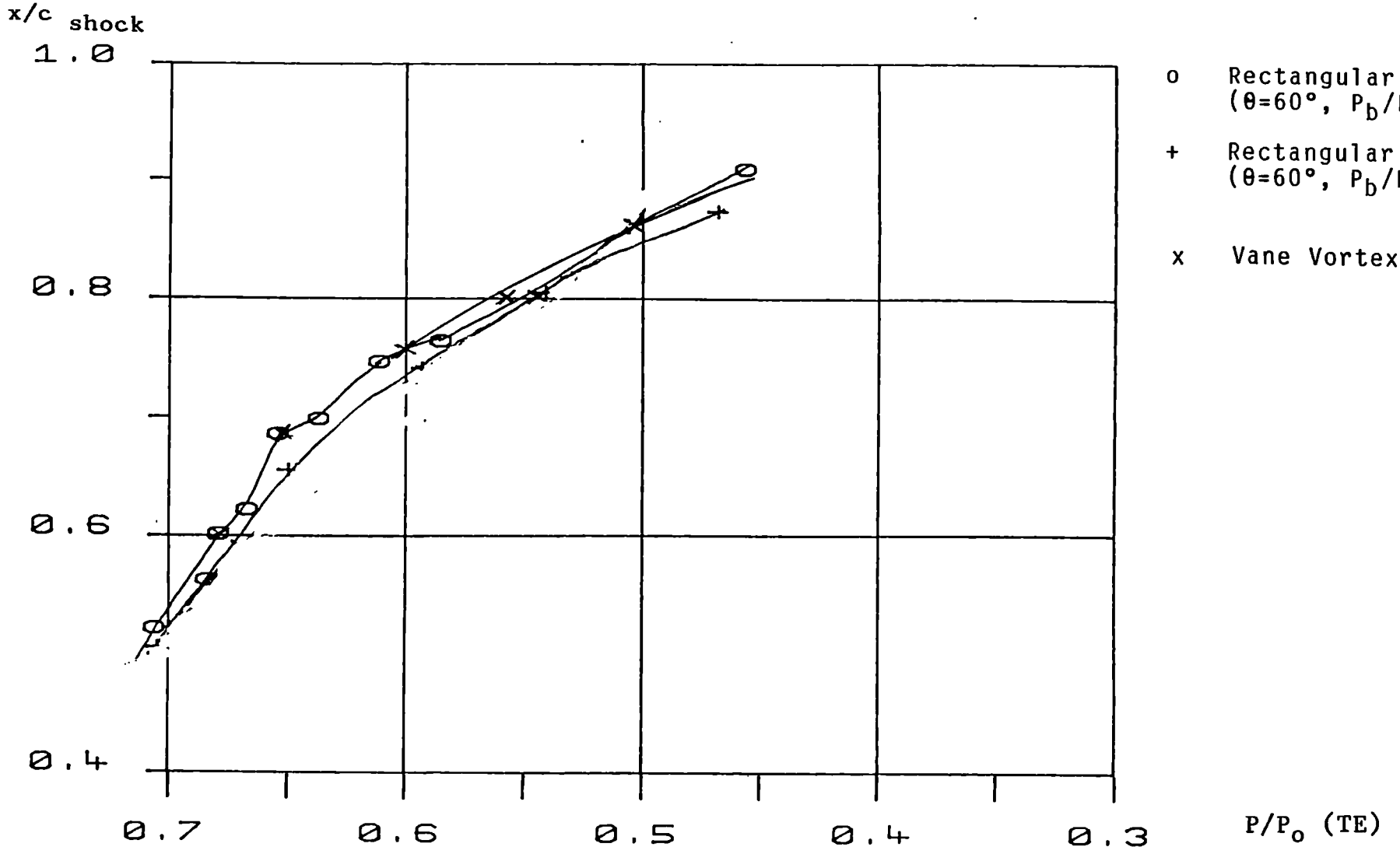

Figure 6.26 Comparison of the loci of Shock Position Against Trailing Edge Pressure for the 8% Bump.

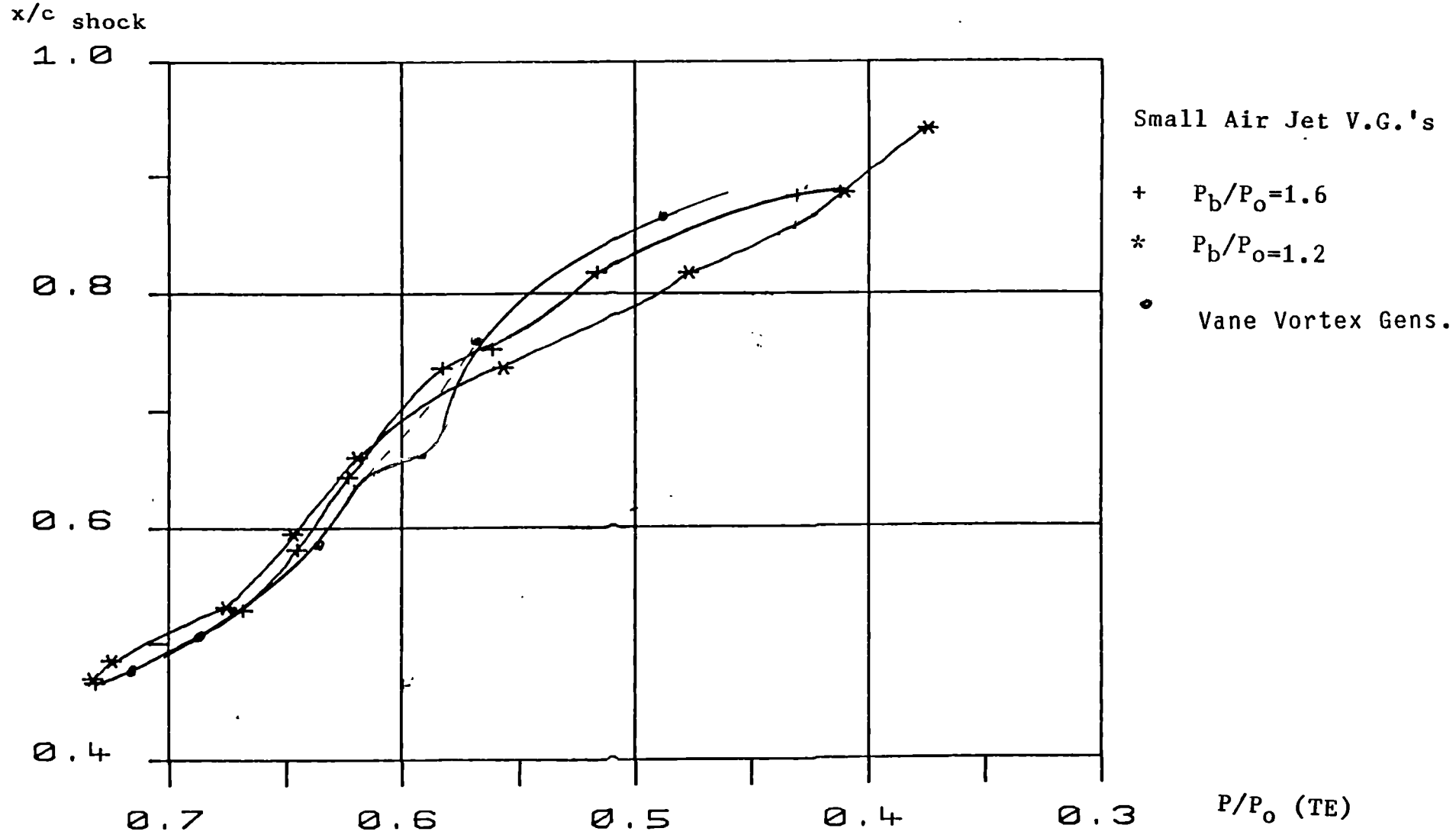

Figure 6.27 Comparison of the Loci of Shock Position Against Trailing Edge Pressure for the 10% Bump.

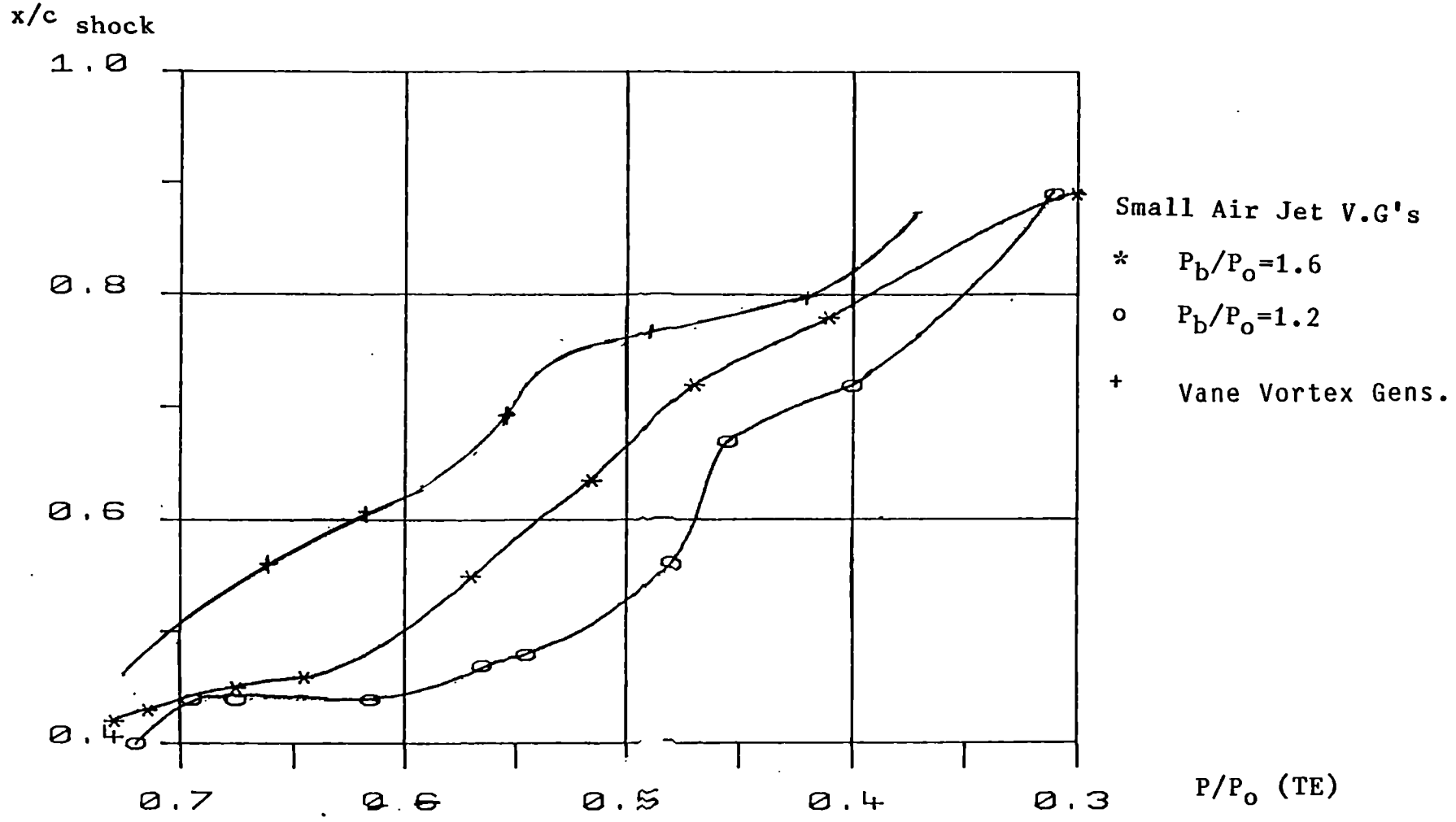

Figure 6.28 Comparison of the Loci of Shock Position Against Trailing Edge Pressure for the 14% Bump.

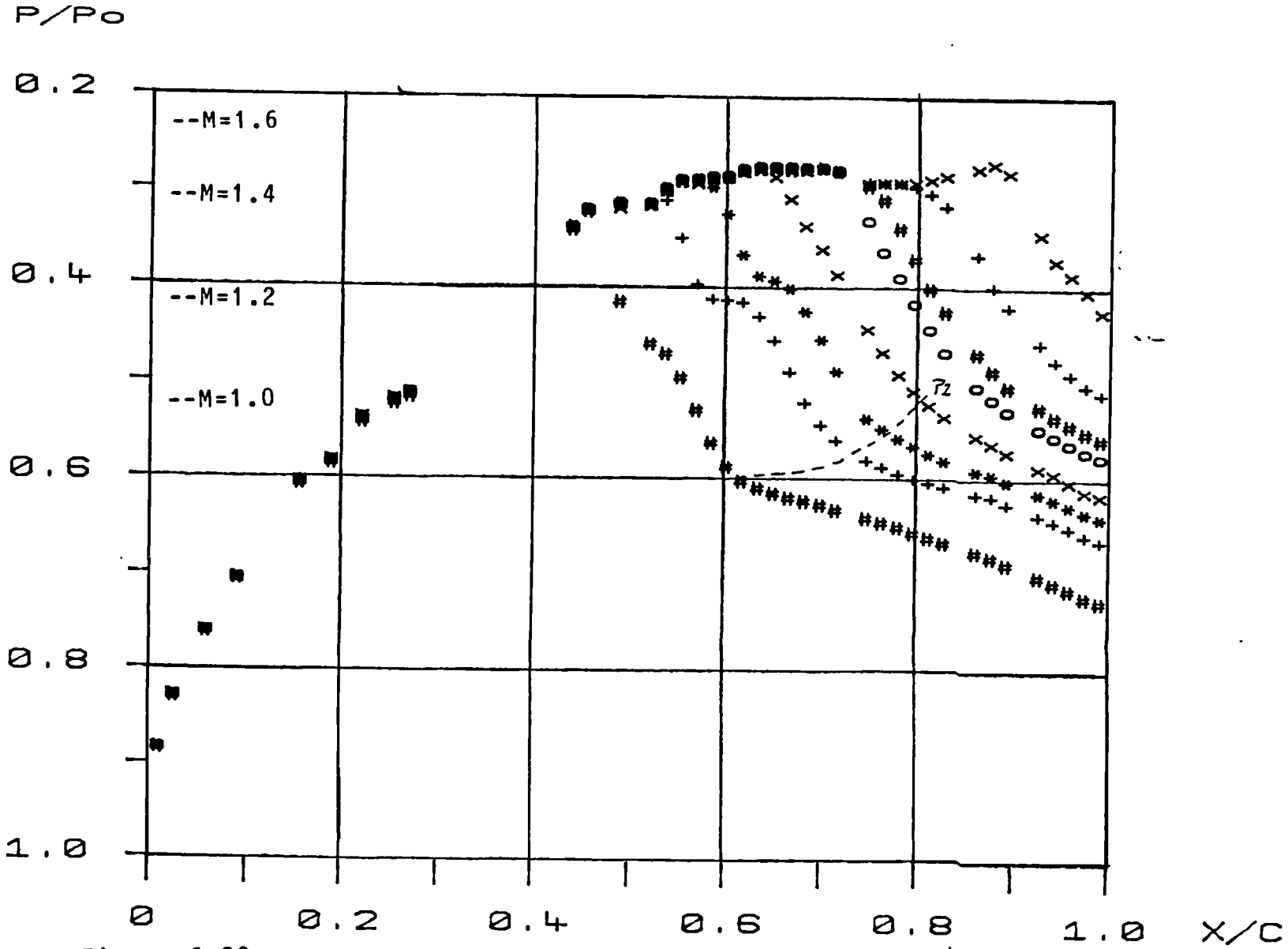

Figure 6.29 Experimental Pressure Distributions for the 10% Bump with Small Air Jet Vortex Generators (P_b/P_o=1.6)

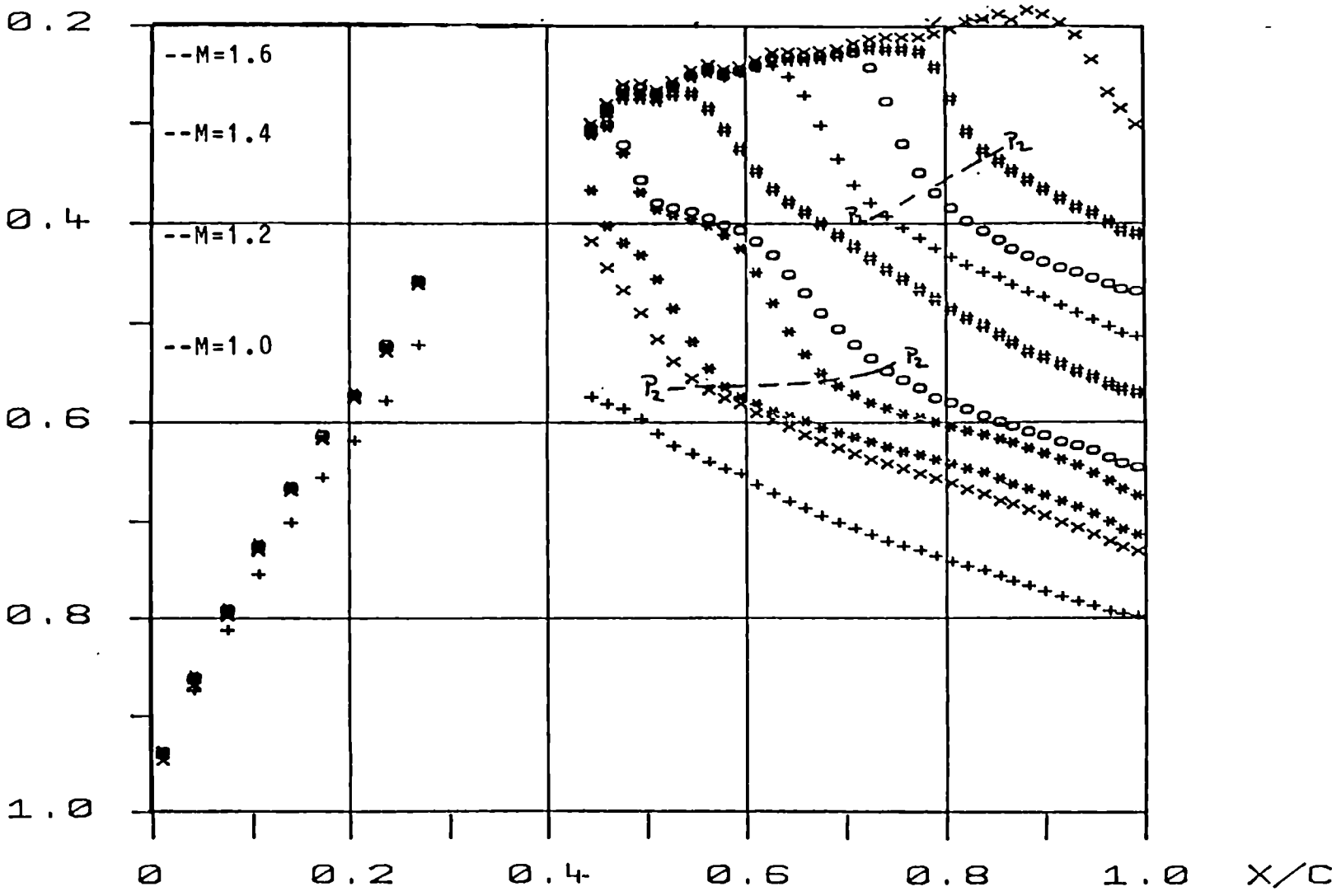

Figure 6.30 Experimental Pressure Distributions for the 14% Bump with Small Air Jet Vortex Generators ($\emptyset$=30°, P_b/P_o=1.6).

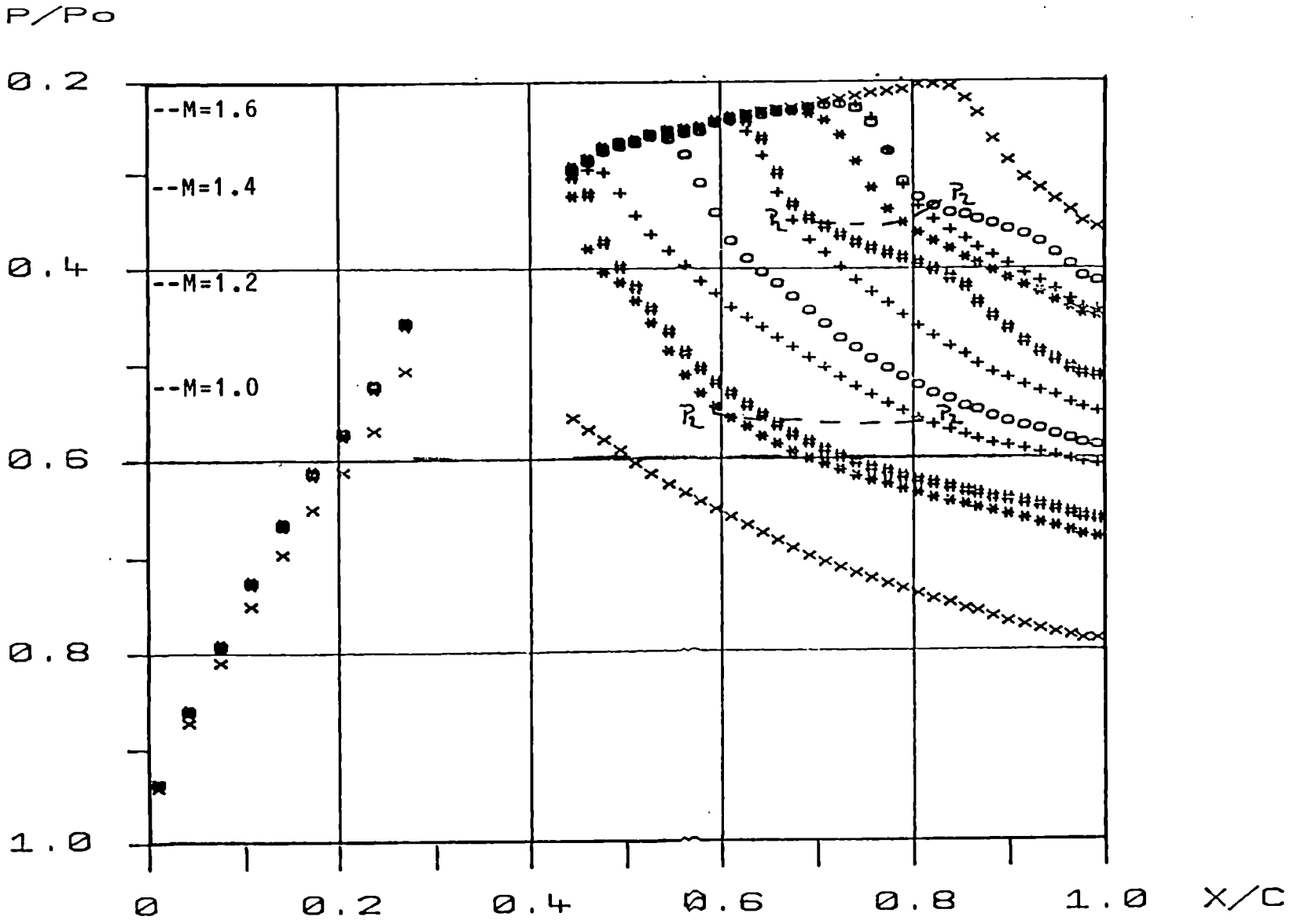

Figure 6.31 Experimental Pressure Distributions for the 14% Bump with Small Air Jet Vortex Generators ($\emptyset$=45°, P_b/P_o=1.2).

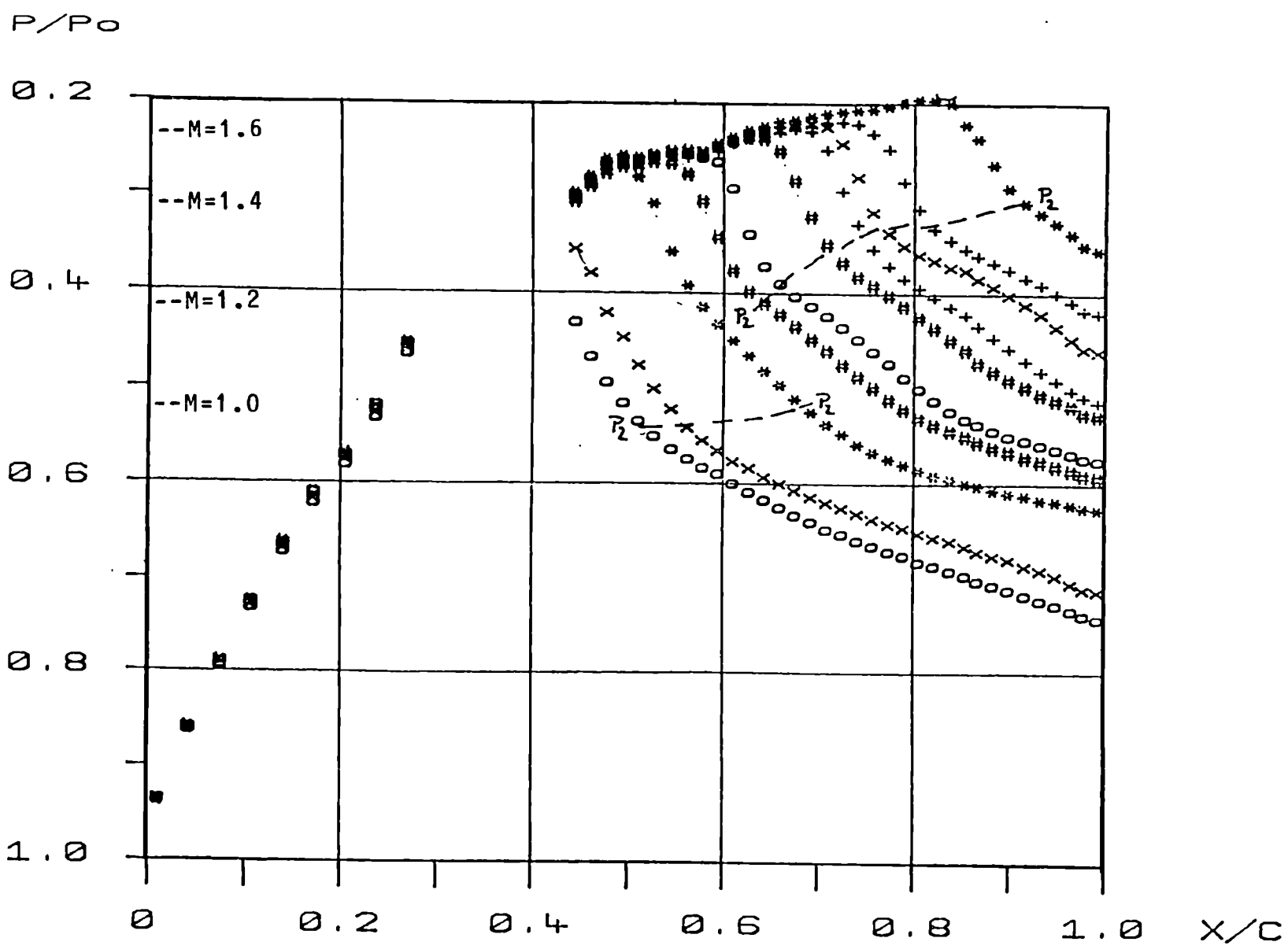

Figure 6.32 Experimental Pressure Distributions for the 14% Bump with Small Air Jet Vortex Generators (Ø=45°, P_b/P_o=1.6).

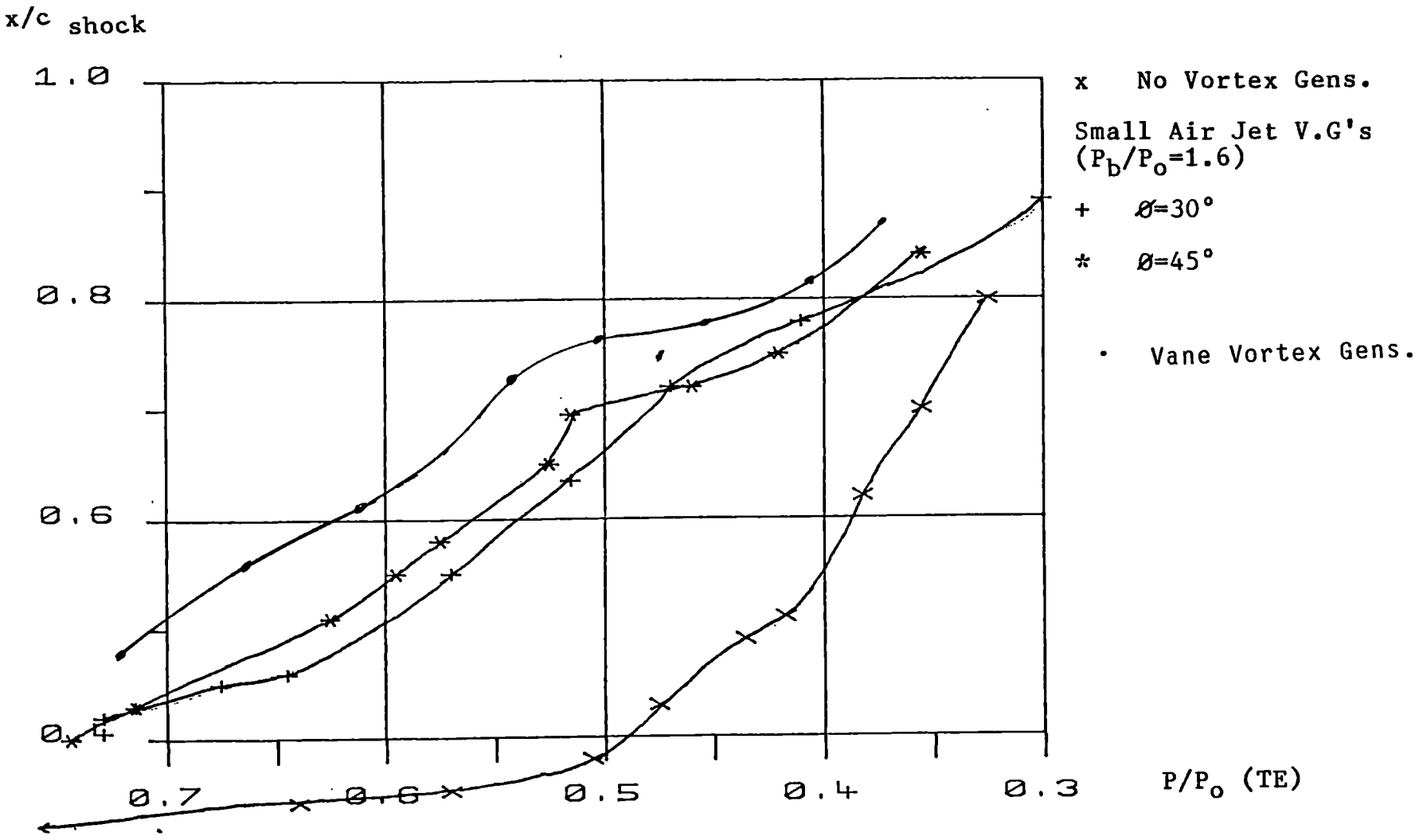

Figure 6.33 Comparison of the Loci of Shock Position Against Trailing Edge Pressure for the 14% Bump.

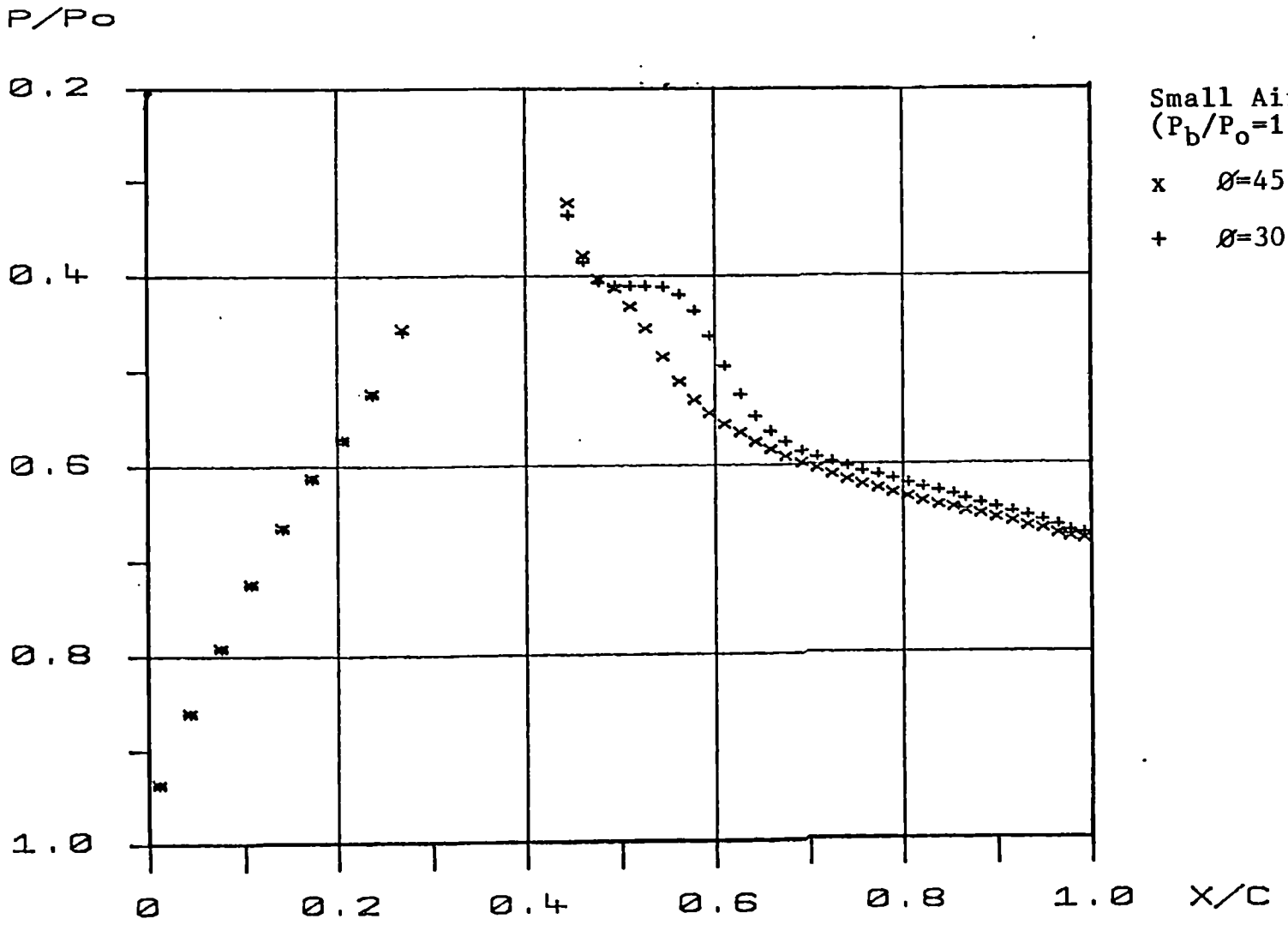

Figure 6.34 Comparison of Experimental Pressure Distributions on the 14% Bump.

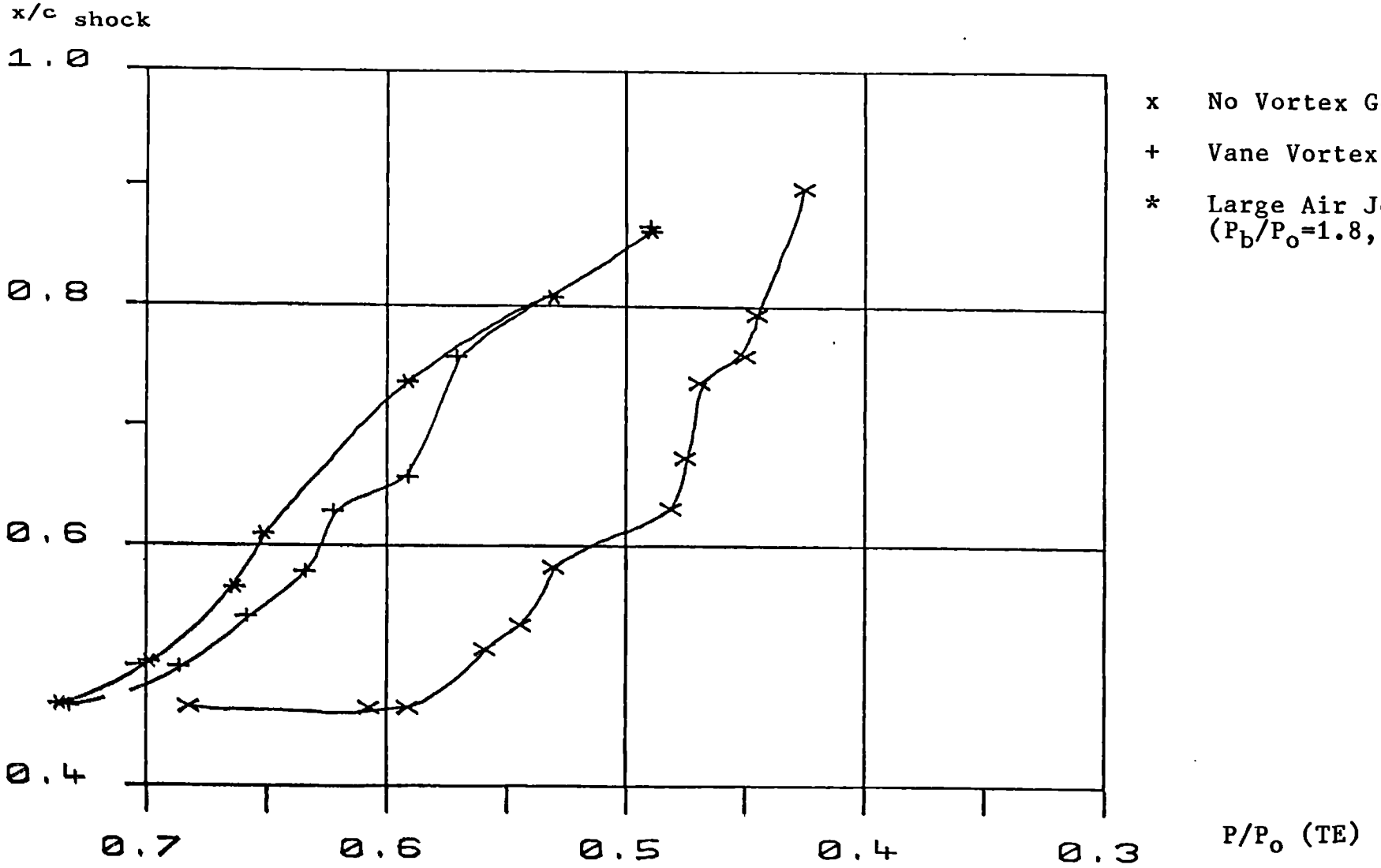

Figure 6.35 Comparison of the Loci of Shock Position Against Trailing Edge Pressure for the 10% Bump.

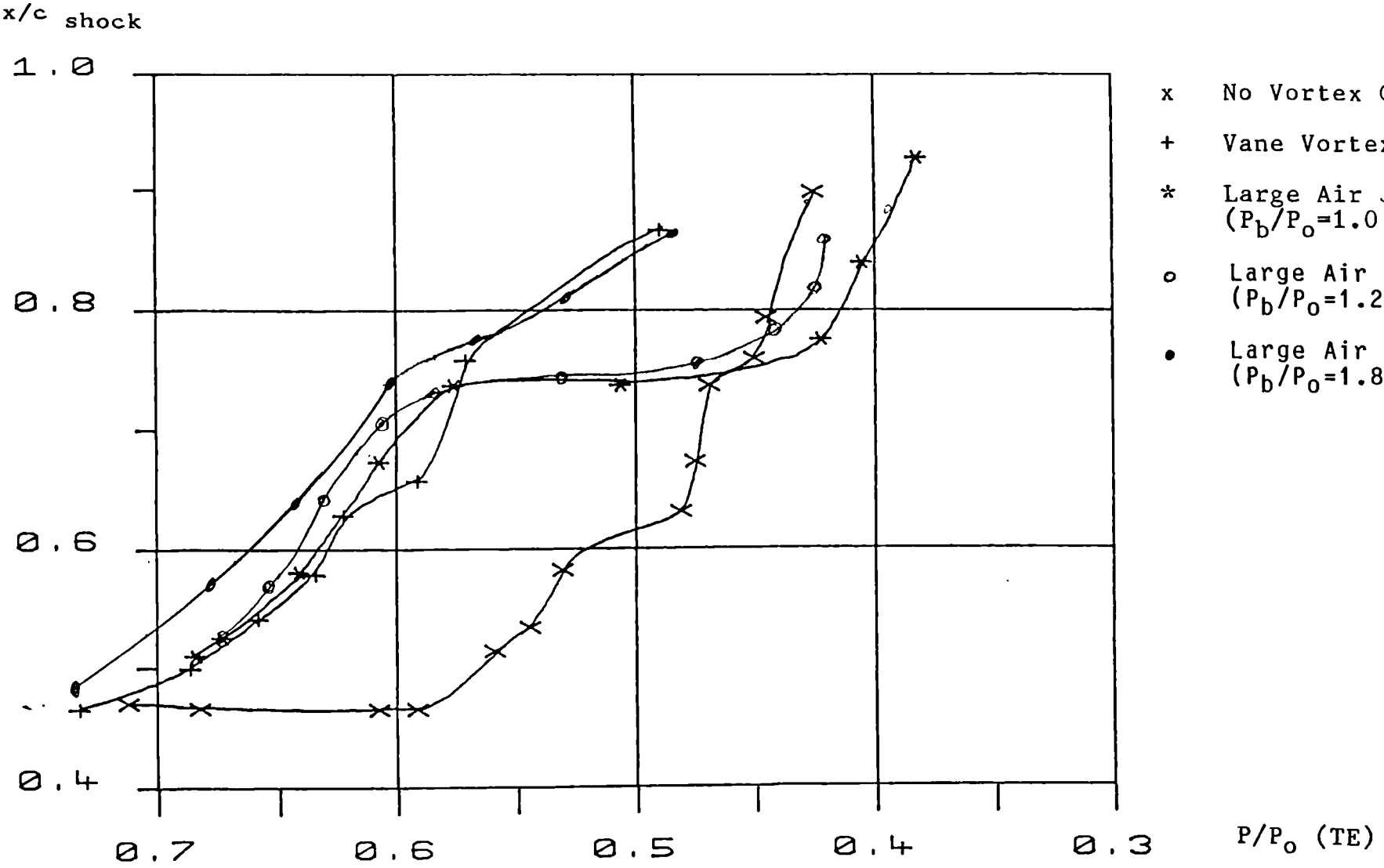

Figure 6.36 Comparison of the Loci of Shock Position Against Trailing Edge Pressure for the 10% Bump.

Figure 6.37 Boundary Layer Profiles With Vane Vortex Generators.

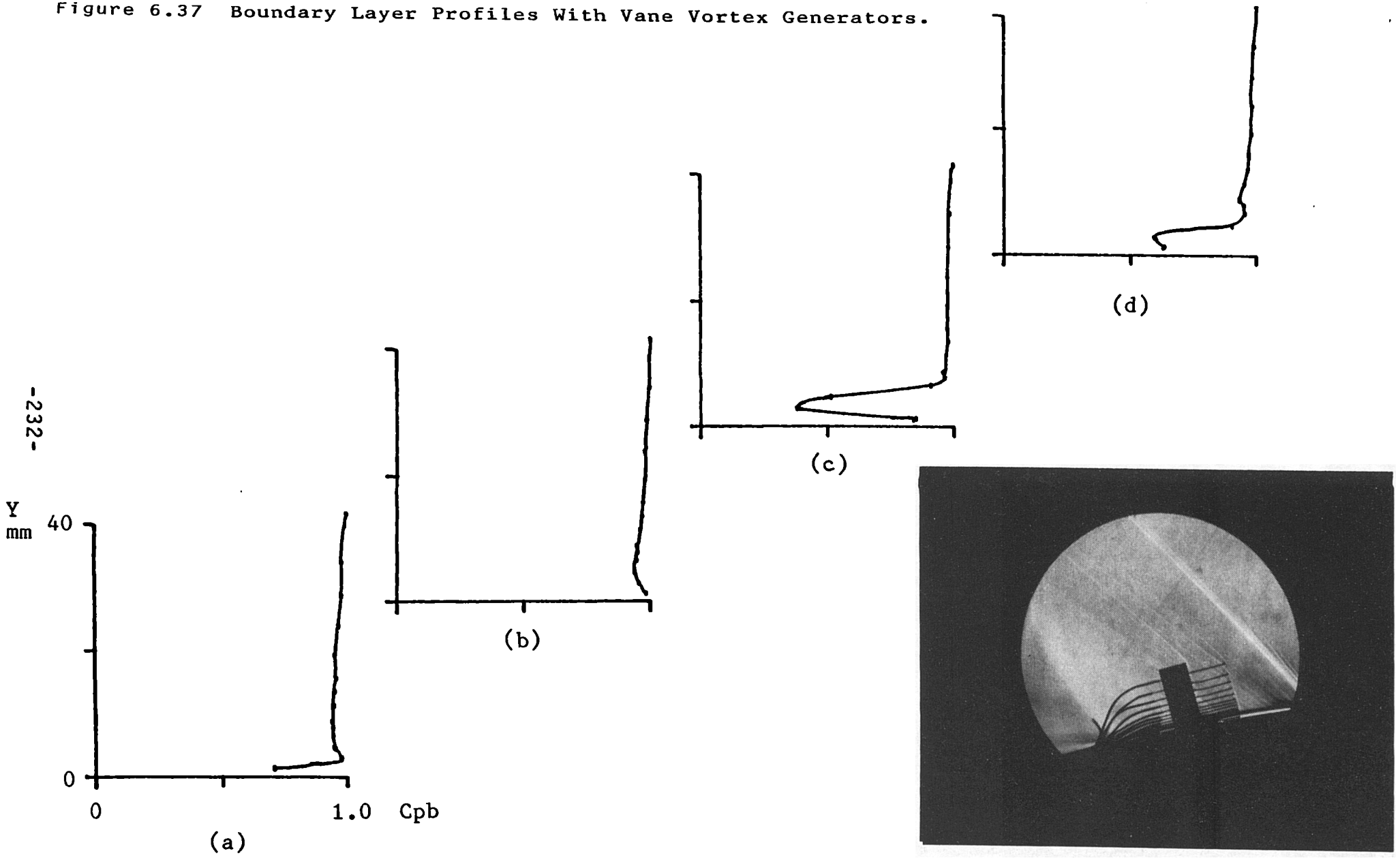

Figure 6.38 Boundary Layer Profiles With Small Air Jet Vortex Generators (P_b/P_o=1.6, Ø=45°).

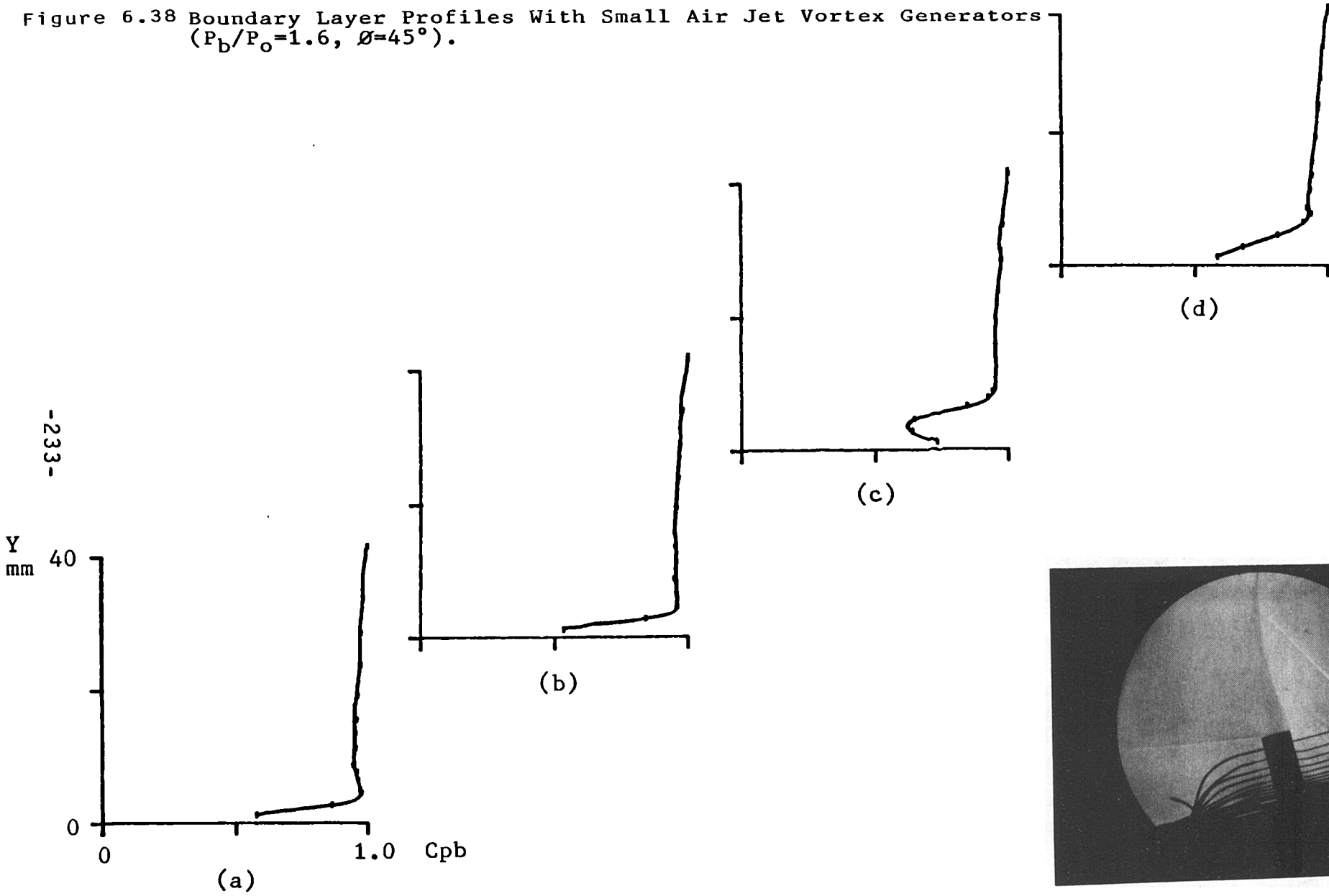

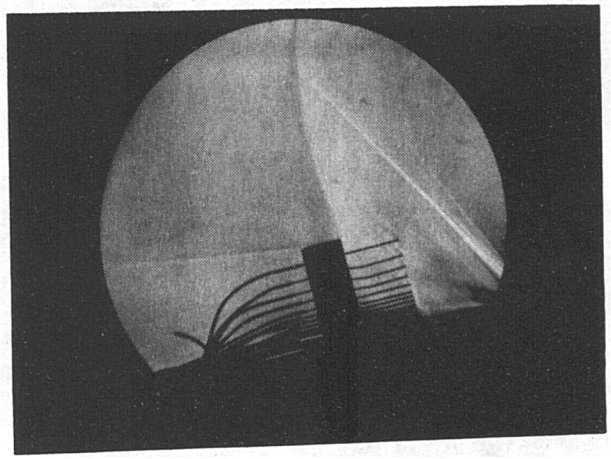

Figure 6.39 Boundary Layer Profiles With Large Air Jet Vortex Generators (P_b/P_o=1.5, θ=60°).

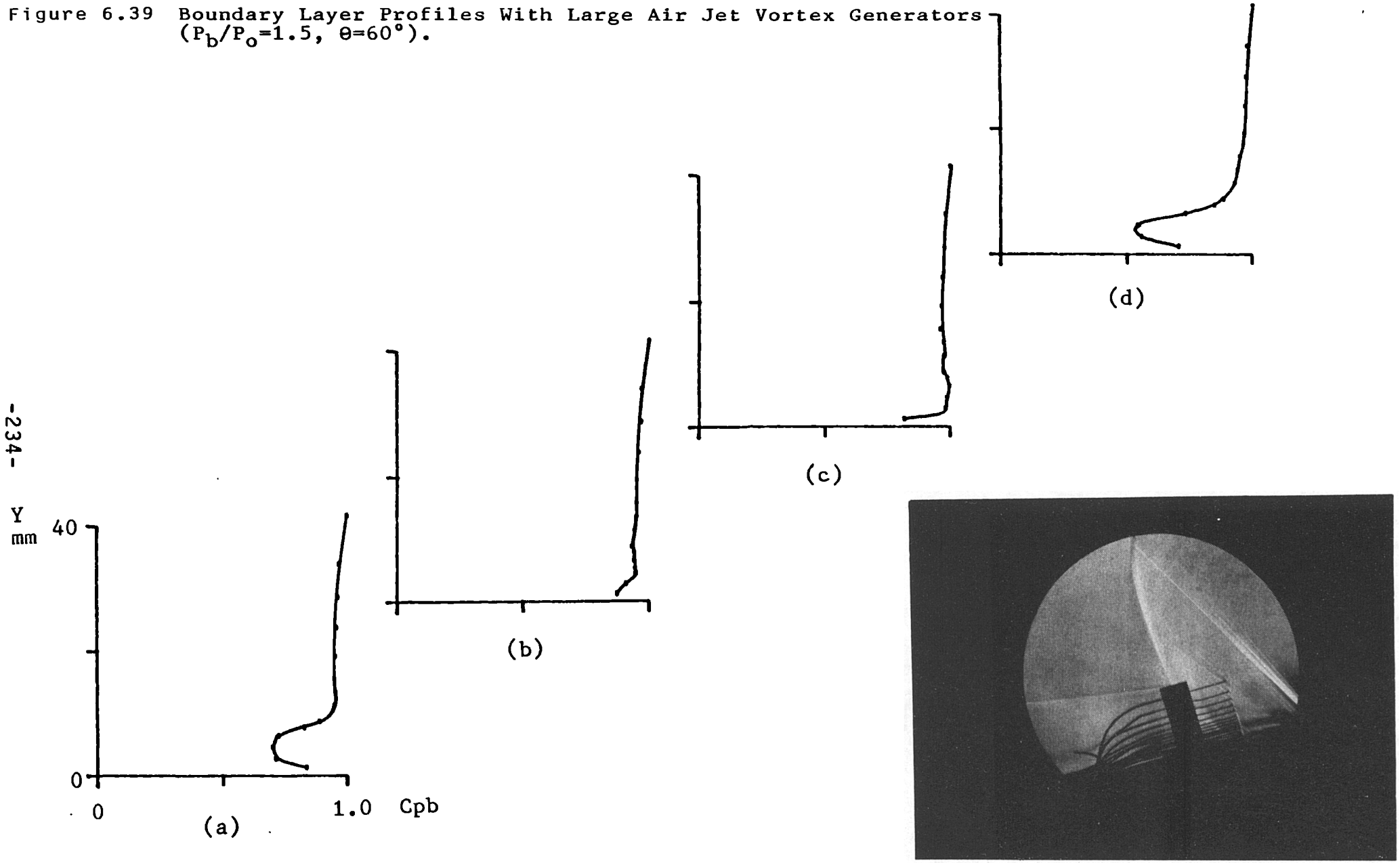

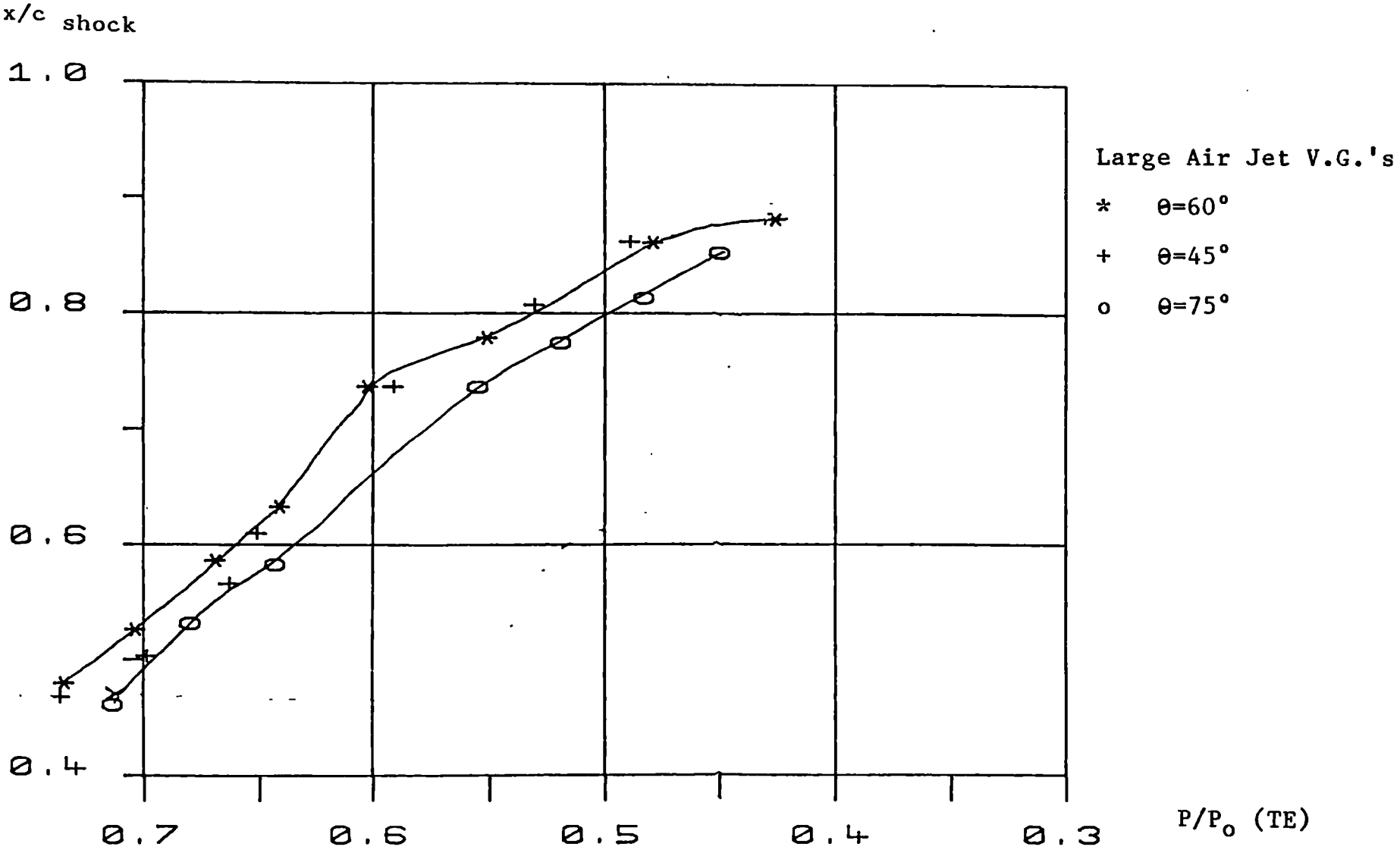

Figure 6.4(Comparison of the Loci of Shock Position Against Trailing Edge Pressure for the 10% Bump.

CONCLUSIONS

1. The bumps of varying thickness to chord ratio displayed significant shock induced boundary layer separation when no vortex generators were used and were therefore judged to be a exacting tests for air jet vortex generators.

2. It was shown that air jet vortex generators could be designed to be as effective in controlling shock induced boundary layer separation as conventional vane type generators, and could do so for relatively low blowing pressures.

3. The method by which an air jet forms a vortex showed that the jet flow formed the core and the mainstream flow wrapped itself around this core to form the vortex.

4. The influence of jet shape, size, direction, inclination and blowing pressure on the vortex characteristics was investigated and there effects are discussed in detail.

5. From the findings discussed in this thesis it was possible to issue a preliminary set of design guidelines.

REFERENCES

1. Pearcey H.H. Shock induced separation and its prevention by design and boundary layer control. (Pergamon Press Oxford, 1961).

2. Wallis R. A. Control of shock induced boundary layer separation with discrete air jets. (N.P.L. (F.M. 2641), 1958).

3. Freestone M. M. Preliminary tests at low speed on vorticity produced by air jet vortex generators. (City University London, RM 85/1 1985).

4. Pearcey H.H. Osborne J. Haines A. B. The interaction between local effects at the shock and rear separation. (AGARD C.P. No. 35, 1968).

5. Delery J. Marvin J. G. Shock wave boundary layer interactions. (AGARDograph No. 280, 1986).

6. Working Group 9 Boundary Layer Simulation and Control in Wind Tunnels, AGARD Advisory Report Number 224, 1988).

7. Delery J. Shock wave/turbulent boundary layer interaction and its control. (Prog in aero sci., vol. 22, Pergamon, 1985).

8. Raghunathan S. Passive control of shock boundary layer interaction. (Prog. in aero. sci., vol. 24, Pergamon, 1988).

9. Mehta R. D. Vortex/separated boundary layer interactions at transonic Mach numbers. (AIAA Journal, vol. 26, no. 1, 1988).

10. Freestone M.M. Effects of vortex spacing on induced lateral velocity. (Unpublished).

11. Sykes D. M. The slotted wall transonic wind tunnel at The City University. (City University RM Aero. 69/3, 1969).

12. Tanner L. H. Curves suitable for families of aerofoils with variable maximum thickness positions, nose radius, camber and nose droop. (HMSO C.P. No. 358, 1957).

13. Wallis R. A. — A preliminary note on a modified type of air jet for boundary layer control. (Dept of Supply, Australia, 1956).

14. Nelson P. — OASIS Handbook. (Peter Nelson Design Consultancy, Norwich, 1986).

15. Pearcey H.H. — Some effects of shock induced separation of turbulent boundary layers in transonic flows past aerofoils. (ARC R and M number 3108, 1955).

16. Delery J. Horowitz E. Leuchter O. Solignac J. — Fundemental studies on vortex flows. (ONERA, Rech. Aerospace, 1984).

17. Pearcey H.H. Osborne J. Sinnott C. — Some effects of wind tunnel interference observed in tests on 2-D aerofoils at high subsonic and transonic speeds. (AGARD 296, 1959).

18. VGK20 — Viscous Garebidian and Korn version 20. Used with the kind permission of RAE. Farnborough.

19. Houghton E.L. Brock A.E. — Tables for the compressible flow of dry air. (Edward Arnold, London, Third Edition, 1975)

APPENDIX A

Boundary Layer Suction

Since the half aerofoil or bump technique was used in the investigation discussed in this thesis it was necessary to devise a method of partially removing the boundary layer ahead of the bump. This was necessary to ensure that the boundary layer approaching the leading edge would be turbulent and of a realistic thickness.

To achieve this objective a plenum chamber was built into the model. The chamber, which spanned the working section, was 254mm by 254mm by 60mm deep and was positioned 20mm ahead of the bump. A perforated plate (of 30% open area ratio) was securely fixed above the chamber and flush with the surface of the model. Figure A.1 shows a diagrammatic representation of the apparatus.

The plenum chamber was connected via a 76.2mm diameter flexible pipe to the secondary ejector of the nearby T6 transonic wind tunnel. The secondary ejector of T6 was used as the low pressure source which when operated in conjunction with the T5 wind tunnel induced part of the boundary layer flow over the perforated liner to pass into the chamber and through to the ejector. Varying the control valve on the T6 secondary ejector gave a control on the amount of suction applied and hence the quantity of air removed through the perforated liner.

To determine the amount of suction required to produce a thin turbulent layer near the leading edge of the model a

Preston tube (1.57mm O/D and 1.00mm I/D) was fitted 50mm aft of the leading edge. For a given downstream pressure on the T5 wind tunnel, the T6 secondary ejector was operated at various pressures. The pressures at the Preston tube (P_p) were recorded for the various secondary ejector feed pressures and were non-dimensionalised with respect to P_o to give P_p/P_o.

The results are presented in graph A.2 and show that as the feed pressure is increased from 0 to 55 psi (indicated value) the pressure recorded at the Preston tube increases, which suggest that the boundary layer height decreases. For secondary ejector pressures greater than 55psi the rate at which the pressure increases falls dramatically and for values greater than 60 psi there is no further increase in P_p/P_o. It can be concluded that for ejector feed pressures greater than 60 psi no further decrease in boundary layer height occurs.

It is evident from the shape of the pressure distributions and the schlieren photographs that the boundary layer ahead of the all shock positions is turbulent. Transition from a laminar layer probably takes place ahead of the bump and is a result of the roughness of the perforated liner and the adverse pressure gradient of the flow over it.

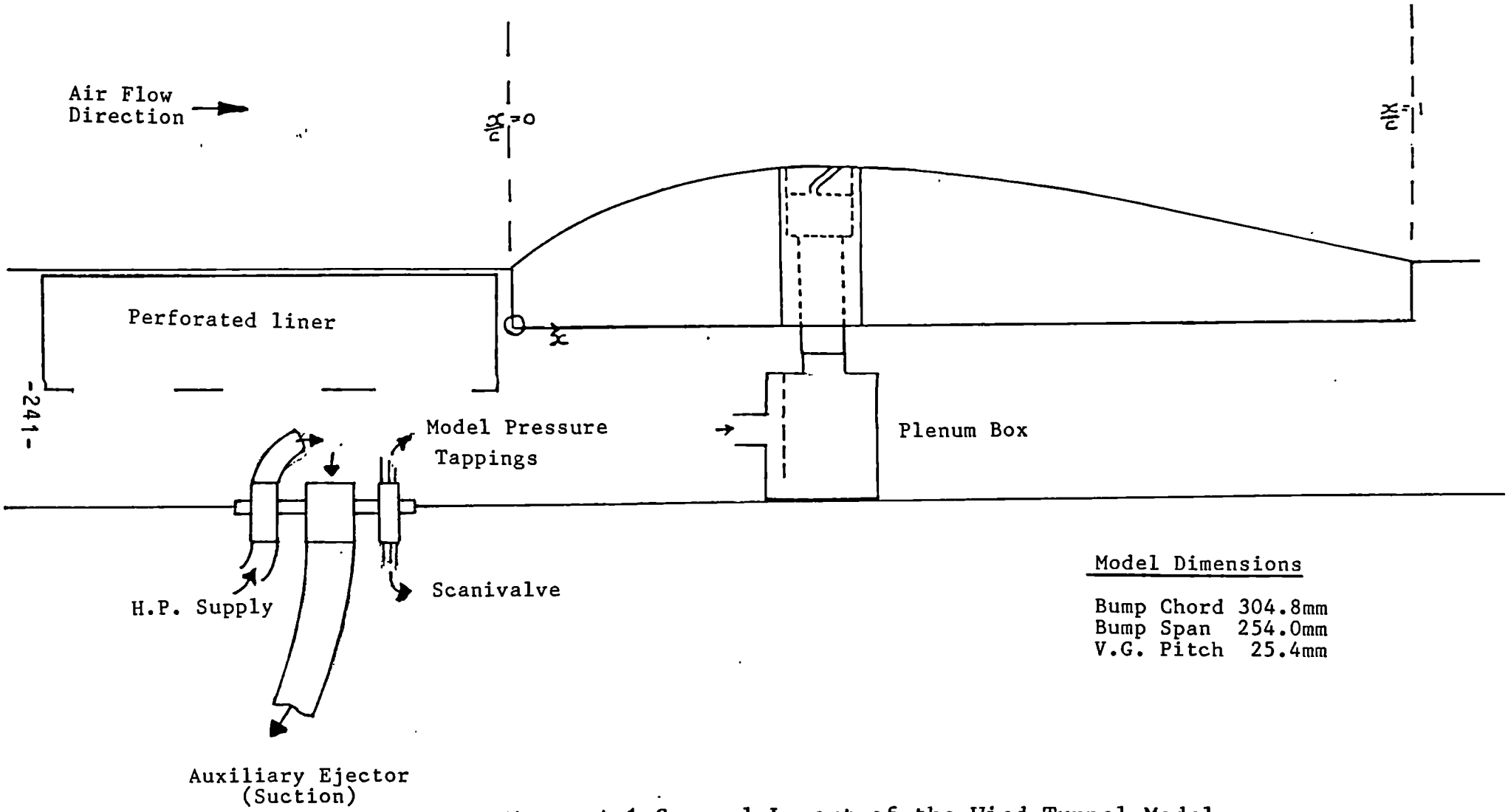

Figure A.1 General Layout of the Wind Tunnel Model.

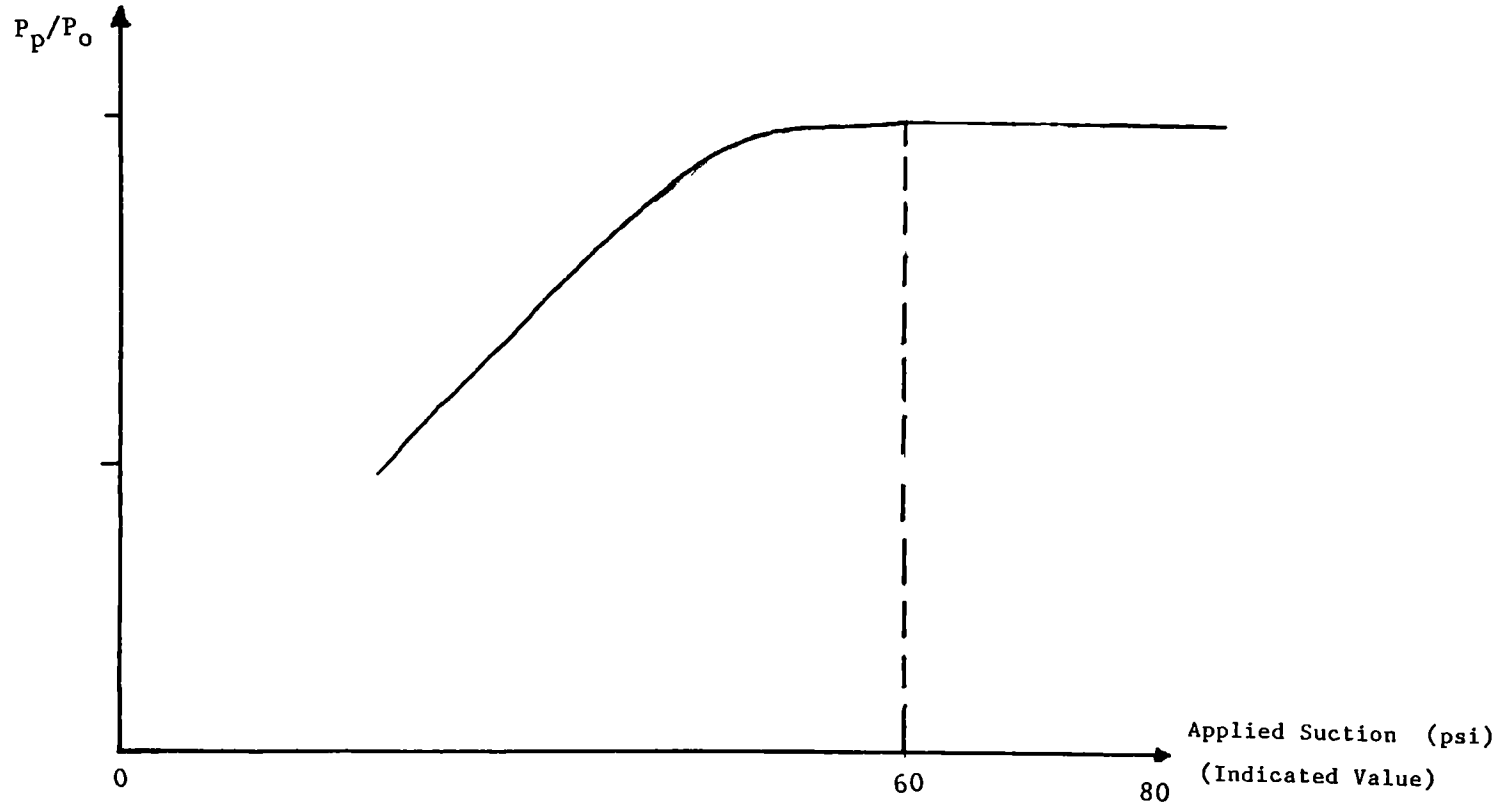

Figure A.2 Graph of Preston Tube Reading against Applied Suction.

APPENDIX B

B.1 Chordwise Position of Pressure Tappings (8% Bump)

Tapping	Position (x/c)
1	0.013
2	0.045
3	0.073
4	0.102
5	0.133
6	0.166
7	0.200
8	0.231
9	0.263
10	0.284
11	0.442
12	0.461
13	0.487
14	0.523
15	0.560
16	0.591
17	0.623
18	0.656
19	0.687
20	0.718
21	0.748
22	0.779
23	0.813
24	0.846
25	0.873
26	0.909
27	0.938
28	0.974
29	0.990

B.2 Chordwise Position of Pressure Tappings (10% Bump)

Tapping	Position (x/c)
1	0.016
2	0.032
3	0.065
4	0.097
5	0.130
6	0.162
7	0.195
8	0.227
9	0.260
10	0.276
11	0.445
12	0.461
13	0.494
14	0.526
15	0.542
16	0.558
17	0.575
18	0.591
19	0.607
20	0.623
21	0.640
22	0.656
23	0.672
24	0.688
25	0.705
26	0.721
27	0.737
28	0.753
29	0.769
30	0.786
31	0.802
32	0.818
33	0.834
34	0.867
35	0.883
36	0.899
37	0.932
38	0.948
39	0.964
40	0.981
41	0.997

B.3 Chordwise Position of Pressure Tappings

Tapping	Position (x/c)
1	0.016
2	0.049
3	0.081
4	0.114
5	0.146
6	0.179
7	0.211
8	0.244
9	0.276
10	0.451
11	0.468
12	0.484
13	0.500
14	0.516
15	0.532
16	0.552
17	0.568
18	0.584
19	0.601
20	0.617
21	0.633
22	0.649
23	0.666
24	0.682
25	0.698
26	0.714
27	0.731
28	0.747
29	0.763
30	0.779
31	0.795
32	0.812
33	0.828
34	0.844
35	0.860
36	0.873
37	0.890
38	0.906
39	0.922
40	0.938
41	0.955
42	0.971
43	0.984
44	0.990

APPENDIX C

Choice of Liner

As described in Chapter 3, the T5 wind tunnel facility at City University was used for the investigation discussed in this thesis. A half aerofoil model of thickness to chord ratio of 8% and chord length of 304.5mm was mounted in the floor of the wind tunnel. The roof of the wind tunnel was fitted with a slotted liner with an open area ratio of 12%. With this arrangement the wind tunnel was able to operate with transonic flow over the bump.

The object of the early tests on the 8% thick bump was to establish the extent of the shock induced boundary layer separation and to compare the findings with the work carried out by Wallis (2), who had used the same section in his investigation into the use of air jet vortex generators in transonic flow.

With no vortex generators fitted to the bump the results obtained, using the slotted liner, did not compare well with those found by Wallis. This observation is illustrated in graph C.2 which shows the loci of shock position against trailing edge pressure for the two cases and it can be seen that Wallis' results showed a more severe shock pause and lower pressures at the trailing edge for given shock positions.The main reason for this discrepancy was due to the fact that Wallis' tests were carried out with a solid liner fitted above the bump.

The slotted liner was sealed and the tests repeated, again with no method of boundary layer control on the bump. Graph C.3 shows the pressure distributions obtained using this arrangement. Comparing with graph C.1, which shows the pressure distribution with the slotted liner, it can clearly be seen that there are significant differences. The local Mach number ahead of the shock decreases and the pressure recoveries achieved after the shock are less when the solid liner is used. Graph C.4 compares the loci of shock position against trailing edge pressure for these two cases. It shows that by sealing the slots in the liner the trailing edge pressure for a given shock position is lower and the distinctive pausing of the shock position for decreasing trailing edge pressure, as found by Wallis and characteristic of Type A shock induced boundary layer separation, is more pronounced.

Tests reported by Pearcey (17) showed that for slotted liners with high open area ratios, distortion of the local supersonic flow occurred resulting in an increase in local Mach number upstream of the shock in some cases and a reduction in others. He found that the onset of shock induced separation was delayed for such walls in a manner that could not be corrected for in any conventional way. He attributed this to the distortion in the upstream supersonic flow.

Pearcey also discusses the abnormally large influence that solid walls can have on the wake interference effects in the presence of separated flow. He suggests that this influence exerts itself by distorting the relationship between the trailing edge pressure and freestream Mach number. As is shown in Chapter 5 the relationship between freestream Mach number and the pressure at the trailing

edge is not required for the analysis of the results in this thesis.

Graph C.5 compares the results obtained using the solid liner with those of Wallis. It can be seen that the behaviour of the shock induced separation is similar for the two cases when considered in terms of shock position and trailing edge pressure. This is despite a 2:1 difference in the ratio of model chord to tunnel height.

The decision to proceed with the solid liner in the investigation discussed in this thesis is supported by the following considerations:

1. It reproduces the conditions used by Wallis in his earlier work on air jet vortex generators.

2. It reproduces the conditions used in the earlier NPL work on which development of vane type vortex generators was based, which in turn was the basis for many subsequent successful applications of vane type vortex generators in practice. Comparisons of the current type of air jet vortex generators with vanes under the conditions for which the latter were developed should therefore be a good background from which to infer the effectiveness of these air jets when used in practice.

3. Solid liners present a more severe shock induced separation than the slots of large open area do and therefore a more severe test for vortex generators.

4. The most important consideration for the present tests is to asses the relative effectiveness of various vortex generators under identical conditions.

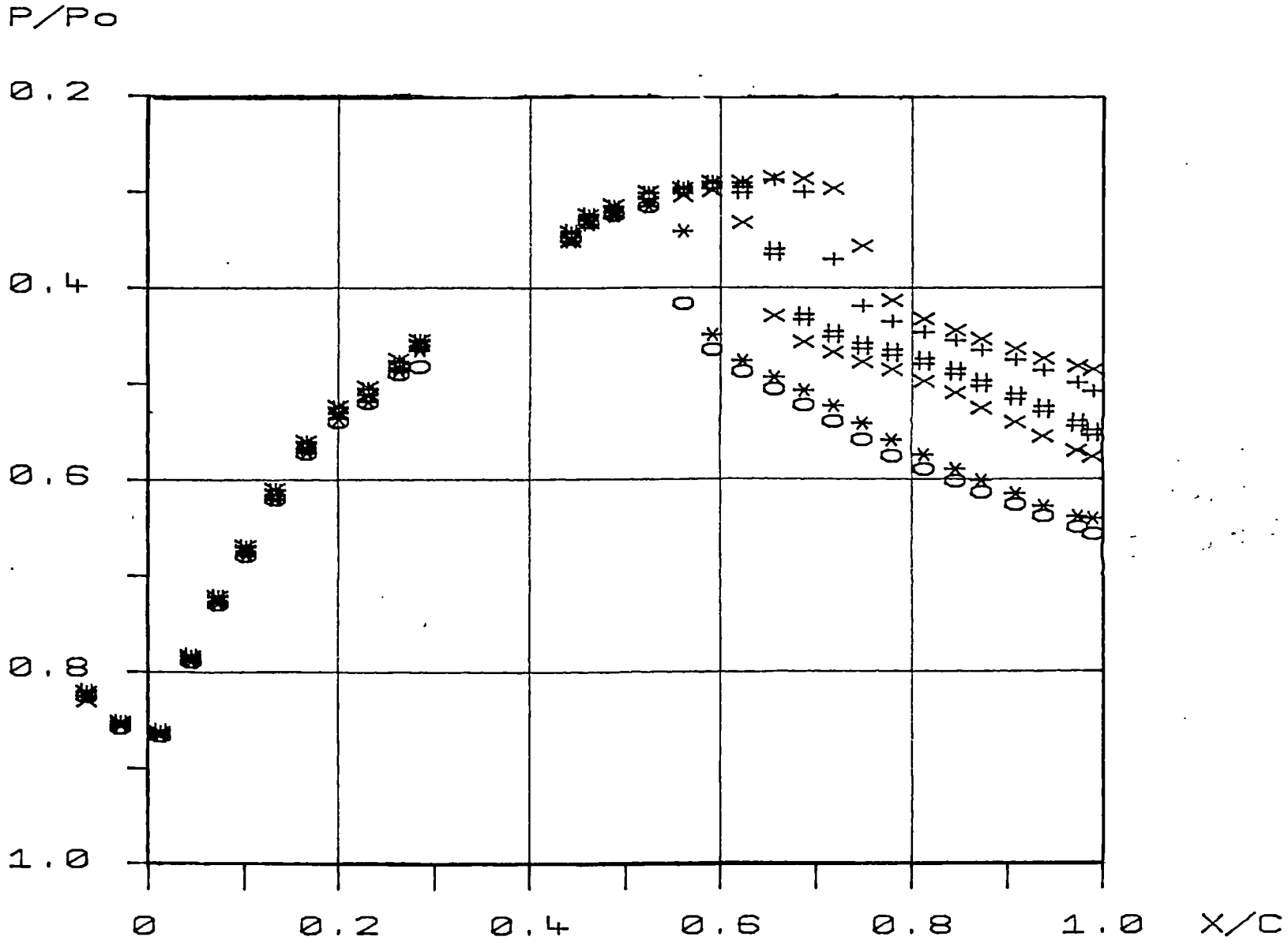

Figure C.1 Experimental Pressure Distribution for the 8% Bump with No Vortex Generators and a slotted Liner.

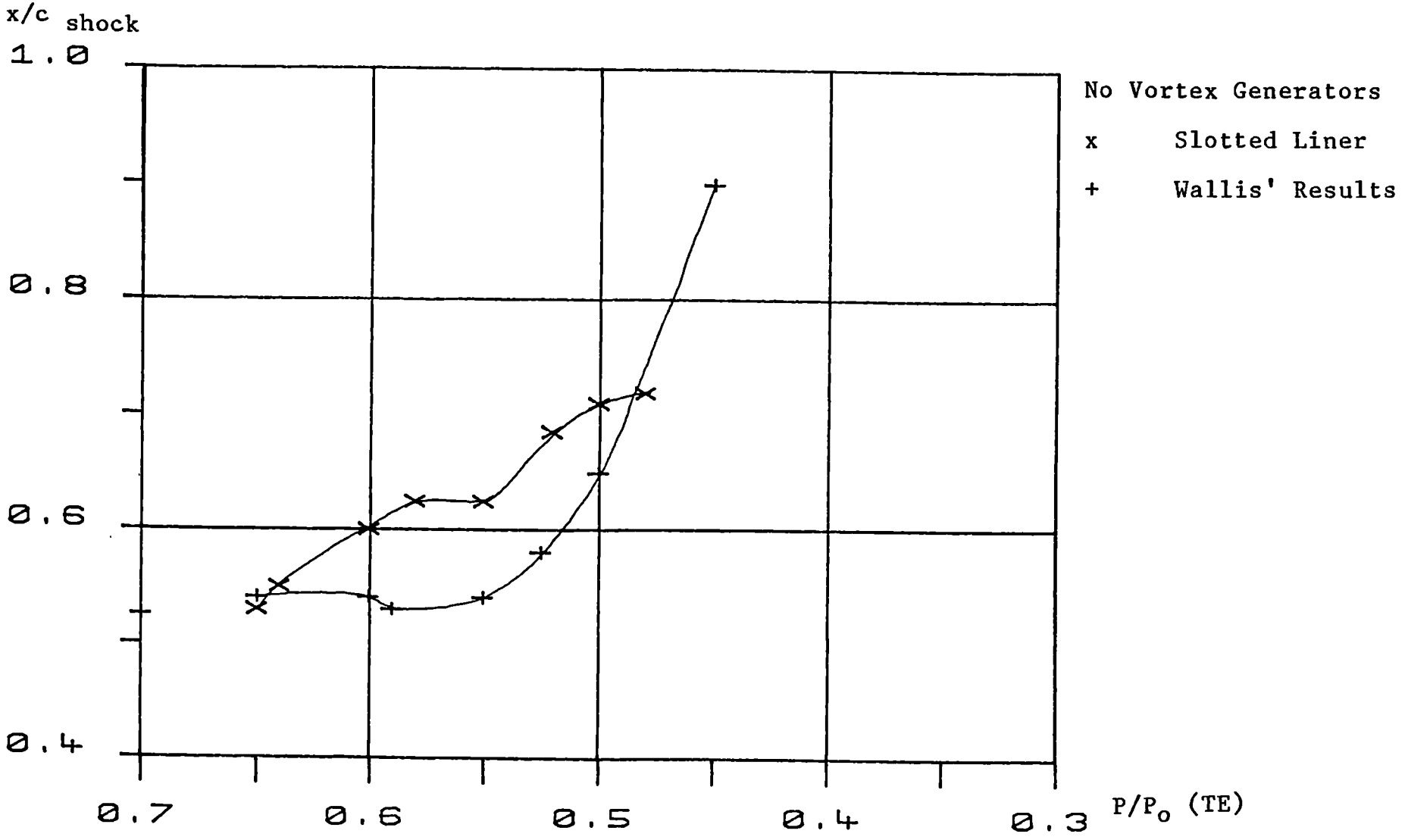

Figure C.2 Comparison of the Loci of Shock Position Against Trailing Edge Pressure for the 8% Bump.

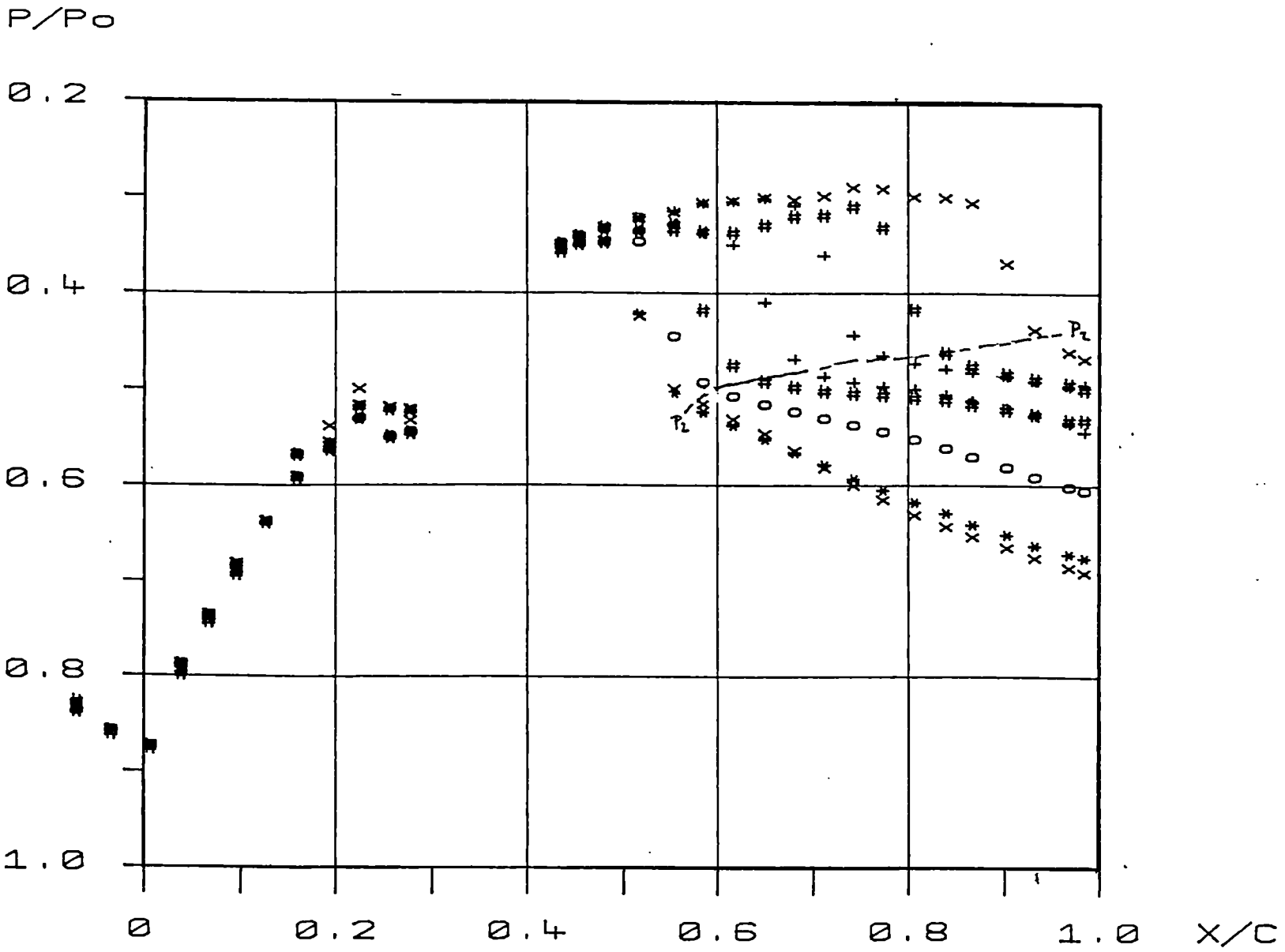

Figure C.3 Experimental Pressure Distribution for the 8% Bump with No Vortex Generators and a solid Liner.

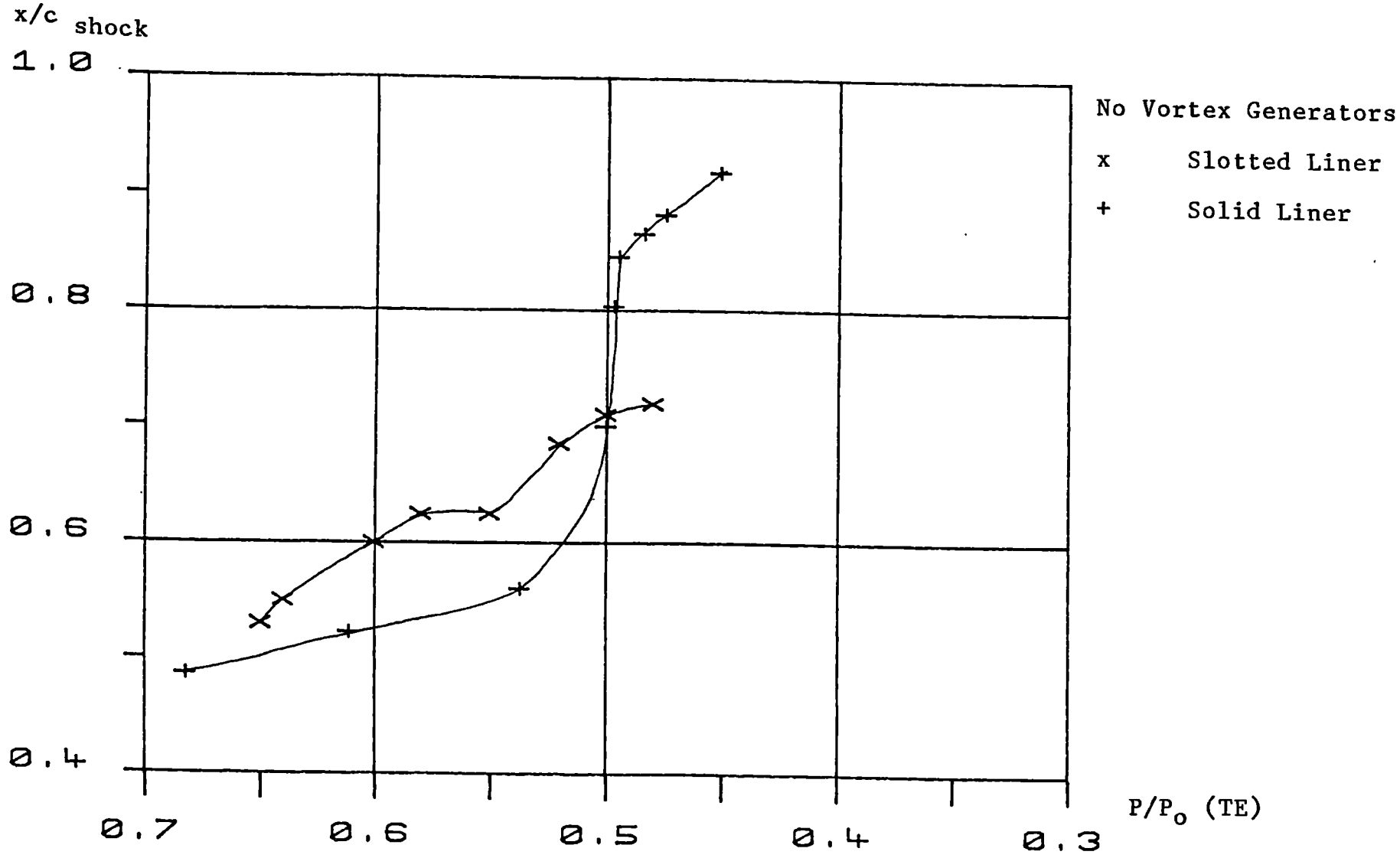

Figure C.4 Comparison of the Loci of Shock Position Against Trailing Edge Pressure for the 8% Bump.

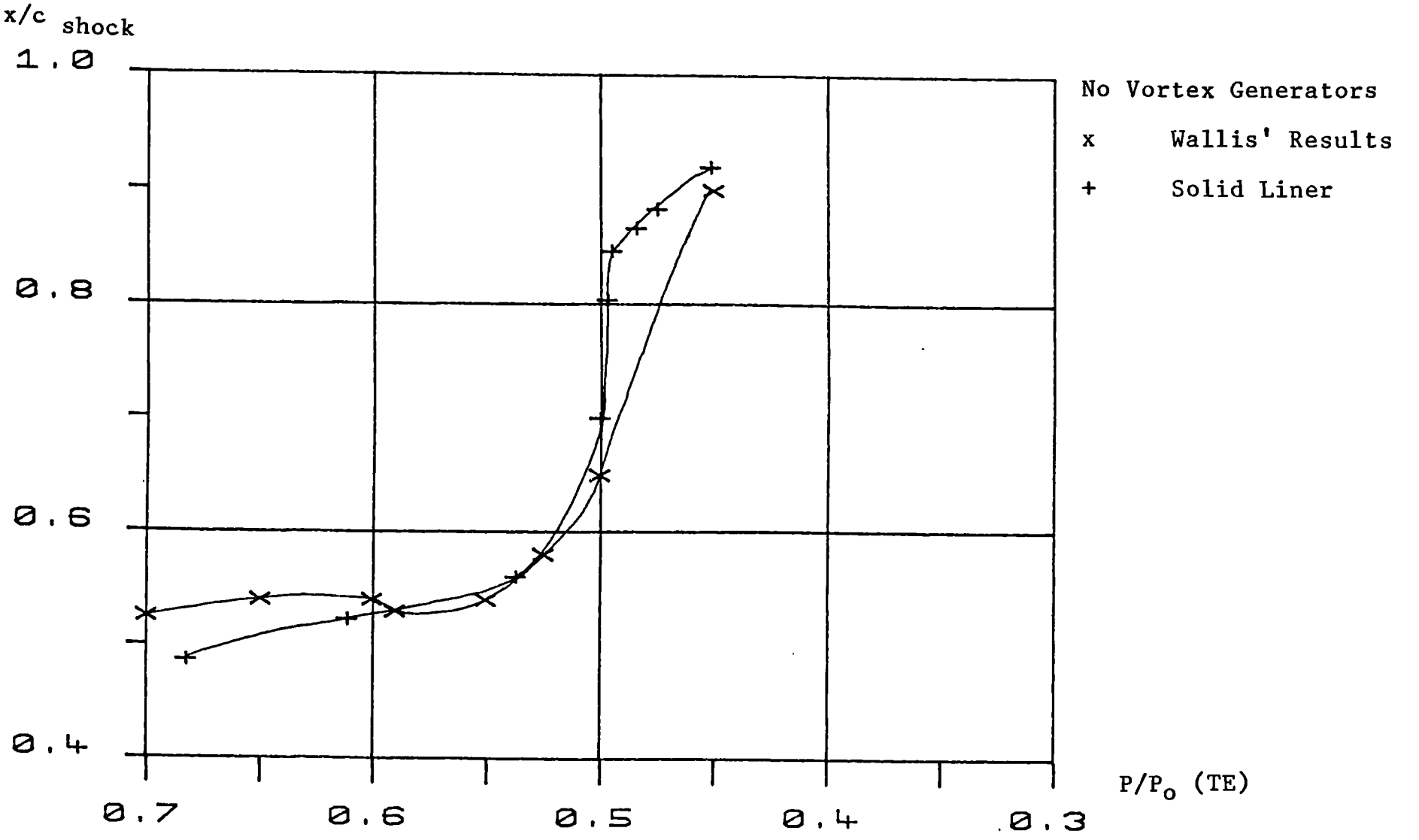

Figure C.5 Comparison of the Loci of Shock Position Against Trailing Edge Pressure for the 8% Bump.

APPENDIX D

Schlieren Investigation

The sidewalls of the T5 wind tunnel facility used for this investigation were fitted with circular windows of 230mm diameter. The windows could be positioned to observe either the forward section or rear section of the half aerofoil. All the results presented in this report are with the windows in the aft position, making it possible to photograph the flow from 40% chord to the trailing edge.

The schlieren investigation was carried out with a continuous light source and the knife edge set parallel to the flow so as to cut off light rays refracted away from the bump, i.e. to give a black image for the boundary layer. The schlieren photographs were made using 120 black and white negative film of 400 ASA.

Diagrams D.1 to D.6 are presented to help in interpreting the schlieren photographs presented in this report. The variation of density through an attached boundary layer is shown in diagram D.1. The corresponding schlieren image would be dark as the rate of change of density with height is always positive, as shown in diagram D.2. Diagram D.3 shows the variation of density through an attached boundary layer with a vortex running parallel with the flow. The resulting schlieren image would be a dark boundary layer followed by a pale and dark band, which represents the vortex. Diagram D.4 shows that the position

of the centre of the vortex is where the band goes from pale to dark.

In some of the schlieren photographs presented, the disappearance of the black boundary layer image towards the rear of the bump might seem to indicate separation. However, as shown in diagrams D.5 and D.6 the white image and corresponding density gradient in the inner part of the vortex may merge with and cancel the dark image and opposite density gradient of the boundary layer.

Figure D Sketch of Boundary Layer Characteristics used to Help Interpret Schlieren Photographs.

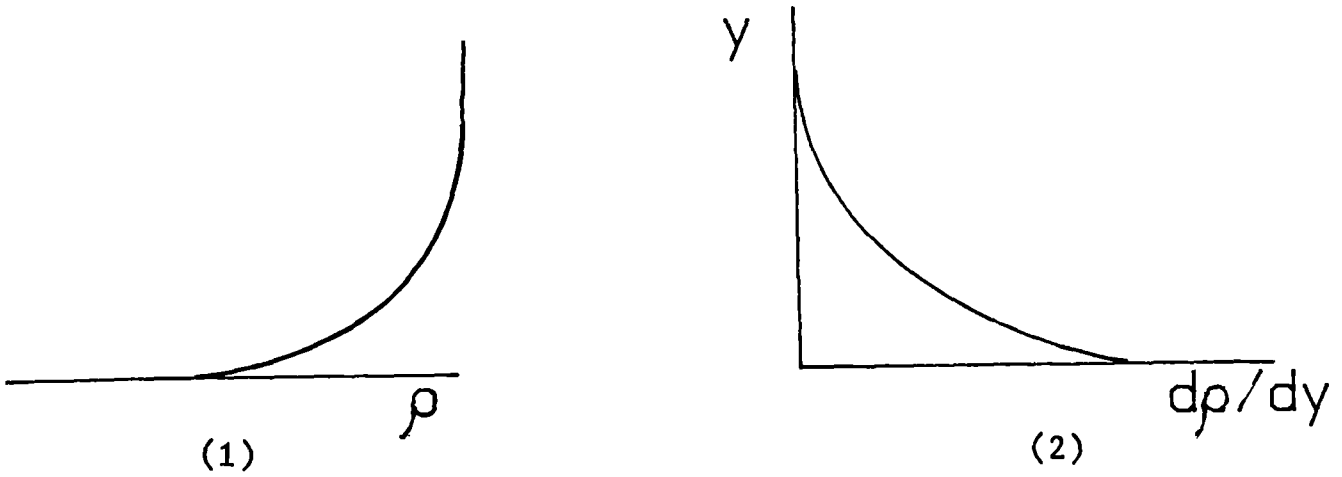

(1) (2)

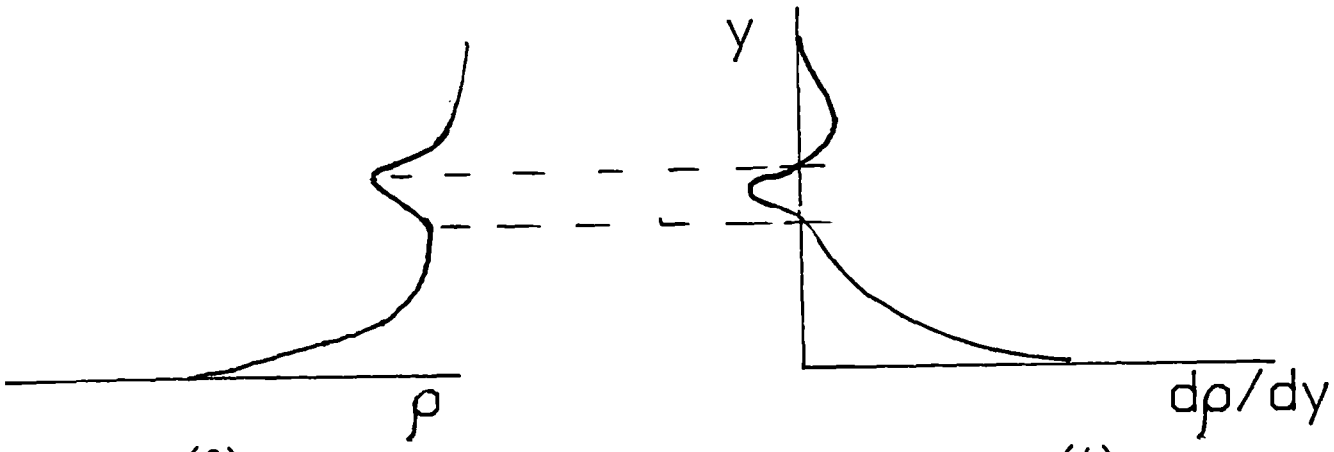

(3) (4)

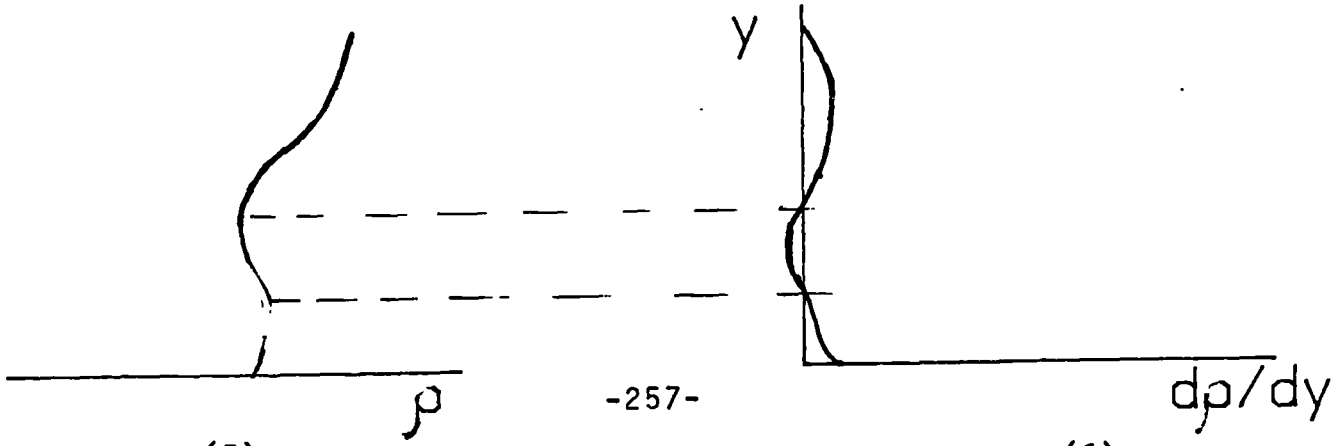

(5) (6)

APPENDIX E

The flow parameters used to interpt the results from the chordwise pressure distributions in the high speed wind tunnel are defined below. A sketch of a pressure distribution is show in Figure E.1 and helps illustrate some of the definitions.

P	Local static pressure
P_0	Freestream stagnation pressure
P_1	Pressure ratio P/P_0 just upstream of the shock
P2	Pressure ratio P/P_0 at the foot of the shock or alternatively, just downstream of the rapid pressure rise through the region of shock boundary layer interaction (which includes the re-attachment if the separation bubble is of limited length).
P/P_0(TE)	Pressure ratio at the trailing edge
x/c_{shock}	Shock position which is defined as the intersection of the steep pressure rise with the locus of the upstream pressure P_1

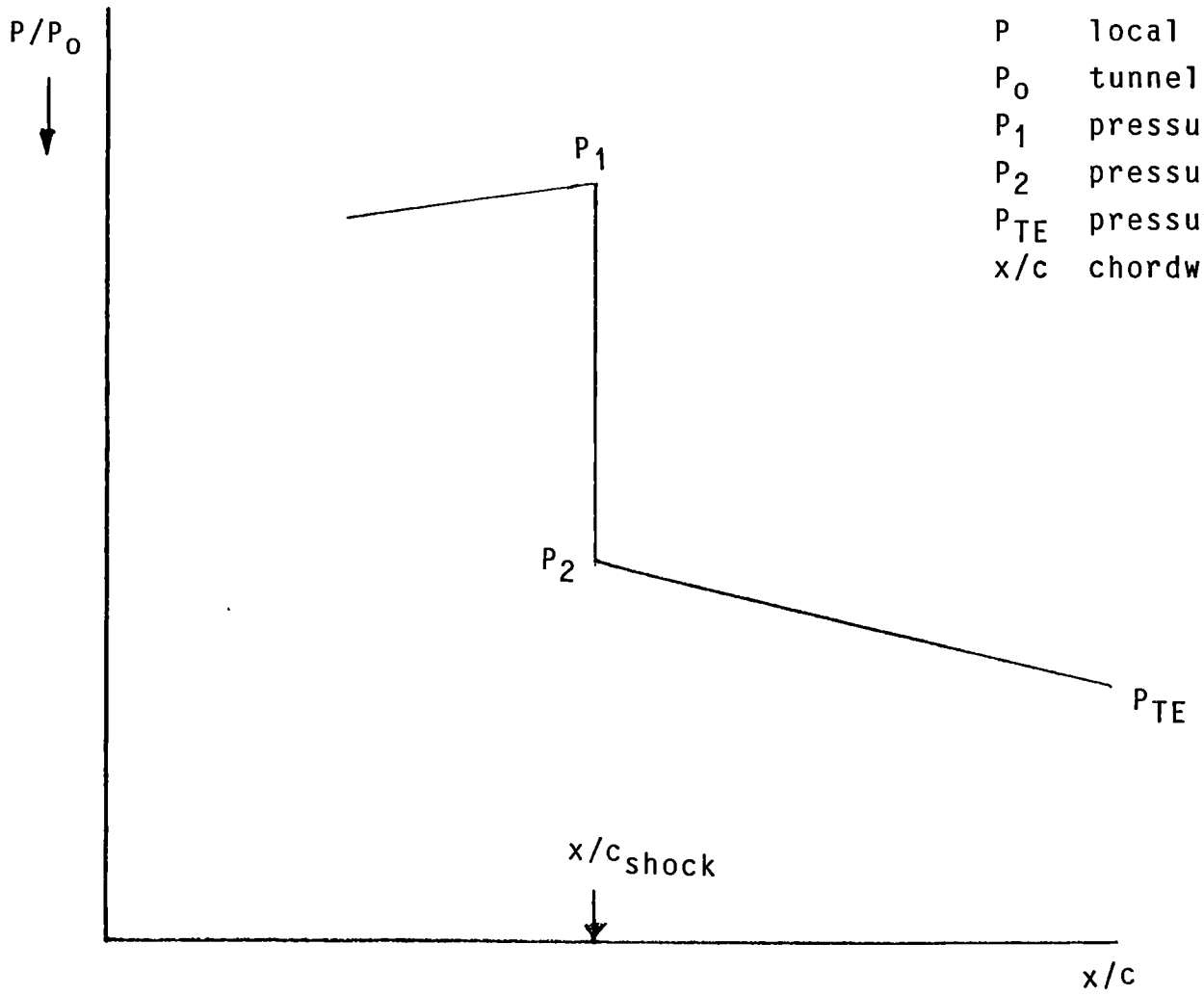

P local static pressure
P_o tunnel stagnation pressure
P_1 pressure just upstream of the shock wave
P_2 pressure at the foot of the shock wave
P_{TE} pressure at the trailing edge
x/c chordwise extent

APPENDIX F

Extrapolation Method to Determine Required t/c Ratio

The first series of tests in the high speed wind tunnel were carried out on the 8% thick bump. Local Mach numbers ahead of the shock increased to a maximum value of 1.40. In order to investigate the effect of increasing the Mach number ahead of the shock wave it was decided to increase the thickness to chord ratio (t/c) of the bump. Mach numbers as high as 1.5 and 1.6 were desired.

To achieve these local Mach numbers ahead of the shock wave a simple extrapolation procedure was adopted to estimate the t/c ratio of the bumps required. This procedure was based on the assumption that the ratio of the theoretical (Prandtl Mayer) Mach number to the experimental or predicted Mach number would remain constant (see Figure F.1).

For the 8% bump, experimental results showed that sonic conditions were reached at x/c=0.22%. The local pressure ratios and therefore local Mach number and flow deflections (u) could be obtained from isentropic flow tables (reference 19). Knowing the equation that defined the 8% bump the theoretical flow deflections (u_T) from the sonic point were calculated and theoretical Mach numbers based on these flow deflections were ascertained from the isentropic flow tables (19). The ratio of theoretical to experimental Mach numbers or flow deflections (u_T/u_E) was thus achieved. From this, theoretical Mach numbers and flow deflections for bumps with increasing t/c ratios

could be used to derive predicted flow deflections (u_p) and Mach numbers. A sample calculation is shown below.

8% Bump

Theoretical calculations:

x/c(%)	dy/dx	u_T(degrees)	Mach No.
0.22	0.152	0.000	1.00
0.30	0.047	5.926	1.29
0.40	-0.017	9.630	1.42
0.50	-0.064	12.264	1.51
0.60	-0.094	14.029	1.57
0.70	-0.113	15.096	1.61

Experimental Results:

x/c(%)	P/P_o	u_E(degrees)	Mach No.
0.22	0.528	0.00	1.00
0.30	0.452	2.94	1.13
0.40	0.378	5.09	1.26
0.50	0.334	7.55	1.35
0.60	0.310	8.97	1.40
0.70	0.310	8.97	1.40

Hence;

x/c(%)	u_T/u_E
0.22	0.000
0.30	3.055
0.40	1.892
0.50	1.624
0.60	1.564
0.70	1.683

10% Bump

Theoretical calculations:

x/c(%)	dy/dx	u_T(degrees)	Mach No.
0.22	0.190	0.000	1.00
0.30	0.079	6.272	1.30
0.40	-0.029	12.432	1.52
0.50	-0.106	16.832	1.67
0.60	-0.158	19.744	1.77
0.70	-0.189	21.489	1.83

Prediction for 10% Bump

x/c(%)	u_T/u_E	u_p(degrees)	Mach No.
0.22	0.000	0.000	1.00
0.30	3.055	2.053	1.14
0.40	1.892	6.571	1.31
0.50	1.624	10.365	1.45
0.60	1.564	12.624	1.52
0.70	1.683	12.768	1.53

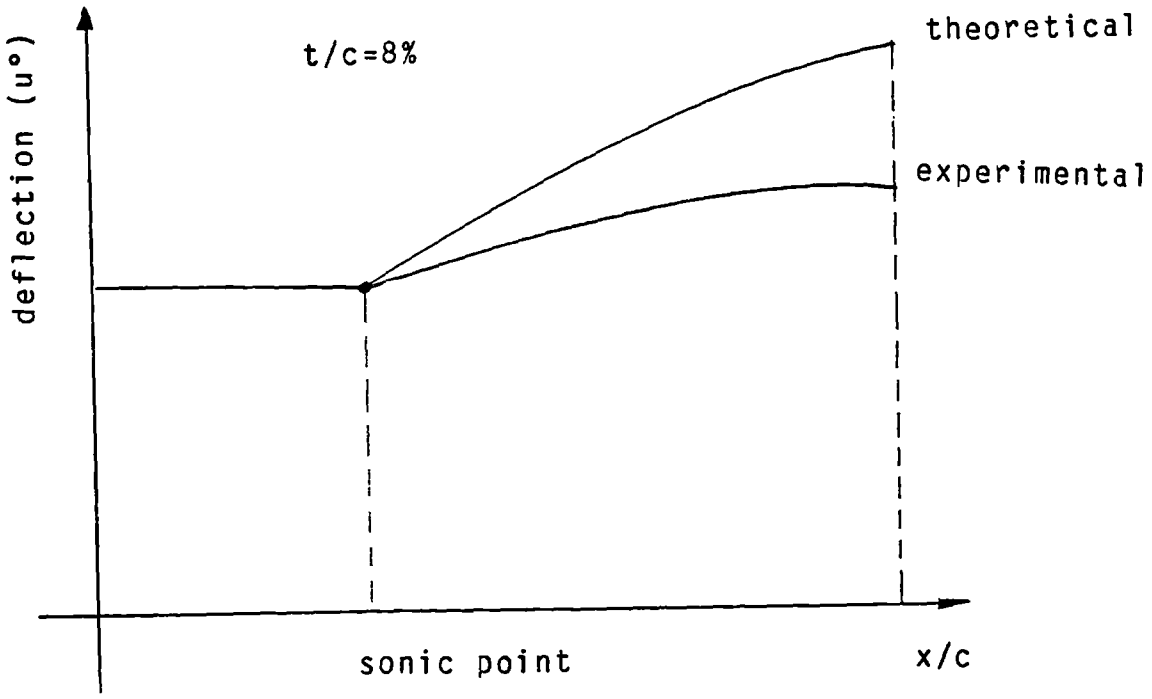

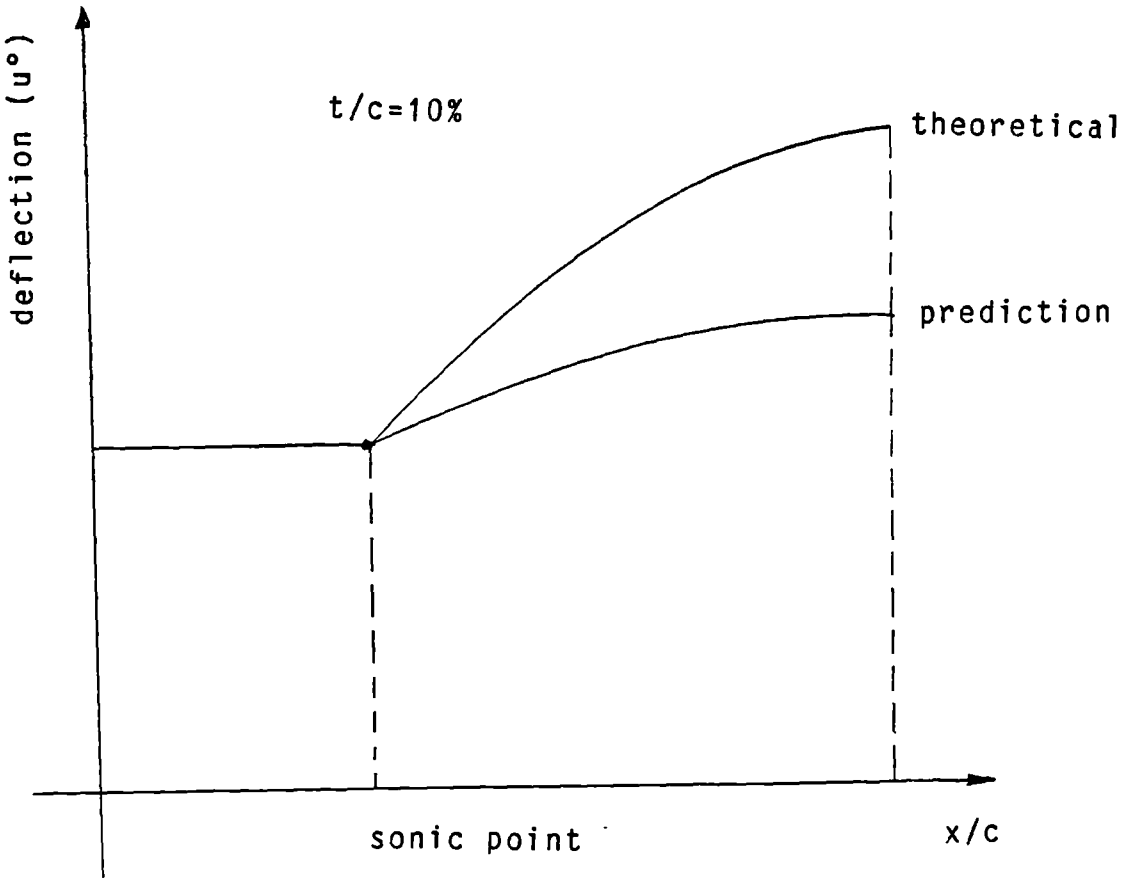

Figure F.1 Assumption for Mach Number Prediction

APPENDIX G

Definition of C_{pb}

The experimental data available for calculating the profiles of the boundary layers measured on the 14% thick bump comprise of, the local static pressure at the rake position, P_s, and the values of the pitot pressure measured on the 14 boundary layer rake tubes, P_{or}. The stagnation pressure measured on the highest rake is referred to as P_{oe}.

The definition of C_{pb} is as follows;

$$C_{pb} = \frac{[P_{or} - P_s]}{P_{oe} - P_s}$$

The significance of this boundary layer coefficient is explained by the following:

(1) If there is a separated flow in the boundary layer or the boundary layer is close to separation this means that the pitot rake method of measurement can no longer be interpreted correctly. However where the pitot pressure becomes close to the local static pressure (as C_{pb} tends to 0) at a significant distance from the surface it is safe to deduce the presence of separation.

(2) The presence of streamwise vortices embedded or partially embedded in the boundary layer is detected by a significant drop in the local pitot pressure which is shown as a drop in Cpb.